

**Dendritic Spine Morphology:
The Role of Microtubules and Endosomes**

Bjorn Robin Dortland

ISBN: 978-90-9024590-4

©Bjorn R. Dortland, 2009

All rights reserved. No part of this publication may be reproduced, stored in a retrieval system or transmitted in any form or by any means, electrical, mechanical, photocopying, recording or otherwise without the permission of the author or, when appropriate, of the scientific journal in which parts of this thesis have been published.

The studies presented in this thesis were performed at the Department of Neuroscience of the Erasmus MC in Rotterdam, The Netherlands. Research was supported by Prinses Beatrix Fonds, The European Community (EEC; SENSOPAC), Netherlands Organization for Scientific Research (NWO-ALW and NWO-CW-ECHO), Netherlands Organization for Health Research and Development (ZonMw-VIDI, ZonMw-TOP), Human Frontier Science Program Career Development Award (HFSP-CDA), European Science Foundation (European Young Investigators (EURYI) Award) and Senter (Neuro-Bsik).

Printed by: Wöhrmann Print Service

Lay-out by: E.A. van der Laan - Reussink

Dendritic Spine Morphology: The Role of Microtubules and Endosomes

Dendritische spine morfologie: De rol van microtubuli en endosomen

Proefschrift

Ter verkrijging van de graad van doctor aan de
Erasmus Universiteit Rotterdam
op gezag van de rector magnificus
Prof.dr.H.G. Schmidt
en volgens besluit van het College voor Promoties

De openbare verdediging zal plaatsvinden op
woensdag 23 september 2009 om 11.30 uur

door

Bjorn Robin Dortland
Geboren te Gouda



Promotiecommissie:

Promotor: Prof. dr. C.I. de Zeeuw

Overige leden: Prof. dr. Y. Elgersma
Dr. A. Akhmanova
Prof. dr. D.N. Meijer

Copromotor: Dr C.C. Hoogenraad

Table of contents

Chapter 1	General Introduction	7
1.1	A brief introduction to the brain, neurons and synapses	9
	<i>1.1.1 Neurons</i>	9
	<i>1.1.2 Synapses</i>	11
1.2	Synaptic transmission and the structure of synapses	12
	<i>1.2.1 Synaptic transmission</i>	12
	<i>1.2.2 Synaptic structure</i>	13
	<i>1.2.3 The postsynaptic compartment</i>	14
1.3	Receptor recycling	15
	<i>1.3.1 Postsynaptic receptor trafficking</i>	15
	<i>1.3.2 AMPA receptor trafficking</i>	16
1.4	Dendritic spines	19
	<i>1.4.1 Spine development and morphology</i>	19
	<i>1.4.2 Spine plasticity</i>	21
1.5	Synaptic pathology in neurological diseases	21
1.6	Scope of this thesis	24
Chapter 2	Dynamic microtubules regulate dendritic spine morphology and synaptic plasticity	31
Chapter 3	Rab4 effector GRASP-1 coordinates endocytic domain coupling and dendritic spine morphology	49
Chapter 4	Deletion of FMR1 in Purkinje cells enhances parallel fiber LTD, enlarges spines, and attenuates cerebellar eyelid conditioning in Fragile X Syndrome	95
Chapter 5	General discussion	111
Summary		125
Samenvatting		127
Portfolio		129
Curriculum Vitae		131
List of publications		133
Dankwoord		135

General Introduction

Chapter 1

1.1 A brief introduction to the brain, neurons and synapses

In Ancient Egypt, the function of the brain was regarded as not much more than cranial stuffing. The brain was regularly removed in preparation for mummification since the heart was assumed to be the organ of intelligence. Over the next five thousand years, this view was reversed; the brain is now known to be the control center of the central nervous system that is responsible for regulating virtually all activities of the body and is the source of perception and higher cognitive functions in humans.

The simplest possible multicellular organisms have very simple nervous systems made up of a few neurons that mediate a reflex action. Smaller invertebrates, such as the flatworm, do not have a centralized brain but loose associations of neurons arranged in simple reflex pathways along the body. Larger invertebrates, such as the lobster have simple “brains” that consist of localized collections of neuronal cell bodies called ganglia. Each ganglion controls sensory and motor functions in its segment through reflex pathways, and the ganglia are linked together to form a simple nervous system. In higher organisms the nervous systems evolve from the chains of ganglia cells into more centralized brain structures. In mammals the brain is extremely complex and is divided in different functional regions, such as for example the brain stem, cerebellum, and cerebral cortex.

1.1.1 Neurons

All regions of the brain contain two classes of cells, neurons and glia, both of which contain several different cell types which perform different functions (Kandel et al., 2000). Glial cells (“glia” is Greek for “glue”) form a support system for neurons. They create the insulating myelin, provide structure to the neuronal network, manage waste, and clean up neurotransmitters.

Neurons are electrically excitable cells that connect with each other, convey information to other cells and form an extensive neuronal network. The human brain consists of more than a 10^{12} (a trillion) neurons which can be divided in three main neuronal cell types: sensory neurons that act to detect stimuli (photoreceptors, olfactory, touch), motor neurons that transmit signals from the central nervous system to muscles (and glands) and interneurons that process signals from other neurons. Although neurons have a variety of shapes such as pyramidal neurons in the cerebral cortex, Purkinje cells in the cerebellum, mitral cells in the olfactory bulb and motor neurons in the spinal cord (Figure 1), they all have three basic parts: cell body that contains all of the necessary components of the cell, such as the nucleus (contains DNA), endoplasmic reticulum (ER) and ribosomes (for protein synthesis) and mitochondria (energy production), axon a long projection that conducts the electrochemical information (nerve impulse or action potential) and dendrites, branch-like projections which receive (and combine) electrochemical information sent by neighboring neurons (Figure 1). The neuron’s place as the primary functional unit of the nervous system was first recognized in the early 20th century through the work of the Spanish anatomist Santiago Ramón y Cajal (Shepherd and Erulkar, 1997). Cajal proposed that neurons were discrete cells that communicated with each other via specialized junctions, or spaces, between cells. This became known as the neuron doctrine, one of the central dogmas of modern neuroscience (Bullock et al., 2005; Richard, 2005).

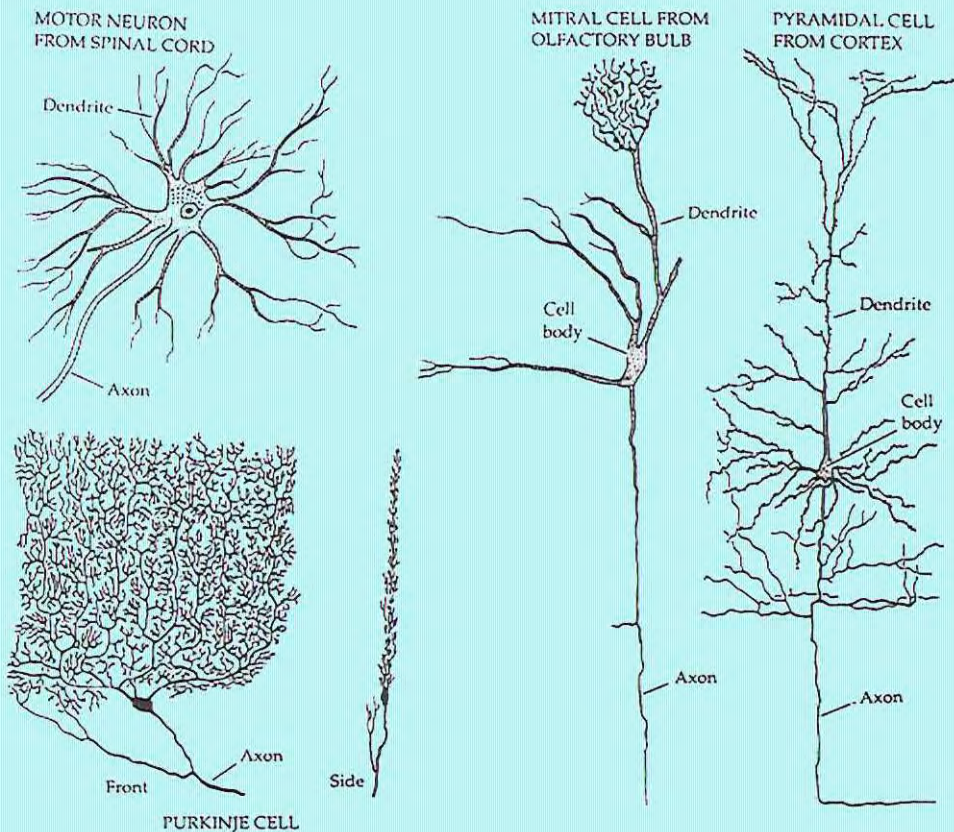


Figure 1: Neuron morphology

Reconstructions (drawn by Cajal and Deiters) of different types of neurons. A motor neuron from the spinal cord (top left), a front and side view from a Purkinje cell found in the cerebellum (bottom left), a mitral cell from the olfactory bulb (middle) and a pyramidal neuron found in the cerebral cortex (right). Although neurons can be very different in appearance, all have a basic structure of a cell body, an axon and dendrites. (Adapted from *From neuron to brain: A Cellular and Molecular Approach to the Function of the Nervous System*, 3rd Ed)

In the late 19th century a big controversy revolved around the question of whether the nervous system is composed of independent cells whose processes contact other cells (neuron theory), or whether the nervous system is a continuous system (reticular theory). In 1906 the Nobel Prize in medicine was shared by two pioneers in neuroanatomy, Camillo Golgi and Santiago Ramon y Cajal (De Carlos and Borrell, 2007). Golgi supported the reticular theory while Ramon y Cajal supported the neuron theory. Cajal experimented on brain tissue with the silver staining that was developed by and named after Golgi, the Golgi-staining. Cajal saw tiny protrusions on the dendrite of stained Purkinje cells. He proposed that these were the places where the neuron could communicate with other cells (Garcia-Lopez et al., 2007). While these and other experiments helped to achieve an eventual consensus in favor of the neuron theory, it was not possible to actually visualize the space between two neurons at the spot where they connect. With the development of the electron microscope (EM) around the mid 20th century it was finally possible to visualize the connections of neurons in great detail, showing a cleft between the two cells, thereby definitely settling the controversy in favor of the neuron theory.

1.1.2 Synapses

In a neuronal network a single neuron may be connected to many other neurons and the total number of neurons and connections in a network may be extensive. The point where two neurons connect with each other and communicate together is called a “synapse”. The term synapse was introduced by Charles Sherrington in 1897 for these connections (Shepherd and Erulkar, 1997). The word “synapse” comes from “synaptein”, created from the Greek “syn-” (“together”) and “haptain” (“to clasp”). It is estimated that the mature human brain has 5×10^{14} (500 trillion) neuronal synapses. Although the term “synapse” commonly refers to a chemical synapse, synaptic connections are categorized in two groups: electrical and chemical. Already in 1860 it was suggested that communication between neurons was an electrical process. A decade later Bois-Reymond was the first to propose that synaptic transmission is a chemical process. The debate whether synapses are electrical or chemical took till the 1950’s when, with improved physiological techniques it became clear that both forms of synaptic transmission exist (Bennett and Zukin, 2004; Connors and Long, 2004). Electron microscope analysis made it possible to show the morphological differences between the two types of synapses. At electrical synapses, the two neurons make direct contact via gap junction channels and approach within about 3.5 nm of each other. The pore of a gap junction channel is wide enough to allow ions and even medium-sized molecules like signaling molecules to flow from one cell to the next, thereby connecting the two cells cytoplasm. At chemical synapses, the two neurons are separated from each other by a synaptic cleft of 20 nm distance. They are not connected via protein channels and thus cannot communicate directly. Instead, small chemicals called neurotransmitters are used to signal from one cell to the next. Most excitatory neurons in the mammalian central nervous system have glutamatergic synapses with glutamate as neurotransmitter. The first neurotransmitter identified was acetylcholine, described by Dale in 1914 (Brown, 2006). Many other small molecules, amino acids and short peptides have been identified as neurotransmitters since then.

1.2 Synaptic transmission and the structure of synapses

1.2.1 Synaptic transmission

Neurons are specially adapted for the transmission of electrical signals by changing their membrane potential (Purves, 2001). The membrane potential is a property of all cells and reflects a difference in charge on either side of the cell membrane. Normally, cells have a negative charge inside the cell which results in a negative resting membrane potential. In response to stimuli, neurons are electrically excitable which means that rapid changes in membrane potential can occur. Within a millisecond, the membrane potential changes from negative to positive and back. This pulse-like wave of voltage is called the action potential or nerve impulse (Kandel et al., 2000). Thus, neurons transport their information by way of action potentials. When a nerve impulse moves along the axon and arrives at the presynapse, it releases neurotransmitters, which influence the postsynaptic neurons, either in an inhibitory way or in an excitatory way. The chemical movement over the synapse caused by the propagation of the action potential is called synaptic transmission (latin: transmitto = send, let through). The next neuron may be connected to many more neurons, and if the total of excitatory influences is sufficient, it will create a new action potential at its axon hillock, in this way passing on the information to yet another neuron, or resulting in an experience or an action.

Whether the result of synaptic transmission will be excitatory or inhibitory depends on the type of neurotransmitter used and the ion channel receptors they interact with (Kandel et al., 2000; Purves, 2001). Glutamate is the most common neurotransmitter for excitatory synaptic transmission in the mammalian brain. This is a common amino acid used throughout the body to build proteins but in the central nervous system (CNS) it is the major excitatory neurotransmitter. It interacts with different classes of glutamate-type receptors in the postsynaptic neuron (Dingledine et al., 1999; Hollmann and Heinemann, 1994). These receptors are named after specific agonists (AMPA (α -amino-3-hydroxy-5-methyl-4-isoxazoleprionic acid) and NMDA (N-methyl-D-aspartic acid)) that can bind the receptors and mimic the effect of glutamate. The receptors are ion channels that are permeable to sodium ions and thus generate depolarisation waves. Inhibitory synaptic transmission uses a neurotransmitter called γ -Aminobutyric acid (GABA) (Hevers and Luddens, 1998; Whiting, 2003). This interacts with GABA receptors, ion channels that are permeable to negatively charged chloride ions. Thus, opening of these channels makes it harder for a neuron to generate an action potential. Long-lasting changes in the efficacy of these synaptic connections (long-term potentiation or depression) between two neurons can involve the making and breaking of synaptic contacts (Malenka and Nicoll, 1999; Malinow et al., 2000; Nelson and Turrigiano, 2008). Understanding the precise control of synaptic transmission in the brain makes it clear how an imbalance in this mechanism could have serious clinical implications. Whether due to genetic defects, drug abuse, the aging process or other various causes, biological dysfunction in synaptic transmission often leads to such imbalances and is the underlying cause of conditions such as schizophrenia, Parkinson's disease, and Alzheimer's disease (Cohen and Greenberg, 2008; Katona and Freund, 2008; Selkoe, 2002; Stephan et al., 2006; Sudhof, 2008).

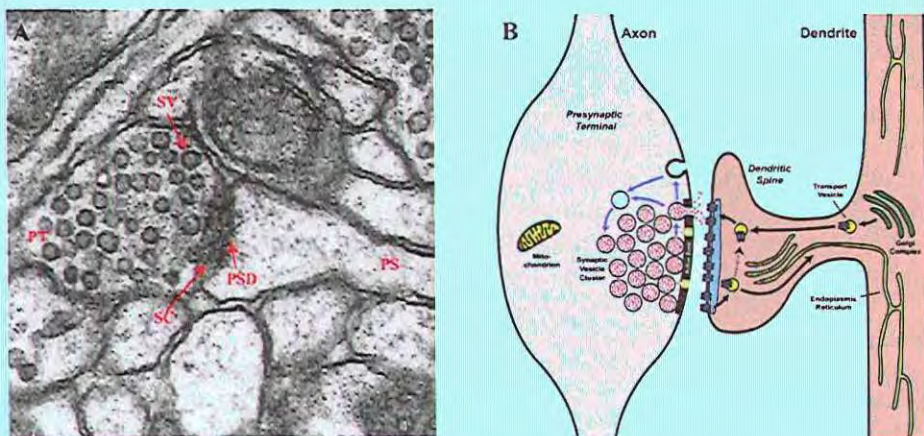


Figure 2: Synapse morphology

A EM image of an excitatory synapse with a presynaptic terminal (PT) and a postsynaptic spine (PS) separated by a synaptic cleft (SC). At the PT, synaptic vesicles (SV) containing neurotransmitter can be seen. A post synaptic density (PSD) can be seen in the PS. B a schematic overview of a synapse with the presynaptic side (left) showing synaptic vesicles docking at the synapse and releasing their neurotransmitters in the synaptic cleft after an electric stimulus. Receptors of the PSD can bind the neurotransmitters and initiate a response in the postsynaptic compartment (right). Transport of receptors from the synaptic membrane to intracellular vesicles or visa versa allows fast adaptation of synaptic strength. The major trafficking organelles, the Golgi complex and the ER are indicated in green. (adapted from Sudhof and Malenka, *Neuron*, 2008)

1.2.2 Synaptic Structure

How does the electrical information from one neuron flows to another neuron across a synapse? Let's first look more closely at the structure and architecture of the synapse. A synapse consists of: a presynaptic ending that contains neurotransmitters, a postsynaptic ending that contains receptor sites for neurotransmitters and, a synaptic cleft between the presynaptic and postsynaptic endings (Figure 2) (Okabe, 2007; Sheng and Hoogenraad, 2007; Waites et al., 2005). Since the action potential cannot cross the synaptic cleft between neurons, the nerve impulse is carried by small chemicals called neurotransmitters. These chemicals are made by the cell that is sending the impulse (the presynaptic neuron) and stored in synaptic vesicles at the end of the axon. Excitatory presynaptic boutons contain clear round vesicles, approximately 35-50 nm in diameter (Figure 2). These vesicles usually contain the neurotransmitter glutamate. Exocytosis of neurotransmitters requires the docking and fusion of vesicles with the plasma membrane and requires ATP and voltage-gated calcium channels (Jin and Garner, 2008; Rosenmund et al., 2003). This initiates the docking and fusion of the vesicles at the presynaptic membrane in an active zone through the action of docking and fusion proteins such as synaptotagmin, synaptobrevin and syntaxin (Sudhof, 2004). The cell that is receiving the nerve impulse (the postsynaptic neuron) has chemical-gated ion channels in its membrane, called neurotransmitter receptors, which have specific binding sites for the neurotransmitters (Figure 2). After its recognition by the receptor, the neurotransmitter must be inactivated so that it does not continually occupy the receptor sites of the postsynaptic cell. Inactivation of the neurotransmitter or recovery by the presynaptic neuron avoids constant stimulation of the postsynaptic cell, while at the same time freeing up the receptor sites so that they can receive additional neurotransmitter molecules, should another action potential arrive. Many psychoactive drugs and neurotoxins can change the properties of neurotransmitter release, neurotransmitter

reuptake and the availability of receptor binding sites (Costa et al., 2008; Luscher and Ungless, 2006).

1.2.3 The Postsynaptic Compartment

At the postsynaptic membrane, both glutamate and GABA receptors are organized by specific scaffolding proteins which concentrate receptors at excitatory or inhibitory synapses. At excitatory synapses, a specialised postsynaptic multiprotein complex, known as the postsynaptic density (PSD) clusters glutamate receptors, scaffolding proteins and signaling elements at the postsynaptic membrane (Kennedy, 2000; Ziff, 1997). The PSD lies adjacent to the cytoplasmic face of the postsynaptic membrane, in close apposition to the active zone of the synapse and the docked synaptic vesicles in the presynaptic terminal. By EM the PSD is clearly visible as an electron-dense postsynaptic structure of ~200-800 nm wide and ~30-50 nm thick (Figure 2). This specialised location places the PSD directly in the path of the intracellular ionic fluxes and second messenger cascades generated by neurotransmitters. It is now apparent that the PSD provides a structural matrix, which clusters ion channels in the postsynaptic membrane and anchors signaling molecules such as kinases and phosphatases at the synapse (Kennedy et al., 2005). These properties suggest that the PSD serves as a general organizer of the postsynaptic signal transduction machinery, which links regulatory molecules to their targets, coordinates developmental and activity-dependent changes in postsynaptic structures, and establishes the functional topography of the postsynaptic membrane. It is now widely believed that the PSD has a central role in synaptic signaling and regulation (Okabe, 2007; Sheng and Hoogenraad, 2007).

Over the years, protein components of the PSD have been discovered by biochemical and yeast two-hybrid approaches. The PSD is typically purified through differential centrifugation, sucrose gradient sedimentation and detergent extraction, because the PSD structure cannot be solubilized with mild nonionic detergents such as Triton X-100. Kennedy and co-workers discovered several PSD proteins by sequencing of protein bands from one-dimensional gels of PSD preparations (Kennedy et al., 1983). Walsh and Kuruc employed two-dimensional gel electrophoresis followed by immunoblotting and amino acid sequencing by traditional N-terminal degradation, and determined more than 30 proteins (Walsh and Kuruc, 1992). Later, many PSD proteins were identified by the yeast two-hybrid system as binding partners of known postsynaptic proteins (Kim and Sheng, 2004). The development of matrix-assisted laser desorption/ionization-time of flight (MALDI-TOF) mass spectrometry allowed several groups to re-analyze constituents of the PSD. Recently, Peng et al., and Cheng et al., identified ~350 PSD components using liquid chromatography coupled with tandem mass spectrometry (LC-MS/MS) (Cheng et al., 2006; Peng et al., 2004). Membrane proteins found in the PSD are ion channels, cell adhesion molecules, G protein-coupled receptors and receptor tyrosine kinases which are involved in communication and linkage with the presynaptic active zone. Cytoplasmic proteins found in the PSD are scaffolding proteins, signaling enzymes and cytoskeletal proteins. The PSD is a highly dynamic structure that can change size or composition in response to synaptic activity, involving mechanisms such as protein phosphorylation, local translation, ubiquitination and degradation, and subcellular redistribution (Kennedy et al., 2005; Okabe, 2007). Important mechanisms for synaptic regulation, including long-term potentiation (LTP) and long-term depression (LTD), are likely to have a basis in the PSD. For example, a major component of the PSD, the subunit of the Ca²⁺/calmodulin-dependent protein

kinase II (CaMKII), has a central role in a current model for long-term memory (Lisman and Goldring, 1988). The NMDA receptor, which is required for several forms of synaptic plasticity (Wilson and Tonegawa, 1997) is clustered at the synapse by components of the PSD (Sheng and Kim, 1996). Thus, the PSD contributes to critical features of synaptic integration and regulation and aberrations therefore may underlie neuronal disorders (Dev, 2004; Li and Jimenez, 2008).

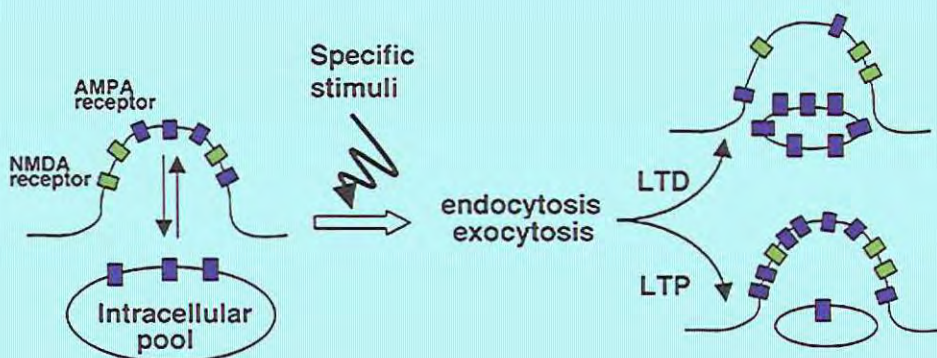


Figure 3: AMPA receptor trafficking during LTP and LTD.

While the total amount of AMPA receptors at a synapse is stable, the individual receptors are constantly recycled, moving from the synaptic membrane to an intracellular pool and back. LTP-inducing stimuli cause more AMPA receptors to enter the synaptic membrane via endocytosis, strengthening the synaps. LTD-inducing stimuli will enhance the internalization of AMPA receptors via exocytosis. (adapted from Craig and Boudin, *Nature Neuroscience*, 2001)

1.3 Receptor recycling

1.3.1 Postsynaptic Receptor Trafficking

Synaptic plasticity is the ability of the synapse to change in strength and is thought to be the cellular basis of learning and memory. There are several underlying mechanisms that cooperate to achieve synaptic plasticity, including changes in the quantity of neurotransmitter released into a synapse and changes in how effectively cells respond to those neurotransmitters. The synaptic strength also depends on the number of ion channels. Importantly, it has been shown that neurons change the density of receptors on their postsynaptic membranes as a mechanism for changing their own excitability in response to stimuli. In a dynamic process that is maintained in equilibrium, neurotransmitter receptors are added to the synaptic membrane by exocytosis and removed by endocytosis (Sheng and Lee, 2001) or recruited and stabilized from a freely diffusing surface pool (Choquet and Triller, 2003). In excitatory synapses, NMDA receptors in the synaptic membrane are quite constant both in number and position, while the amount of AMPA receptors in these synapses can change quickly. AMPA receptors are constantly recycled from the synaptic membrane to an intracellular vesicle pool and back. These processes, and by extension the number of receptors on the membrane, can be altered by synaptic activity (Bredt and Nicoll, 2003; Greger and Esteban, 2007; Newpher and Ehlers, 2008). In fact, it is widely believed that AMPA receptors are delivered to the membrane due to repetitive NMDA receptor activation.

Importantly, the delivery of AMPA receptors to the synapse during synaptic stimulation is independent of protein synthesis. This is achieved by having a nonsynaptic pool of AMPA receptors adjacent to the postsynaptic membrane. When the appropriate LTP-inducing stimulus arrives, nonsynaptic AMPA receptors are rapidly trafficked into the postsynaptic membrane under the influence calcium influx and activation of protein kinases, such as CaMKII and protein kinase A (PKA) (Derkach et al., 2007). By increasing the efficiency and number of AMPA receptors at the synapse, future excitatory stimuli will generate larger postsynaptic responses.

1.3.2 AMPA receptor trafficking

AMPA receptors are the brain's most abundant glutamate receptors and mediate the majority of its excitatory activity (Cull-Candy et al., 2006; Derkach et al., 2007). As indicated above, understanding the cellular machinery behind AMPA receptor trafficking is relevant for understanding synaptic plasticity. Important processes in AMPA receptor dynamics are receptor assembly, sorting and trafficking. AMPA receptor trafficking includes mechanisms such as vesicular transport to get the receptors to synaptic sites (Bredt and Nicoll, 2003), endocytic recycling and degradation (Sheng and Lee, 2001) and surface receptor diffusion (Choquet and Triller, 2003) for local trafficking near the synaptic membrane.

AMPA receptors are hetero-tetramers composed of different combinations of GluR1, GluR2, GluR3, and GluR4 subunits (Hollmann and Heinemann, 1994). Each subunit is composed of 4 transmembrane domains, an extracellular N-terminus and an intracellular C-terminus. In the mature hippocampus, most AMPA receptors are composed of GluR1–GluR2 or GluR2–GluR3 combinations, whereas GluR4-containing AMPA receptors are expressed mainly in early postnatal development (Wenthold et al., 1996). These oligomeric combinations are formed in the endoplasmic reticulum (ER), possibly assembling as dimers of dimers via interactions between the luminal, N-terminal domains of the subunits. After assembly, exit from the ER is tightly regulated by quality control mechanisms that monitor the competency of newly synthesized receptors for ligand binding and gating (Fleck, 2006). Interestingly, a fraction of the GluR2 subunits remains unassembled within the ER, which seems to depend on a single amino acid located at position 607 at the channel pore region. In GluR1, GluR3 and GluR4 this is a glutamine residue gln607 but in GluR2 it is an arginine residue arg607. After mutation of gln607 into arg607 in GluR2, GluR2 will behave like the other subunits and quickly exported from the ER (Greger and Esteban, 2007). Interactions with cytosolic proteins also control trafficking through the ER. For example, the GluR2 C-terminus has a PDZ (PSD-95/Discs-Large/ZO-1) binding motif (-SVKI) that interacts with the PDZ domain-containing protein PICK1 (Protein Interacting with C-Kinase 1) (Bredt and Nicoll, 2003) which is required for GluR2's exit from the ER. Additionally, export of AMPA receptors from the ER and surface expression is also facilitated by direct interaction with a family of transmembrane AMPA receptor regulatory proteins (TARPs) (Nicoll et al., 2006). Mutant *stargazer* mice lacking TARP γ 2 have no delivery of functional receptors to the cell surface, which leads to ataxia and epilepsy in these mice (Chen et al., 2000). The four last C-terminal amino acids of TARP form a PDZ binding domain which can bind to PSD-95, a scaffolding protein in the PSD, indicating an additional role for TARPs in the clustering of AMPA receptors at the synapse. In fact, TARPs may well be considered auxiliary subunits of AMPA receptors (Fukata et al., 2005), which assist in their proper folding and affect channel kinetics (Bedoukian et

al., 2006).

The newly synthesized AMPA receptors travel long distances from their point of biosynthesis to their final synaptic targets. The long-range dendritic transport of AMPA receptors is likely to depend on the microtubule cytoskeleton that runs along dendritic shafts. The transport of membrane organelles on microtubule tracks is an active process powered by motor proteins of the kinesin and dynein superfamilies (Hirokawa and Takemura, 2005; Vale, 2003). Membrane vesicles bearing AMPA receptors are likely to be transported by some of these motor proteins; however the molecular mechanisms underlying these processes are still not clear. The PDZ domain-containing protein Glutamate Receptor Interacting Protein (GRIP) interacts directly with the heavy chain of conventional kinesin (kinesin-1) and with the C-terminal PDZ motif of GluR2 and GluR3 (Dong et al., 1997; Setou et al., 2002), and hence, may serve as the link between synaptic receptors and microtubule dependent motor protein transport (Hoogenraad et al., 2005). In addition, it has recently been reported that the transport of AMPA receptors to synaptic sites depends on actin-based motor protein transport (Wang et al., 2008).

The final steps in the synaptic trafficking of AMPA receptors strongly depend on their subunit composition, and specifically, on cis-signals contained within their cytosolic carboxy termini (Shi et al., 2001). The extracellular domains and the trans-membrane domains of AMPA receptors are very similar in all four subunits but the C-terminus varies in the different subunits. GluR1 and GluR4 have long cytoplasmic C-terminal tails while GluR2 and GluR3 have short cytoplasmic tails (Shepherd and Huganir, 2007). The different C-terminal tails bind to specific cytoplasmic proteins which lead to subunit-specific receptor dynamics. In hippocampus, hetero-tetramers formed by GluR1-GluR2 and GluR2-GluR3 subunits, together with a smaller contribution from GluR homo-tetramers, represent the most common combinations in excitatory synapses. GluR2-GluR3 hetero-tetramers continuously cycle in and out of synapses in a manner largely independent from synaptic activity (constitutive pathway) (Passafaro et al., 2001). Activity-dependent receptor endocytosis responsible for long term depression (LTD) requires the GluR2 subunit (Lee et al., 2004). The C-terminal tail of GluR2 specifically binds to several proteins involved in receptor trafficking; GRIP1 anchors AMPA receptors at synaptic and intracellular membranes and PICK1 binds to the GluR2 C-tail at the same region as GRIP/ABP. Transfer of AMPA receptor from ABP/GRIP to PICK1, facilitated by GluR2 S880 phosphorylation is a critical step in controlling GluR2 trafficking (Lu and Ziff, 2005). GluR1 on the other hand is the key subunit that “drives” AMPA receptors to the surface and to synapses in response to NMDA receptor stimulation and activation of CaMKII, resulting in synaptic potentiation. In heteromeric receptors, GluR1 acts “dominantly” over GluR2 (Shi et al., 2001). This regulated pathway is triggered transiently upon induction of long-term potentiation (LTP), and results in a net increase in the number of AMPA receptors present at synapses. This leads to activation of previously silent synapses that lacked AMPA receptors or to further strengthening of synapses that already had AMPA receptors. Although the mechanisms behind AMPA receptor delivery during LTP are not yet completely known, several experiments have shown that GluR1 containing receptors are critical for LTP induction. Mature GluR1-knockout mice show no LTP, while GluR2-knockout mice show enhanced LTP (Meng et al., 2003). Furthermore, overexpression of the GluR1 C-terminus abolishes LTP in neurons (Bredt and Nicoll, 2003). How is the behavior of GluR subunits differentially regulated? There is compelling

evidence that phosphorylation of AMPA receptors plays an important role during plasticity. Previous studies indicate that especially phosphorylation of the GluR1 subunit of AMPA receptors changes with LTP and LTD induction (Shepherd and Huganir, 2007). LTP is associated with an increase in phosphorylation of GluR1 and LTD is correlated with a dephosphorylation of GluR1 (Lee et al., 2000). CaMKII can directly phosphorylate GluR1 at Ser831 and PKA can phosphorylate GluR1 at Ser845. Preventing phosphorylation by either inhibiting CaMKII or mutating GluR1 Ser831 and Ser845 blocks LTP induction in hippocampal slices. Furthermore, mice with knock-in mutations in these GluR1 phosphorylation sites show deficits in LTD and LTP and have memory defects in spatial learning tasks (Lee et al., 2003), demonstrating that Ser831 and Ser845 phosphorylation of GluR1 are critical for LTD and LTP expression and memory retention.

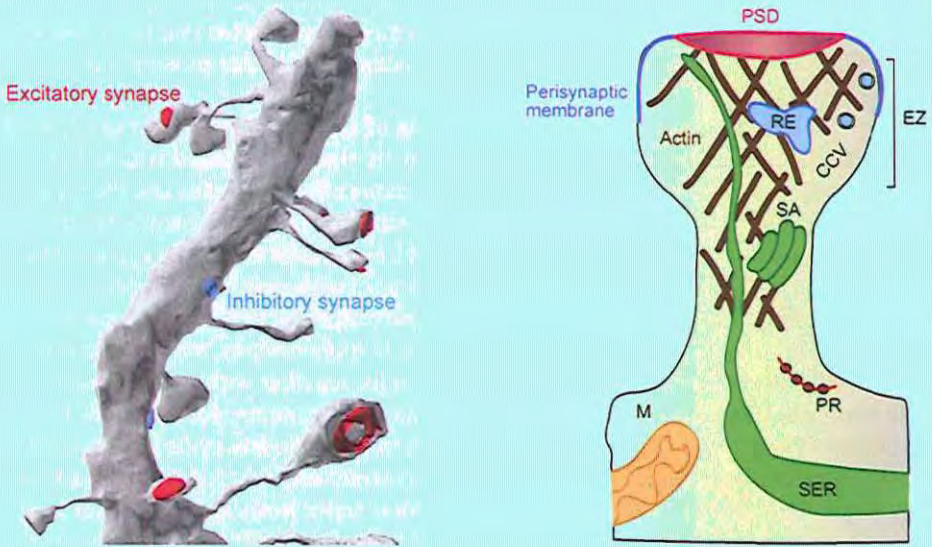


Figure 4: Spine morphology

A 3-Dimensional reconstruction of a piece of dendrite with mushroom shaped and thin spines. Several excitatory synapses (red) can be seen on the spines and inhibitory synapses (blue) on the dendritic shaft.

B Schematic overview of a mushroom-shaped spine containing several organelles. Actin is shown in brown forming the exoskeleton of the spine. The endocytic zone (EZ) is located in the perisynaptic membrane lateral of the PSD. Clathrin coated vesicles (CCV) and recycling endosomes can be found in the spine head. The spine apparatus (SA) can be found in the spine shaft or at the base of the spine. Polyribosomes (PR) found at the base or shaft of the spine allow local protein synthesis. In larger spines smooth endoplasmatic reticulum (SER) can sometimes be found all the way into the spine head. Mitochondria are normally located in the dendritic shaft near the spine but extend into the spine.

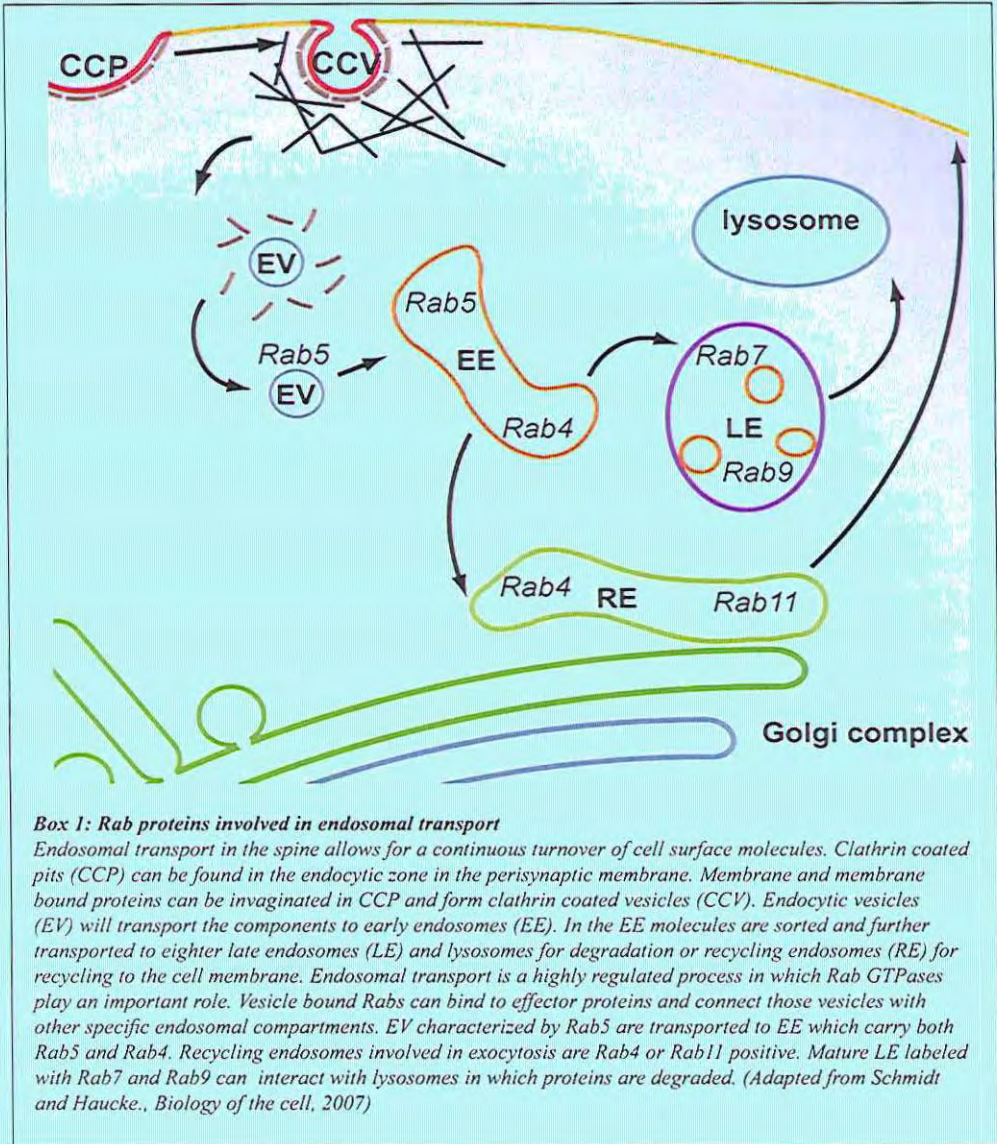
(adapted from Sheng and Hoogenraad, *Annu. Rev. Biochem.* 2007)

1.4 Dendritic Spines

1.4.1 Spine development and morphology

In mammalian brains excitatory synapses are often found on top of tiny structures called “spines”. These spines protrude from dendrites, form microcompartments for individual synapses and vary widely in shape, size and density. Microscopic studies on fixed brain tissue have identified several categories of spines based on their shape (thin, stubby, mushroom or cup shaped) (Hering and Sheng, 2001). Postsynaptic spines are highly diverse among synapses on the same dendrite and across different cell types in the brain; their size can vary with lengths of 0.5-6 μm and volumes of 0.01-0.8 μm^3 . For example, neighboring dendritic spines on a single hippocampal dendritic segment can vary more than 10 fold in their dimensions (Bourne and Harris, 2008). Spines are very dynamic during development of the brain; spine shape and density quickly change during early synaptogenesis (Bourne and Harris, 2007). In neuron cultures some spines are very dynamic and able to change shape and size in matter of seconds or minutes while others are stable for hours or even days (Hering and Sheng, 2001). During rat brain development, dendritic filipodia, which are thought to be the precursors of spines, emerge during the first postnatal week and quickly extend and retract while they search for interactions with axons of neighboring neurons. Once the axonal connection is established filopodia develop into stubby and mushroom-shaped spines. During postnatal week two the amount of stubby and shaft spines decreases and the first thin and mushroom-shaped spines emerge (Bourne and Harris, 2007). In mature brain, mushroom-shaped spines are the most abundant spine form although filopodia can also still be found. Overall, the adult brains show up to 50% fewer spines than developing brains.

Beside the variation in shape and size, spines also vary in their content (Figure 4). All spines have a filamentous actin cytoskeleton and all but very thin and developing spines contain a PSD. The reconstructed surface area of the PSD correlates nearly perfectly with the volume and surface area of the spine head. The PSD area and spine head volume also correlates nearly perfectly with the total number of presynaptic vesicles and the number of vesicles docked at the presynaptic active zone (Bourne and Harris, 2008), suggesting a strong structure-function relationship between dendritic spines and their presynaptic axons. Polyribosomes have been described in both dendrites and dendritic spines which indicates that local protein synthesis could exist close to the synapse (Steward and Levy, 1982). Smooth endoplasmatic reticulum (SER) can be found in dendrites from where it extends into a subset of larger spines, where it transports lipids and membrane-bound proteins (Sheng and Hoogenraad, 2007). A special organelle made of stacks of SER named the spine apparatus is often present in larger spines and thought to be involved in calcium storage (Sheng and Hoogenraad, 2007). Several types of vesicular organelles, like endosomes and clathrin-coated vesicles are also found in spines and are believed to play important roles in the recycling and degradation of receptors and other membrane proteins. Recently it was shown that local endosomal compartments in close proximity to synapses, or even within dendritic spines, mediate the delivery of AMPA receptors into the synaptic membrane (Park et al., 2004; Park et al., 2006). The endosomal Rab GTPase family with well-defined functions in non-neuronal cells has been shown to be of key importance for regulating postsynaptic AMPA receptor endocytosis (Box 1).



Box 1: Rab proteins involved in endosomal transport

Endosomal transport in the spine allows for a continuous turnover of cell surface molecules. Clathrin coated pits (CCP) can be found in the endocytic zone in the perisynaptic membrane. Membrane and membrane bound proteins can be invaginated in CCP and form clathrin coated vesicles (CCV). Endocytic vesicles (EV) will transport the components to early endosomes (EE). In the EE molecules are sorted and further transported to either late endosomes (LE) and lysosomes for degradation or recycling endosomes (RE) for recycling to the cell membrane. Endosomal transport is a highly regulated process in which Rab GTPases play an important role. Vesicle bound Rabs can bind to effector proteins and connect those vesicles with other specific endosomal compartments. EV characterized by Rab5 are transported to EE which carry both Rab5 and Rab4. Recycling endosomes involved in exocytosis are Rab4 or Rab11 positive. Mature LE labeled with Rab7 and Rab9 can interact with lysosomes in which proteins are degraded. (Adapted from Schmidt and Haucke., *Biology of the cell*, 2007)

1.4.2 Spine plasticity

Changes in spine morphology and density can lead to changes in the synaptic strength of neurons. Much evidence suggests that learning can cause alterations in synaptic strength of synapses by changing the structure of the postsynaptic side of the synapse. It has been suggested that memories are retained when spine and synapses alterations are stabilized and persist over time (Bourne and Harris, 2007). In the brain, mushroom-shaped spines are stable over months; therefore bigger spines are thought to be “memory spines”.

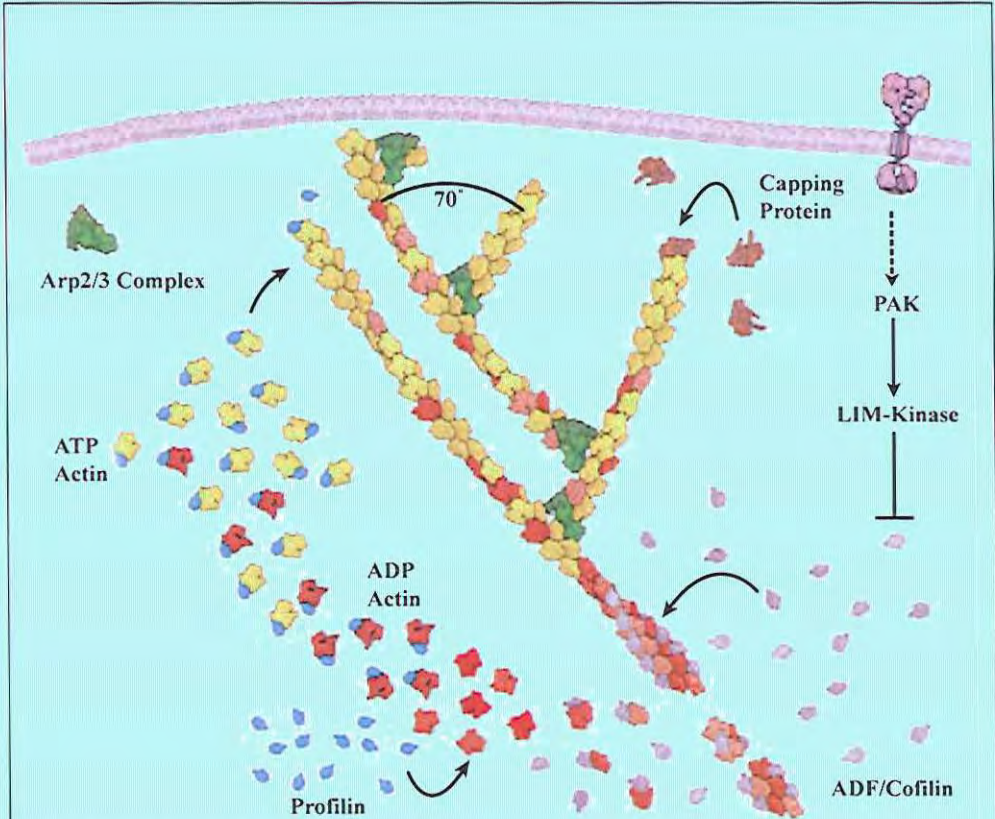
In contrast, thin spines are much more flexible and tend to enlarge or shrink. Thin spines can emerge and collapse or develop into mature spines within a few days and are therefore thought to be “learning spines”. The molecular mechanisms behind this structural plasticity are not yet fully understood, but more and more molecules and signaling pathways involved are identified. One attractive mechanism for refining spine morphology is local addition or removal of membrane by exocytosis and endocytosis. Indeed, the observation that spine volume correlates with the size of the PSD, the number of postsynaptic AMPA receptors and the abundance of spine endomembranes suggests a quantitative coupling between membrane trafficking, synaptic strength, and spine size (Park et al., 2004; Park et al., 2006). Consistent with this notion, LTP- and LTD-inducing stimuli trigger an increase or decrease in spine size, respectively (Matsuzaki et al., 2004).

Alternatively, it seems that most if not all other signaling pathways control spine shape by regulating actin cytoskeleton dynamics. For example both Rac and Rho GTPases are important protein kinases found to regulate actin dynamics (Ethell and Pasquale, 2005).

Actin is present in its monomeric form which provides a pool easily available for polymerization in the spine. Many proteins have been identified in the spine that can bind to or affect actin polymerization (Box 2). LTP-inducing stimuli will activate pathways that promote actin dynamics, stabilization and branching which results in a growing actin network and thus enlargement of the spine (Carlisle and Kennedy, 2005; Ethell and Pasquale, 2005; Tada and Sheng, 2006). A larger spine head can accommodate a larger PSD which can recruit more AMPA receptors to the synaptic membrane, resulting in increased synaptic strength. Alternatively, LTD-inducing stimuli will activate pathways involved in actin depolymerization and lead to spine shrinkage or even spine loss and thus a decreased synaptic strength. Therefore, the tight regulation of receptor trafficking and membrane material together with well coordinated actions of cytoskeleton dynamics provides an attractive mechanism for coupling functional and structural plasticity at glutamatergic synapses.

1.5 Synaptic Pathology in neurological diseases

Abnormal spine morphology or density has been reported in a broad range of neuropsychiatric disorders. Alcohol or drug addiction can lead to spine abnormalities. After chronic alcohol abuse, spine abnormalities can be found in the hippocampus (affecting memory), the cerebellum (affecting motor performance) and in the nucleus accumbens which is the reward centre of the brain (Blanpied and Ehlers, 2004). Consistently, defects in synaptic properties have been reported in animal models of drug addiction (Boudreau and Wolf, 2005). Altered synaptic connections are also found in mental retardation, dementia and neurodevelopmental disorders such as autism and schizophrenia (Lau and Zukin, 2007). For example, two major mental retardation



Box 2: Actin dynamics in spines

The cytoskeleton of a spine is made of filaments of polymerized F-actin and a soluble pool of monomeric G-actin. The actin cytoskeleton is very dynamic, enabling the spine to quickly grow or shrink. Several direct binding partners of actin regulate the growth of the actin polymers. Profilin is a small protein that can bind monomeric actin and transfers the monomers to the vicinity of the growing tip of the actin filament, thus enhancing actin polymerization. Capping proteins can bind to the tip of an actin polymer and inhibit further growth. The actin-related proteins 2/3 (Arp2/3) complex can bind to the side of actin filaments. From Arp2/3 a new actin filament can form which leads to branching of the actin skeleton. Cofilin and actin depolymerizing factor (ADF) can bind to the side of actin filaments and cause structural changes enhancing actin depolymerization. ADF/Cofilin can be inhibited by PAK1 an LIM-Kinase activation after LTP induction. A complex network of signaling pathways influences the actin dynamics in the spine (Ethell and Pasquale, 2005). To illustrate the complexity of this network increased Ca^{2+} concentrations in the spine can lead to opposite effects on actin dynamics. High levels of Ca^{2+} for a longer period lead to spine shrinkage or even spine collapse, while small increases of Ca^{2+} levels leads to spine growth and the formation of new spines. (Adapted from <http://www.boil.vt.edu/research/mcdeb.html>)

syndromes, Down syndrome and Fragile X syndrome, show less mature mushroom-shaped spines and more immature filopodia (Bear et al., 2004; Blanpied and Ehlers, 2004). FMRP, the protein affected in Fragile X patients, can indirectly influence Rac GTPase activity which is involved in regulating actin dynamics in spines (Blanpied and Ehlers, 2004). In Williams syndrome, one of the genes found to be affected is LIM kinase (Meng et al., 2002). Mice lacking LIM kinase have small and thin spines most likely caused by alteration in the actin cytoskeleton. Other proteins, such as PAK3 and oligophrenin1, whose mutated forms cause nonsyndromic mental retardation, are also known to regulate actin dynamics in the spines (Blanpied and Ehlers, 2004).

Recent studies indicate that abnormal synapse formation and maturation is the lead-

ing cause of autism (Zoghbi, 2003). Autism and Asperger syndrome are classified as pervasive developmental disorders, also referred to as autism-spectrum disorders (ASD). Rearrangement of chromosomal regions harboring synaptic adhesion molecules neuroligin-1 and neuroligin-2 and postsynaptic scaffolding protein (PSD-95) genes have been associated with autism (Zoghbi, 2003). Two mutations in the X-chromosomal neuroligin genes, neuroligin-3 and -4, have been directly linked to Asperger syndrome (Jamain et al., 2003). These mutations impair the expression of neuroligins at the plasma membrane, and are likely to have important consequences on synaptic properties given the importance of these adhesion molecules in the clustering of other postsynaptic proteins (Sudhof, 2008). Recent linkage and copy number variation analyses also implicated other genes encoding synaptic proteins associated with autism, such as the neuroligin interacting partners neurexins (Szatmari et al., 2007). In addition, mutations in the adhesion molecule NrCam and the scaffolding protein Shank3 have been linked to autism (Durand et al., 2007). Thus, dysfunction in adhesion and scaffolding PSD proteins might be a common defect in ASD.

Furthermore, recent findings show an interesting link between synaptic proteins and neurodegenerative diseases. For example, the Huntington's disease protein huntingtin binds to proteins such as HIP14 (huntingtin interacting protein 14) which participate in receptor function and trafficking (Huang and El-Husseini, 2005) by regulating the palmitoylation of several scaffolding proteins (Kang et al., 2008). In addition, the role of postsynaptic mechanisms in Alzheimer's disease (AD) is particularly interesting. Recent data indicate that the processing of the amyloid precursor protein during β -amyloid ($A\beta$) production is activity-dependent, and liberated $A\beta$ in turn attenuates synaptic strength (Kamenetz et al., 2003). Conversely, $A\beta$ oligomers block LTP (Walsh et al., 2002). Consistently, the memory loss found in AD patients correlates with the lower density of large spines at pyramidal neurons in the hippocampus. From these studies it is tempting to speculate that at its early stages AD is a disorder of abnormal postsynaptic trafficking and synapse dysfunction.

1.6 Scope of the thesis

Synaptic plasticity is thought to be the cellular basis of learning and memory. The regulation of synaptic plasticity is a complex system in which many basic cell biological pathways are involved. Different postsynaptic signaling routes affect the shape of the spine by regulating actin cytoskeleton dynamics or synaptic strength by controlling receptor trafficking. This thesis aims to address the following questions. What are the molecular mechanisms underlying spine morphology and synaptic receptor trafficking?

In **chapter 1** we give an overview of the current knowledge of excitatory synapses, spine morphology and molecular processes involved in synaptic receptor trafficking. In **chapter 2** we show that microtubule plus ends decorated with EB3 enter dendritic spines and can modulate spine shape. These data provide a new mechanism for dendritic spine morphogenesis and synaptic plasticity through a novel signaling pathway that connects dynamic microtubule and actin cytoskeleton.

In *chapter 3* we show that GRASP-1 connects early and late recycling endosomal compartments by bringing together Rab4/Rab11-positive membrane domains with the fusion machinery, providing a new mechanism to achieve specificity and directionality in neuronal membrane receptor trafficking.

In **chapter 4** we show that deficits in spine morphology are an important aspect of Fragile X syndrome. This syndrome is caused by a mutation in the gene FMR1 which leads to an absence of functional FMRP. We show that lack of FMRP in neurons leads to an altered spine morphology in Purkinje cells in the cerebellum of mice. These cellular changes cause cerebellar dysfunctions which lead to motor learning deficits, that are also found in Fragile X patients.

In **chapter 5** we discuss the results of the studies described in this thesis.

References

- Bear, M. F., Huber, K. M., and Warren, S. T. (2004). The mGluR theory of fragile X mental retardation. *Trends Neurosci* 27, 370-377.
- Bedoukian, M. A., Weeks, A. M., and Partin, K. M. (2006). Different domains of the AMPA receptor direct stargazin-mediated trafficking and stargazin-mediated modulation of kinetics. *J Biol Chem* 281, 23908-23921.
- Bennett, M. V., and Zukin, R. S. (2004). Electrical coupling and neuronal synchronization in the Mammalian brain. *Neuron* 41, 495-511.
- Blanpied, T. A., and Ehlers, M. D. (2004). Microanatomy of dendritic spines: emerging principles of synaptic pathology in psychiatric and neurological disease. *Biol Psychiatry* 55, 1121-1127.
- Boudreau, A. C., and Wolf, M. E. (2005). Behavioral sensitization to cocaine is associated with increased AMPA receptor surface expression in the nucleus accumbens. *J Neurosci* 25, 9144-9151.
- Bourne, J., and Harris, K. M. (2007). Do thin spines learn to be mushroom spines that remember? *Curr Opin Neurobiol* 17, 381-386.
- Bourne, J. N., and Harris, K. M. (2008). Balancing structure and function at hippocampal dendritic spines. *Annu Rev Neurosci* 31, 47-67.
- Bredt, D. S., and Nicoll, R. A. (2003). AMPA receptor trafficking at excitatory synapses. *Neuron* 40, 361-379.
- Brown, D. A. (2006). Acetylcholine. *Br J Pharmacol* 147 Suppl 1, S120-126.
- Bullock, T. H., Bennett, M. V., Johnston, D., Josephson, R., Marder, E., and Fields, R. D. (2005). Neuroscience. The neuron doctrine, redux. *Science* 310, 791-793.
- Carlisle, H. J., and Kennedy, M. B. (2005). Spine architecture and synaptic plasticity. *Trends Neurosci* 28, 182-187.
- Chen, L., Chetkovich, D. M., Petralia, R. S., Sweeney, N. T., Kawasaki, Y., Wenthold, R. J., Bredt, D. S., and Nicoll, R. A. (2000). Stargazin regulates synaptic targeting of AMPA receptors by two distinct mechanisms. *Nature* 408, 936-943.
- Cheng, D., Hoogenraad, C. C., Rush, J., Ramm, E., Schlager, M. A., Duong, D. M., Xu, P., Wijayawardana, S. R., Hanfelt, J., Nakagawa, T., et al. (2006). Relative and absolute quantification of postsynaptic density proteome isolated from rat forebrain and cerebellum. *Mol Cell Proteomics* 5, 1158-1170.
- Choquet, D., and Triller, A. (2003). The role of receptor diffusion in the organization of the postsynaptic membrane. *Nat Rev Neurosci* 4, 251-265.
- Cohen, S., and Greenberg, M. E. (2008). Communication between the synapse and the nucleus in neuronal development, plasticity, and disease. *Annu Rev Cell Dev Biol* 24, 183-209.
- Connors, B. W., and Long, M. A. (2004). Electrical synapses in the mammalian brain. *Annu Rev Neurosci* 27, 393-418.
- Costa, L. G., Giordano, G., Guizzetti, M., and Vitalone, A. (2008). Neurotoxicity of pesticides: a brief review. *Front Biosci* 13, 1240-1249.
- Cull-Candy, S., Kelly, L., and Farrant, M. (2006). Regulation of Ca²⁺-permeable AMPA receptors: synaptic plasticity and beyond. *Curr Opin Neurobiol* 16, 288-297.
- De Carlos, J. A., and Borrell, J. (2007). A historical reflection of the contributions of Cajal and Golgi to the foundations of neuroscience. *Brain Res Rev* 55, 8-16.

- Derkach, V. A., Oh, M. C., Guire, E. S., and Soderling, T. R. (2007). Regulatory mechanisms of AMPA receptors in synaptic plasticity. *Nat Rev Neurosci* 8, 101-113.
- Dev, K. K. (2004). Making protein interactions druggable: targeting PDZ domains. *Nat Rev Drug Discov* 3, 1047-1056.
- Dingledine, R., Borges, K., Bowie, D., and Traynelis, S. F. (1999). The glutamate receptor ion channels. *Pharmacol Rev* 51, 7-61.
- Dong, H., O'Brien, R. J., Fung, E. T., Lanahan, A. A., Worley, P. F., and Huganir, R. L. (1997). GRIP: a synaptic PDZ domain-containing protein that interacts with AMPA receptors. *Nature* 386, 279-284.
- Durand, C. M., Betancur, C., Boeckers, T. M., Bockmann, J., Chaste, P., Fauchereau, F., Nygren, G., Rastam, M., Gillberg, I. C., Anckarsater, H., *et al.* (2007). Mutations in the gene encoding the synaptic scaffolding protein SHANK3 are associated with autism spectrum disorders. *Nat Genet* 39, 25-27.
- Ethell, I. M., and Pasquale, E. B. (2005). Molecular mechanisms of dendritic spine development and remodeling. *Prog Neurobiol* 75, 161-205.
- Fleck, M. W. (2006). Glutamate receptors and endoplasmic reticulum quality control: looking beneath the surface. *Neuroscientist* 12, 232-244.
- Fukata, Y., Tzingounis, A. V., Trinidad, J. C., Fukata, M., Burlingame, A. L., Nicoll, R. A., and Bredt, D. S. (2005). Molecular constituents of neuronal AMPA receptors. *J Cell Biol* 169, 399-404.
- Garcia-Lopez, P., Garcia-Marin, V., and Freire, M. (2007). The discovery of dendritic spines by Cajal in 1888 and its relevance in the present neuroscience. *Prog Neurobiol* 83, 110-130.
- Greger, I. H., and Esteban, J. A. (2007). AMPA receptor biogenesis and trafficking. *Curr Opin Neurobiol* 17, 289-297.
- Hering, H., and Sheng, M. (2001). Dendritic spines: structure, dynamics and regulation. *Nat Rev Neurosci* 2, 880-888.
- Hevers, W., and Luddens, H. (1998). The diversity of GABAA receptors. Pharmacological and electrophysiological properties of GABAA channel subtypes. *Mol Neurobiol* 18, 35-66.
- Hirokawa, N., and Takemura, R. (2005). Molecular motors and mechanisms of directional transport in neurons. *Nat Rev Neurosci* 6, 201-214.
- Hollmann, M., and Heinemann, S. (1994). Cloned glutamate receptors. *Annu Rev Neurosci* 17, 31-108.
- Hoogenraad, C. C., Milstein, A. D., Ethell, I. M., Henkemeyer, M., and Sheng, M. (2005). GRIP1 controls dendrite morphogenesis by regulating EphB receptor trafficking. *Nat Neurosci* 8, 906-915.
- Huang, K., and El-Husseini, A. (2005). Modulation of neuronal protein trafficking and function by palmitoylation. *Curr Opin Neurobiol* 15, 527-535.
- Jamain, S., Quach, H., Betancur, C., Rastam, M., Colineaux, C., Gillberg, I. C., Soderstrom, H., Giros, B., Leboyer, M., Gillberg, C., and Bourgeron, T. (2003). Mutations of the X-linked genes encoding neuroligins NLGN3 and NLGN4 are associated with autism. *Nat Genet* 34, 27-29.
- Jin, Y., and Garner, C. C. (2008). Molecular mechanisms of presynaptic differentiation. *Annu Rev Cell Dev Biol* 24, 237-262.
- Kamenez, F., Tomita, T., Hsieh, H., Seabrook, G., Borchelt, D., Iwatsubo, T., Sisodia, S., and Malinow, R. (2003). APP processing and synaptic function. *Neuron* 37, 925-937.
- Kandel, E. R., Schwartz, J. H., and Jessell, T. M. (2000). *Principles of Neural Science*, 4th ed. edn, McGraw-Hill).

Kang, R., Wan, J., Arstikaitis, P., Takahashi, H., Huang, K., Bailey, A. O., Thompson, J. X., Roth, A. F., Drisdell, R. C., Mastro, R., *et al.* (2008). Neural palmitoyl-proteomics reveals dynamic synaptic palmitoylation. *Nature* 456, 904-909.

Katona, I., and Freund, T. F. (2008). Endocannabinoid signaling as a synaptic circuit breaker in neurological disease. *Nat Med* 14, 923-930.

Kennedy, M. B. (2000). Signal-processing machines at the postsynaptic density. *Science* 290, 750-754.

Kennedy, M. B., Beale, H. C., Carlisle, H. J., and Washburn, L. R. (2005). Integration of biochemical signaling in spines. *Nat Rev Neurosci* 6, 423-434.

Kennedy, M. B., Bennett, M. K., and Erondy, N. E. (1983). Biochemical and immunochemical evidence that the "major postsynaptic density protein" is a subunit of a calmodulin-dependent protein kinase. *Proc Natl Acad Sci U S A* 80, 7357-7361.

Kim, E., and Sheng, M. (2004). PDZ domain proteins of synapses. *Nat Rev Neurosci* 5, 771-781.

Lau, C. G., and Zukin, R. S. (2007). NMDA receptor trafficking in synaptic plasticity and neuropsychiatric disorders. *Nat Rev Neurosci* 8, 413-426.

Lee, H. K., Barbarosie, M., Kameyama, K., Bear, M. F., and Huganir, R. L. (2000). Regulation of distinct AMPA receptor phosphorylation sites during bidirectional synaptic plasticity. *Nature* 405, 955-959.

Lee, H. K., Takamiya, K., Han, J. S., Man, H., Kim, C. H., Rumbaugh, G., Yu, S., Ding, L., He, C., Petralia, R. S., *et al.* (2003). Phosphorylation of the AMPA receptor GluR1 subunit is required for synaptic plasticity and retention of spatial memory. *Cell* 112, 631-643.

Lee, S. H., Simonetta, A., and Sheng, M. (2004). Subunit rules governing the sorting of internalized AMPA receptors in hippocampal neurons. *Neuron* 43, 221-236.

Li, K. W., and Jimenez, C. R. (2008). Synapse proteomics: current status and quantitative applications. *Expert Rev Proteomics* 5, 353-360.

Lisman, J. E., and Goldring, M. A. (1988). Feasibility of long-term storage of graded information by the Ca²⁺/calmodulin-dependent protein kinase molecules of the postsynaptic density. *Proc Natl Acad Sci U S A* 85, 5320-5324.

Lu, W., and Ziff, E. B. (2005). PICK1 interacts with ABP/GRIP to regulate AMPA receptor trafficking. *Neuron* 47, 407-421.

Luscher, C., and Ungless, M. A. (2006). The mechanistic classification of addictive drugs. *PLoS Med* 3, e437.

Malenka, R. C., and Nicoll, R. A. (1999). Long-term potentiation--a decade of progress? *Science* 285, 1870-1874.

Malinow, R., Mainen, Z. F., and Hayashi, Y. (2000). LTP mechanisms: from silence to four-lane traffic. *Curr Opin Neurobiol* 10, 352-357.

Matsuzaki, M., Honkura, N., Ellis-Davies, G. C., and Kasai, H. (2004). Structural basis of long-term potentiation in single dendritic spines. *Nature* 429, 761-766.

Meng, Y., Zhang, Y., and Jia, Z. (2003). Synaptic transmission and plasticity in the absence of AMPA glutamate receptor GluR2 and GluR3. *Neuron* 39, 163-176.

Meng, Y., Zhang, Y., Tregoubov, V., Janus, C., Cruz, L., Jackson, M., Lu, W. Y., MacDonald, J. F., Wang, J. Y., Falls, D. L., and Jia, Z. (2002). Abnormal spine morphology and enhanced LTP in LIMK-1 knockout mice. *Neuron* 35, 121-133.

- Nelson, S. B., and Turrigiano, G. G. (2008). Strength through diversity. *Neuron* 60, 477-482.
- Newpher, T. M., and Ehlers, M. D. (2008). Glutamate receptor dynamics in dendritic microdomains. *Neuron* 58, 472-497.
- Nicoll, R. A., Tomita, S., and Brecht, D. S. (2006). Auxiliary subunits assist AMPA-type glutamate receptors. *Science* 311, 1253-1256.
- Okabe, S. (2007). Molecular anatomy of the postsynaptic density. *Mol Cell Neurosci* 34, 503-518.
- Park, M., Penick, E. C., Edwards, J. G., Kauer, J. A., and Ehlers, M. D. (2004). Recycling endosomes supply AMPA receptors for LTP. *Science* 305, 1972-1975.
- Park, M., Salgado, J. M., Ostroff, L., Helton, T. D., Robinson, C. G., Harris, K. M., and Ehlers, M. D. (2006). Plasticity-induced growth of dendritic spines by exocytic trafficking from recycling endosomes. *Neuron* 52, 817-830.
- Passafaro, M., Piech, V., and Sheng, M. (2001). Subunit-specific temporal and spatial patterns of AMPA receptor exocytosis in hippocampal neurons. *Nat Neurosci* 4, 917-926.
- Peng, J., Kim, M. J., Cheng, D., Duong, D. M., Gygi, S. P., and Sheng, M. (2004). Semiquantitative proteomic analysis of rat forebrain postsynaptic density fractions by mass spectrometry. *J Biol Chem* 279, 21003-21011.
- Purves, D. (2001). *Neuroscience*, 2nd edn, Sinauer Associates).
- Richard, L. (2005). *Nerve Endings: The Discovery of the Synapse*, W.W. Norton).
- Rosenmund, C., Rettig, J., and Brose, N. (2003). Molecular mechanisms of active zone function. *Curr Opin Neurobiol* 13, 509-519.
- Selkoe, D. J. (2002). Alzheimer's disease is a synaptic failure. *Science* 298, 789-791.
- Setou, M., Seog, D. H., Tanaka, Y., Kanai, Y., Takei, Y., Kawagishi, M., and Hirokawa, N. (2002). Glutamate-receptor-interacting protein GRIP1 directly steers kinesin to dendrites. *Nature* 417, 83-87.
- Sheng, M., and Hoogenraad, C. C. (2007). The postsynaptic architecture of excitatory synapses: a more quantitative view. *Annu Rev Biochem* 76, 823-847.
- Sheng, M., and Kim, E. (1996). Ion channel associated proteins. *Curr Opin Neurobiol* 6, 602-608.
- Sheng, M., and Lee, S. H. (2001). AMPA receptor trafficking and the control of synaptic transmission. *Cell* 105, 825-828.
- Shepherd, G. M., and Erulkar, S. D. (1997). Centenary of the synapse: from Sherrington to the molecular biology of the synapse and beyond. *Trends Neurosci* 20, 385-392.
- Shepherd, J. D., and Huganir, R. L. (2007). The cell biology of synaptic plasticity: AMPA receptor trafficking. *Annu Rev Cell Dev Biol* 23, 613-643.
- Shi, S., Hayashi, Y., Esteban, J. A., and Malinow, R. (2001). Subunit-specific rules governing AMPA receptor trafficking to synapses in hippocampal pyramidal neurons. *Cell* 105, 331-343.
- Stephan, K. E., Baldeweg, T., and Friston, K. J. (2006). Synaptic plasticity and dysconnection in schizophrenia. *Biol Psychiatry* 59, 929-939.
- Steward, O., and Levy, W. B. (1982). Preferential localization of polyribosomes under the base of dendritic spines in granule cells of the dentate gyrus. *J Neurosci* 2, 284-291.
- Sudhof, T. C. (2004). The synaptic vesicle cycle. *Annu Rev Neurosci* 27, 509-547.

- Sudhof, T. C. (2008). Neuroligins and neuexins link synaptic function to cognitive disease. *Nature* 455, 903-911.
- Szatmari, P., Paterson, A. D., Zwaigenbaum, L., Roberts, W., Brian, J., Liu, X. Q., Vincent, J. B., Skaug, J. L., Thompson, A. P., Senman, L., et al. (2007). Mapping autism risk loci using genetic linkage and chromosomal rearrangements. *Nat Genet* 39, 319-328.
- Tada, T., and Sheng, M. (2006). Molecular mechanisms of dendritic spine morphogenesis. *Curr Opin Neurobiol* 16, 95-101.
- Vale, R. D. (2003). The molecular motor toolbox for intracellular transport. *Cell* 112, 467-480.
- Waites, C. L., Craig, A. M., and Garner, C. C. (2005). Mechanisms of vertebrate synaptogenesis. *Annu Rev Neurosci* 28, 251-274.
- Walsh, D. M., Klyubin, I., Fadeeva, J. V., Cullen, W. K., Anwyl, R., Wolfe, M. S., Rowan, M. J., and Selkoe, D. J. (2002). Naturally secreted oligomers of amyloid beta protein potently inhibit hippocampal long-term potentiation in vivo. *Nature* 416, 535-539.
- Walsh, M. J., and Kuruc, N. (1992). The postsynaptic density: constituent and associated proteins characterized by electrophoresis, immunoblotting, and peptide sequencing. *J Neurochem* 59, 667-678.
- Wang, Z., Edwards, J. G., Riley, N., Provance, D. W., Jr., Karcher, R., Li, X. D., Davison, I. G., Ikebe, M., Mercer, J. A., Kauer, J. A., and Ehlers, M. D. (2008). Myosin Vb mobilizes recycling endosomes and AMPA receptors for postsynaptic plasticity. *Cell* 135, 535-548.
- Wenthold, R. J., Petralia, R. S., Blahos, J., II, and Niedzielski, A. S. (1996). Evidence for multiple AMPA receptor complexes in hippocampal CA1/CA2 neurons. *J Neurosci* 16, 1982-1989.
- Whiting, P. J. (2003). The GABAA receptor gene family: new opportunities for drug development. *Curr Opin Drug Discov Devel* 6, 648-657.
- Wilson, M. A., and Tonegawa, S. (1997). Synaptic plasticity, place cells and spatial memory: study with second generation knockouts. *Trends Neurosci* 20, 102-106.
- Ziff, E. B. (1997). Enlightening the postsynaptic density. *Neuron* 19, 1163-1174.
- Zoghbi, H. Y. (2003). Postnatal neurodevelopmental disorders: meeting at the synapse? *Science* 302, 826-830.

Dynamic microtubules regulate dendritic spine morphology and synaptic plasticity

Jacek Jaworski,^{1,4,7} Lukas C. Kapitein,^{1,7} Susana Montenegro Gouveia,^{2,7} Bjorn R. Dortland,^{1,7} Phebe S. Wulf,¹ Ilya Grigoriev,² Paola Camera,⁶ Samantha A. Spangler,¹ Paola Di Stefano,⁶ Jeroen Demmers,³ Harm Krugers,⁵ Paola Defilippi,⁶ Anna Akhmanova,² and Casper C. Hoogenraad,¹

¹Department of Neuroscience, ²Department of Cell Biology and Genetics, ³Proteomics Center Erasmus Medical Center, 3015 GE, Rotterdam, The Netherlands, ⁴International Institute of Molecular and Cell Biology, Warsaw, Poland, ⁵Swammerdam Institute for Life Sciences, University of Amsterdam, The Netherlands, ⁶Molecular Biotechnology Center, University of Torino, Italy, ⁷These authors contributed equally to this work.

Neuron 61, 85–100, January 15, 2009

Chapter 2

Dynamic Microtubules Regulate Dendritic Spine Morphology and Synaptic Plasticity

Jacek Jaworski,^{1,4,7} Lukas C. Kapitein,^{1,7} Susana Montenegro Gouveia,^{2,7} Bjorn R. Dortland,^{1,7} Phebe S. Wulf,¹ Ilya Grigoriev,² Paola Camera,⁶ Samantha A. Spangler,¹ Paola Di Stefano,⁶ Jeroen Demmers,³ Harm Krugers,⁵ Paola DeFilippi,⁶ Anna Akhmanova,² and Casper C. Hoogenraad^{1,*}

¹Department of Neuroscience

²Department of Cell Biology and Genetics

³Proteomics Center

Erasmus Medical Center, 3015 GE, Rotterdam, The Netherlands

⁴International Institute of Molecular and Cell Biology, Warsaw, Poland

⁵Swammerdam Institute for Life Sciences, University of Amsterdam, The Netherlands

⁶Molecular Biotechnology Center, University of Torino, Italy

⁷These authors contributed equally to this work

*Correspondence: c.hoogenraad@erasmusmc.nl

DOI 10.1016/j.neuron.2008.11.013

SUMMARY

Dendritic spines are the major sites of excitatory synaptic input, and their morphological changes have been linked to learning and memory processes. Here, we report that growing microtubule plus ends decorated by the microtubule tip-tracking protein EB3 enter spines and can modulate spine morphology. We describe p140Cap/SNIP, a regulator of Src tyrosine kinase, as an EB3 interacting partner that is predominately localized to spines and enriched in the postsynaptic density. Inhibition of microtubule dynamics, or knockdown of either EB3 or p140Cap, modulates spine shape via regulation of the actin cytoskeleton. Fluorescence recovery after photobleaching revealed that EB3-binding is required for p140Cap accumulation within spines. In addition, we found that p140Cap interacts with Src substrate and F-actin-binding protein cortactin. We propose that EB3-labeled growing microtubule ends regulate the localization of p140Cap, control cortactin function, and modulate actin dynamics within dendritic spines, thus linking dynamic microtubules to spine changes and synaptic plasticity.

INTRODUCTION

Dendritic spines are membrane protrusions that are the major sites of glutamatergic presynaptic input in the mammalian central nervous system. Although small in size (up to a few microns in length), spines are motile and remarkably diverse in size and shape, ranging from long, thin filopodia-like protrusions to mushroom-shaped spines (Harris and Kater, 1994; Hering and Sheng, 2001). Nearly all dendritic spines contain a postsynaptic density (PSD), a complex matrix of postsynaptic receptors, signaling molecules and cytoskeletal proteins involved in postsynaptic signaling and plasticity (Kennedy et al., 2005; Sheng

and Hoogenraad, 2007). The strong correlation between the size of the spine and the strength of the synapse makes spine remodeling an attractive structural mechanism underlying learning and memory (Kasai et al., 2003; Lamprecht and LeDoux, 2004; Yuste and Bonhoeffer, 2001). In addition, several human mental retardation syndromes have been linked to altered spine morphology (Hering and Sheng, 2001; Kaufmann and Moser, 2000; Newey et al., 2005).

Biochemical events that regulate dendritic spine remodeling are poorly understood. It is generally believed that changes in spine morphology are based on rearrangements of the actin cytoskeleton (Ethell and Pasquale, 2005; Matus, 2000; Tada and Sheng, 2006). Within spines, actin is present as a soluble pool of monomeric G-actin and as polymerized F-actin filaments that confer the characteristic spine shape. Multiple signaling pathways, particularly those involving small GTPases of the Rho and Ras family, control actin organization (Ethell and Pasquale, 2005; Newey et al., 2005; Tada and Sheng, 2006). Recently, members of the Src family of non-receptor tyrosine kinases were also found in dendritic spines and implicated in spine reorganization, most likely through controlling actin polymerization (Morita et al., 2006; Webb et al., 2007). However, it remains unclear how different signal transduction pathways converging on the actin-based processes within spines are coordinated.

There is strong evidence that in nonneuronal cells the microtubule (MT) cytoskeleton serves as a primary spatial regulator of cell shape. MTs are highly dynamic and can interact with actin in areas of cellular growth or reorganization during cell division, polarization, and migration (Rodríguez et al., 2003; Siegrist and Doe, 2007). In developing neurons, the actin and MT cytoskeleton also act together to guide and support the growth and differentiation of axons and dendrites (Dent and Gertler, 2003). In contrast to these well-studied examples of MT-actin cooperativity, it is widely accepted that in dendrites of mature neurons the two cytoskeletal domains are spatially separated; while actin filaments are predominately concentrated in spines, stable MTs are confined to the dendritic shaft and do not branch off into spines (Matus, 2000). This view is based on ultrastructural and

fluorescent imaging studies showing that MTs and MT-associated protein 2 (MAP2) are absent from dendritic spines (Kaech et al., 2001; Landis and Reese, 1983). While this revealed that stable MTs, decorated with MAP2, are predominantly present as bundles in dendritic shafts, it is currently unknown whether dynamic MTs are involved in the regulation of dendritic spine morphology and synaptic plasticity.

Dynamic MTs can be distinguished from stable ones by a number of markers; in particular, growing MTs specifically accumulate a set of factors known as MT plus-end tracking proteins, or +TIPs at their ends (Akhmanova and Hoogenraad, 2005). +TIPs are thought to be important for cross-talk between dynamic MTs and actin (Basu and Chang, 2007; Rodríguez et al., 2003); moreover, they can be used as tools to visualize growing MT ends even within dense MT networks (Morrison et al., 2002; Stepanova et al., 2003). Among +TIPs, proteins of the EB family directly interact with the majority of other known plus-end binding proteins and have been implicated as key regulators of MT-associated signaling pathways (Jaworski et al., 2008; Lansbergen and Akhmanova, 2006).

Here, we use a large variety of biochemical, cell-biological, and quantitative/high-resolution microscopic approaches to determine the potential role of +TIPs in spine morphogenesis. We show that dynamic EB3 positive MT plus ends can enter dendritic spines, are required for controlling the levels of F-actin within the spines, and are essential for the maintenance of spine morphology and mature synapses. Furthermore, we found that p140Cap, a regulator of Src tyrosine kinase, associates with EB3 and F-actin binding protein cortactin. We propose a model in which EB3 regulates spine size by modulating the turnover of p140Cap in spines, thereby altering actin dynamics through the regulation of cortactin.

RESULTS

EB3 Expression Increases during Neuronal Maturation

Several +TIPs have been shown to localize to MT plus ends in developing neuronal cells (reviewed in Jaworski et al., 2008). However, very little is known about localization and function of +TIPs in mature neurons. To identify +TIPs abundant in hippocampal neurons at the time of spine maturation we probed western blots of homogenates of cultured hippocampal neurons for different +TIPs (Figure 1A and data not shown). Most +TIPs analyzed were already expressed at *in vitro* day 3 (DIV 3) and slightly increased during neuronal development. However, EB3 was undetectable in young neurons (<DIV 7) and began to elevate throughout development with the strongest expression in more mature neurons (>DIV 17) (Figure 1A). This is consistent with high levels of EB3 expression *in vivo* in the adult hippocampus and cerebral cortex compared to embryonic and post-natal stages (Figure 1B).

Next, we stained different stages of developing and mature hippocampal neurons (from DIV 3 to DIV 21) with antibodies against the three mammalian EB family members, EB1, EB2, and EB3. While anti-EB2 antibodies produced no clear pattern (data not shown), EB1, and EB3-specific staining appeared as dashes or comets, which have been shown to correspond to growing MT tips in numerous studies (Komarova et al., 2005;

Stepanova et al., 2003). Interestingly, EB1 and EB3 displayed different developmental patterns: EB1-positive dashes were clearly visible in young hippocampal neurons at < DIV 7 but not in mature cells, whereas EB3 immunoreactivity was hard to detect in developing neurons but was highly prominent in mature neurons at > DIV17 (Figures 1C, 1D, 1F, S1A, S1B, and S1D). High levels of EB3 expression correlate with fully developed neurons with mushroom-headed spines positive for the postsynaptic marker PSD-95 (Figures S1C and S1E). The lack of changes in EB1 expression by immunoblot (Figure 1A) can be attributed to the abundance of EB1 in glial cells in both developing and mature neuronal cultures (Figure 1F).

The robust switch in EB family proteins during neuronal development is most likely regulated at the level of gene expression. To test whether reduced EB3 expression is able to induce EB1 levels in older neurons, we used DNA plasmid (pSuper)-based RNA interference to knock down endogenous EB3 (Komarova et al., 2005). Dissociated hippocampal neurons in culture at DIV13 were transfected with EB3-shRNA together with β -galactosidase (β -gal), to highlight shRNA expressing cells. Four days after transfection, the EB3-specific antibody showed ~90% reduction in staining intensity in neurons transfected with the EB3-shRNA construct (Figures 1E and 1G). EB1 staining was unchanged in neurons transfected with EB3-shRNA (Figures 1E and 1G), indicating that EB1 expression is not increased by reduction of EB3 levels. We conclude that EB3 protein levels are steadily increased during neuronal development and its expression and abundance at MT tips peaks in mature neurons.

MT Plus Ends Labeled with Endogenous EB3 or EB3-GFP Enter Dendritic Spines

Next, we examined in detail the subcellular distribution of EB3 in mature dendrites. Cultured hippocampal neurons (> DIV 17) stained with EB3-specific antibodies showed characteristic comet-like MT plus-end patterns (Figure 2A). Similar to non-neuronal cells (Figure S2A) (Mimori-Kiyosue et al., 2000), blocking MT dynamics by the addition of 200 nM nocodazole completely abolished EB3-positive comets (Figures 2B and S2E; Stepanova et al., 2003). This effect was specific, since the MT network was still present, as indicated by MAP2 and tubulin costaining (Figures S2B and S2C); EB3 and tubulin expression was unchanged (Figure S2F) and polymerized MT levels measured by tubulin pre-extraction (He et al., 2002) were not significantly affected (Figures S2C and S2D). As expected (Mimori-Kiyosue et al., 2000; Stepanova et al., 2003), treatment with a low dose of taxol (200 nM) showed similar effects (Figures S2B–S2E). Taken together, these results suggest that in mature neurons endogenous EB3 specifically associates with the ends of growing MTs.

Although present in axons, EB3 staining was predominantly localized within the dendritic compartment, as revealed by the dendritic marker MAP2 (Figure 2A). However, to our surprise, EB3-labeled comets occasionally extended beyond the dendritic shaft (arrowheads in Figure 2A), overlapped with the synaptic marker Bassoon (arrowheads in Figure 2B) and localized within the dendritic spines visualized in β -gal filled neurons (Figure 2C). At DIV 17, we observed that a small fraction (on average 4%) of dendritic spines contained endogenous EB3

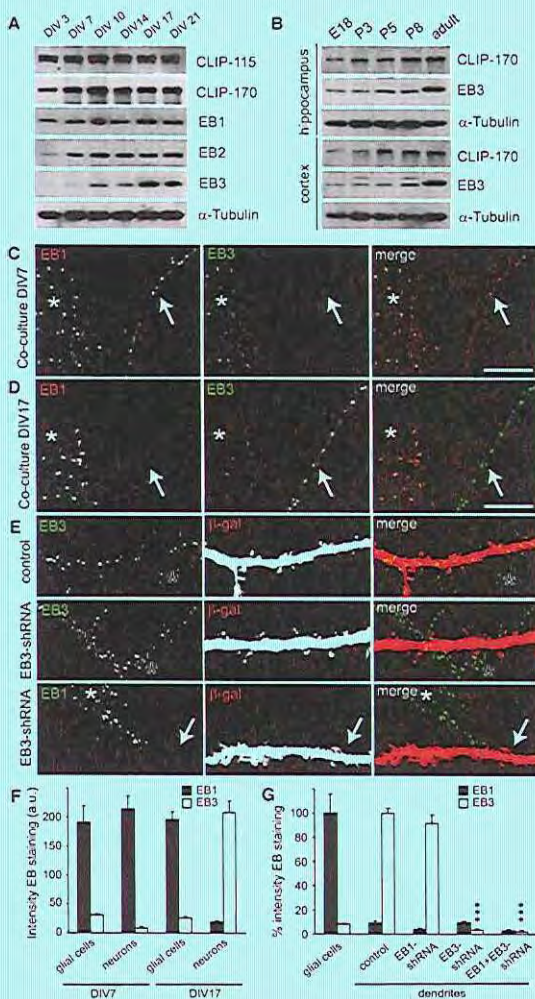


Figure 1. EB3 Expression Increases during Neuronal Development

(A) +TIP developmental expression patterns in cultured hippocampal neurons from DIV 3 to DIV 21 (20 μ g of protein/lane).

(B) Patterns of developmental expression of CLIP-170 and EB3 in E18, P3, P5, P8, and 6-month-old (adult) rat hippocampus and cortex (20 μ g of protein/lane).

(C and D) Representative images of rat hippocampal neurons at 7 DIV and 17 DIV double labeled with mouse anti-EB1 antibody (red) and rabbit anti-EB3 antibody (green). Only the merge is shown in color. Glial cells are indicated by a filled asterisk, and arrows point to neurons.

(E) Representative images of hippocampal neurons transfected at DIV 13 with control pSuper vector or EB3-shRNA and double labeled with anti-EB1 or anti-EB3 antibody (green) and for cotransfected β -gal (red). Nontransfected neurons are indicated by an open asterisk.

(F) Quantification of EB1 and EB3 immunostaining intensities (as arbitrary units) in dendrites of hippocampal neurons and glial cells in the same culture at DIV 7 and DIV 17.

(G) Quantification of EB1 and EB3 immunostaining intensities (mean \pm SEM) in dendrites of hippocampal neurons transfected at DIV 13 for 4 days with control pSuper vector, EB1-shRNA, EB3-shRNA, or a combination of EB1-shRNA and EB3-shRNA. EB3 intensity in neurons is normalized to dendritic EB3 staining in pSuper control neurons. EB1 intensity in neurons is normalized to EB1 staining in glial cells. *** $p < 0.0005$.

observed bidirectional displacements of EB3-GFP comets in hippocampal dendrites, whereas in axons the movements were unidirectional, reflecting different MT organization in axons and dendrites (Jaworski et al., 2008; Stepanova et al., 2003). The average velocity of EB3-GFP movement in mature hippocampal neurons was $0.12 \pm 0.03 \mu\text{m/s}$ (mean \pm SD; $n > 500$) and 1.8-fold lower than previously reported for young neurons (Stepanova et al., 2003). Although most EB3-GFP-positive comets moved along the dendritic shaft, a number of EB3-GFP dashes entered the spines and disappeared close to the head of the spine, most likely because of MT catastrophe (Figure 2E; Movie S1). EB3-GFP comets could target numerous spines on a single dendrite (Movie S2) or repeatedly enter the same spine (Figure 2F; Movie S3).

Overexpression of EB3 resulted in even distribution along the MT lattice (Komarova et al., 2005) and showed a significant increase of EB3-positive MTs pointing into the dendritic spines and colocalizing at their tips with synaptic markers (Figures 2D and 7F).

Quantification revealed that EB3-positive MTs could be detected in $\sim 30\%$ of dendritic spines in EB3-GFP overexpressing neurons. Together these data indicate the presence of EB3-labeled MT tips in dendritic protrusions of mature neurons.

Dynamic MTs Affect Synaptic Plasticity and Spine Morphology in Hippocampal Slices

What is the function of dynamic MTs in mature neurons? To address this question, we utilized low concentrations of nocodazole to inhibit MT dynamics (Figure S2) (Mimori-Kiyosue et al.,

staining. Among these, mushroom-shaped spines were slightly more frequent than thin filopodia; the few EB3-positive filopodia-like protrusions were typically long ($>5 \mu\text{m}$) and could represent newly forming dendritic arbors (data not shown). These data indicate that MT tips decorated with endogenous EB3 can enter dendritic spines.

To confirm this remarkable finding, we used the Semliki Forest virus (SFV) to deliver EB3-GFP to mature (DIV 21) hippocampal neurons in culture and analyzed its dynamics by live cell imaging. In cases when the expression level of EB3-GFP was low, we

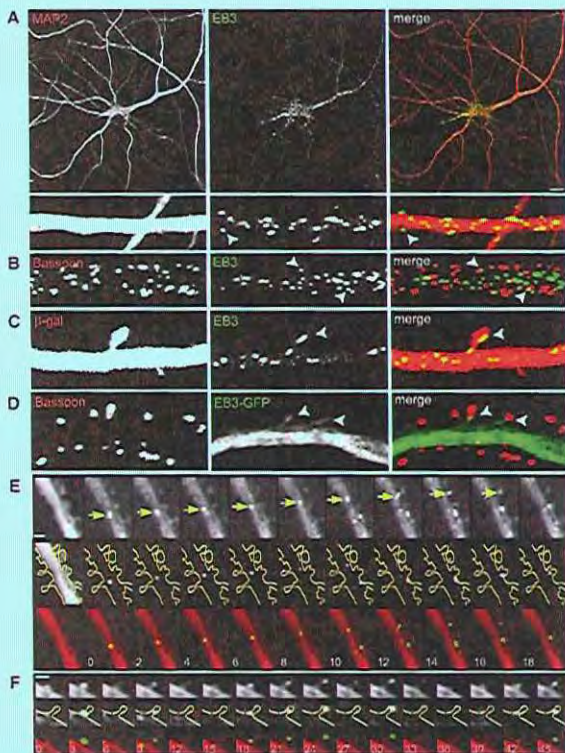


Figure 2. MT Plus-End-Bound EB3 Enters Dendritic Spines

(A) Representative images of rat hippocampal neurons (DIV 17) double labeled with rabbit anti-EB3 antibody (green) and mouse anti-MAP2 antibody (red). Only the merge is shown in color. Dendritic segments (lower panels) are enlarged to show the localization of EB3 and MAP2. Arrowheads indicate EB3 comets outside the dendritic shaft. Scale bar, 10 μ m. (B) Dendrites of hippocampal neurons labeled with rabbit anti-EB3 antibody (green) and mouse anti-Bassoon (red). Arrowheads indicate colocalization between EB3 and Bassoon. (C) Hippocampal neurons transfected at DIV 13 with β -gal construct to visualize neuronal morphology and labeled with rabbit anti-EB3 antibody (green) and mouse anti- β -gal (red). Arrowheads indicate endogenous EB3 in dendritic spines. (D) Hippocampal neurons transfected at DIV 13 with EB3-GFP and labeled with mouse anti-Bassoon (red). Arrowheads indicate colocalized EB3-GFP with Bassoon. (E and F) Time-lapse recordings of EB3-GFP-infected neurons showing one (E) and multiple (F) EB3-GFP comets penetrating into spines. First image in all three rows shows neuron morphology obtained by averaging all frames from the time-lapse recording. Subsequent images show low-pass-filtered time series in row 1, low-pass-filtered time series with average of all frames subtracted and dendrite outline traced in yellow in row 2, and a merge of row 2 and the average of all frames in row 3. Scale bar is 1 μ m, time in seconds.

2000; Vasquez et al., 1997) and abolish the binding of EB3 to MT ends in brain slices. We used organotypic slices of the hippocampus biologically transfected with GFP to visualize neuronal morphology. CA1 neurons of hippocampal slice cultures treated for 4 hr with 200 nM nocodazole lost most of their mushroom-headed spines and instead displayed filopodia-like processes with reduced heads both on the apical and basal dendrites (Figure 3A). Next, dendritic protrusions were classified as filopodia-shaped protrusions and mushroom-shaped spines based on the ratio of spine head width to protrusion length (see Experimental Procedures). Nocodazole treatment decreased the number of mushroom-headed spines and increased the number of filopodia (Figure 3B), while the total number of dendritic protrusions was unaffected (Figure 3B). Nocodazole did not alter cell soma circumference, dendrite length, or dendrite width (Figure 3C and data not shown).

Since several studies have demonstrated a strong correlation between defects in synaptic plasticity and abnormalities in dendritic spine morphology (Yuste and Bonhoeffer, 2001), we next tested the effect of low doses of nocodazole on long-term potentiation in the Schaffer collateral-CA1 pathway in acute

mouse hippocampal slices. High-frequency stimulation in the hippocampal CA1 area in control slices caused a transient and highly robust posttetanic rise in the slope of the field excitatory postsynaptic potentials (fEPSP) followed by a sustained increase in the synaptic response (Figure 3D). This stable synaptic potentiation was significantly suppressed in slices treated with 200 nM nocodazole (Figure 3D). Synaptic responses were depressed to almost baseline levels after 2 hr exposure to

the drug (Figure 3D), suggesting a link between dynamic MTs and synaptic plasticity. Control experiments show no decline in fEPSP size 2 hr after nocodazole treatment. Although we cannot exclude that nocodazole treatment has an indirect effect on the synaptic response, it seems likely that the defects in synaptic plasticity in the absence of dynamic MTs are secondary to the disruption of spine/synaptic architecture.

EB3 Depletion Causes Spine Loss

To investigate the relationship between dynamic MTs and spines in more detail, we again switched to dissociated neuronal cultures. At DIV 17, control neurons exhibited mostly mushroom-shaped spines (Figure 4A). Treatment with low doses of nocodazole (200 nM, 4 hr) did not affect the total number of dendritic protrusions, but markedly reduced the number of spines and increased the number of filopodia, similar to the effects observed in slices. Loss of spines was already visible after 2 hr of nocodazole treatment but was not detectable within 30 min of incubation (data not shown), indicating that dynamic MTs influence the maintenance of mature spine morphology with relatively slow kinetics (>30 min). Consistently, nocodazole

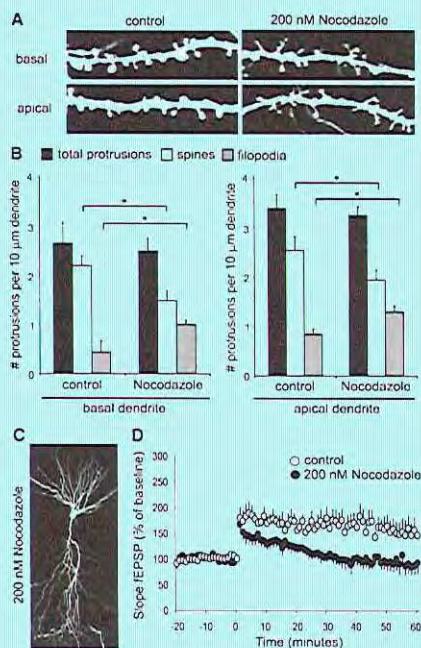


Figure 3. Dynamic MTs Are Required for Synaptic Transmission and Spine Maintenance in Hippocampal Slices

(A) Representative images of basal and apical dendrites from CA1 pyramidal neurons in hippocampal slice cultures from P7 rats transfected with GFP and incubated for 4 hr with 200 nM nocodazole.

(B) Quantification of number of protrusions per 10 μm basal and apical dendrites in pyramidal neurons treated as in (A). Histogram shows mean \pm SEM, $^*p < 0.05$.

(C) Representative image of CA1 pyramidal neuron in hippocampal slice cultures from P7 rats transfected with GFP and incubated for 4 hr with 200 nM nocodazole. Scale bar, 10 μm .

(D) Hippocampal long-term potentiation induced by high-frequency stimulation. Mouse hippocampal slices were treated with vehicle (control) or 200 nM nocodazole for 1 hr before and during recording. Subsequently, fEPSPs were recorded at 0.0166 Hz from CA1 dendritic fields upon Schaffer Collateral stimulation. After 20 min of baseline recordings, slices were stimulated using high-frequency stimulation (1 s at 100 Hz) followed by 60 min of fEPSP recording at 0.0166 Hz.

washout for 3 hr restored normal spine morphology (Figures S3A–S3C), indicating that the effect on spines is reversible and most likely due to reduced MT dynamics.

The effect of nocodazole on spine shape might be explained by the loss EB3 from MT tips. To test this idea, we used RNA interference (RNAi) to suppress endogenous EB3. Hippocampal neurons transfected at DIV 14 for 4 days with EB3-shRNA (Figure 1) did not significantly affect the number of protrusions but resulted in a spine phenotype similar to that induced by

nocodazole treatment; namely, a loss of mushroom-headed spines and an increase of thin, long filopodia-like spines (Figures 4A–4C). In contrast, overexpression of EB3-GFP induced a robust increase in the number of mushroom spines (Figures 4A–4C), suggesting that increased MT targeting might change spine morphology. No effect on spines could be seen with expression of other MT binding proteins, such as CLIP-115 and MAP2c or treatments with 2 μM of the MT stabilizing drug Taxol (Figures S3D–S3F). Moreover nocodazole treatment prevented the EB3-GFP effect on spines (Figures S3G–S3I), implying that the interaction of EB3 with MTs is necessary for spine growth.

EB3-GFP Entry in Spines Accompanies Spine Enlargement

To explore the relationship between EB3-GFP entry and spine growth, the spine area of preexisting spines was monitored for extended periods (>10 min) before and after EB3-GFP comet entry. On average 10% \pm 7% (mean \pm SD, $n = 227$ spines in 12 neurons) of the spines were targeted by EB3-GFP within a 10 min time frame. We rarely observed a decrease in spine size correlated with EB3-GFP entry, whereas often spine growth was observed after EB3-GFP entry (Figures 5A–5C; Movie S4). Detailed analysis of several events ($n = 20$ spines) revealed that 60% of the spines have a >20% increase in spine growth upon EB3 entry under basal culture conditions (Figure 5F). In contrast, control spines that existed throughout the imaging without EB3 entry events show only a slight variation in spine size; only 15% of the control spines showed >20% increase in spine area. Typically, the increase in spine size is correlated with just one or two entries of EB3-GFP (67% of spines) (Figure 5E), or occasionally repeated movements of EB3-GFP in the same spine (Figure 5D). We did not find a correlation between the number of comet entries (within 3 min) and subsequent changes in spine size (data not shown). Consistent with the changes in spine shape found in fixed cells (Figures 4A–4C), these results demonstrate that the entry of EB3-GFP decorated MT tips into dendritic spines is associated with spine growth, further indicating a role for MT targeting in spine morphological plasticity.

EB3 Regulates Actin Dynamics within Spines

Since +TIPs have been implicated in the regulation of actin remodeling in various systems, we next tested if altered spine shape was correlated with actin reorganization. Consistent with previous studies, in control DIV 17 neurons, F-actin appeared as patches and puncta along the dendrites and was enriched in the heads of dendritic spines (Figure 4A). Nocodazole treatment or expression of EB3-shRNA resulted in a pronounced loss of F-actin from dendritic protrusions (Figures 4A and 4D). Conversely, expression of EB3-GFP increased F-actin abundance (Figures 4A and 4D).

To extend this observation, we treated control and EB3 knock-down neurons with two actin-directed drugs, latrunculin B and jaspilakinolide, that are known to shift the equilibrium toward G-actin and F-actin, respectively (Okamoto et al., 2004). Treatment of EB3-shRNA-transfected neurons with latrunculin B (10 μM , 2 hr) showed a further increase in filopodia and decrease in spines compared to nontreated EB3-deficient or control

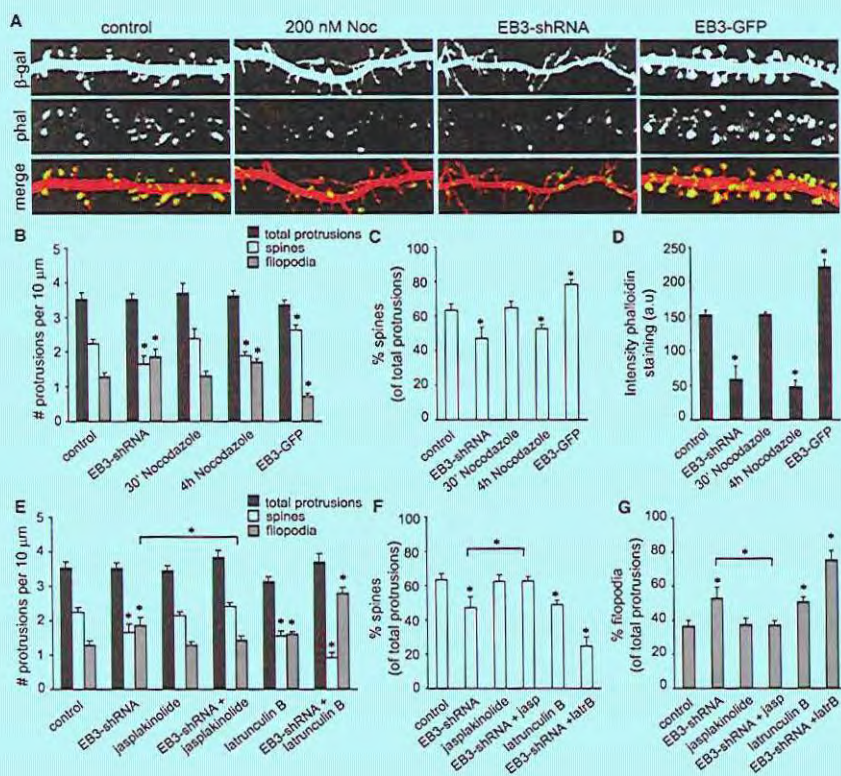


Figure 4. MT Plus-End-Bound EB3 Regulates Actin Dynamics within Spines

(A) High-magnification images of dendrites of hippocampal neurons transfected at DIV 13 for 4 days with the control pSuper vector, EB3-shRNA, or EB3-GFP and treated with 200 nM nocodazole for 4 hr and double-labeled with phalloidin-AS94 and the cotransfected β -gal (red) to visualize the neuronal morphology. (B) Quantification of number of protrusions per 10 μ m dendrites in hippocampal neurons transfected at DIV 13 with the control pSuper vector, EB3-shRNA, or EB3-GFP or treated with 200 nM nocodazole for 30 min or 4 hr. Histograms show mean \pm SEM, * p < 0.05. (C) Percentage of spines (C) of hippocampal neurons transfected and treated as indicated in (B). (D) Quantification of phalloidin immunostaining intensities (as arbitrary units) in dendrites of hippocampal neuron transfected and treated as indicated in (B). (E) Quantification of the number of protrusions per 10 μ m dendrites in hippocampal neurons transfected at DIV 13 with control pSuper vector or EB3-shRNA, either untreated or treated with 10 μ M latrunculin B or 10 μ M jasplakinolide for 2 hr. (F and G) Percentage of spines (F) and filopodia (G) in hippocampal neurons transfected and treated as indicated in (E).

neurons (Figures 4E–4G). On the other hand, treatment of EB3-depleted neurons with jasplakinolide (10 μ M, 2 hr) rescued the EB3 knockdown phenotype (Figures 4E–4G). These data support the idea that the MT plus-end-bound EB3 regulates actin dynamics within dendritic spines.

p140Cap Binds to EB3 and Associates with Growing MT Ends

To investigate the mechanism by which EB3 influences the actin cytoskeleton in spines, we searched for EB3 binding partners in hippocampal neurons. We performed glutathione S-transferase

(GST) pull-down assays with extracts from primary hippocampal neurons (DIV 21) using GST-EB3 fusions and analyzed the isolated proteins by mass spectrometry. Among the proteins which were highly enriched in the GST-EB3 pull down and not present in the control GST pull down, were several known +TIP partners of EB3, such as CLIP-115 and CLASP2 (reviewed in Jaworski et al., 2008; Lansbergen and Akhmanova, 2006) (Table S1). The most significant novel hit in this experiment was p140Cap (also known as SNIP; SNAP-25 interacting protein) (Chin et al., 2000) (Figure 6A; Table S1). p140Cap is a recently discovered Src-binding protein which inhibits Src kinase activity, regulates

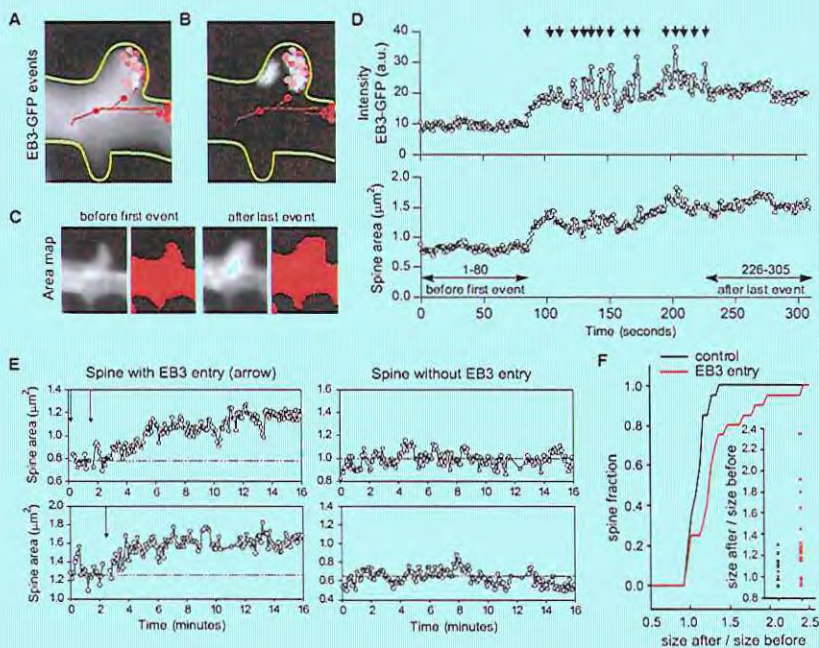


Figure 5. EB3-GFP Entry into Dendritic Spines Is Associated with Spine Growth

(A) Average spine morphology obtained by averaging the time-lapse recording, overlaid with the trajectories of EB3-GFP comets detected during the recording. Progression of time is color coded from dark to light and circles indicate end of trajectories. (B) Image representing the intensity standard deviation per pixel, overlaid with trajectories of EB3 comets. Bright regions have varying intensities due to moving EB3-GFP comets and spine growth. (C) Quantitative changes in spine area. Average spine area of 80 frames before/after the first/last EB3-GFP comet entering the spine, respectively. The binary image for measuring spine size is shown in red. (D) Time trace of spine total intensity (upper panel) and spine total area (lower panel) for 300 s (5 min). Images were taken every 1 s. Arrows indicate events of entering EB3-GFP comets, corresponding with temporarily increased intensities. (E) Examples of spine growth upon EB3-GFP comet entry. Representative traces of spine sizes with (left) or without (right) EB3 entry (depicted by arrows) over longer time (16 min). Images were taken every 2 s to resolve all EB3 entry events. Every three consecutive frames were averaged to enhance visibility. (F) Cumulative probability distribution of the ratio of spine size before and after EB3 entry (red line, $n = 20$), compared with control spines without EB3 entry (ratio of spine size after 10 and 5 min, see methods, $n = 20$).

the actin cytoskeleton and suppresses tumor growth (Di Stefano et al., 2007). To confirm the interaction of p140Cap with EB3 and other EB family members, we performed GST pull down assays with extracts of HEK293 cells expressing GFP alone or GFP-p140Cap. While GFP alone did not interact with any GST fusions (data not shown), the full-length p140Cap (amino acids 1–1216) strongly associated with all members of the EB family and GST-EB1 C terminus but not with GST alone or GST-EB1 N terminus (Figures 6B and 6C). This is in line with the data on other EB binding partners, which all bind to the C-terminal portion of the protein (reviewed in Jaworski et al., 2008; Lansbergen and Akhmanova, 2006). By expressing truncated versions of GFP-p140Cap (Figure 6A), we mapped the minimal EB-binding region of p140Cap. While the large N-terminal part of p140Cap (amino

acids 1–1164) did not interact with any EB proteins, the short 92 amino acid C-terminal region of p140Cap (amino acids 1124–1216) bound to all three GST-EB fusions (Figure 6B). It is likely that the positively charged S/P-rich region within the C terminus of p140Cap is involved in associating with the EB C terminus, because similar domains within other EB-binding partners have also been implicated in this function (Jaworski et al., 2008; Lansbergen and Akhmanova, 2006). The interaction between EB3 and p140Cap under physiological conditions was confirmed by coimmunoprecipitation of endogenous proteins from synaptosome fractions (Figure 6D). In the same experiment, p140Cap was also able to coimmunoprecipitate Src kinase (Figure 6D), consistent with the data from tumor cells (Di Stefano et al., 2007).

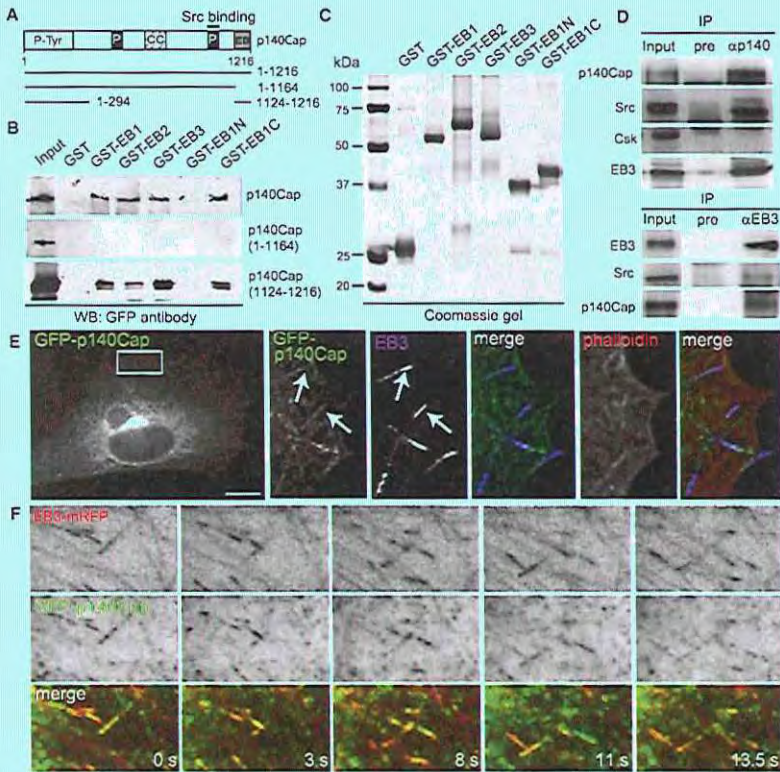


Figure 6. p140Cap Interacts with EB3

(A) Diagram of p140Cap structure and mutant constructs (GFP tag was placed at N terminus). P-Tyr, stretch of phosphorylated tyrosine residues; P, proline-rich domain; CC, coiled coil; EB, minimal EB-binding domain. The second proline-rich region binds to Src kinase.
 (B) GST pull-down assays with the indicated GST fusions and extracts of HEK293 cells overexpressing GFP-p140Cap, GFP-p140Cap(1-1164), or GFP-p140Cap(1124-1216). GFP fusions were detected by western blotting with antibodies against GFP.
 (C) Coomassie-stained gels are shown for GST fusions.
 (D) Immunoprecipitation from mouse crude synaptosomes with anti-p140Cap or anti-EB3 antibodies and proimmune serum (pro) as negative control. Three milligrams of the crude synaptosomal fraction (input = 50 μ g) were immunoprecipitated and analyzed by western blotting for indicated proteins.
 (E) COS-7 cells were transfected with GFP-p140Cap (green), methanol fixed and stained for endogenous EB3 (blue) and F-actin, by phalloidin-AS94 (red). The insets show enlargements of the boxed area. The merge of GFP-p140Cap and endogenous EB3 (green/blue) and GFP-p140Cap/EB3/F-actin (green/blue/red) is shown. Scale bar, 10 μ m.
 (F) Simultaneous imaging of GFP-p140Cap (green) and EB3-mRFP (red) in transfected MRC5-SV cells. Successive frames are shown. Time is indicated in the merge panel.

Next, we investigated the localization of GFP-p140Cap in non-neuronal cells. As previously observed (Di Stefano et al., 2007), GFP-p140Cap localized throughout the cytoplasm and showed a modest colocalization with F-actin (Figure 6E). In addition, we observed GFP-p140Cap-positive comet-like structures, which coincided with some of the MT plus ends labeled for endogenous EB3 (Figure 6E). Further indications of an interaction between the two proteins were provided by coexpression

of GFP-p140Cap and EB3-mRFP. At low expression levels, EB3-mRFP colocalized with GFP-p140Cap on MT plus ends (Figure S4A). However, when EB3 was distributed evenly along the MTs due to overexpression, GFP-p140Cap also decorated the whole MT lattice (Figure S4B).

The ability of p140Cap to associate with growing MT ends was further confirmed by simultaneous dual color live imaging of GFP-p140Cap and EB3-mRFP: GFP-p140Cap was observed

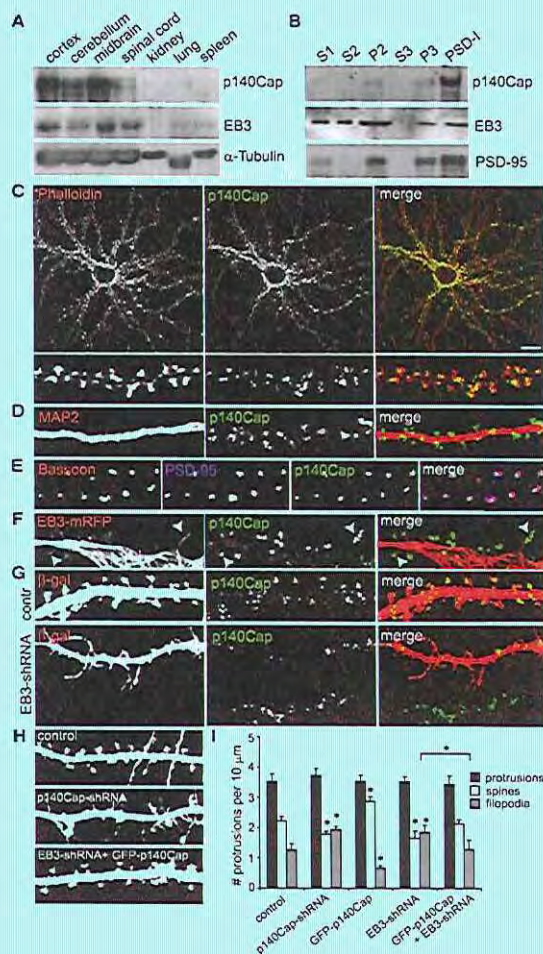


Figure 7. p140Cap Localizes to Synapses and Is Required for Spine Maintenance

(A) Tissue expression of p140Cap. Mouse tissue homogenates (20 μg of protein/lane) were analyzed by SDS-PAGE and immunoblotting using anti-p140Cap and anti-EB3 antibodies. α -Tubulin as is used as a loading control.

(B) Enrichment of p140Cap in the PSD fraction. Hippocampal neurons at DIV 21 were homogenized, fractionated by differential centrifugation, and analyzed by immunoblotting using anti-p140Cap, anti-EB3 and anti-PSD-95 antibodies.

(C) Representative images of rat hippocampal neurons (DIV 17) labeled with rabbit anti-p140Cap antibody (green) and phalloidin-A594 (red), to visualize F-actin. Dendritic segments (lower panels) are enlarged to show the colocalization of p140Cap and F-actin in spines. Scale bar, 10 μm .

(D) Dendrites of hippocampal neurons labeled with rabbit anti-p140Cap antibody (green) and mouse anti-MAP2 (red).

(E) Dendrites of hippocampal neurons triple labeled with rabbit anti-p140Cap antibody (green), guinea pig anti-PSD-95 antibody (blue), and mouse anti-Bassoon (red).

(F) Hippocampal neurons transfected at DIV 13 with EB3-mRFP and labeled with mouse anti-p140Cap (red). Arrowheads indicate colocalized EB3-mRFP and p140Cap.

(G) Representative images of hippocampal neurons transfected at DIV 13 with control pSuper vector or EB3-shRNA and double labeled with anti-p140Cap (green) and cotransfected β -gal (red). (H) Representative images of hippocampal neurons transfected at DIV 13 with control pSuper vector, p140Cap-shRNA, or EB3-shRNA and GFP-p140Cap and stained for cotransfected β -gal to highlight neuronal morphology.

(I) Quantification of number of protrusions per 10 μm dendrites in hippocampal neurons transfected at DIV 13 with control pSuper vector, p140Cap-shRNA, GFP-p140Cap, EB3-shRNA, and a combination of EB3-shRNA and GFP-p140Cap. Error bars indicate SEM, * $p < 0.05$.

as small granular particles that showed diffusive behavior and concentrated at EB3-positive growing MT ends (Figure 6F; Movie S5). These data indicate that, similar to other EB-binding partners, p140Cap can behave as a +TIP.

p140Cap Localizes to Synapses in Hippocampal Neurons

Western blot analyses showed that both p140Cap and EB3 are predominantly expressed in the central nervous system and present in different brain regions (Figure 7A), consistent with previous studies (Chin et al., 2000; Di Stefano et al., 2004; Nakagawa et al., 2000). Several PSD proteome studies have identified

p140Cap/SNIP as an abundant constituent of the PSD (Dosemeci et al., 2007; Peng et al., 2004; Trinidad et al., 2006), but its function at the synapse has not yet been studied. Our biochemical fractionation experiments confirmed the presence of p140Cap in synaptosomal membrane fractions and its enrichment in PSD fractions, similar to core PSD components such as PSD-95 (Figure 7B). In agreement with the biochemical experiments, immunofluorescent staining of p140Cap in cultured neurons revealed granular puncta of different size that were distributed along dendrites and concentrated within F-actin-enriched dendritic spines (Figure 7C). The p140Cap puncta were not restricted to the spine head but often extended toward the dendritic shaft, suggesting that the zone of p140Cap accumulation might include the neck of the spine. More than 70% of the dendritic p140Cap showed overlap with the postsynaptic marker PSD-95 and presynaptic protein Bassoon (Figure 7E). The punctate distribution of p140Cap showed little colocalization with MTs in the dendritic shaft, as revealed by costaining with MAP2 (Figure 7D). Furthermore, very little overlap of p140Cap and EB3 positive MT plus end in the dendritic shaft could be observed, in spite of the marked colocalization between mRFP-EB3 and p140Cap within the spines (Figure 7F). Thus,

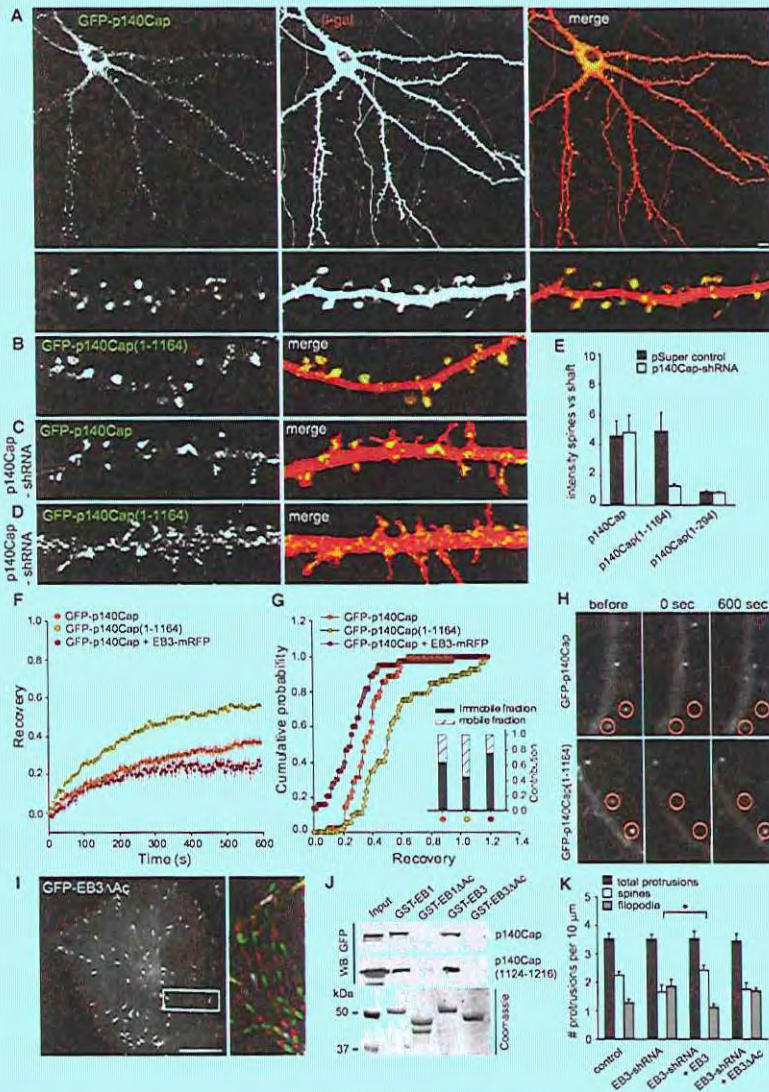


Figure 8. EB3 Is Required for p140Cap Distribution in Hippocampal Neurons

(A–D) Representative images of hippocampal neurons cotransfected at DIV 13 with full-length GFP-p140Cap or GFP-p140Cap(1-1164) with pSuper control vector (A and B) or p140Cap-shRNA (C and D) and labeled for cotransfected β -gal (red). Dendritic segments are enlarged to show the distribution of GFP-p140Cap. Only the merge is shown in color. Scale bar, 10 μ m.

(E) Quantification of GFP-p140Cap spine targeting. Numbers indicate the ratio of fluorescence intensity in spines versus dendritic shafts of each indicated p140Cap construct with pSuper control vector or p140Cap-shRNA (mean \pm SEM), as index of spine targeting.

p140Cap appears to be a synaptic protein which concentrates in spines and may interact with EB3-labeled MT tips entering the spines.

Loss of p140Cap Causes a Decrease in Spine Density

To investigate the role of p140Cap in dendritic spine morphology, we knocked down endogenous p140Cap using plasmid-based RNAi. Transfection of the p140Cap-shRNA construct caused an ~70% reduction in immunostaining for p140Cap in dendrites and the cell body (Figures S5A and S5B) but induced no change in other proteins, such as MAP2 (data not shown). Knockdown of p140Cap caused a significant decrease in the number of spines and an increase in the number of filopodia, while the total protrusion density was unchanged (Figures 7H and 7I). The density of F-actin in dendrites of p140Cap-deficient neurons was significantly diminished (data not shown), similar to the EB3 knock-down neurons. In contrast, GFP-p140Cap overexpression caused an opposite effect on the ratio between spines and filopodia and an increase in F-actin abundance (Figures 7H and 7I). Taken together, these results imply that p140Cap is involved in stabilization of mushroom-like spines.

EB3 and p140Cap Cooperate in Regulating Spine Morphology

Since EB3 and p140Cap interact with each other and their depletion causes similar spine phenotypes, the two proteins may act in the same pathway. To test this possibility, we investigated p140Cap localization in EB3-deficient neurons. We transfected neurons at DIV 13 with EB3-shRNA; 4 days later we observed that the staining of p140Cap in the dendritic protrusions was significantly reduced (Figure 7G). Quantification revealed a 75% reduction in p140Cap protrusion staining intensity in EB3 knockdown neurons compared to control neurons.

To obtain insight in to how EB3 might regulate p140Cap localization, we determined whether the EB3-binding domain of p140Cap is required for its targeting to spines. Neurons were transfected with full-length p140Cap or its truncated versions, GFP-p140Cap(1-1164), that lacks the EB3-binding site, and GFP-p140Cap(1-294) that also lacks the Src-binding site (Figure 6A). GFP-p140Cap(1-1164) accumulated in spines as efficiently as the full-length protein (Figures 8A and 8E), while GFP-p140Cap(1-294) lost its spine targeting (Figure 8E). Since p140Cap has a coiled-coil in the middle of the protein and could interact with itself, endogenous p140Cap may stabilize exogenous p140Cap protein within the spines. To test this hypothesis,

we cotransfected neurons at DIV 13 with p140Cap-shRNA and full-length GFP-p140Cap or GFP-p140Cap(1-1164); 4 days later we observed that the accumulation of GFP-p140Cap(1-1164) in the dendritic protrusions was significantly reduced compared to full-length GFP-p140Cap (Figures 8C–8E). To interfere with the specific interaction between EB3 and p140Cap, we overexpressed the EB3-binding C terminus of p140Cap (1124-1216) (Figures S4B) and observed a significant decrease in the number of mushroom-shaped spines (Figures S5D and S5E). In addition, expressing a 23 aa C-terminally truncated EB3 construct (GFP-EB3ΔAc), which is unable to bind to p140Cap (Figure 8J) but can bind to MT plus ends and regulate MT dynamics (Figure 8I), does not increase the number of mushroom spines compared to full-length EB3-GFP (Figures S3D–S3F). Furthermore, full-length EB3-GFP but not GFP-EB3ΔAc is able to rescue the EB3 knockdown phenotype (Figure 8K). Together these data indicate that the EB3-p140Cap interaction is necessary for regulating spine morphology.

We hypothesized that the EB3-binding region might affect the turnover of p140Cap in spines. Fluorescence recovery after photobleaching (FRAP) revealed that on average, full-length GFP-p140Cap fluorescence recovers to $36\% \pm 2\%$ (mean \pm SEM, $n = 35$ spines) of prebleach intensity with an average recovery half-time of $\tau_{1/2} = 148 \pm 11$ s (mean \pm SEM) (Figure 8F). Fitting a single-exponential recovery curve to the average recovery time trace yielded similar results ($\tau_{1/2} = 153 \pm 36$ s, Recovery level $R_{\text{final}} = 38\% \pm 4\%$), indicating that there are two p140Cap populations; one mobile fraction with a turnover time of minutes and another, more stable fraction that turns over on a timescale much longer than 15 min (Figures 8G and 8H). FRAP analysis of GFP-p140Cap(1-1164) showed not much change in the recovery half-time ($\tau_{1/2} = 125 \pm 9$ s, mean \pm SEM, $n = 52$ spines), but a much higher recovery level than full-length GFP-p140Cap ($R_{\text{final}} = 55\% \pm 4\%$, mean \pm SEM), indicating that the fraction of stably incorporated p140Cap has decreased by almost 30% (Figures 8F–8H). Coexpression of GFP-p140Cap and EB3-mRFP revealed a lower GFP recovery level compared to p140Cap alone ($R_{\text{final}} = 23\% \pm 3\%$, mean \pm SEM, $n = 43$ spines) (Figures 8G and 8H). Although we cannot exclude that other factors also influence p140Cap turnover in spines, the FRAP data reveal that the EB3 interaction is important for regulation of p140Cap accumulation within spines.

Next, we tested whether p140Cap acts up- or downstream of EB3 in regulating spine shape. While overexpression of GFP-p140Cap fully restored the number of mushroom-shaped spines in EB3 depleted neurons (Figures 7H and 7I), GFP-EB3

(F) Averaged time traces of fluorescence recovery after photobleaching for full-length GFP-p140Cap (orange circles, 35 spines), GFP-p140Cap(1-1164) (green circles, 52 spines) or GFP-p140Cap coexpressing EB3-mRFP (red circles, 43 spines). Error bars show SEM.

(G) Cumulative probability distribution of the recovery levels 595 s after bleaching. Inset shows the average size of the mobile and immobile fractions of GFP-p140Cap, GFP-p140Cap(1-1164) and GFP-p140Cap plus EB3-mRFP.

(H) Examples of the fluorescence distribution and intensity of GFP-p140Cap and GFP-p140Cap(1-1164) before, directly after and 600 s after bleaching the spines indicated with circles.

(I) CHO cells were transfected with GFP-EB3ΔAc and imaged every 500 ms. The GFP-EB3ΔAc positive growing MT ends are color coded for each fifth frame (2.5 s). Frame 1 is shown in white (at left) and every subsequent fifth frame is alternately colored red and green in the enlargement (at right). Scale bar, 10 μm .

(J) GST pull-down assays with the indicated GST fusions and extracts of HEK293 cells overexpressing GFP-p140Cap and GFP-p140Cap(1124-1216). GFP fusions were detected by western blotting with antibodies against GFP. Coomassie-stained gel is shown for GST fusions.

(K) Quantification of the number of dendritic protrusions per 10 μm in hippocampal neurons transfected at DIV 13 with empty vector (control), EB3-shRNA alone, or EB3-shRNA with EB3 or EB3ΔAc. Error bars indicate SEM. * $p < 0.05$.

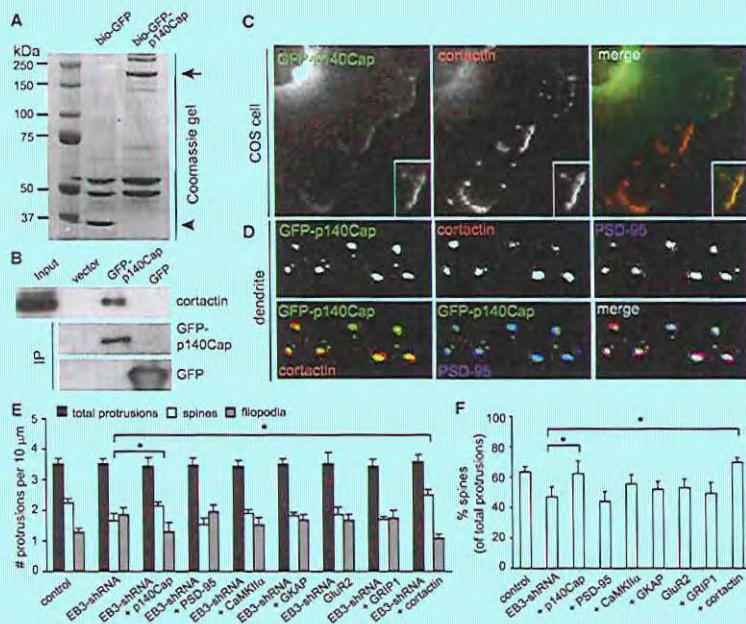


Figure 9. p140Cap Interacts with Cortactin

(A) Streptavidin pull-down assays were performed with lysates of HeLa cells coexpressing bio-GFP-p140Cap or bio-GFP together with BirA. Proteins bound to streptavidin beads were analyzed on a Coomassie-stained gel. The arrowhead and the arrow indicate bio-GFP and bio-GFP-p140Cap protein bands, respectively. (B) Immunoprecipitations from extracts of transfected HeLa cells with the indicated constructs and probed for cortactin. (C) COS-7 cells were transfected with GFP-p140Cap, formaldehyde fixed and stained for endogenous cortactin (red). The insets show enlargements of cortactin and p140Cap colocalization at cortical membrane ruffles. (D) Dendrites of hippocampal neurons triple labeled for transfected GFP-p140Cap (green), rabbit anti-cortactin (red), and guinea pig anti-PSD-95 antibody (blue). (E) Quantification of number of protrusions per 10 μm dendrite in hippocampal neurons transfected at DIV 13 with control pSuper vector, EB3-shRNA, or EB3-shRNA plus the indicated constructs. Histograms show mean ± SEM, **p* < 0.05. (F) Percentage of spines of hippocampal neurons transfected with constructs indicated in (E).

expression was unable to rescue the p140Cap phenotype (data not shown). Taken together, our data suggest that EB3 located at the growing MT ends regulates the distribution of p140Cap, which in its turn controls dendritic spine morphology.

p140Cap Binds to Cortactin

While EB3-positive MT plus ends regulates the stability of p140Cap and modulates actin dynamics within dendritic spines, we wanted to gain a better understanding of how EB3/p140Cap regulates the actin cytoskeleton. We next searched for p140Cap binding partners using pull-down assays combined with mass spectrometry. Biotinylation and GFP-tagged p140Cap (bio-GFP-p140Cap) and bio-GFP as a control were transiently coexpressed in HeLa cells together with the protein-biotin ligase BirA and isolated with streptavidin beads (Figure 9A). Mass-spectrometry analysis of the whole bio-GFP-p140Cap lane revealed several actin-related proteins, including Crk (Bougneres et al.,

2004), CD2-associated protein (CD2AP) (Lynch et al., 2003), cortactin (Wu and Parsons, 1993), and Shank (Naisbitt et al., 1999) that were not present in the control lane (Table S2). Interestingly, all the identified proteins have previously been shown to interact with cortactin (Ammer and Weed, 2008), suggesting that p140Cap in HeLa cells associates with a cortactin-containing protein complex. Additional bio-p140Cap mass-spectrometry experiments using MCF7 and brain extract all identified cortactin while the other cortactin interacting proteins were not found (data not shown). The interaction between p140Cap and cortactin was confirmed by immunoprecipitation experiments (Figure 9B). Cortactin is an F-actin-binding protein implicated in the stabilization and branching of actin filaments and shown to concentrate with F-actin at cortical membrane in nonneuronal cells (Wu and Parsons, 1993) and dendritic spines of cultured hippocampal neurons (Hering and Sheng, 2003). Expression of GFP-p140Cap revealed colocalization with cortactin at membrane

ruffles and lamellipodia in COS-7 cells (Figure 9C) and dendritic spines positive for the postsynaptic marker PSD-95 (Figure 9D). It has been shown that loss of cortactin results in a decrease of F-actin staining and reduction of dendritic spines (Hering and Sheng, 2003), similarly to the effects seen with EB3 and p140Cap knockdown. We confirmed the loss-of-function experiments by using cortactin shRNA (data not shown) and tested whether cortactin regulates spine morphology downstream of EB3 in controlling spine shape. Overexpression of myc-tagged cortactin fully restored the number of mushroom-shaped spines in EB3 depleted neurons, similarly to expression of GFP-p140Cap (Figures 9E and 9F). In contrast no rescue of the EB3 knockdown spine phenotype could be seen by overexpressing other major postsynaptic proteins, such as PSD-95, CaMKII α , GKAP, GluR2, or GRIP1 (Figures 9E and 9F). These findings show that p140Cap and its interacting partner cortactin specifically rescue the EB3 depletion phenotype and strengthens the link between EB3, p140Cap and the actin cytoskeleton.

DISCUSSION

In this study we describe a structural and functional interplay between dendritic MTs and actin cytoskeleton within spines. Unexpectedly, dynamic MTs can penetrate into dendritic spines and are required to maintain their shape. EB3-bound MT plus ends modulate spine shape by affecting the abundance of F-actin. This view is supported by the observation that EB3 knockdown phenotype is rescued by jasplakinolide, a drug that promotes actin polymerization. These findings are in line with genetic studies in yeast where +TIPs regulate cell shape by affecting the actin cytoskeleton (Basu and Chang, 2007). Furthermore, we identified an EB3 binding partner, p140Cap, a regulator of Src kinase activity shown to be involved in controlling actin organization (Di Stefano et al., 2007). In this study we also found that p140Cap binds to the Src kinase substrate and F-actin binding protein cortactin (Wu and Parsons, 1993). Overexpression of p140Cap or cortactin rescues the EB3 depletion phenotype. The interactions of EB3-positive MT plus-ends, p140Cap and cortactin may therefore represent a link between the local signaling of MTs and the actin cytoskeleton within the dendritic spines.

Regulation of Spine Morphology by Dendritic MTs

It is widely accepted that in dendrites of mature neurons, the cytoskeletal microdomains are spatially separated: actin filaments are predominately concentrated in spines while MTs are restricted to the dendritic shaft and rarely observed within dendritic spines (Kaech et al., 2001; Westrum et al., 1980). This conclusion is mainly based on ultrastructural studies as well as live imaging experiments using MAP2-GFP, which revealed that stable MTs are absent from spines (Kaech et al., 2001; Landis and Reese, 1983). In this study, we particularly focus on dynamic MTs by using EB3-GFP and show that growing MTs can enter dendritic spines. In accord with these data it was shown previously that the large dendritic spines of CA3 pyramidal neurons frequently contain MTs (Chicurel and Harris, 1992) and that some MT components and associated proteins are present in spines and PSD fractions (Sheng and Hoogen-

raad, 2007; van Rossum and Hanisch, 1999). Thus, it seems that stable MTs are predominantly present as bundles in dendritic shafts whereas dynamic MTs can enter dendritic spines.

Furthermore, we show that entry of dynamic MT plus ends is physiologically relevant. First, EB3-GFP entry in spines frequently accompanies spine enlargement. Second, a low dose of nocodazole abolishes EB3 accumulation at MT tips and leads to changes in spine morphology and synaptic transmission. Third, reduction of EB3 expression decreases F-actin staining and spine size, whereas EB3 overexpression correlates with an increase in polymerized actin and the number of mushroom-like spines. Fourth, a binding partner of EB3, p140Cap, co-localizes with F-actin in spines and its distribution is influenced by EB3 expression. We propose a model in which dynamic EB3-labeled MT ends grow into dendritic spines and influence their morphology by controlling the actin cytoskeleton by acting, at least in part, through p140Cap.

The functions of dynamic MT penetration in spines described here may extend beyond the regulation of the actin cytoskeleton. MTs within spines may be important for organizing membrane traffic and could reflect the need for cargo delivery to the postsynaptic site, analogous to the accumulation of synaptic vesicles in axonal growth cones (Dent and Gertler, 2003). It is generally believed the synaptic cargo travels along the MT transport system in the dendrite shaft and switches to the actin-dependent myosin motor system to reach the postsynaptic membrane (Kennedy and Ehlers, 2006). However, with our finding that MTs grow into spines, it is possible that cargos are also transported by MT-dependent motors toward synaptic sites (Hirokawa and Takemura, 2005; Kneussel, 2005). Furthermore, additional studies are required to determine whether neuronal activity or local calcium influx influences MTs dynamics within dendritic spines.

The Functional Significance of the EB3-p140Cap Interaction

Recent studies in various organisms have provided strong evidence that EB family proteins are conserved key molecules at growing MT plus ends. The localization of most, if not all, other plus-end tracking proteins is influenced by the presence of EBs at the MT plus-ends (Lansbergen and Akhmanova, 2006). Although p140Cap can track on EB3 labeled MT plus-ends in fibroblasts (Figure 6), the primary localization of endogenous p140Cap within hippocampal neurons is in dendritic spines. We propose that growing EB3-positive MT ends influence dendritic spine morphology by altering the turnover of p140Cap.

Several lines of evidence support this model. First, knockdown of EB3 disrupts the localization of endogenous p140Cap within the dendritic spines and FRAP analysis shows that the EB3-binding is required for p140Cap immobilization within spines. Second, p140Cap overexpression rescues the EB3 knockdown phenotype. Third, p140Cap binds EB3 via its C-terminal tail region (amino acid 1124–1216), and p140Cap(1124–1216) has a dominant-negative effect on spine morphology. Fourth, C-terminally truncated EB3 (EB3 Δ Ac) can interact with MT plus ends and regulate MT dynamics but it cannot bind to p140Cap and is unable to increase the number of mushroom spines in

- Shaw, R.M., Fay, A.J., Puthonveedu, M.A., von Zastrow, M., Jan, Y.N., and Jan, L.Y. (2007). Microtubule plus-end-tracking proteins target gap junctions directly from the cell interior to adherens junctions. *Cell* 128, 547–560.
- Sheng, M., and Hoogenraad, C.C. (2007). The postsynaptic architecture of excitatory synapses: a more quantitative view. *Annu. Rev. Biochem.* 76, 823–847.
- Siegrist, S.E., and Doe, C.Q. (2007). Microtubule-induced cortical cell polarity. *Genes Dev.* 21, 483–496.
- Stohbens, S.J., Paterson, A.D., Crampton, M.S., Shewan, A.M., Ferguson, C., Akhmanova, A., Parton, R.G., and Yap, A.S. (2006). Dynamic microtubules regulate the local concentration of E-cadherin at cell-cell contacts. *J. Cell Sci.* 119, 1801–1811.
- Stepanova, T., Slemmer, J., Hoogenraad, C.C., Lansbergen, G., Dortland, B., De Zoouw, C.I., Grosveld, F., van Cappellen, G., Akhmanova, A., and Gallart, N. (2003). Visualization of microtubule growth in cultured neurons via the use of EB3-GFP (end-binding protein 3-green fluorescent protein). *J. Neurosci.* 23, 2655–2664.
- Suter, D.M., Schaefer, A.W., and Forscher, P. (2004). Microtubule dynamics are necessary for SRC family kinase-dependent growth cone steering. *Curr. Biol.* 14, 1194–1199.
- Tada, T., and Sheng, M. (2006). Molecular mechanisms of dendritic spine morphogenesis. *Curr. Opin. Neurobiol.* 16, 95–101.
- Trinidad, J.C., Specht, C.G., Thalhammer, A., Schoepfer, R., and Burlingame, A.L. (2006). Comprehensive identification of phosphorylation sites in postsynaptic density preparations. *Mol. Cell. Proteomics* 5, 914–922.
- van Rossum, D., and Hanisch, U.K. (1999). Cytoskeletal dynamics in dendritic spines: direct modulation by glutamate receptors? *Trends Neurosci.* 22, 290–295.
- Vasquez, R.J., Howell, B., Yvon, A.M., Wadsworth, P., and Cassimeris, L. (1997). Nanomolar concentrations of nocodazole alter microtubule dynamic instability in vivo and in vitro. *Mol. Biol. Cell* 8, 973–985.
- Weaver, A.M., Young, M.E., Lee, W.L., and Cooper, J.A. (2003). Integration of signals to the Arp2/3 complex. *Curr. Opin. Cell Biol.* 15, 23–30.
- Webb, D.J., Zhang, H., Majumdar, D., and Horwitz, A.F. (2007). $\alpha 5$ integrin signaling regulates the formation of spines and synapses in hippocampal neurons. *J. Biol. Chem.* 282, 6929–6935.
- Westrum, L.E., Jones, D.H., Gray, E.G., and Barron, J. (1980). Microtubules, dendritic spines and spine apparatuses. *Cell Tissue Res.* 208, 171–181.
- Wu, H., and Parsons, J.T. (1993). Cortactin, an 80/85-kilodalton pp60src substrate, is a filamentous actin-binding protein enriched in the cell cortex. *J. Cell Biol.* 120, 1417–1426.
- Yuste, R., and Bonhoeffer, T. (2001). Morphological changes in dendritic spines associated with long-term synaptic plasticity. *Annu. Rev. Neurosci.* 24, 1071–1089.

Neuron specific Rab4 effector GRASP-1 coordinates membrane specialization and maturation of recycling endosomes

Casper C. Hoogenraad¹, Ioana Popa², Kensuke Futai³, Emma Sanchez-Martinez², Phebe S. Wulf¹, Thijs van Vlijmen², Bjorn R. Dortland¹, Viola Oorschot^{2,4}, Roland Govers⁵, Maria Monti⁶, Albert J. R. Heck⁶, Morgan Sheng³, Judith Klumperman^{2,4}, Holger Rehmann⁷, Dick Jaarsma¹, Lukas C. Kapitein¹, Peter van der Sluijs²

¹Department of Neuroscience, Erasmus Medical Center, Rotterdam; ²Department of Cell Biology, UMC Utrecht, Utrecht; ³The Picower Institute for Learning and Memory, Massachusetts Institute of Technology, Cambridge; ⁴Cell Microscopy Center, UMC Utrecht, Utrecht; ⁵Department of Functional Genomics, Centre for Neurogenomics and Cognitive Research, VU Amsterdam; ⁶Department of Biomolecular Mass Spectrometry and Proteomics Group, Bijvoet Centre for Biomolecular Research and Utrecht Institute for Pharmaceutical Sciences, Utrecht University, Utrecht; ⁷Department of Physiological Chemistry, Centre for Biomedical Genetics and Cancer Genomics Centre, UMC Utrecht, Utrecht.

Submitted

Chapter 3

SUMMARY

The endosomal pathway in neuronal dendrites is essential for membrane receptor trafficking and proper synaptic function and plasticity. However, the molecular mechanisms that organize specific endocytic trafficking routes are poorly understood. Here, we identify GRIP-associated protein-1 (GRASP-1) as a neuron-specific effector of Rab4 and key component of the molecular machinery that coordinates recycling endosome maturation in dendrites. We show that GRASP-1 is necessary for AMPA receptor recycling, maintenance of spine morphology and synaptic plasticity. At the molecular level, GRASP-1 segregates Rab4 from EEA1/Neep21/Rab5-positive early endosomal membranes and coordinates the coupling to Rab11-labelled recycling endosomes by interacting with the endosomal SNARE syntaxin 13. We propose that GRASP-1 connects early and late recycling endosomal compartments by forming a molecular bridge between Rab-specific membrane domains and the endosomal SNARE machinery. The data uncover a new mechanism to achieve specificity and directionality in neuronal membrane receptor trafficking.

INTRODUCTION

In order to receive, process, and transmit information, neurons need substantially regulated mechanisms to locally redistribute membranes and proteins to synaptic sites. Multiple lines of evidence suggest that the endosomal pathway plays a crucial role in synaptic function and plasticity. At excitatory synapses, the postsynaptic membrane composition is subject to continuous and activity-dependent endocytic cycling of postsynaptic molecules. Based on uptake of extracellular gold particles, visualization of clathrin assembly in living neurons and pre-embedding immunogold electron microscopy, it was shown that endosomal compartments are present in the dendritic shaft and spines and that endocytosis occurs at specialized endocytic zones lateral to the postsynaptic density (PSD) (Kennedy and Ehlers, 2006; Sheng and Hoogenraad, 2007). Using live-cell imaging and serial section electron microscopy it was demonstrated that recycling endosomes are required for the growth and maintenance of dendritic spines (Park et al., 2006). Membrane recruitment from recycling endosomes is a common mechanism that cells employ to expand the plasma membrane and targets proteins in a polarized manner in such distinct processes as cytokinesis, cell-cell adhesion, phagocytosis, and cell fate determination (Gruenberg, 2001; Maxfield and McGraw, 2004; Gould and Lippincott-Schwartz, 2009).

Perhaps the strongest evidence for the importance of endocytic recycling in synaptic function originates from the analysis of AMPA-type glutamate receptor (AMPA) trafficking (Bredt and Nicoll, 2003; Malinow and Malenka, 2002; Shepherd and Huganir, 2007). AMPARs are the major excitatory neurotransmitter receptors in the brain and redistribution of AMPARs in and out of the synapse has emerged as an important mechanism for information storage in the brain (Malinow and Malenka, 2002). Increased delivery of AMPARs to the postsynaptic membrane leads to long-term potentiation (LTP), whereas net removal of AMPARs by internalization from the surface through endocytosis seems to underlie long-term depression (LTD) (Bredt and Nicoll, 2003; Malinow and Malenka, 2002; Shepherd and Huganir, 2007). Like any other internalized membrane protein, endocytosed AMPARs undergo endosomal sorting; they can be degraded in lysosomes or recycled back to the surface membrane (Ehlers, 2000;

Lee et al., 2004). A popular model is that the recycling endosomes provides the local intracellular pool of glutamate receptors for LTP (Park et al., 2004). Neuron-enriched endosomal protein of 21 kD (Neep21) and its interacting protein syntaxin 13 are endosomal proteins implicated in regulating AMPAR trafficking during synaptic plasticity (Steiner et al., 2002). However, it remains unclear how endocytic receptor sorting and recycling is organized and coordinated in neuronal dendrites.

Multiple proteins identified as regulators of endosomal traffic in non-neuronal cells are also important in neuronal endosomes (Cai et al., 2007; Maxfield and McGraw, 2004). Dendritic spines contain the basic components of the endocytic machinery, postsynaptic receptor endocytosis occurs through a dynamin-dependent pathway and Rab GTPases and their effectors regulate endosomal traffic (Kennedy and Ehlers, 2006). The classic endosomal Rab proteins, Rab5, Rab4 and Rab11 have all been implicated in endosomal receptor and membrane trafficking in dendrites (Greger and Esteban, 2007; Kennedy and Ehlers, 2006). Rab5 controls transport to early endosomes (also called sorting endosomes) whereas Rab4 and Rab11 are involved in the regulation of endosomal recycling back to the plasma membrane (Sönnichsen et al., 2000). Active membrane-bound Rabs can bind to specific effector proteins and regulate membrane specialization and protein sorting by connecting specific endosomal compartments (Grosshans et al., 2006; Gruenberg, 2001, Zerial and McBride, 2001). The endosomal pathway can be considered as a mosaic of discrete but overlapping domains that are controlled by Rab proteins and their interacting networks. The communication and transport between sequentially organized Rab domains is thought to be mediated via proteins that are 'shared' by both domains. Bivalent effectors, such as Rabenosyn-5 and Rabaptin-5 have been found that connect proximal Rab5 and distal Rab4 domains on early endosomes (de Renzis et al., 2002). However, how Rab4 and Rab11 recycling endosomal domains are coupled is poorly understood.

To gain a better mechanistic understanding of endosome recycling in neurons, we searched for neuronal interacting partners of Rab4 (van der Sluijs et al., 1992). Using a pull-down and mass spectrometry approach, we identified GRASP-1 as neuron-specific effector of Rab4 and key component of endocytic recycling in dendrites. GRASP-1 was originally found to interact with glutamate receptor interacting protein (GRIP) and shown to be involved in regulating AMPAR distribution (Ye et al., 2000). We show that GRASP-1 is necessary for AMPAR recycling and synaptic plasticity, essential for maintenance of spine morphology and important for endosomal trafficking. GRASP-1 segregates Rab4 from EEA1/Neep21/Rab5-positive early endosomal membranes and coordinates the coupling to Rab11-labelled recycling endosomes via the interaction with t-SNARE syntaxin 13. These results describe a molecular mechanism for regulating recycling endocytosis by GRASP-1.

RESULTS

GRASP-1 is a Rab4-GTP-binding protein

To identify Rab4-interacting proteins we performed glutathione S-transferase (GST) pull-down assays with pig brain extracts using GTP γ S-loaded GST-Rab4 affinity columns and analyzed the isolated proteins by mass spectrometry (Fig. 1A). Among the proteins that were highly enriched in the GST-Rab4-GTP γ S pull-downs but were not detected by mass spectrometry in the pull-down assays using GST-Rab4-GDP or GST alone, we found known binding partners of Rab4, such as the bivalent Rab effectors

Rabaptin-5 and Rabenosyn-5 (Table 1) (de Renzis et al., 2002; Vitale et al., 1998).

Identified protein	MW (kDa)	Pept. total	NCBI GI number	References
Rabaptin-5	99.7	68	1050523	
GRASP-1	96.3	9	16758652	
Rabenosyn-5	89.5	3	58037445	

Table 1. Binding partners of GST-Rab4-GTP in pig brain extracts identified by mass spectrometry
The table shows proteins identified with a significant Mascot score in GST-Rab4-GTP pull downs from pig brain extracts. The list is corrected for background proteins which were identified in a control GST-Rab4-GDP and GST pull-down. For each identified protein, the list is filtered for duplicates and shows only the hits with identified peptides.

The most significant novel hit was GRASP-1, which was originally identified as a GRIP/AMPA interacting protein which regulates AMPAR targeting and Jun-N-terminal kinase (JNK) signaling (Ye et al., 2000; Ye et al., 2007). The association between GRASP-1 and Rab4 was confirmed by immunoblotting with an antibody against GRASP-1 (Fig. 1B). Binding of GRASP-1 to Rab4 was direct and specific since GRASP-1 associates with GST-Rab4, but not with the other tested Rab proteins, such as Rab3, Rab5, Rab7 and Rab11 (Fig. 1C). Immunoprecipitation experiments from COS-7 cells co-expressing myc-GRASP-1 and Flag-Rab4 or Flag-Rab5 further confirmed the interaction of GRASP-1 with Rab4 (Fig. 1D). Fluorescence microscopic analysis of Hela cells transfected with myc-GRASP-1 and GFP-Rab4, showed that the distribution of GRASP-1 fully coincided with GFP-Rab4 (Fig. 1E). Analysis of the endosomal compartment in the same cells, as visualized by internalized Alexa594-Transferrin (Tf-594), indicated that GRASP-1 localizes to the Rab4-positive domain of the early endosomal recycling system. These immunofluorescence data are in line with the reported endosomal localization of GRASP-1 in Hep-2 cells, detected with an autoimmune GRASP-1 serum from a patient with recurrent infections and a presumed immune deficiency (Stinton et al., 2005).

GRASP-1 has an extensive propensity to form coiled-coils and contains a caspase-3 cleavage site, a PDZ-like GRIP binding domain, and a central glutamate-rich stretch (Fig. 1F). To define the minimal Rab4 binding domain on GRASP-1 we generated a series of myc-GRASP-1 truncations (Fig. 1F, 2B). GST-Rab4 pull down assays with COS-7 cell extracts expressing GRASP-1 mutants showed that the N-terminal domain of GRASP-1 binds to Rab4, and that the coiled-coil region between amino acid 280-300 is required for this interaction (Fig. 1G, 2A). However, this region alone is not sufficient for Rab4 binding. Full length GRASP-1 lacking amino acid 280-300, partially retained (50%) Rab4 binding (Fig. 2C) and colocalized, although to a lesser extent, with the small GTPase in Hela cells (Fig. 2D). Taken together, these data argue for an important role of the N-terminal coiled-coil region in Rab4 binding. It has been reported that GRASP-1 may serve as a guanine nucleotide exchange factor (GEF) for H-ras (Ye et al., 2000). We tested whether GRASP-1 might be a GEF for Rab4 by analyzing recombinant GRASP-1(1-594) in a GEF assay using fluorescent mantGDP. GRASP-1 did not act as GEF for Rab4 (Fig. 3A,B).

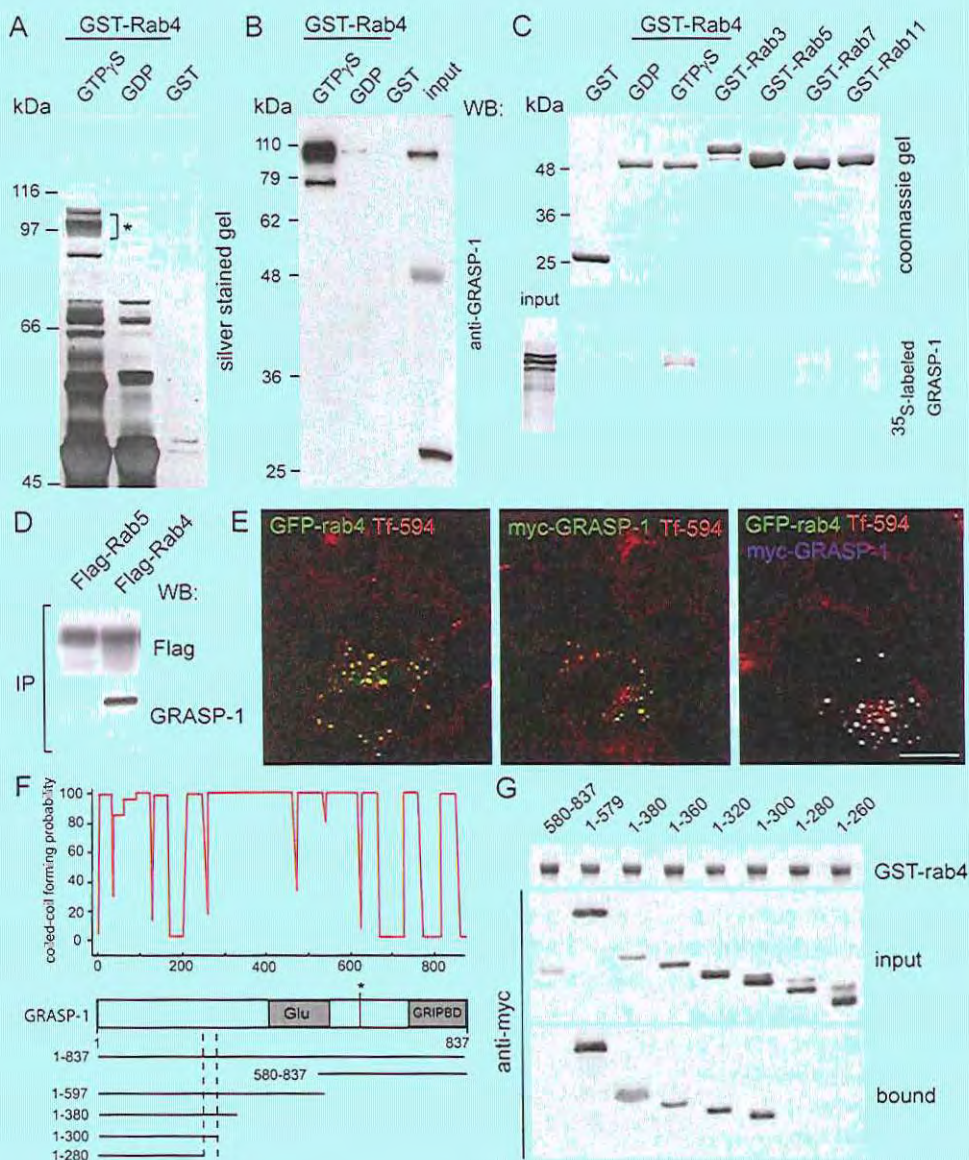


Figure 1. GRASP-1 is a Rab4GTP-binding protein

A) Silver stained gel showing isolation of GST-Rab4-GTP γ S binding proteins from brain cytosol. Asterisk denotes band from which GRASP-1 was identified.

B) Western blot of samples from (A) probed with GRASP-1 antibody.

C) Binding assay of 35 S-labeled GRASP and immobilized GST-Rab proteins.

D) FLAG-tagged Rabs were co-expressed with myc-GRASP-1 in COS-7 cells. Anti-FLAG immunoprecipitates were analyzed by Western blot with myc antibody.

E) HeLa cells were transfected with GFP-Rab4, myc-GRASP-1 or both. Prior to fixation, cells were incubated for 60 min with Alexa594-labeled Tf at 37°C. Bar is 10 μ m.

F) Coiled-coil prediction and domain architecture of GRASP-1. Glu; glutamic acid rich domain, asterisk; caspase-3 cleavage site, GRIPBD; GRIP1 binding domain.

G) Binding domain analysis using lysates of COS-7 cells expressing myc-tagged GRASP-1 truncations, and GTP γ S-charged GST-Rab4.

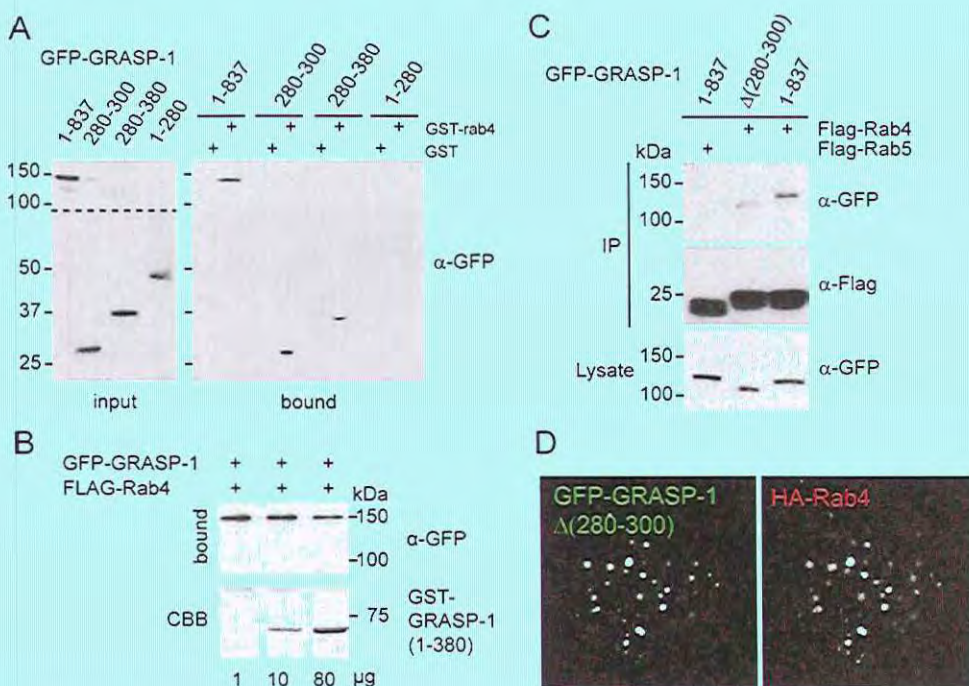


Figure 2. GRASP-1(280-300) interact with Rab4

A) Binding assay of GFP-GRASP-1 truncations and GST-rab4 showing that rab4 interacts with amino acid 280-300 of GRASP-1.

B) FLAG-Rab4-GRASP-1 complexes were isolated from COS-7 cell lysates on anti-FLAG antibody-coated beads and incubated for 1 hr with 1, 10 and 80 μg purified GST-GRASP-1(1-380). Immune complexes were eluted with 0.15 mg/ml FLAG peptide and analyzed by Western blot with monoclonal GFP antibody and polyclonal FLAG antibody. The amount of GFP-GRASP-1 on the beads remained relatively constant upon increasing the amount of competing GRASP-1 fragment containing the rab4 binding region.

C) FLAG-tagged Rabs were co-expressed with GFP-GRASP-1 constructs in COS-7 cells. Anti-FLAG immunoprecipitations were analyzed by Western blot with monoclonal GFP antibody. Note that GRASP-1 retained ~50% Rab4 binding after deletion of amino acid 280-300.

D) Image of cell body of a hippocampal neuron cotransfected at DIV13 for 2 days with GFP-GRASP-1(Δ280-300) and HA-Rab4 and labeled with anti-HA antibody (red).

However, unlike the positive control *cdc25*, GRASP-1 also did not exhibit noticeable GEF activity towards H-ras (Fig. 3B). GRASP-1 also failed to increase GTP-loading of H-Ras in vivo as measured in pull down assays with the recombinant ras binding domain of Raf-1, while the GEF Ras-GRP markedly enhanced the amount of H-Ras in the GTP state (Fig. 3C). In line with these results, careful sequence analysis of GRASP-1 did not reveal significant homology to any known rasGEF. Together these data suggest that GRASP-1 is not a rasGEF but a Rab4 effector.

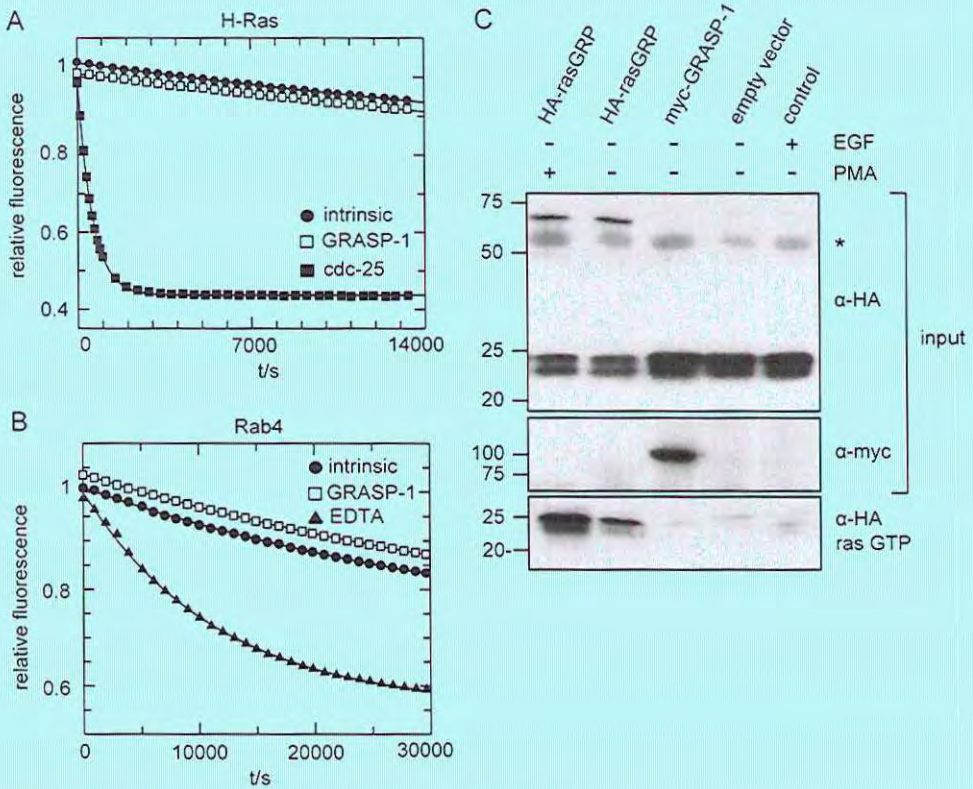


Figure 3. GRASP-1 does not have GEF activity on H-ras and Rab4

A-B) 200 nM H-ras or Rab4 loaded with fluorescent mantGDP was incubated with an excess of GDP at 25°C, in the absence or in the presence of GRASP-1(1-594), cdc-25, or EDTA, at the indicated concentrations. Dissociation of mGDP was monitored by measuring the decrease in relative fluorescence that accompanies release of mGDP from the GTPase.

C) COS-7 cells were transfected with HA-Hras in combination with indicated constructs and treated with or without EGF and PMA, respectively. Ras-GTP was isolated on GSH beads containing the ras binding domain of the ras effector raf and analyzed by Western blot with HA antibody. Note that GRASP-1 did not increase rasGTP level above non-transfected control. Asterisk (*) denotes background band.

GRASP-1 localizes to a sub-domain of Rab4-positive early recycling endosomes in neurons

We examined GRASP-1 expression in mouse tissues and cell lines and showed by Western blot that GRASP-1 is highly expressed throughout the central nervous system, including cortex, cerebellum, midbrain and spinal cord and in primary cultured hippocampal neurons but is absent in non-neuronal tissues and cell types with the exception of neuroendocrine insulinoma cells (Fig. 4A). These results are consistent with previous immunoblot and immunohistochemistry analyses (Ye et al., 2000), indicating that GRASP-1 is expressed in neurons throughout the CNS, with highest expression levels in the hippocampus. Double labeling confocal immunofluorescence on mouse brain and spinal cord sections, showed that GRASP-1 immunoreactivity was associated with punctate structures throughout the somato-dendritic compartment of neurons (Fig. 5). These punctate structures generally were immunoreactive for Rab4, although various GRASP-1 positive structures did not label for Rab4 and vice versa (Fig. 5).

Immunofluorescence labeling in mature hippocampal neurons (> days in vitro 17 (DIV 17)), revealed that endogenous GRASP-1, although present in axons, is predominantly localized within the somatodendritic compartment, as evidenced by its labeling pattern and the codistribution with the dendritic marker MAP2 (Fig. 4B). GRASP-1 is associated with punctate structures which occasionally extend beyond the dendritic shaft (arrowheads in Fig. 4C), overlap with the synaptic markers Bassoon (arrowheads in Fig. 4D) and PSD-95 (not shown) and localize within the dendritic spines visualized in β -galactosidase (β -gal) filled neurons (data not shown). In line with the mouse spinal cord and brain sections (Fig. 5), colocalization of endogenous Rab4 and GRASP-1 is observed in primary hippocampal neurons (Fig. 4E). Immunoelectron microscopy showed that endogenous GRASP-1 and Rab4 localize on an extensive tubular network that appeared to emanate from endosomes with a morphology that is characteristic of recycling tubules (Fig. 4F). The ability of GRASP-1 to associate with Rab4 positive endosomes was further confirmed by simultaneous dual color live imaging of mRFP-GRASP-1 and GFP-Rab4: GRASP-1 was observed on mobile Rab4-positive vesicles and tubular structures which dock and fuse with larger GRASP-1/Rab4 endosomal domains (Fig. 4G). Overexpression of GFP-Rab4 in hippocampal neurons increased the size of the endosomal structures where GRASP-1 and Rab4 coincide (Fig. 4H). Close inspection of these structures revealed that endogenous GRASP-1 localizes to a sub-domain of the large Rab4-positive endosome (Fig. 4H, inset), suggesting that GRASP-1 might regulate a particular step in the endosomal recycling pathway. To test whether endosomal GRASP-1 localization depends on Rab4 activity, neurons were transfected with dominant negative Rab4 (Rab4S22N). Expression of Rab4S22N redistributed GRASP-1 away from punctate endosomes, while other endosomal proteins were unaffected (Fig. 4I and Fig. 6). Together these data show that GRASP-1 is selectively expressed in neurons, where it is partially localized to Rab4-positive endosomes in dendrites and present in spines near postsynaptic structures.

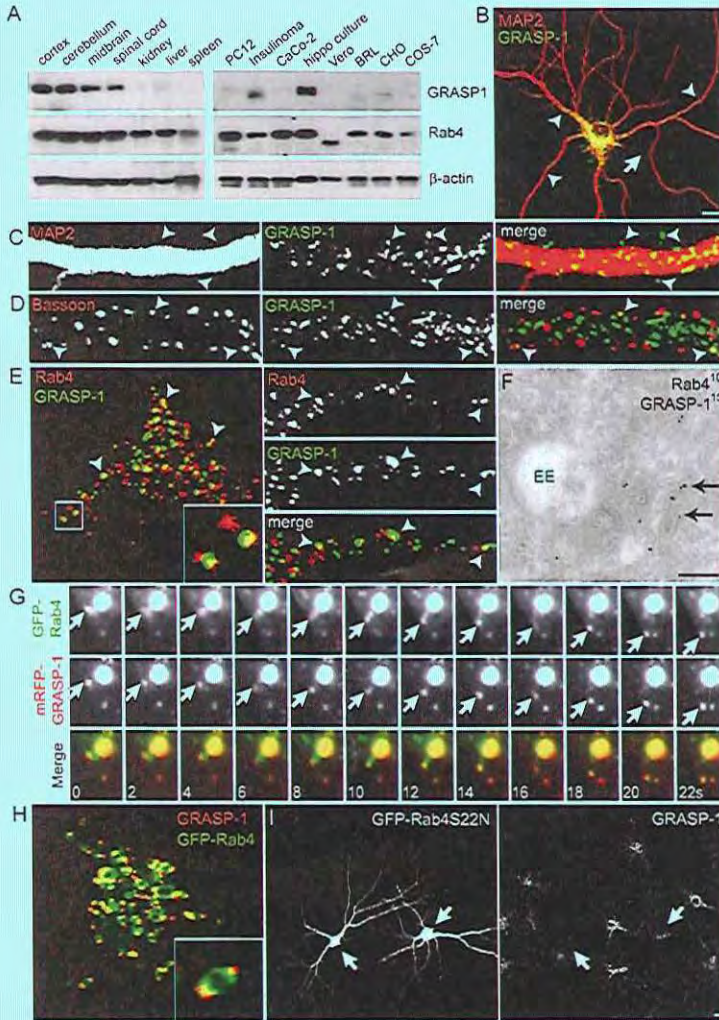


Figure 4. Colocalization of GRASP-1 and Rab4 in hippocampal neurons

A) Expression pattern of Rab4 and GRASP-1 in mouse tissue and cultured cells.

B-E) Representative images of hippocampal neurons double-labeled with antibodies against GRASP-1 and endogenous markers. B) MAP2 and GRASP-1, arrow denotes axon and arrowheads dendrites

C) MAP2 and GRASP-1, arrow heads mark GRASP-1 signal beyond the dendritic shaft. D) Bassoon and GRASP-1, arrowheads denote localization of GRASP-1 to synaptic sites. E) Rab4 and GRASP-1 in the cell body (left) and dendrites (right). Arrowheads denote areas of colocalization, inset show magnified regions. Bar is 10 μ m.

F) Immunogold EM of hippocampal neurons labeled with 10 nm protein A gold for endogenous Rab4 and with 15 nm protein A gold for GRASP-1. Arrow denotes tubular membrane to

which GRASP-1 and Rab4 colocalized. Scale bar is 100 nm.

G) Simultaneous imaging of GFP-Rab4 (green) and mRFP-GRASP-1 (red) in transfected hippocampal neurons. Successive frames are shown and time (seconds) is indicated in the merge panel.

H) Images of the cell body of hippocampal neurons transfected at DIV13 with GFP-Rab4 and stained for GRASP-1. Magnified region is shown as inset; note the partial localization of GRASP-1 on the distal domain of GFP-Rab4 endosomes.

I) Representative images of hippocampal neurons transfected at DIV13 with GFP-Rab4S22N and stained after 2 days for GRASP-1. Arrows indicates loss of GRASP-1 puncta in transfected neurons. Bar is 10 μ m.

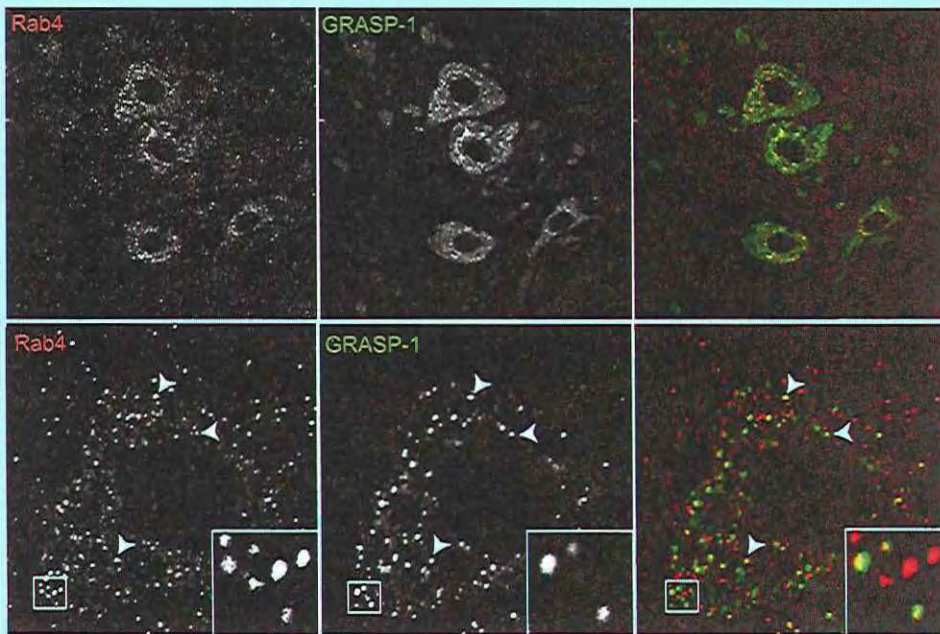


Figure 5. Colocalization of Rab4 and GRASP in vivo

Mouse spinal cord sections of 40 μm were double-labeled for endogenous GRASP-1 (green) and Rab4 (red). Sections were examined on a Zeiss LSM510 at low magnification to obtain the overview image (top row), or high magnification (bottom row). Arrow heads denote colocalization between GRASP-1 and Rab4 as also shown in the inset with merged colors.

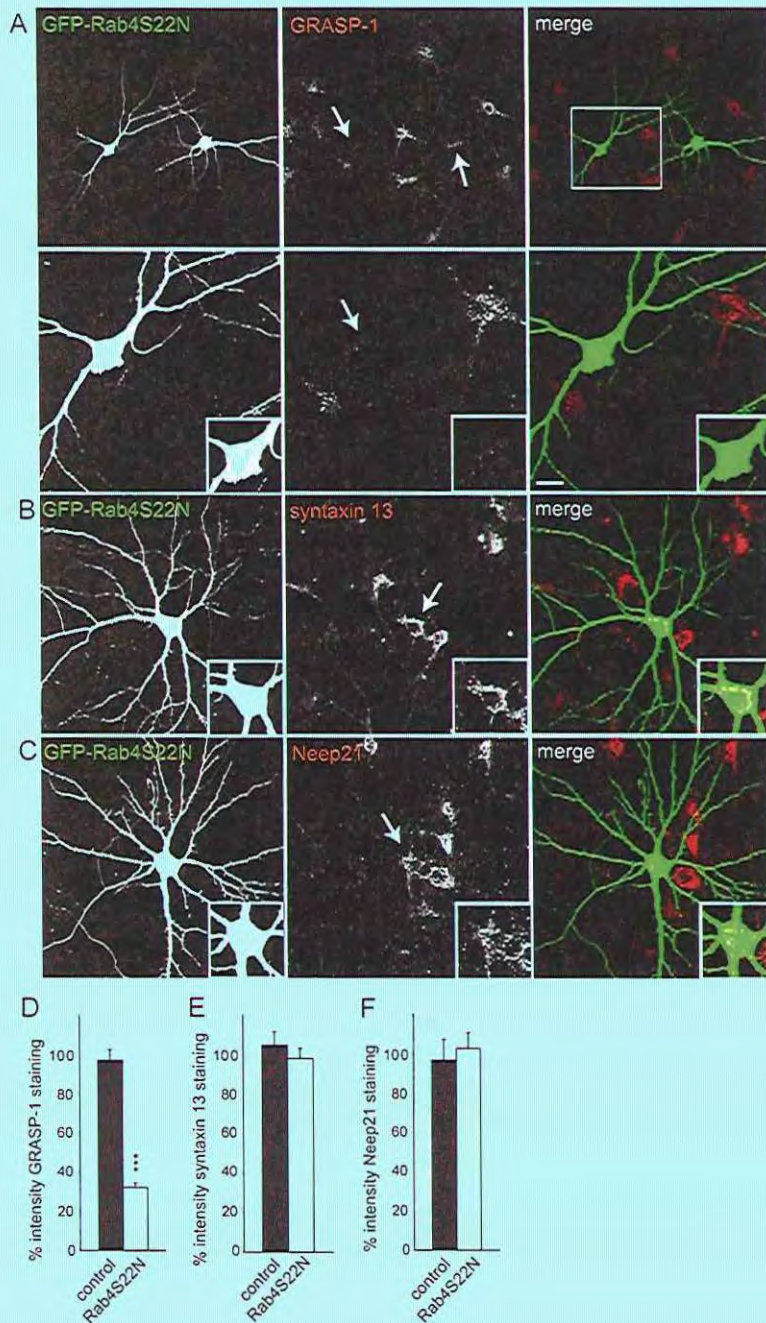


Figure 6. Rab4 dominant negative mutant affects GRASP-1 localization

A-C) Representative images of hippocampal neurons transfected with GDP-bound dominant negative mutant GFP-Rab4S22N at DIV13 for 2 days and stained for endogenous GRASP-1 (A), syntaxin 13 (B) or Neep21 (C). Note that in the neurons transfected with Rab4S22N almost no GRASP-1 puncta are present in somato-dendritic compartments while the localization of syntaxin 13 and Neep21 is unchanged. Bar is 10 μ m.

D-F) Quantification of GRASP-1 fluorescence intensities in cell body of hippocampal neurons transfected as indicated in A-C. Graphs show mean \pm SEM normalized to neighboring neurons. *** $p < 0.0005$

GRASP-1 is required for dendritic spine morphology

To explore the function of GRASP-1, we used RNA interference to knock down expression of GRASP-1 in mature hippocampal neurons. We found two independent GRASP-1-shRNA sequences (#2 and #5) that specifically inhibited expression of GRASP-1 in hippocampal neurons (Fig. 7). GRASP-1 antibodies detected more than ~80% reduction of GRASP-1 staining intensity in the cell body as well as in dendrites in GRASP-1-shRNA transfected neurons (Fig. 7), while other antibody staining, such as of MAP2 were unaffected (data not shown). Both GRASP-1-shRNAs constructs produced similar phenotypic effects.

In view of previous observations that inhibition of endosomal recycling by dominant negative forms of Rab4 and Rab11 alters the morphology of dendritic spines (Park et al., 2006) we first examined the effect of GRASP-1 knock-down on dendritic spines. In neurons co-expressing GRASP-1-shRNA and β -gal, we observed a marked decrease in the total number of protrusions (Fig. 8A). The remaining dendritic protrusions were classified as filopodia-shaped protrusions and mushroom-shaped spines based on the ratio of spine head width to protrusion length. Quantification revealed that knockdown of GRASP-1 decreased the number of mushroom-headed spines (Fig. 8B,C). Neurons expressing GRASP-1* (which is resistant to GRASP-1-shRNA#2 knockdown) largely reversed the spine phenotype (Fig. 8A-C). A similar spine phenotype was observed by expressing dominant negative forms of Rab11 (Rab11S25N) and Rab4 (Rab4S22N) (Fig. 8B,C). We next tested whether GRASP-1 knockdown could inhibit LTP-induced spine growth by glycine stimulation, a protocol used to induce chemical LTP in cultured hippocampal neurons (Park et al., 2006). In control neurons, glycine treatment induced new spine formation and preexisting spine growth while in the absence of GRASP-1 spine growth is blocked (Fig. 8D,E). Together these data indicate that GRASP-1 plays an essential role within the recycling endosomal pathway to maintain dendritic spine morphology and regulate LTP-induced spine growth.

GRASP-1 regulates recycling endosome distribution

To directly examine the effect of GRASP-1 knock-down on recycling endosomes into spines, we analyzed its localization with GFP-tagged transferrin receptor (GFP-TfR), which is an archetype recycling cargo that at steady state resides in recycling endosomes (Park et al., 2006). As expected GRASP-1 and GFP-TfR showed a strong colocalisation within dendrites (Fig. 8F). TfR-GFP-labeled endosomes were present in the dendritic shaft at the base of spines (a), in the spine neck (b) and in the spine head (c) (Fig. 8G). In neurons transfected with GRASP-1-shRNA, GFP-TfR labeled endosomes were abundantly present in the dendritic shaft at the base of spines but were depleted from the spines (Fig. 8H). Quantitative analysis revealed that in control neurons ~50% of the spines had TfR-GFP-labeled endosomes in their neck and head (b, c and b+c), whereas in the absence of GRASP-1 only ~10% of the spines contained recycling endosomes (Fig. 8G). These data show that GRASP-1 regulates recycling endosomal localization into dendritic spines and most likely explains the observed GRASP-1 knock down spine phenotype.

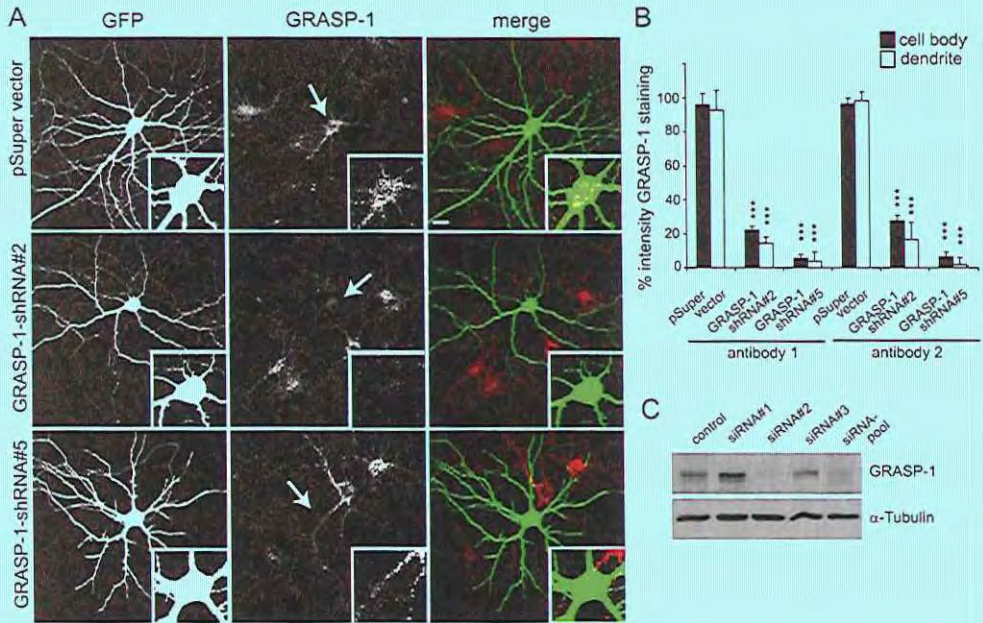


Figure 7. GRASP-1 shRNA suppresses expression of GRASP-1

A) Representative images of hippocampal neurons cotransfected at DIV13 with GFP and either pSuper, pSuper-GRASP-1-shRNA#2 or -shRNA#5, and visualized after 4 days with rabbit antibody against GRASP-1 (red) and GFP (green). Cell body (inset) is enlarged to show loss of GRASP-1 immunoreactivity in GRASP-1-shRNA transfected neurons. Bar is 10 μ m.

B) Quantification of GRASP-1 fluorescence intensities in cell body and dendrites of hippocampal neurons transfected at DIV13 for 4 days with GFP and either pSuper, pSuper-GRASP-1-shRNA#2 or -shRNA#5. Staining was done with two distinct rabbit anti-GRASP-1 antibodies; clone JH 2730 and AB96361. Graph shows mean \pm SEM normalized to pSuper control neurons. *** $p < 0.0005$

C) Western blot of lysates prepared from INS-1 cells transfected with 100 nM (final concentration) of three siRNAs (Ambion), a smartpool (Dharmacon) or control scrambled siRNA (Dharmacon) for 3 days. siRNA#2 and the smartpool reduced GRASP-1 expression to 15% and 23%, respectively.

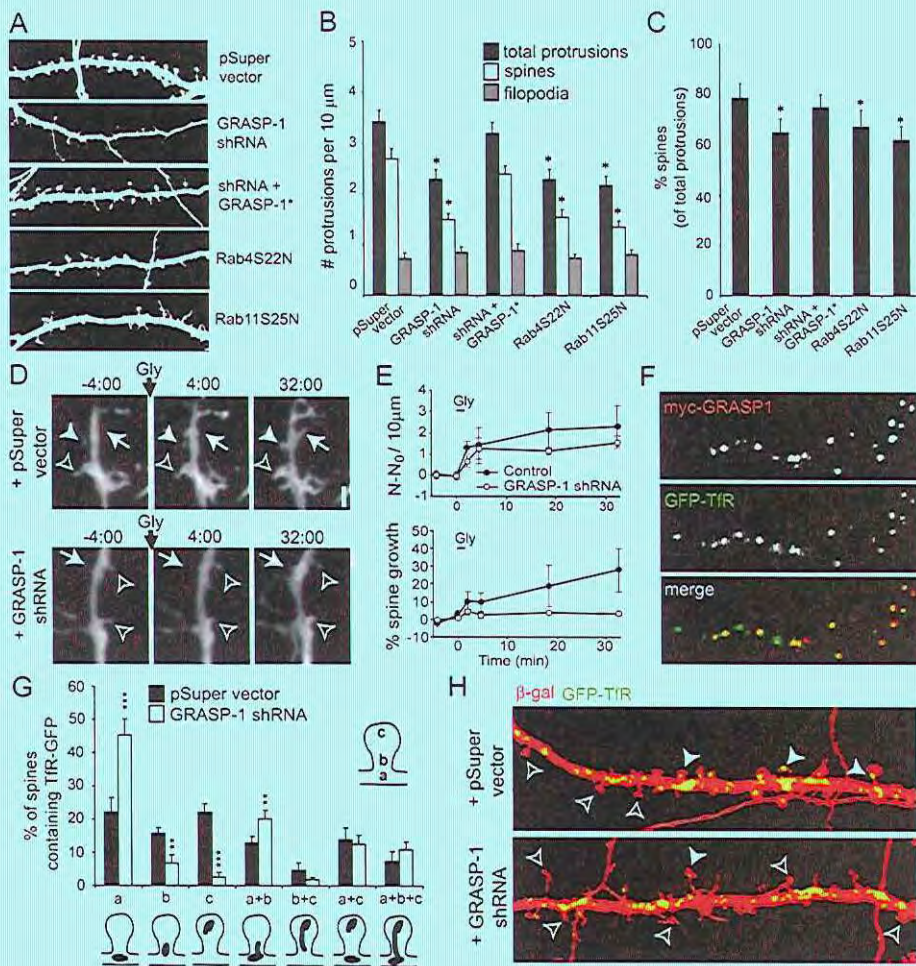


Figure 8. GRASP-1 is required for the maintenance of dendritic spines

A) Representative high magnification images of dendrites of hippocampal neurons co-transfected at DIV13 for 4 days with β -galactosidase (to mark the dendrites), and either pSuper, pSuper-GRASP-1-shRNA#2, GRASP-1-shRNA#2 and GFP-GRASP-1*, Rab4S22N or Rab11S25N, and labeled with anti- β -galactosidase.
B) Quantification of number of protrusions per 10 μm dendrites in hippocampal neurons transfected as indicated in (A).
C) Percentage of spines of hippocampal neurons transfected as indicated in (A).
D) Neurons expressing GFP (to mark the dendrite), and either pSuper or pSuper-GRASP-1-shRNA#2 were stimulated with glycine (200 mM, 3 min), and then imaged for >30 min after glycine stimulation. Arrows indicated spine formation. Closed and open arrow heads spine growth and stable protrusions, respectively
E) Quantification of the spine formation (top) and spine growth (bottom) following glycine stimulation. N_t , number of dendritic protrusions per 10 μm at the indicated time. N_0 indicates the average of spine areas before application of glycine. Glycine-stimulated preexisting spine growth is blocked by GRASP-1-shRNA#2 (bottom).
F) High magnification images of dendrites of hippocampal neurons cotransfected at DIV13 for 4 days with myc-GRASP-1 (red) and GFP-TjR.
G,H) Percentage of spines containing TjR-GFP positive endosomes at the indicated locations. Hippocampal neurons were co-transfected at DIV13 for 4 days with β -galactosidase (to mark dendrites) and GFP-TjR (to mark endosomes) and pSuper control vector or pSuper-GRASP-1-shRNA#2 as shown in (H). Closed and open arrow heads denote protrusions with and without GFP-TjR marked endosomes in the spine head, respectively. Error bars indicate S.E.M. ** $p < 0.005$. *** $p < 0.0005$.

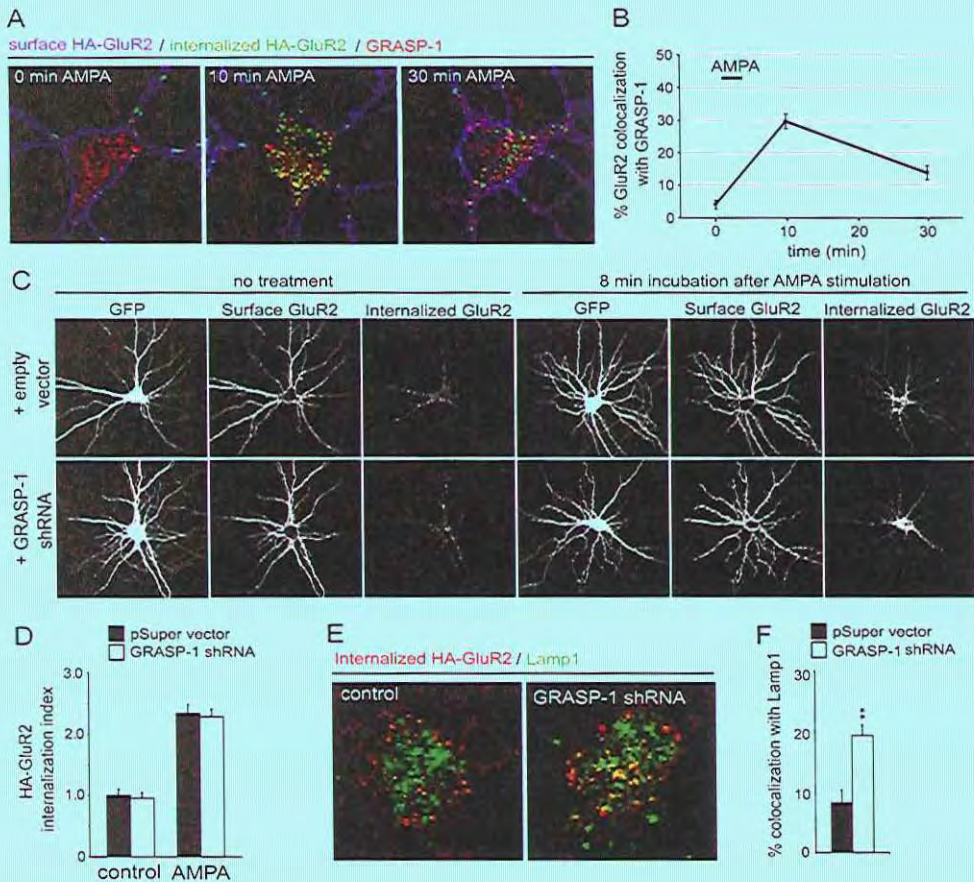


Figure 9. Internalized HA-GluR2 colocalizes with GRASP-1

- A*) Representative merge image of surface HA-GluR2 (blue) and internalized HA-GluR2 (green) in soma and dendrites of hippocampal neurons labeled for GRASP-1 (red) after 0, 10 and 30 minutes 100 μ M AMPA plus 50 μ M APV (AMPA) stimulation.
- B*) Quantification of the percentage of colocalization of internalized GluR2 with GRASP1 after AMPA/APV treatment at different time points. Each data point represents mean \pm S.E.M. (5 neurons for each time point).
- C*) Representative images of neurons triple transfected at DIV13 with GFP and HA-GluR2 and either pSuper control vector or pSuper-GRASP-1-shRNA#2. After 4 days, neurons are "live" labeled with anti-HA antibody for 15 min, followed by 10 min incubation in conditioned medium (Control, no treatment) or 2 min incubation in conditioned medium containing 100 μ M AMPA plus 50 μ M APV (AMPA) followed by additional 8 min in conditioned medium. The neurons are stained for surface and internalized HA-GluR2.
- D*) Quantification of intracellular accumulation assays, measured as the ratio of internalized/surface fluorescence (internalization index), normalized to GluR2 10 min control (no treatment). Graph shows mean \pm S.E.M. (10 neurons for each condition).
- E*) Representative merge images of neurons cotransfected at DIV13 with HA-GluR2 and either pSuper control vector or pSuper-GRASP-1-shRNA#2 and stained for internalized HA-GluR2 (red) and lysosomal marker Lamp1 (green) in the cell body after stimulation for 30 min with AMPA.
- F*) Quantification of the percentage of colocalization of internalized GluR2 with Lamp1 as indicated in E). Graph shows mean \pm S.E.M. (5 neurons each). ** $p < 0.005$

GRASP-1 regulates AMPAR recycling

To further explore the functional importance of GRASP-1 in endosomal recycling we studied the effect of GRASP-1 knock-down on endocytic trafficking of AMPAR. First, we analyzed GRASP-1 colocalization with internalized AMPARs by using the fluorescence-based antibody feeding assay (Lee et al., 2004). Live hippocampal neurons expressing extracellular HA-tagged GluR1 or GluR2 subunits were surface labeled with HA antibody, stimulated with AMPA (100 μ M, in the presence of 50 μ M APV), fixed, permeabilized and stained for internalized GluR subunits and endogenous GRASP-1. At 2 minutes after AMPA stimulation, only ~5% of internalized HA-GluR1 or HA-GluR2 colocalized with GRASP-1 (Fig. 9A,B). After 10 minutes following stimulation colocalization between internalized GluR subunits with GRASP-1 was increased to ~30% (Fig. 10A, Fig. 9A,B), which is consistent with the kinetics of internalized AMPAR colocalization with Rab4 (Ehlers, 2000).

Next, we transfected hippocampal neurons either with GFP and control vector or GFP with GRASP-1-shRNA and analyzed internalization and recycling of endogenous AMPAR following AMPA stimulation by immunolabeling for surface GluR1 and GluR2. At steady state, GRASP-1 knock down neurons showed a modest but significant reduction (~15%) in surface labeling for GluR1 (Fig. 10B, D) and GluR2 (Fig. 10C, E) compared to controls. After 10 minutes stimulation, GluR1 and GluR2 decreased at the neuronal surface in both control and GRASP-1 shRNA expressing neurons, reflecting receptor internalization (Fig. 10B,C). At 60 min, reappearance of both GluR1 and GluR2 was strongly impaired (~50%) by GRASP-1 shRNA compared to controls (Fig. 10B-E). Consistently, in a protocol where surface HA-GluR2 receptors were stripped away after labeling (Lu and Ziff, 2005), recycling of HA-GluR2 back to the surface was significantly decreased in neurons expressing GRASP-1-shRNA compared to control neurons (Fig. 10F). No difference was observed in the level of intracellular HA-GluR2 after 8 min AMPA stimulation (Fig. 9C,D). However, we observed that in GRASP-1 knockdown neurons more intracellular HA-GluR2 is present in LAMP-1 positive lysosomal compartments after AMPA treatment (Fig. 9E,F). These data show that GRASP-1 is important for activity-induced AMPAR recycling.

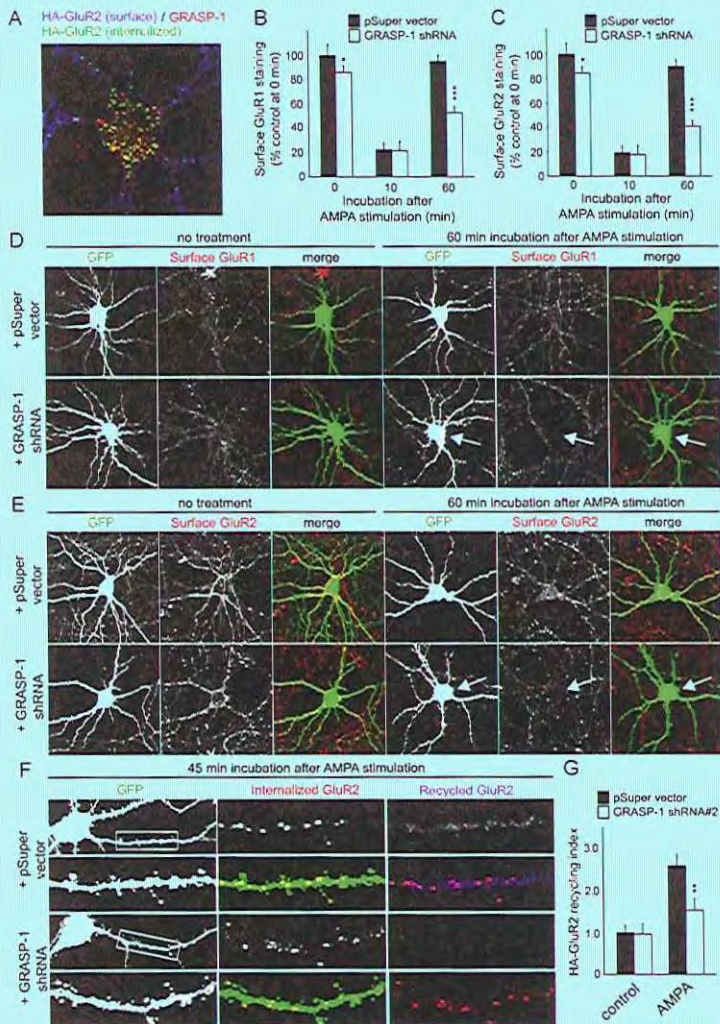


Figure 10. Knock down of GRASP-1 reduces AMPAR recycling

A) Representative merge image of surface HA-GluR2 (blue) and internalized HA-GluR2 (green) in soma and dendrites of hippocampal neurons labeled for GRASP-1 (red) after 10 minutes AMPA stimulation.

B,C) Quantification of the surface fluorescence intensities of endogenous GluR1 (*B*) and GluR2 (*C*) in control pSuper vector or GRASP-1-shRNA#2 transfected neurons. The cells were untreated (0 min) or stimulated with AMPA for indicated times. Histograms show fluorescent intensity of surface GluR subunit staining relative to the intensity of GFP transfected control neurons at basal levels. $n = 20$ cells for each group.

D,E) Representative images of hippocampal neurons stained for endogenous surface GluR1 (*D*) and GluR2 (*E*). Hippocampal neurons at DIV13 were cotransfected with GFP and pSuper control vector or GRASP-1-shRNA#2. At DIV17, neurons were fixed (0 min, no treatment), or stimulated for 2 min with 100 μ M AMPA in the presence of 50 μ M APV and further incubated for a total of 10 or 60 min before fixation. Endogenous surface GluR1 (*D*) or GluR2 (*E*) was revealed by immunofluorescence labeling without permeabilization using specific extracellular AMPAR antibodies.

F) Neurons transfected with GFP, HA-GluR2 and either pSuper control vector or GRASP-1-shRNA#2 were stained live with an anti-HA antibody, stimulated for 2 min with AMPA/APV, acid stripped and incubated in conditioned media for 45 min. Recycled HA-GluR2 (blue) and internalized HA-GluR2 (red) were sequentially labeled.

G) Quantification of the ratio of recycled to internalized HA-GluR2 in neurons as indicated in (*F*). Error bars indicate S.E.M. * $p < 0.05$, ** $p < 0.005$, *** $p < 0.0005$.

GRASP-1 regulates synaptic plasticity

Next we examined the role of GRASP-1 in excitatory transmission and LTP and recorded excitatory synaptic responses from CA1 pyramidal neurons in organotypic cultures of hippocampal slices. Simultaneous recordings were obtained from both transfected neurons (identified by cotransfected GFP) and a neighboring untransfected neuron. Both control luciferase-shRNA and GRASP-1-shRNA expressing cells had no effect on basal AMPAR-mediated excitatory postsynaptic currents (EPSCs) (GRASP-1 shRNA#5: 0.93 ± 0.09 -fold relative to untransfected cells, luciferase shRNA: 1.21 ± 0.18) and NMDAR-EPSCs (GRASP-1 shRNA#5: 0.86 ± 0.09 -fold, luciferase shRNA: 1.03 ± 0.32) (Fig. 11A, B). The importance of GRASP-1-mediated AMPAR recycling in slices became more evident by testing for synaptic plasticity. After induction of LTP, cells expressing GRASP-1 shRNA induced comparable levels of potentiation to that of neighboring untransfected cells up to 20 min after the LTP induction protocol. Subsequently, however, the response from GRASP-1 shRNA transfected cells started to fall and eventually returned to the baseline level at 30 min after LTP induction (Fig. 11C, untransfected neuron: 1.75 ± 0.18 -fold enhancement of EPSC at 29-30 min after LTP induction, transfected neuron: 1.17 ± 0.10). In contrast, control luciferase shRNA transfected, and neighboring untransfected neurons expressed stable LTP lasting for at least 30 min (Fig. 11D, untransfected neuron: 2.04 ± 0.16 -fold enhancement of EPSC, transfected neuron: 2.45 ± 0.44). These data indicate that GRASP-1 is important for synaptic plasticity and particularly for the phase of LTP after the first 20 min. The results suggest that delivery of AMPAR from recycling endosomes might be important for this later phase of LTP.

GRASP-1 segregates Rab4 from EEA1/Neep21 endosomal membranes

To define more precisely the function of GRASP-1 within the endosomal system we first examined the localization of exogenous GRASP-1 with respect to early endosomal marker proteins in HeLa cells. We found little if any co-distribution with GFP-Rab5, but extensive colocalization with GFP-Rab4 (Fig. 12). The same results were obtained in transfected hippocampal neurons, where $> 80\%$ of Rab4 structures contained GRASP-1 both in dendrites and the cell body, while little overlap was seen with Rab5 (Fig. 13A,B, 14). In agreement with this observation, the Rab5 domain marker EEA1 and endogenous GRASP-1 displayed mutually exclusive distributions (Fig. 13D), whereas $\sim 40\%$ of EEA1 structures in the cell body and dendrites colocalized with GFP-Rab4 (Fig. 13C,E top row). These results suggested that Rab4 in neurons is interfaced between a proximal EEA1 and distal GRASP-1 endosomal domain. To determine whether the endosomal domain organization is regulated by GRASP-1, we knock down the expression of GRASP-1 and then assayed the co-distribution of EEA1 and GFP-Rab4. Hippocampal neurons transfected with GRASP-1-shRNA showed a strong increase in colocalized EEA1 and GFP-Rab4 ($\sim 80\%$) compared to control neurons ($\sim 40\%$) (Fig. 13C,E). In contrast, in neurons transfected with myc-GRASP-1 the overlap between EEA1 and GFP-Rab4 was significantly decreased ($\sim 20\%$) (Fig. 13C,E). Similar results were obtained in HeLa cells, where myc-GRASP-1 strongly reduced colocalization between GFP-Rab4 and EEA1, while the co-distribution of GFP-Rab5 and EEA1 was not affected (Fig. 15). To confirm our results we tested the effect of GRASP-1 on the localization of other early endosomal markers, such as Neep21 (Steiner et al., 2002).

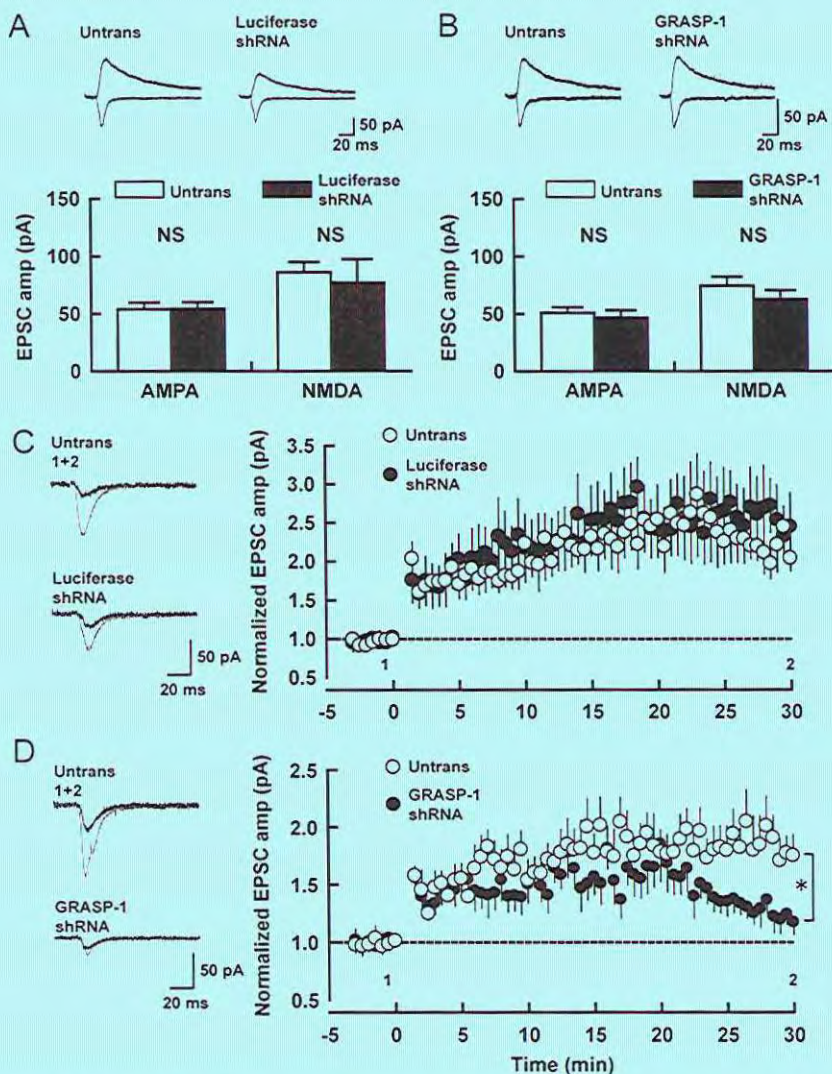
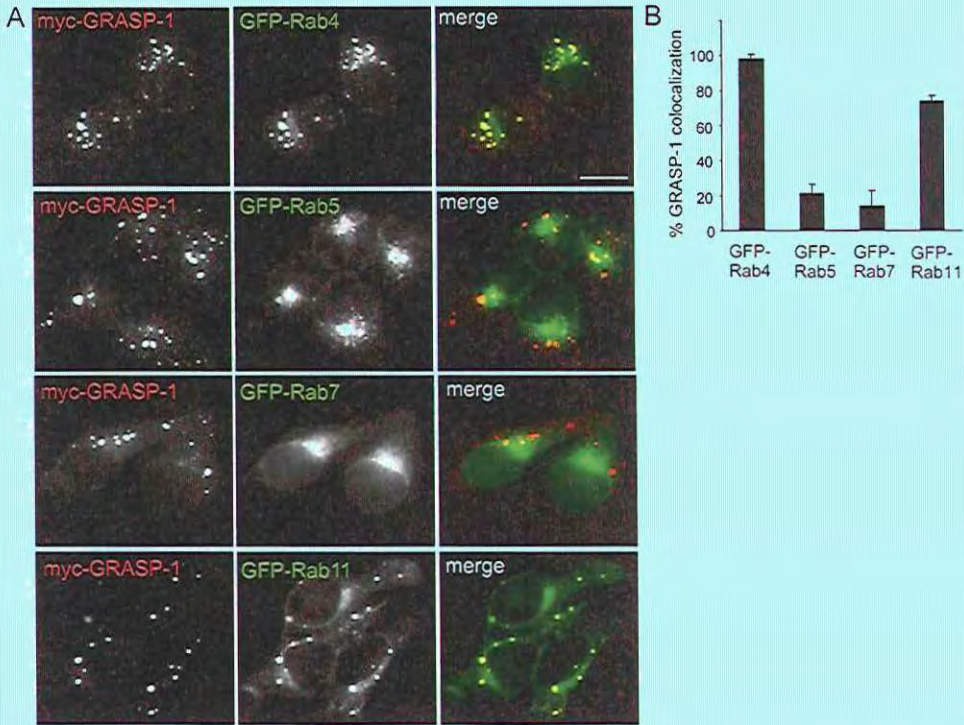


Figure 11. Effect of GRASP-1 knock down on synaptic transmission and plasticity in hippocampal slice

A,B) AMPA and NMDA receptor-mediated excitatory synaptic responses were measured from neurons transfected with Luciferase-shRNA (*A*, control), and GRASP-1-shRNA#5 (*B*). Top, sample traces mediated by AMPAR (downward) and NMDAR (upward) from pairs of shRNA transfected (Luciferase or GRASP-1-shRNA#5) and neighboring untransfected (Untrans) neurons. Stimulus artifacts were truncated from the traces. Bottom, summary graphs of EPSC amplitudes (AMPA-R-EPSCs and NMDA-R-EPSCs) from shRNA transfected and neighboring untransfected cells. Number of cell pairs: Luciferase-shRNA, 18 and 10; GRASP-1-shRNA#5, 15 and 8 for AMPA and NMDAR-EPSC. NS, not significant. Error bars indicate S.E.M.

C,D) LTP was induced in shRNAs expressing and neighboring untransfected cells by pairing depolarization to 0 mV with 2Hz stimulation for 100s. Left, sample AMPAR-EPSC traces from untransfected and Luciferase or GRASP-1 shRNA transfected neurons. Currents before (black) and after (gray) are superimposed. Right, time course of AMPA-EPSCs after LTP induction (LTP was induced at $t = 0$). The time points at which sample traces were obtained are indicated by 1 and 2. Number of cell pairs: Luciferase-shRNA, 6; GRASP-1-shRNA#5, 8. * $p < 0.05$.



GRASP-1 regulates endosome recycling

Figure 12. GRASP-1 colocalizes with Rab4 and Rab11

A) Hela cells co-transfected with myc-GRASP-1 and GFP-Rab4, GFP-Rab5, GFP-Rab7 or GFP-Rab11. Bar is 10 μ m.

B) Percentage of colocalization between GRASP-1 and Rab proteins in Hela cells as indicated in (A).

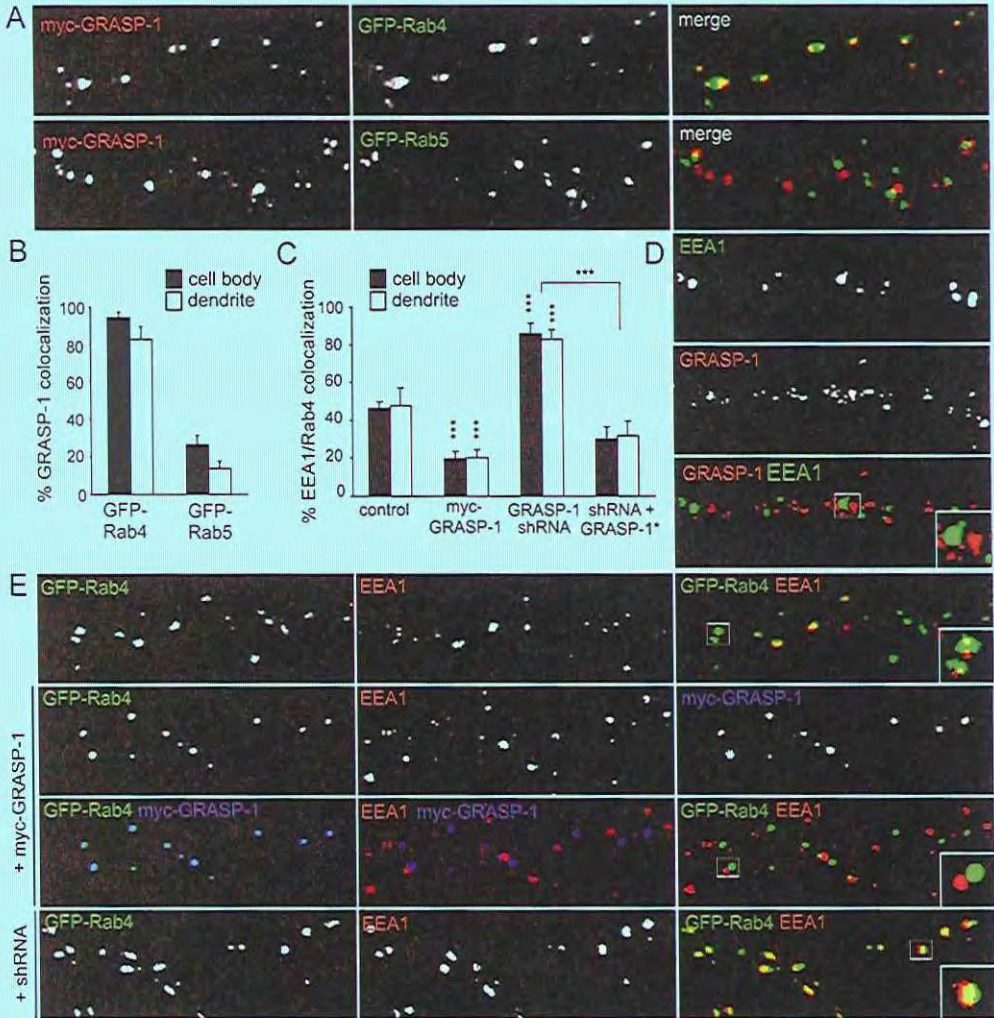


Figure 13. GRASP-1 segregates Rab4 from EEA1 positive endosomal membranes

A) Representative images of dendrites of hippocampal neurons cotransfected at DIV13 for 4 days with myc-GRASP-1 (red) and either GFP-Rab4 (upper row) or GFP-Rab5 (bottom row).

B) Percentage of colocalization between myc-GRASP-1 and Rab proteins in neurons as indicated in (*A*).

C) Percentage of Rab4 and EEA1 colocalization in cell body and dendrites as indicated in (*E*). Error bars indicate S.E.M. *** $p < 0.0005$.

D) Representative images of dendrites of hippocampal neurons double-labeled with anti-GRASP-1 (red) and anti-EEA1 (green) antibodies.

E) Representative images of dendrites of hippocampal neurons cotransfected at DIV13 for 4 days with GFP-Rab4 and pSuper control vector, myc-GRASP-1 or pSuper-GRASP-1-shRNA#2 and labeled with anti-EEA1 (red) and anti-myc (blue) antibodies.

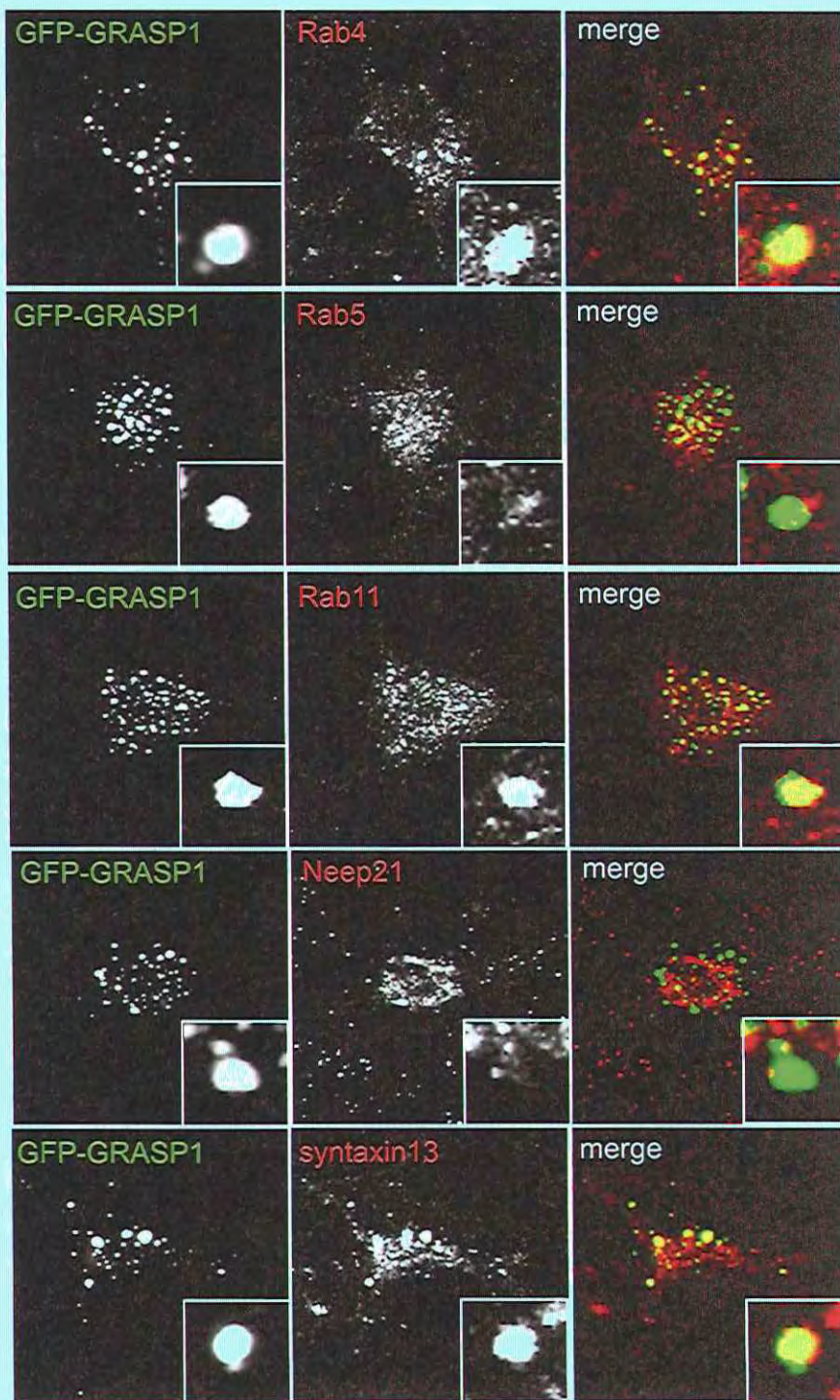


Figure 14. The effect of GRASP-1 expression on endogenous endosomal markers
Representative images of cell bodies of hippocampal neurons transfected with GFP-GRASP-1 and labeled with anti-Rab4, anti-Rab5, anti-Rab11, anti-NEEP21 or anti-syntaxin 13 antibodies (all red).

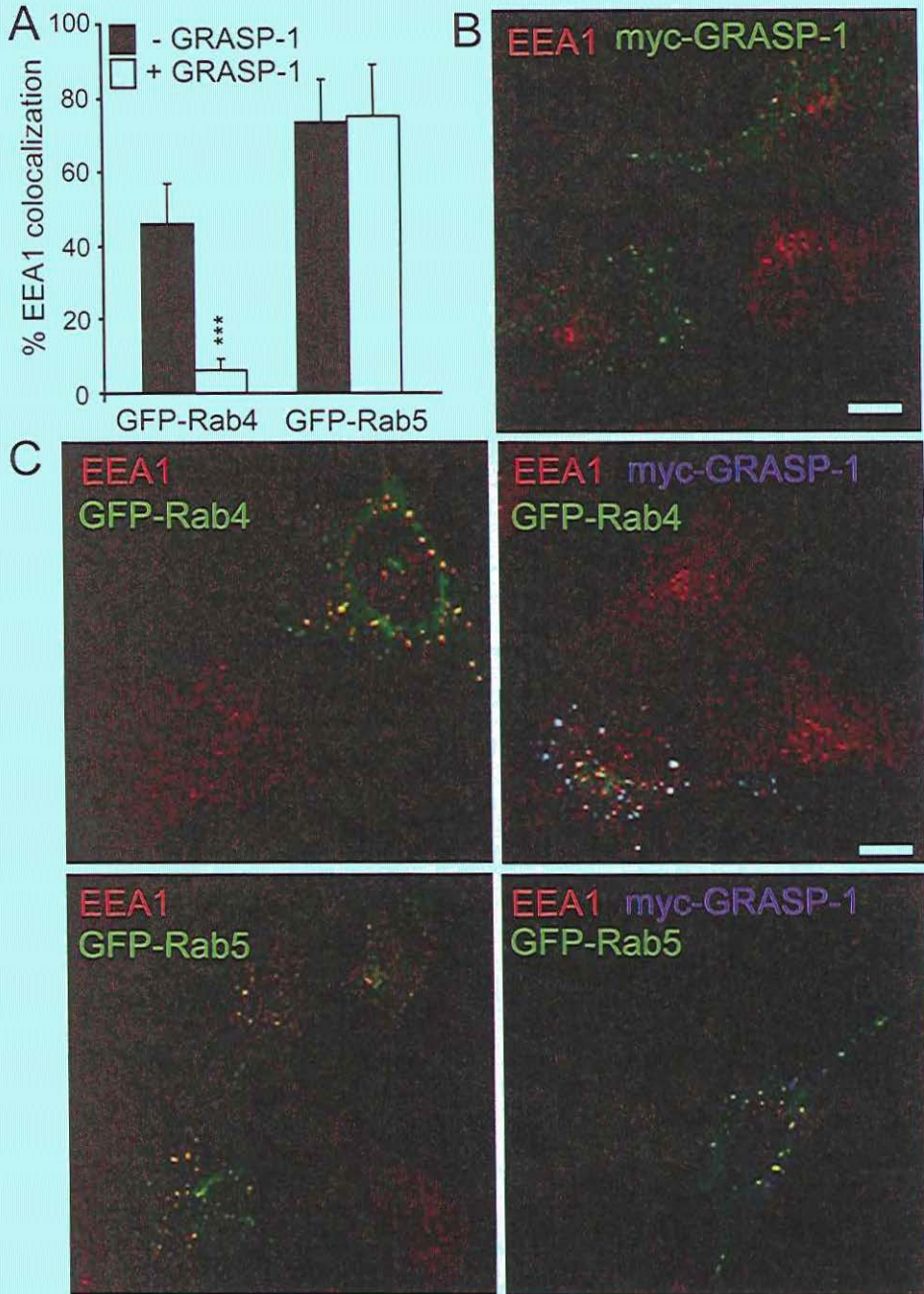


Figure 15. GRASP-1 regulates EEA1 distribution in HeLa cells

A) Percentage of colocalization between EEA1 and Rab4 or Rab5 in HeLa cells with and without transfected myc-GRASP-1 as shown in (B,C). Error bars indicate S.E.M. *** $p < 0.0005$.

B) HeLa cells transfected with myc-GRASP-1 and double labeled with anti-EEA1 (red) and anti-myc (green) antibodies.

C) HeLa cells co-transfected with GFP-Rab4 or GFP-Rab5 with and without myc-GRASP-1. Cells were labeled with anti-EEA1 (red) and anti-myc (blue) antibodies. Bar is 10 μ m.

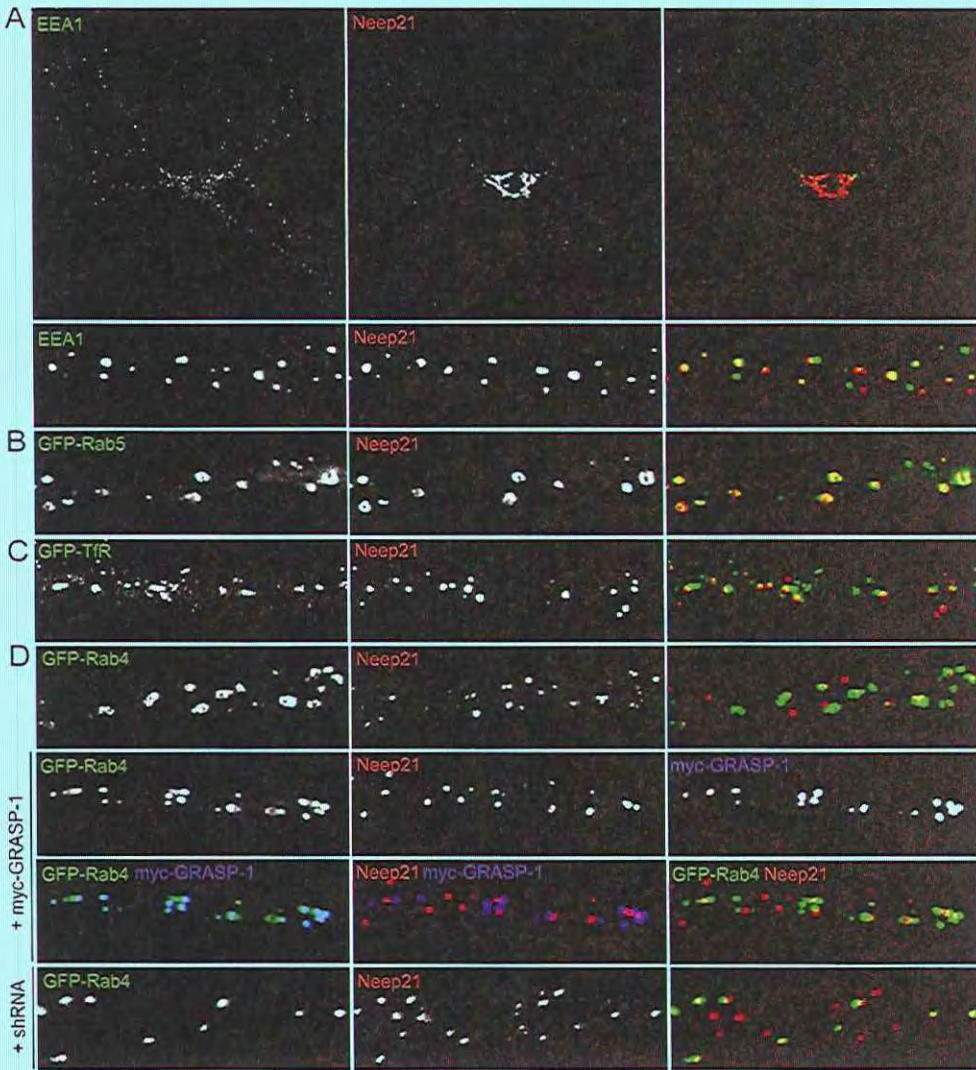


Figure 16. GRASP-1 segregates Rab4 from NEEP21 positive endosomal membranes

A) Representative images of hippocampal neurons double labeled with anti-EEA1 (green) and anti-NEEP21 (red) antibodies. Dendritic segments are enlarged to show the distribution of the markers (bottom).

B, C) Representative images of dendrites of hippocampal neurons cotransfected at DIV13 for 4 days with GFP-Rab5 (*B*) or GFP-TfR (*C*) and labeled with anti-NEEP21 (red).

D) Representative images of dendrites of hippocampal neurons cotransfected at DIV13 for 4 days with GFP-Rab4 and pSuper control vector, myc-GRASP-1 or pSuper-GRASP-1-shRNA#2 and labeled with anti-NEEP21 (red) and anti-myc (blue) antibodies.

Endogenous Neep21 staining strongly coincides with Rab5 and EEA1 (~80%) and to a lesser extent with Rab4 (~40%) (Fig. 16 and data not shown). However in neurons transfected with myc-GRASP-1 the overlap between Neep21 and GFP-Rab4 was significantly reduced (~20%), consistent with the effect on EEA1 distribution (Fig. 16D). In contrast, GRASP-1-shRNA enhances Neep21/Rab4 colocalization (Fig. 16D). Together these results suggest that GRASP-1 is able to separate Rab4 from EEA1/Neep21 endosomal domains.

GRASP-1 regulates the coupling between Rab4 and Rab11 domains

We next determined GRASP-1 localization with respect to late and recycling endosomal markers in HeLa cells (Fig. 12) and hippocampal neurons (Fig. 17A). We found little GRASP-1 colocalization with the Rab7 endosomal domains whereas GRASP-1 labeling coincided extensively with Rab11-positive compartments (~70%) (Fig. 17A,C, 12). These data strongly suggest that GRASP-1 is localized to distal aspects of the endosomal recycling pathway and might serve to couple Rab4 and Rab11 domains. This observation was confirmed by simultaneous dual color live imaging of mRFP-GRASP-1 and GFP-Rab11: GRASP-1 and Rab11 colocalize on larger endosomal domains while dynamic Rab11-positive structures segregate into distinct tubular or vesicular structures (Fig. 17B). Most motile Rab11-positive tubules only transiently overlap with GRASP-1-positive endosomes. Rab4, Rab11 and GRASP-1 largely localized to overlapping regions on these large endosomal structures in the neuronal cell bodies and dendrites (Fig. 17E). We further explored a possible role for GRASP-1 in coupling Rab4 and Rab11 domains by determining the Rab4/Rab11 co-distribution when GRASP-1 was knocked down as well as after overexpression of myc-GRASP-1. In absence of GRASP-1 we observed a significant decreased Rab4/Rab11 colocalization (15%), compared to control neurons (30% Rab4/Rab11 colocalization). While transfected myc-GRASP-1 robustly enhanced the coalescence of Rab4 and Rab11 domains (80% Rab4/Rab11 colocalization) (Fig. 17D,F). Importantly, the observed decrease in EEA1/Rab4 and Neep21/Rab4 domain coupling after myc-GRASP-1 transfection (Fig. 13C,E) is consistent with an increase in Rab4/Rab11 domain coupling, while the reverse occurred after GRASP-1 knock down. These data therefore show that GRASP-1 is a positive regulator of endosomal recycling membrane maturation, via coupling of Rab4- and Rab11-positive endosomal domains.

Syntaxin 13 binds to GRASP-1 and connects recycling endosomal domains

GRASP-1 colocalized with endogenous Rab11 (Fig. 14) and GFP-Rab11 (Fig. 17A) in neurons, however did not directly bind to Rab11 (Fig. 1C). These observations suggest a crosstalk between GRASP-1 and other proteins on Rab11 endosomal domains in hippocampal neurons. One of these candidate proteins is the SNARE syntaxin 13, a transmembrane domain protein that localizes to Rab11 positive tubular recycling endosomes (Park et al., 2006; Prekeris et al., 1998) and is important for AMPAR recycling, spine morphology and endosomal mobility (Park et al., 2006; Trischler et al., 1999). We investigated the possible interaction between GRASP-1 and syntaxin 13 by co-immunoprecipitation experiments from COS-7 cells transfected with GFP-GRASP-1 and different myc-syntaxin constructs. GFP-GRASP-1 precipitated syntaxin 13 and not myc-syntaxin 1 and myc-syntaxin 2 (Fig. 18A). Consistent, GRASP-1 colocalized with syntaxin 13 (Fig. 18D,J) and not with syntaxin 1 (Fig. 18J, 19B, 20A). Moreover, overexpression of GRASP-1 strongly accumulates syntaxin 13 in GRASP-1/Rab4/Rab11

positive structures in neurons (Fig. 18C, 14, S19A) and HeLa cells (Fig. 20A,B). Immunogold EM of neurons revealed that syntaxin 13 colocalized with GRASP-1 (Fig. 18E) and with Rab4 (Fig. 18F) on endosomal tubulovesicular recycling structures, reminiscent of the rab4-GRASP-1 organelles (Fig. 4F), suggesting that these proteins might be engaged in a complex on endosomal membranes. Indeed, myc-syntaxin 13 could be isolated from COS-7 lysates on GST-rab4 beads, only if GRASP-1 was co-transfected (Fig. 19C). The interaction required the PDZ-like domain containing C-terminal region of GRASP-1, but not the N-terminal Rab4 binding domain (Fig. 18B, Fig. 20C,D) and could be recapitulated with purified GST-syntaxin 13 and ³⁵S-labeled GRASP-1 (Fig. 19D). Since syntaxin 13 has a transmembrane domain it could be an anchor for GRASP-1 on endosomal membranes. In accord, the C-terminal part of GRASP-1 is necessary for the localization of GRASP-1 to TfR containing endosomes (Fig. 21). However, GRASP-C alone is not sufficient for GRASP-1 membrane localization since the Rab4 binding domain is also required (Fig. 21).

Previously, syntaxin 13 was found in a complex with early endosomal protein Neep21 (Steiner et al., 2002). To better understand the role of syntaxin 13 in both early and recycling endosomes, we first investigated the distribution of syntaxin 13 in dendrites of hippocampal neurons and found ~40% overlap between Neep21 and syntaxin 13 (Fig. 18H,K), ~40% colocalization between GRASP-1 and endogenous syntaxin 13 (Fig. 18D, Fig. 14), while no co-distribution of Neep21 with GRASP-1 was observed (Fig. 18G, Fig. 6). These data suggest that GRASP-1/syntaxin 13 and Neep21/syntaxin 13 are associated with distinct endosomal structures. Since expression of GFP-GRASP-1 strongly accumulates endogenous syntaxin 13 in the cell body and dendrites without recruiting Neep21 (Fig. 14), we examined whether GRASP-1 influences the Neep21/syntaxin 13 complex. Overexpression of GRASP-1 strongly reduced the colocalization between syntaxin 13 and Neep21 (~15%) compared to control neurons (~40%) (Fig. 18H,K), suggesting that GRASP-1 competes with Neep21 for binding to syntaxin 13 thereby affecting the integrity of the Neep21/syntaxin 13 complex. These data are consistent with the observation that GRASP-1 separates Rab4 from Neep21 endosomal domains.

To evaluate whether syntaxin 13 is important for GRASP-1 association with Rab11 domains, we triple transfected GFP-Rab4, HA-Rab11 and a myc-tagged dominant negative syntaxin 13 Δ TM mutant lacking the transmembrane domain. Hippocampal neurons transfected with syntaxin 13 Δ TM showed a strong decrease in Rab4/Rab11 colocalization (~10%) compared to control neurons (~30%) (Fig. 18I,L), while the co-distribution of Rab4 and GRASP-1 was not affected (data not shown). These data indicate that syntaxin 13 regulates Rab4/GRASP-1 association with Rab11 endosomes.

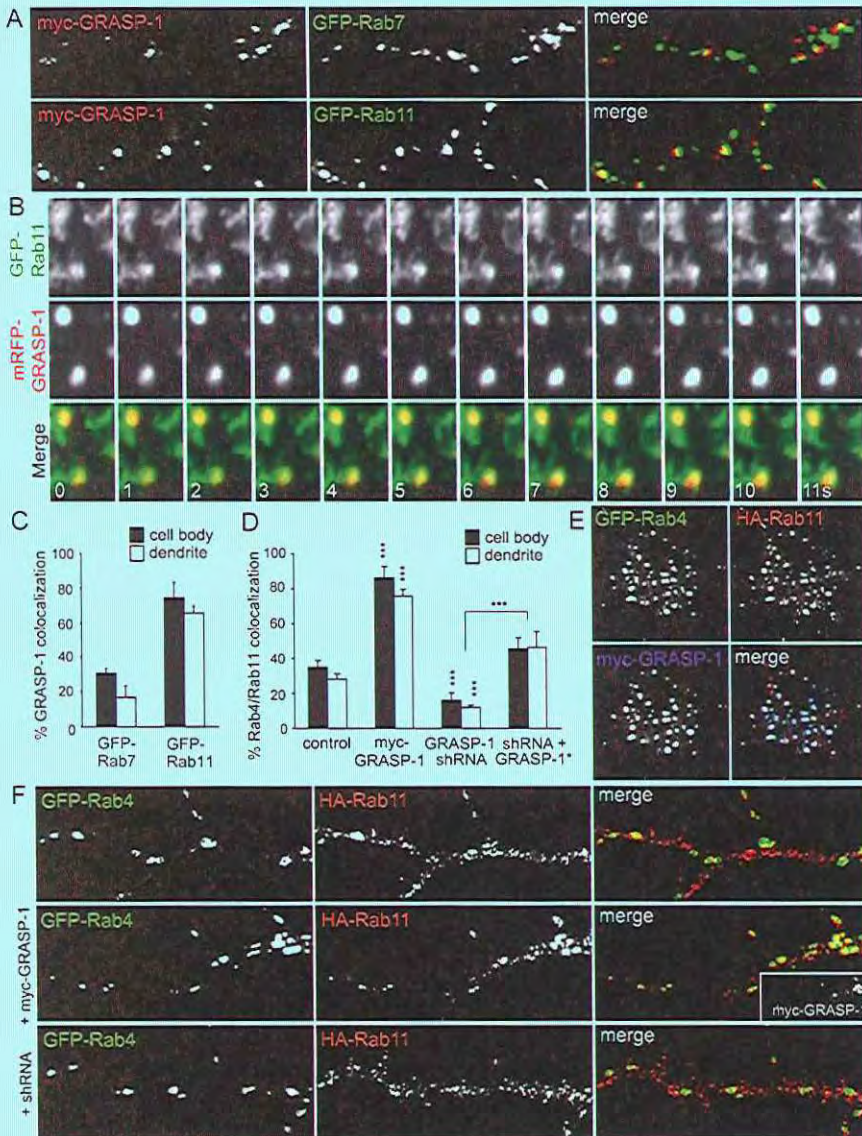


Figure 17. GRASP-1 couples Rab4 and Rab11 domains

A) Representative images of dendrites of hippocampal neurons cotransfected at DIV13 for 4 days with myc-GRASP-1 and either GFP-tagged Rab7 or Rab11 and labeled with anti-myc (red).

B) Simultaneous imaging of GFP-Rab11 (green) and mRFP-GRASP-1 (red) in transfected hippocampal neurons. Successive frames are shown and time (seconds) is indicated in the merge panel.

C) Percentage of colocalization between myc-GRASP-1 and Rab proteins in neurons as indicated in (A). Error bars indicate S.E.M. *** $p < 0.0005$.

D) Percentage of colocalization between Rab4 and Rab11 domains in neurons co-transfected with GFP-Rab4 and HA-Rab11 with either myc-GRASP-1, pSuper-GRASP-1-shRNA#2 or pSuper-GRASP-1-shRNA#2 and GFP-GRASP-1* as indicated in (F).

E) Images of cell body of hippocampal neurons triple transfected at DIV13 for 4 days with GFP-Rab4, HA-Rab11, and myc-GRASP-1 and labeled with anti-HA (red) or anti-myc (blue) antibodies.

F) Representative images of dendrites of hippocampal neurons cotransfected at DIV13 for 4 days with GFP-Rab4 and HA-Rab11 and pSuper control vector, myc-GRASP-1 or pSuper-GRASP-1-shRNA#2 and labeled with anti-HA (red) or anti-myc (blue) antibodies.

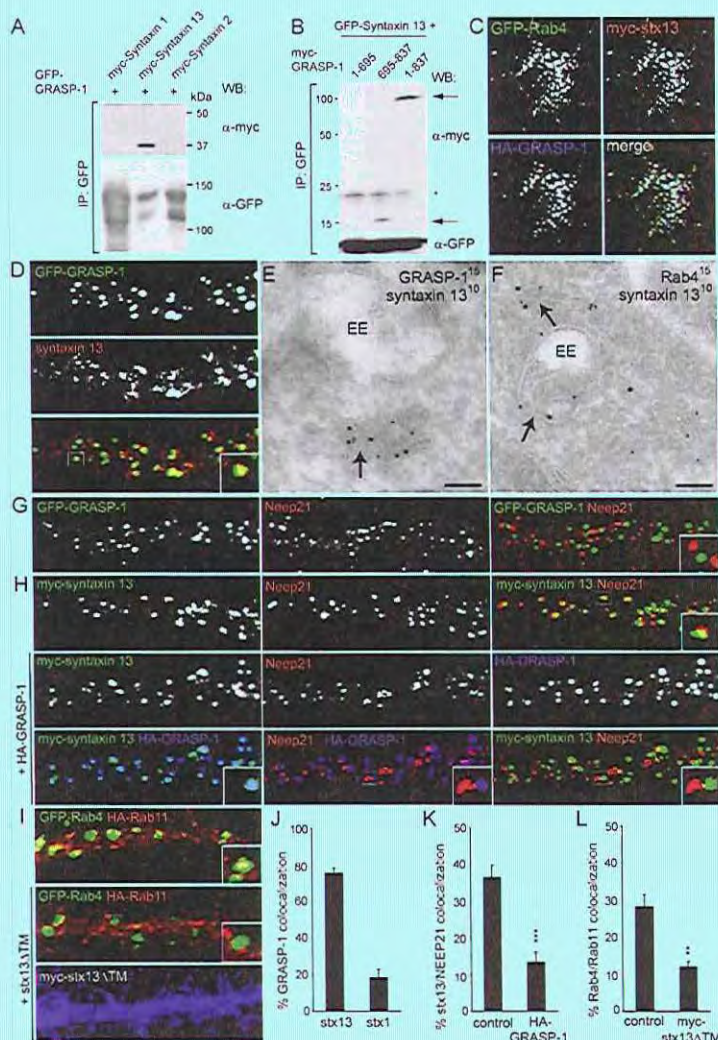


Figure 18. Syntaxin 13 binds to GRASP-1 and segregates Rab4/Rab11 domains

A) Lysates of COS-7 cells cotransfected with GFP-GRASP-1 and myc-syntaxins were immunoprecipitated with anti-GFP antibody and analyzed by Western blot.

B) Lysates of COS-7 cells cotransfected with GFP-syntaxin 13 and full length myc-GRASP-1 (1-837) or truncated myc-GRASP-1 constructs (1-695 or 695-837) were immunoprecipitated with anti-GFP antibody and analyzed by Western blot. Asterisk indicates background band. Arrows point to co-precipitated GRASP-1 proteins.

C) Images of cell body of hippocampal neurons triple transfected at DIV13 for 4 days with GFP-Rab4, HA-GRASP-1, and myc-syntaxin 13 and labeled with anti-HA (blue) or anti-myc (red) antibodies.

D) Representative images of dendrites of hippocampal neurons transfected at DIV13

with GFP-GRASP-1 for 4 days and labeled with anti-syntaxin 13 (red).

E, F) Immunogold EM of hippocampal neurons labeled with 10 nm protein A gold for endogenous syntaxin 13 and with 15 nm protein A gold for GRASP-1 (**E**) or with 15 nm protein A gold for Rab4 (**F**). Arrow denotes tubular endosomal membrane to which GRASP-1, syntaxin 13 and Rab4 localized. Scale bar is 100 nm.

G) Representative images of dendrites of hippocampal neurons transfected at DIV13 with GFP-GRASP-1 for 4 days and labeled with anti-Neep21 (red).

H) Representative images of dendrites of hippocampal neurons cotransfected at DIV13 for 4 days with myc-syntaxin 13 and control vector or HA-GRASP-1 and labeled with anti-myc (green), anti-HA (blue) and anti-Neep21 (red).

I) Representative images of dendrites of hippocampal neurons cotransfected at DIV13 for 4 days with GFP-Rab4, HA-Rab11 and control vector or myc-syntaxin 13 Δ TM and labeled with anti-myc (blue) and anti-HA (red).

J) Percentage of colocalization between HA-GRASP-1 and myc-syntaxin 1 or myc-syntaxin 13 in neurons.

K) Percentage of colocalization between myc-syntaxin 13 and Neep21 in dendrites as indicated in (**H**).

L) Percentage of colocalization between GFP-Rab4 and HA-Rab11 domains in dendrites expressing myc-syntaxin 13 Δ TM as indicated in (**I**). Error bars indicate S.E.M. ** $p < 0.005$. *** $p < 0.0005$.

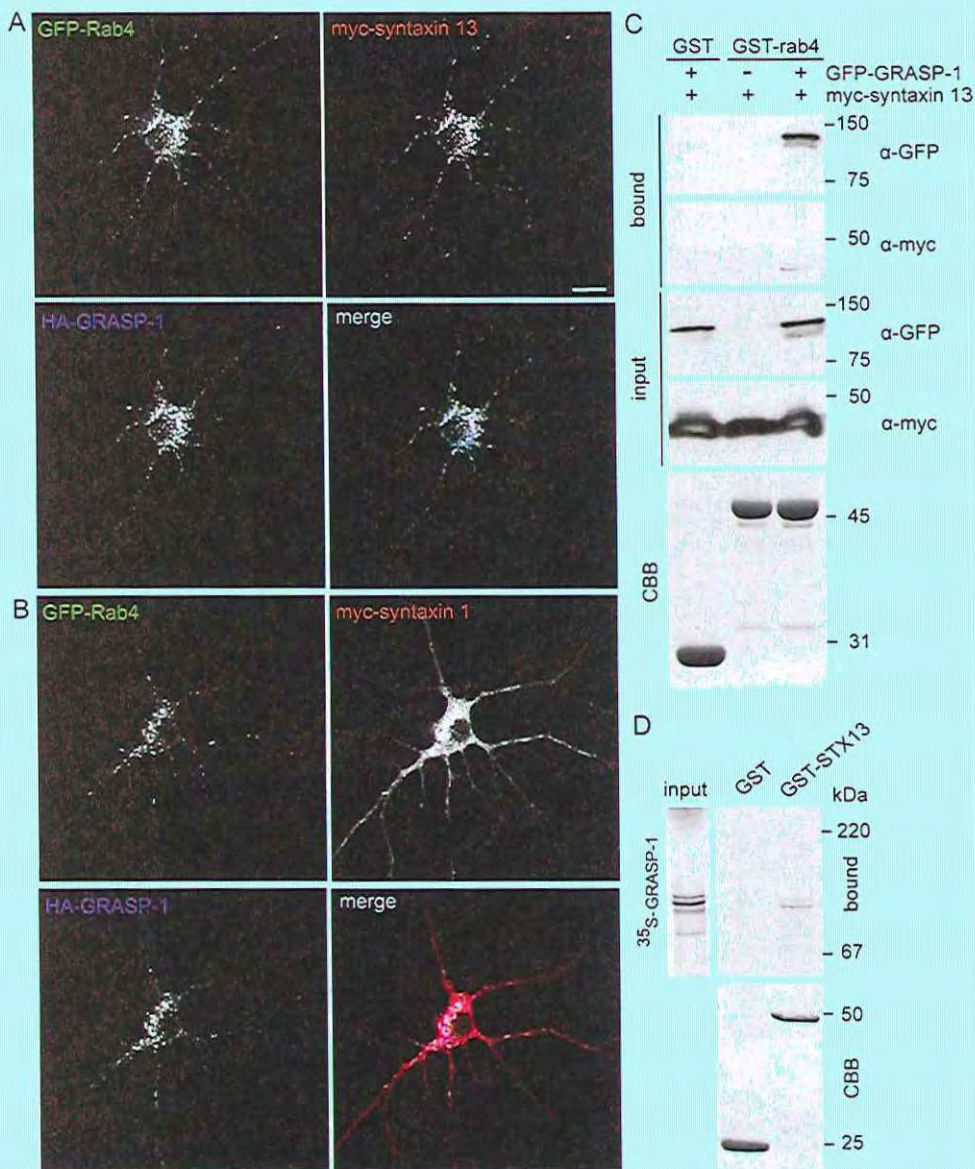


Figure 19. GRASP-1 interacts and coincides with Rab4 and syntaxin 13

A-B) Representative images of hippocampal neurons transfected with GFP-GRASP-1 and HA-Rab4 and myc-syntaxin 13 (*A*) or myc-syntaxin 1 (*B*).

C) Binding assay using lysates of COS-7 cells expressing myc-syntaxin 13 with or without GFP-GRASP-1, and GMP-PNP-charged GST-rab4. Note that myc-syntaxin 13 is only isolated on the beads in the presence of GRASP-1.

D) Binding assay of ³⁵S-labeled GRASP-1 and immobilized GST-syntaxin 13ΔTM.

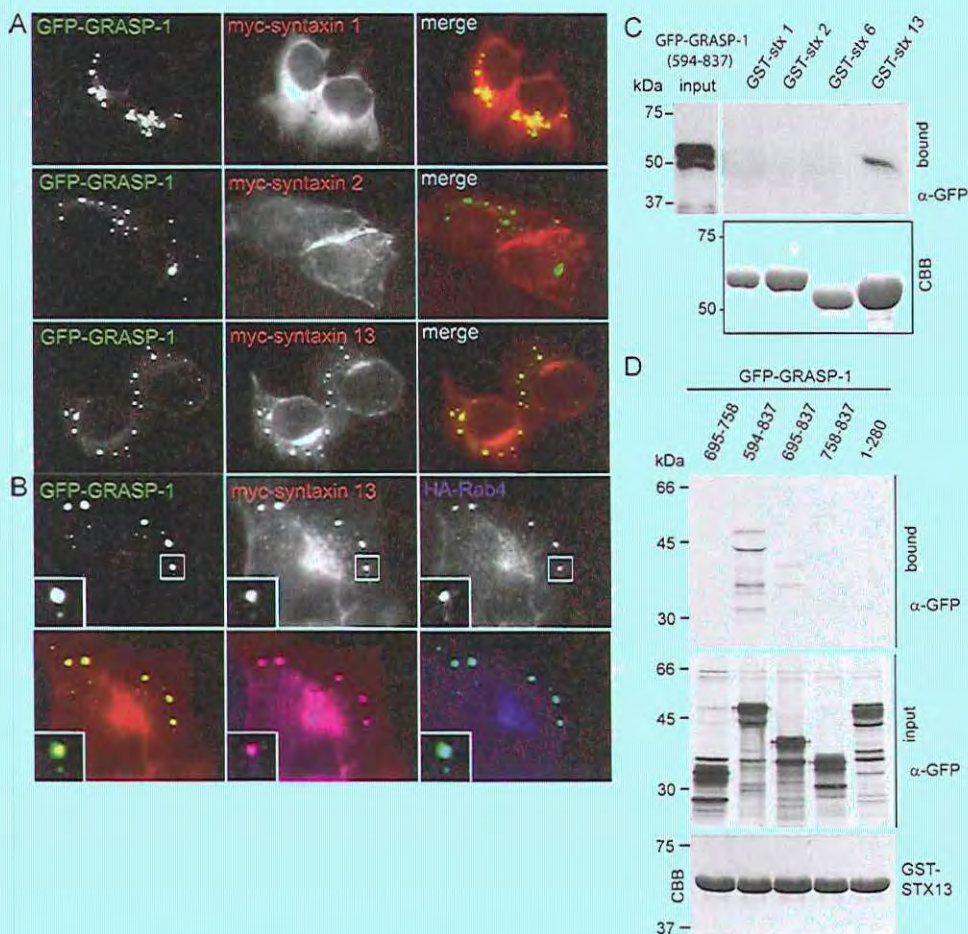


Figure 20. Syntaxin 13 interacts with the C-terminal part of GRASP-1

A) HeLa cells co-transfected with GFP-GRASP-1 and myc-syntaxin 1, myc-syntaxin 2 or myc-syntaxin 13.

B) HeLa cells triple transfected with GFP-GRASP-1, myc-syntaxin 13 and HA-Rab4.

C) Binding assay using lysate of COS-7 cells transfected with GFP-GRASP-1(594-837) and GST-syntaxins without transmembrane domain. GRASP-1 was analyzed by Western blot with antibody against GFP.

D) Binding assay using lysates of ^{35}S -methionine labeled COS-7 cells expressing GFP-GRASP-1 truncations and GST-syntaxin 13 ΔTM .

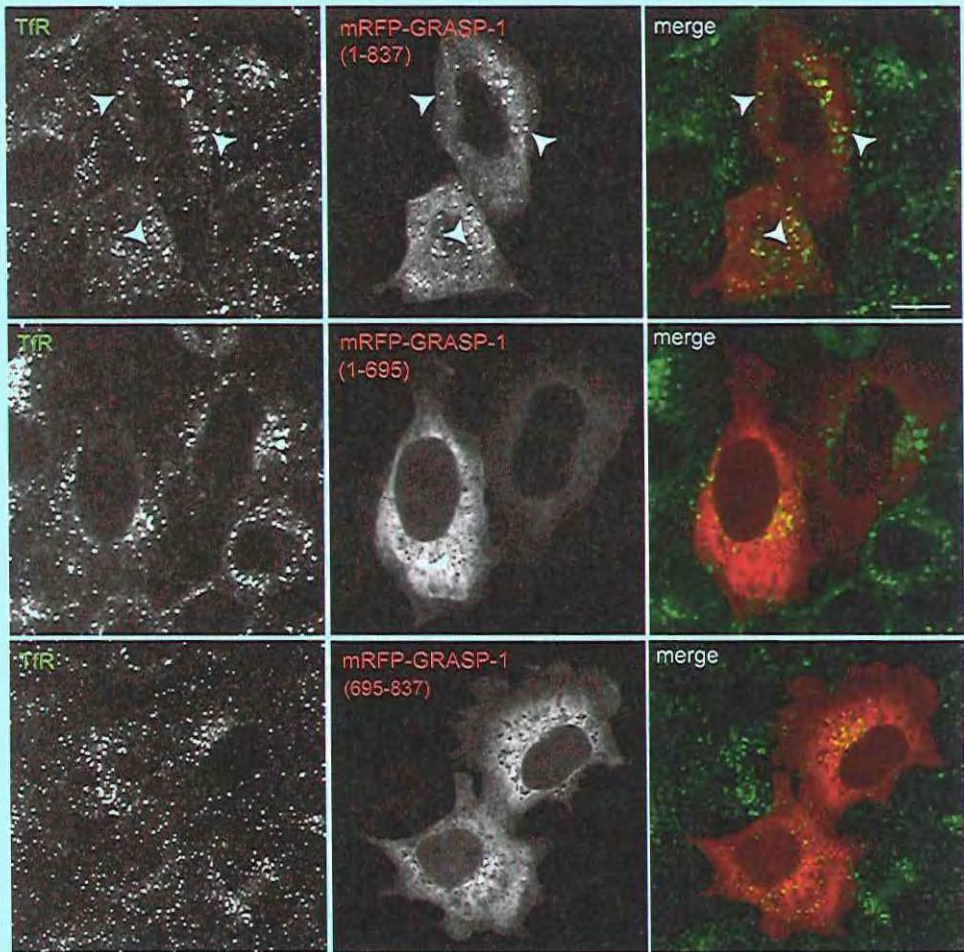


Figure 21. Both N- and C-terminus are necessary for GRASP-1 localization to endosomes
HeLa cells transfected with full length mRFP-GRASP-1 (1-837) or truncated mRFP-GRASP-1 constructs and labeled with anti-TfR antibodies (green). Bar is 10 μ m.

DISCUSSION

Complex processes that govern neuronal function have adapted basic cellular pathways to perform the elaborate information processing achieved by the brain. Some of these processes, such as cargo trafficking require additional layers of control and fine-tuning. Here, we describe a new molecular mechanism for regulating endosomal membrane and receptor recycling by GRASP-1 in neuronal cells. GRASP-1 is a neuronal effector of Rab4, binds syntaxin 13, and couples Rab4 and Rab11 endosomal domains. This mechanism has two distinct roles in neuronal function; first it is required for AMPAR recycling and second it is critical for dendritic spine morphology.

Regulation of recycling endosome maturation by GRASP-1

Each organelle carries its own set of Rabs which ensures the specificity of intracellular membrane transport. Ample examples show that Rab GTPases and their effectors can confer directionality to membrane traffic and couple different traffic steps (Zerial and McBride, 2001). Here, we show that GRASP-1 is a new component of the molecular machinery that regulates directionality in endosomal trafficking in neurons. First, GRASP-1 is a novel Rab4 effector and binds specifically to its active GTP-bound state. Second, knock-down of GRASP-1 separates Rab4 and Rab11 domains and moves Rab4 in EEA1/Neep21 positive early endosomal structures. Accordingly, knock down of GRASP-1 mimics the effects of dominant-negative Rab4 and Rab11 on dendritic spine morphology. Third, GRASP-1 overexpression strongly increases Rab4/Rab11 colocalization in both neurons and Hela cells. We propose a model in which GRASP-1 coordinates recycling endosomal maturation (Fig. 22). The term recycling endosome maturation is used here to discern it from the other endosomal exit routes, such as the degradative multivesicular body/endosome maturation pathway, the retrieval route of mannose 6-phosphate receptors to the trans Golgi network, or the pathway for melano-genic enzymes to melanosomes (Bonifacino and Rojas, 2006).

How does GRASP-1 couple specific Rab domains? Along the endosomal pathway bivalent effectors have been found that connect proximal Rab5 and Rab4 domains on early endosomes (de Renzis et al., 2002). Since GRASP-1 binds directly to Rab4 but not to Rab11 additional factors are needed. We found that GRASP-1 binds to endosomal SNARE protein syntaxin 13. Overexpression of GRASP-1 separates syntaxin 13 from Neep21 positive structures and strongly recruits syntaxin 13 to Rab4 positive membranes. Previous studies have shown that syntaxin 13 is involved in recycling of endosomal domains (Prekeris et al., 1998; Steiner et al., 2002) and is enriched in Rab11 endosomal fractions (Trischler et al., 1999). We found that mutant syntaxin 13 separates Rab4/GRASP-1 and Rab11 positive endosomal domains, suggesting that the coupling of Rab4 and Rab11 domains by GRASP-1 is, at least in part, through the interaction with syntaxin 13. Since syntaxin 13 is a constituent of the SNARE core complex (Prekeris et al., 1998) and shown to be involved in membrane fusion (McBride et al., 1999), it is tempting to speculate that the binding between GRASP-1 and syntaxin 13 recruits the fusion machinery necessary to connect with Rab11 positive membranes. Additional studies are required to determine the precise functional relationship between GRASP-1 binding to syntaxin 13 and the SNARE function of syntaxin 13. The property to bind Rab4 via the N-terminus and syntaxin 13 via the C-terminus of GRASP-1 supports the model that membrane bound active Rab4 retains or recruits GRASP-1 on endosomes and forms a complex with syntaxin 13.

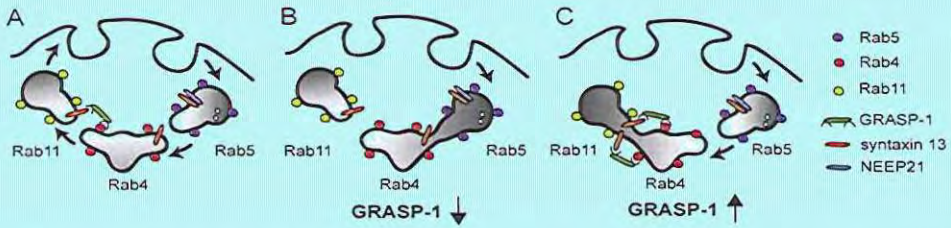


Figure 22. Model for the role of GRASP-1 in endosome recycling

Endosomes can be viewed as mosaic distribution of Rab4, Rab5 and Rab11 domains that dynamically interact via effector proteins and SNAREs. The Rab5 domain allows entry into the early/sorting endosome, whereas the Rab4 and Rab11 domains contain the machinery that is necessary for sorting and recycling membranes and receptors back to the plasma membrane.

A) GRASP-1 binds to Rab4 and syntaxin 13 and couples Rab4 and Rab11 recycling endosomes. The complex formed between GRASP-1 and t-SNARE syntaxin 13 might mediate fusion between Rab4 and Rab11 endosomes.

B) Absence of GRASP-1 interferes with complex formation at the recycling step, causing cargo accumulation in early endosomes, impairment of receptor expression and changes in spine morphology.

This sequence of interactions could then structurally and functionally link Rab4 to Rab11 membrane domains (Fig. 22). Subsequent recruitment of the other factors on to Rab4-defined membrane domains could strengthen the interaction with Rab11. It has been speculated that the GTPase-activating proteins (GAPs) that act on the upstream Rabs might be effectors of the downstream Rabs (Grosshans et al., 2006). These Rab cascades and conversions might serve as a positive feedback loop to specifically concentrate activated Rab4 on Rab11 positive endosomes. Additional regulation of GRASP-1 by caspase-3 cleavage (Ye et al., 2000) could separate the N-terminal Rab4 binding domain from the C-terminal syntaxin 13 binding site, potentially disrupting the interaction between Rab4 and Rab11 endosomes (Fig. 22).

Role of GRASP-1 in endosomal AMPAR recycling

GRASP-1 was originally found to act as a neuronal Ras guanine nucleotide exchange factor (GEF) and regulate synaptic AMPAR trafficking (Ye et al., 2000). We could not measure detectable GEF activity of GRASP-1 for Ras *in vivo*, by filter binding (not shown) or sensitive fluoro-metric mantGDP assays, nor did we find homology between the GRASP-1 sequence and known rasGEF domains. Here, we provide an alternative model for the role of GRASP-1 in AMPAR traffic and show that GRASP-1 is part of the molecular machinery that controls endosomal membrane receptor recycling in dendrites. Indeed, we show that GRASP-1 colocalizes with internalized AMPARs and that knock down of GRASP-1 decreases recycling of GluR subunits after AMPA application. Moreover GRASP-1 regulates synaptic plasticity, especially the late phase of LTP in hippocampal slices. Previous results show that Rab11 and syntaxin 13 dominant negative mutants were critical for the entire time course of LTP (Park et al., 2004). We propose that GRASP-1 regulates a particular step in the endosomal trafficking and is important for a specific-phase of AMPA receptor recycling (Fig. 22). In addition to supplying AMPARs, membrane trafficking from recycling endosomes also mediates the growth of dendritic spines (Park et al., 2006). In accord, GRASP-1 knock down decreased the total number of protrusions and mushroom-shaped spines and regulates endosomal mobility into dendritic spines. As discussed above, the coupling of endosomal Rab4 and Rab11 domains by GRASP-1 is an attractive possibility to explain the

effects on AMPAR recycling and spine morphology.

GRASP-1 binds to the seven PDZ domain-containing scaffolding protein GRIP (Ye et al., 2000) that transports and stabilizes GluR2 containing AMPAR at synapses and intracellular compartments (Bredt and Nicoll, 2003; Hoogenraad et al., 2005). Rab4 dominant negative and GRASP-1 knock down had no effect on GRIP-1 distribution and Rab4/GRASP-1 positive endosomal structures did not recruit endogenous GRIP (data not shown), suggesting that GRIP functions in an alternative trafficking pathway independent of GRASP-1 or the interaction with GRASP-1 is transient and highly regulated. Interestingly, GRIP also binds to the early endosomal protein Neep21 which is crucial for AMPAR sorting through endosomes (Kulangara et al., 2007; Steiner et al., 2005). Since neuronal activity determines the phosphorylation status of GRIP and enhances the binding of GRIP and GluR2 with Neep21 (Kulangara et al., 2007; Steiner et al., 2005), it is possible that GRIP is under tight control of specific phosphorylation signaling mechanisms in order to allow for consecutive protein binding and temporal receptor interactions (Kulangara et al., 2007). Additional studies are required to determine the precise role of GRIP in endosomal receptor trafficking.

In contrast to AMPA stimulation, GRASP-1 staining strongly decreased by bath application of NMDA (Lee et al., 2004; Ye et al., 2000). It has been shown that AMPA and NMDA stimulation induce differential AMPAR sorting; AMPA stimulation allows AMPARs to enter the normal recycling pathway, whereas NMDA stimulation diverts AMPARs to Neep21-positive endosomes and the lysosome degradation pathway (Lee et al., 2004; Steiner et al., 2002). It is tempting to speculate that GRASP-1 in AMPA stimulated neurons allows sorting of internalized AMPARs to the recycling endosomes, while in response to NMDA, absence of GRASP-1 drives receptors to the lysosomes. It is possible that different neuronal stimulatory inputs dynamically control activity of effector complexes and endosomal trafficking pathways. In this model, GRASP-1 might be part of the machinery on endosomes that senses and reacts on NMDA receptor-mediated Ca²⁺ influx, which is of key importance to understand internalized AMPAR and membrane sorting during plasticity and neuronal circuitry remodeling.

MATERIAL AND METHODS

Antibodies and reagents

The following primary and secondary antibodies were used in this study. Rabbit anti-GRASP-1 (JH 2730) (Ye et al., 2000), rabbit anti-NEEP21 (Steiner et al., 2002), rabbit anti-GRIP1 (Hoogenraad et al., 2005), rabbit anti-Rab4 (Bottger et al., 1996), rabbit anti-GFP (van Vlijmen et al., 2008), rabbit anti-syntaxin 13 (Prekeris et al., 1998), rabbit anti-rab4 (Bottger et al., 1996). Rabbit anti-Rab11 was generated by immunizing animals with GST-Rab11a and affinity purified on His-Rab11a columns. Anti-GRASP-1 (#5285) was generated by immunizing rabbits with GST-GRASP-1(1-378) and used for immuno electronmicroscopy.

The following antibodies were obtained from commercial sources: rabbit anti-GRASP-1 (AB96361), mouse anti- β -actin, mouse anti-GluR2 (Chemicon), mouse anti-Rab4, mouse anti-EEA1 (BD Biosciences), mouse anti-FLAG, mouse anti-MAP2, mouse anti- α -tubulin (Sigma), mouse anti-GFP (Roche), mouse anti-bassoon (Stressgen), rabbit anti- β -galactosidase (MP Biomedicals), mouse anti- β -galactosidase (Promega), rabbit anti-GluR1 (Calbiochem), mouse anti-HA (Roche), rabbit anti-myc (Upstate

Biotechnology), mouse LAMP-1 (Stressgen), mouse anti-myc, rabbit anti-Rab5 (Santa Cruz Biotechnology), rabbit anti-syntaxin 13 (Synaptic Systems), human anti-EEA1, mouse anti-human TfR (ATCC). TfR-594, HRP and fluorescently labeled secondary antibodies were from Molecular Probes and Jackson Laboratories and agarose beads conjugated with mouse anti-FLAG antibody were purchased from Sigma.

Expression constructs

The following mammalian expression plasmids have been described: pRK5-myc-GRASP-1 (Ye et al., 2000), pEF-Flag-Rab4 and pEF-Flag-Rab5 (Fukuda, 2003), pEGFP-Rab7 (Jordens et al., 2001), p β actin-HA- β -galactosidase (Hoogenraad et al., 2005), pJPA5-TfR-GFP (Burack et al., 2000), Rab3, Rab4, Rab5, Rab7 and Rab11 cDNA in pGEX, pEGFP or pcDNA3 (Cormont et al., 2001; de Graaf et al., 2004; Deneka et al., 2003; Roberts et al., 2001; van Vlijmen et al., 2008), pGEX-Hras(1-166) and pGEX-cdc25(974-1260) (Rehmann, 2005), pcDNA3-NEEP21-GFP, pcDNA3-myc-syntaxin 13 (Steiner et al., 2002), pEGFP-Rab11S25N (Wilcke et al., 2000), pEGFP-Rab4S22N (de Wit et al., 2001) pGW1-HA-GluR2 (Lee et al., 2004), pSuper vector (Brummelkamp et al., 2002) and pSuper-GRIPI-shRNA (Hoogenraad et al., 2005). pMT2HA-rasGRP and pMT2HA-ras were obtained from Hans Bos (University Medical Center, Utrecht). Syntaxin constructs were obtained as indicated; pGEX-syntaxin1 Δ TM and pGEX-syntaxin2 Δ TM (Ruud Toonen, CNCR, VU, Amsterdam), pGEX-syntaxin6 Δ TM (Suzanne Pfeffer, Stanford School of Medicine), and pGEX-syntaxin13 Δ TM (Andrew Peden, CIMR, Cambridge).

GRASP-1 truncation constructs and GRASP-1 mutant lacking aa280-300 were made with PCR from full length GRASP-1 cDNA 1 (Ye et al., 2000). GRASP-1* rescue constructs were prepared by a PCR-based strategy to introduce 4 silent substitutions in the target site. The target sequence GCTCTCTGAGAAATTGAAA was modified into GCTTTCGGAAAAGTTGAAA. Syntaxin-1A (BC100446; image: 6595634), syntaxin-2 (BC047496; image: 5296500), syntaxin-6 (BC009944; image: 4122224) cDNA was purchased from Geneservice. For neuronal expression, all cDNAs were subcloned in pGW1- and p β actin-expression vectors with various tags (Hoogenraad et al., 2005). Myc-syntaxin 13 Δ TM (aa1-245) was made by PCR from full length syntaxin 13 cDNA. The rat GRASP-1 (accession NM_053807) smartpool siRNA (cat# L-096315-01) was from Dharmacon. Another set of 3 separate siRNAs targeting rat GRASP-1 was purchased from Ambion (cat# AM16798A). GRASP-1 siRNA2 (siRNA ID#192942, GCU-CUCUGAGAAAUUGAAAtt) yielded most efficient knock down in INS1 cells and was cloned in pSuper plasmid for knock down of GRASP-1 in rat hippocampal neurons. GRASP-1 shRNA#5 (GTCCCAGCACAAAGAAGAA) was designed by using the siRNA selection program at the Whitehead Institute for Biomedical Research (Yuan et al., 2004) (jura.wi.mit.edu/bioc/siRNAext). The sequence for the Luciferase shRNA is: CGTACGCGGAATACTTCGA (Zhang and Macara, 2006).

Preparation of tissue extracts

For tissue Western blots, cerebral cortex, cerebellum, midbrain, spinal cord, kidney, liver and spleen were dissected from P30 mice. Frozen tissue samples and cultured cells were homogenized in PBS/1%Triton-X100, and then an equal volume of 2X SDS sample buffer was added, and the samples were boiled. Protein concentrations were measured using a BCA protein assay kit (Pierce) and 20 μ g of protein was loaded in each lane for a subsequent Western blot analysis.

GST-Rab pull down assays

Preparation of pig brain cytosol, purification of GST-Rab fusion proteins, isolation of Rab4GTP-interacting proteins in pull down assays and binding assays with ^{35}S -labeled GRASP-1 were done as described (Deneka et al., 2003; Neeft et al., 2005). To determine the Rab4 binding region on GRASP-1, we expressed pRK5-myc GRASP-1 or pGW1-GFP-GRASP-1 truncations in COS-7 cells. Cells were washed in ice-cold PBS and lysed in 20 mM Hepes pH 7.4, 100 mM NaCl, 5 mM MgCl_2 (lysis buffer) containing 0.5% NP-40, 5 $\mu\text{g}/\text{ml}$ leupeptin, 10 $\mu\text{g}/\text{ml}$ aprotinin, 1 $\mu\text{g}/\text{ml}$ pepstatin, 1 mM PMSF, 20 μM GMP-PNP, 1 mM DTT. Detergent lysates were shaken for 20 min at 4°C, centrifuged for 10 min at maximum speed in a cooled Eppendorf centrifuge, diluted with lysis buffer to 0.2% NP-40 and incubated with Rab4-GMP-PNP beads for 2 hrs at 4°C. Beads were washed 4 times with lysis buffer containing 0.2% NP-40, 20 μM GMP-PNP, 1 mM DTT. Bound proteins were eluted in Laemmli sample buffer and analyzed by Western blot and detection with anti-myc antibody. To determine whether Rab4, GRASP-1 and syntaxin 13 can form a ternary complex, we transfected COS-7 cells with pGW1-myc-syntaxin 13 with and without pGW1-GFP-GRASP-1. Cells were lysed in 20 mM Na Hepes pH 7.5, 100 mM NaCl, 1% TX-100 and cleared detergent lysates were incubated with GST-Rab4 or GST beads. Beads were washed 3 times with lysis buffer, and bound protein was assayed by Western blot with monoclonal antibodies against GFP and myc epitope tags.

Binding assays with GST-syntaxins

GST-syntaxin fusion proteins lacking the transmembrane domain were expressed in *E. coli* BL21(DE3), immobilized on GSH beads and used for binding assays with lysates of COS-7 cells transfected with GFP-GRASP-1(594-837). Binding assay of GST-syntaxin13 ΔTM and ^{35}S -labeled GRASP-1, produced in a coupled in vitro transcription-translation reaction was done as described (Neeft et al., 2005). For mapping the syntaxin 13 binding domain on GRASP-1 we expressed C terminal pGW1-GFP-GRASP-1 constructs in COS-7 cells. The cells were metabolically labeled for 30 min with 0.5 mCi/ml ^{35}S -methionine/Pro-Mix (Perkin Elmer), and detergent lysates were then subjected to a GST pull down assay on GST-syntaxin13 ΔTM as described above. Bound proteins were released by boiling the beads 8 min in 0.1 ml 1% SDS/PBS and GFP-tagged GRASP-1 truncations were immunoprecipitated with a rabbit GFP antibody and analyzed by phosphorimaging as before (Gerez et al., 2000).

Mass spectrometry

Eluates were boiled in Laemmli sample buffer, resolved on a 7.5% SDS-PAA gel and silver-stained. Bands of interest were excised and in-gel digested using modified trypsin (Roche Diag-nostics, Indianapolis, IN) in 50 mM ammonium bicarbonate. The peptide mixtures were analyzed by LC/MS/MS using a Q-ToF hybrid mass spectrometer (Micromass, Waters) equipped with a Z-spray source and coupled online with a capillary chromatography system. The peptide mixtures were delivered to the system using a Famos autosampler (LC Packing) at 3 $\mu\text{l}/\text{min}$ and trapped on an AquaTM C18RP column (Phenomenex; column dimension 1 cm x 100 μm i.d., packed in house). The sample was then fractionated onto a C_{18} reverse-phase capillary column (PepMap, LC Packing; column dimension 25 cm x 75 μm i.d.) at a flow rate of 150-200 nl/min using a linear gradient of acetonitrile. The mass spectrometer was set up in a data-dependent MS/MS mode where a full scan spectrum (m/z acquisition range from 400

to 1600 Da/e) was followed by a tandem mass spectrum (m/z acquisition range from 100 to 1800 Da/e). The pre-cursor ions were selected as the most intense peaks of the previous scan. Suitable collision energy was applied depending on the mass and charge of the precursor ion. ProteinLynx software, provided by the manufacturers, was used to analyze raw MS and MS/MS spectra and to generate a peak list which was introduced in the MASCOT MS/MS ion search software for protein identification.

Immunoprecipitation

COS-7 cells were cotransfected with pEF-FLAG-Rab4 or pEF-FLAG-Rab5 and GRASP-1 constructs and co-immunoprecipitations were done as described (van Vlijmen et al., 2008). Immune complexes were eluted with FLAG peptide, and analyzed by Western blot with a mouse monoclonal antibody against GFP, and rabbit antibody against FLAG. For interaction studies between GRASP-1 and syntaxin 13, COS-7 cells were transfected with pGW1-GFP-GRASP-1, and pGW1-myc-syntaxin 1, pGW1-myc-syntaxin 2, or pGW1-myc-syntaxin 13. To determine the region of GRASP-1 that bound to syntaxin13, we transfected COS-7 cells with pGW1-myc-GRASP-1, pGW1-myc-GRASP-1(1-695) or pGW1-myc-GRASP-1(695-837) and pGW1-GFP-syntaxin-13. Cells were lysed in 20 mM Hepes pH 7.4, 200 mM NaCl, 1% NP-40, and protease inhibitors. Detergent lysates were passed 20 x through a 27-gauge needle, and centrifuged at maximum speed in a cooled Eppendorf centrifuge. The supernatant was incubated for 2 hr with Rabbit GFP antibody coated beads at 4°C. Beads were washed four times with 20 mM Hepes pH 7.4, 200 mM NaCl, 1% NP-40, and immune complexes were eluted by heating for 5 min in reducing Laemmli sample buffer. Eluates were resolved by SDS-PAGE and analyzed by Western blot with monoclonal antibody against myc.

In vitro GEF assay

GST-Rab4, H-ras(1-166), GST-GRASP-1(1-594), GST-cdc25(974-1260) were expressed in E.coli CK600K. Bacteria were grown at 37°C until OD_{600} of 0.8. IPTG was added to 1 mM and bacteria were incubated overnight at room temperature. Cells were resuspended in 50 mM Tris HCl pH 7.5, 50 mM NaCl, 5% glycerol, 5 mM DTE and 5 mM $MgCl_2$ and lysed by sonication. Insoluble material was removed by centrifugation at 30,000 g and in case of GST fusion proteins the supernatant was loaded on a 20 ml GSH-column (Pharmacia). The column was washed with 5 volumes 50 mM Tris HCl pH 7.5, 400 mM NaCl, 5% glycerol 5 mM $MgCl_2$ and 5 mM DTE and 2 volumes of 50 mM Tris HCl pH 7.5, 50 mM NaCl, 2.5% glycerol 10 mM $CaCl_2$, 5 mM $MgCl_2$ and 5 mM DTE (buffer T). The proteins were cleaved with 80 units of thrombin (Serva) in buffer T on the column and elute with buffer T. Protein containing fractions were concentrated using a Millipore concentrator unit. Further purification was achieved by gel filtration on a Superdex 75 (16/60) column (Pharmacia), equilibrated with 50 mM Tris HCl pH 7.5, 50 mM NaCl, 2.5% glycerol, 5 mM $MgCl_2$ and 5 mM DTE. GTPases were loaded with 2'-(3')-O-(N-methylanthraniloyl)-guanosinediphosphate (mantGDP) as described for rap (Rehmann, 2005). Nucleotide exchange reactions were carried out as described (Rehmann, 2005). In brief, 200 nM mantGDP loaded GTPase was incubated at 25°C in 50 mM Tris HCl pH 7.5, 50 mM NaCl, 5 mM $MgCl_2$, 5 mM DTE and 5% glycerol in the presence of an 100 fold molar excess of GDP. Exchange factors were added as indicated. The fluorescence intensity was measured over time in a Cary Eclipse Spectrofluorometer (Varian), with excitation at 340 nm and emission at 460 nm.

IN VIVO GEF ASSAY

COS-7 cells were transfected with pMT2HA-Hras together with pMT2HA-rasGRP, pGW1-myc GRASP-1 or pGW1-myc. Cells expressing HA-ras were incubated with and without 10 ng/ml EGF and cells co-expressing HA-ras and HA-rasGRP were incubated with or without 10 μ M Phorbol 12-Myristate 13-Acetate (PMA). After 5 min, the cells were lysed in 100 mM NaCl, 1% NP40, 20 mM Hepes pH 7.5. Cleared lysates were incubated for 3 hr with GSH beads containing the ras binding domain of Raf-1 (de Rooij and Bos, 1997). Beads were washed in lysis buffer. Bound HARas-GTP and expression levels of HA-Hras, HA-rasGRP, and myc-GRASP-1 was determined by Western blot with monoclonal HA and myc antibodies, respectively.

Cultured cells and transfection

Hela cells and COS-7 cells were grown in DMEM containing 10% fetal calf serum, antibiotics and 2 mM glutamine. Transferrin (Tf) uptake experiments in Hela cells were done as described (Deneka et al., 2003). INS1 cells were grown in RPMI 1640 with the same additions and 0.2 μ M Na pyruvate, and 50 μ M β -mercaptoethanol. Cells were transfected using FuGENE6 (Roche) or Lipofectamine 2000 (Invitrogen) and used in experiments after 16-24 hrs. siRNAs (100 nM final concentration) were transfected with Lipofectamine 2000 in INS1 cells. After 3 days cells were lysed and expression level of endogenous GRASP-1 was determined by Western blot.

Primary hippocampal neuron cultures, transfection and immunohistochemistry

Primary hippocampal cultures were prepared from embryonic day 18 (E18) rat brains (Goslin and Banker, 1990). Cells were plated on coverslips coated with poly-L-lysine (30 μ g/ml) and laminin (2 μ g/ml) at a density of 75,000/well. Hippocampal cultures were grown in Neurobasal medium (NB) supplemented with B27, 0.5 mM glutamine, 12.5 μ M glutamate and penicillin/streptomycin. Hippocampal neurons were transfected using Lipofectamine 2000 (Invitrogen). Briefly, DNA (3.6 μ g/well) was mixed with 3 μ l Lipofectamine 2000 in 200 μ l NB, incubated for 30 minutes and then added to the neurons in NB at 37°C in 5% CO₂ for 45 min. Next, neurons were washed with NB and transferred in the original medium at 37°C in 5% CO₂ for 2-4 days.

For immunohistochemistry, neurons were fixed for 5 minutes with ice-cold 100% methanol/1mM EGTA at -20°C, followed by 5 minutes with 4% formaldehyde/4% sucrose in phosphate-buffered saline (PBS) at room temperature. After fixation cells were washed three times in PBS for 30 min at room temperature, and incubated with primary antibodies in GDB buffer (0.2% BSA, 0.8 M NaCl, 0.5% Triton X-100, 30 mM phosphate buffer, pH 7.4) overnight at 4°C. Neurons were then washed three times in PBS for 30 min at room temperature and incubated with Alexa-conjugated secondary antibodies in GDB for 2 hr at room temperature and washed three times in PBS for 30 min. Slides were mounted using Vectashield mounting medium (Vector laboratories). Confocal images were acquired using a Zeiss LSM 510 confocal laser-scanning microscope with a 40x or 63x oil objective.

Surface and Intracellular Staining of AMPA Receptors

Surface staining of endogenous AMPARs was performed as described (Hoogenraad et al., 2005; Lee et al., 2004). Hippocampal neurons were "live" incubated with 10 μ g/ml rabbit anti-GluR1 (Calbiochem (1:8)) and mouse anti-GluR2 (Zymed (1:80)) N-terminal antibodies at 37°C for 15 min. After brief washing in prewarmed

DMEM, neurons were either returned to conditioned medium (for control incubation) or stimulated for 2 min with 100 μ M AMPA and 50 μ M APV or 50 μ M NMDA, washed in DMEM, returned to conditioned medium and incubated for the given time. The neurons were fixed for 5 min with 4% formaldehyde/4% sucrose in phosphate-buffered saline (PBS), followed by three washes in PBS (30 min at room temperature) and incubated with secondary antibody conjugated to Alexa488 (1:400) or Alexa568 (1:400) in GDB buffer without detergent (0.2% BSA, 0.8 M NaCl, 30 mM phosphate buffer, pH 7.4) overnight at 4°C followed by a further three washes in PBS (30 min at room temperature).

The fluorescent-based AMPAR internalization assay was performed as described (Lee et al., 2004). Hippocampal neurons transfected with HA-tagged GluR2 subunits were “live” labeled with 10 μ g/ml mouse anti-HA antibody (12CA5, Roche) by incubating coverslips in conditioned medium for 10 min at 37°C. After brief washing in prewarmed DMEM, neurons were either returned to conditioned medium (for control incubation) or stimulated for 2 min with 100 μ M AM-PA and 50 μ M APV or 50 μ M NMDA, returned to conditioned medium and incubated for the given time. Neurons were fixed in 4% formaldehyde/4% sucrose for 8 min at room temperature and surface-remaining receptors were visualized with Alexa633-conjugated secondary antibody. Internalized receptors were detected with Alexa488-conjugated secondary antibody after permeabilizing cells in methanol (-20°C) for 2 min. To determine colocalization, the neurons were immunostained with antibodies against GRASP-1 in GDB without detergent overnight at 4°C and incubated with Alexa568-conjugated secondary antibodies for 2 hr at room temperature.

The AMPAR recycling assay was performed as described (Lu and Ziff, 2005). After live staining for surface HA-GluR2 as indicated above, neurons were washed and either returned to conditioned medium (for control incubation) or stimulated for 2 min with 100 μ M AMPA and 50 μ M APV. The remaining surface anti-HA antibodies were stripped away by stripping buffer (0.5 M NaCl / 0.2 M acetic acid) on ice for 4 min and washed extensively with cold TBS (Tris-buffered saline) and returned back to conditioned media at 37°C for 45 min for recycling. After recycling, neurons were fixed in 4% formaldehyde/4% sucrose, and HA-GluR2 recycled back to the surface was detected with Alexa633-conjugated secondary antibodies. Neurons were permeabilized, and internal HA-GluR2 was detected with Alexa568-conjugated secondary antibodies.

Immunohistochemistry and confocal immunofluorescence

The mouse spinal cord was sectioned at 40 μ m with a freezing microtome. Sections were processed free floating, employing double-labeling immunofluorescence (Jaarsma et al., 2001). The antibodies were diluted in Tris-Buffered-Saline (TBS, pH 7.6) containing 1% normal horse serum and 0.2% Triton X-100. Sections stained for immunofluorescence were analyzed with a Zeiss LSM 510 confocal laser-scanning microscope.

Time-lapse live cell imaging

During imaging, neurons were maintained at 37°C in standard culture medium in a closed chamber with 5% CO₂ (Tokai Hit; INUG2-ZILCS-H2). To visualize mRFP-GRASP-1 and GFP-Rab4 or mRFP-GRASP-1 and GFP-Rab11 in neurons, near-simultaneous dual color (green and red) time-lapse live cell imaging was performed using Total Internal Reflection Fluorescence microscopy (TIRFM) on a Nikon Eclipse

TE2000E (Nikon), equipped with Nikon TIRF arm, CFI Apo TIRF 100x 1.49 N.A. oil objective (Nikon), Coolsnap camera (Roper Scientific), and controlled by MetaMorph 7.1 software (Molecular Devices). For excitation, the 488nm laser line of an argon laser (Spectra-Physics Lasers) and a 561 nm laser (Spectra-Physics) were used in combination with a ETGFP/mCherry filter cube (Chroma). A filterwheel (Sutter instruments) with GFP and Cherry emission filters (both Chroma) and synchronized with laser emission alternately exposed the camera to GFP or Cherry emission. For glycine treatments, the same microscope was used with regular widefield illumination by a mercury lamp. Glycine treatments were performed as described in (Park et al., 2006). Images of live cells were processed and analyzed using MetaMorph, Adobe Photoshop or LabVIEW (National Instruments) software.

Image Analysis and Quantification

Confocal images of transfected neurons were obtained with sequential acquisition settings at the maximal resolution of the microscope (1024 x 1024 pixels). Each image was a z-series of 6-8 images each averaged 2 times was chosen to cover the entire region of interest from top to bottom. The resulting z-stack was 'flattened' into a single image using maximum projection. Images were not further processed and were of similar high quality to the original single planes. The confocal settings were kept the same for all scans when fluorescence intensity was compared. Morphometric analysis, quantification and colocalization were performed using MetaMorph software (Universal Imaging Corporation).

Morphometric analyses of hippocampal neurons. To visualize the dendritic protrusions we used β -gal or GFP as an unbiased cell-fill. Because protrusions often crossed several z planes, we took series of stacks from the bottom to the top of all dendrites and used the LSM software to generate image projections for quantitative analyses. All morphological experiments were repeated at least three times with an $n > 7$ for individual experiments were analyzed in a double-blind manner. Between 150-300 protrusions were scored for every neuron and expressed per 10 μ m length of dendrite. Measurements of length and width of the protrusions were performed as described previously (Jaworski et al., 2009) and were classified based on the ratio of spine head width to protrusion length according to the following ratios: the spine whose width was equal to or more than half the size of its length was judged as standard mushroom spine. The protrusion whose width was smaller than half the size of its length was judged as filopodia or thin spine. In those cases where the total length of the spine could not be adequately seen or its length was $> 5 \mu$ m, protrusions were excluded from analysis.

Quantification of TfR-GFP distribution in spines. Measurements of TfR-GFP localization in spines and dendrites was performed as described (Park et al., 2006). Confocal images of hippocampal neurons filled with β -gal (red) and labeled for TfR-GFP were analyzed using MetaMorph software. The dendritic localization of TfR positive structures relative to spines was categorized according to the presence of GFP signal at the base (a), in the neck (b), or in the head (c) of spines.

Colocalization of fluorescent signals in dendrites and cell body. Colocalization of two fluorescent signals was determined using "colocalization" module in MetaMorph software as described (Lee et al., 2004). The colocalization module provides intensity measurements of the region overlap between signals in red and green channels of image projections. To minimize random overlap due to projection of confocal images, a single optical section from the z series stack that showed the largest amount of fluo-

REFERENCES

- Bonifacino, J. S., and Rojas, R. (2006). Retrograde transport from endosomes to the trans Golgi network. *Nature Rev Mol Cell Biol* 7, 568-579.
- Bredt, D. S., and Nicoll, R. A. (2003). AMPA receptor trafficking at excitatory synapses. *Neuron* 40, 361-379.
- Cai, H., Reinisch, K., and Ferro-Novick, S. (2007). Coats, tethers, Rabs, and SNAREs work together to mediate the intracellular destination of a transport vesicle. *Dev Cell* 12, 671-682.
- de Renzis, S., Sönnichsen, B., and Zerial, M. (2002). Divalent rab effectors regulate the sub-compartmental organization and sorting function of early endosomes. *Nature Cell Biol* 4, 124-133.
- Ehlers, M. D. (2000). Reinsertion or degradation of AMPA receptors determined by activity-dependent endocytic sorting. *Neuron* 28, 511-525.
- Gould, G. W., and Lippincott-Schwartz, J. (2009). New roles for endosomes: from vesicular carriers to multi-purpose platforms. *Nat Rev Mol Cell Biol* 10, 287-292.
- Greger, I. H., and Esteban, J. A. (2007). AMPA receptor biogenesis and trafficking. *Curr Opin Neurobiol* 17, 289-297.
- Grosshans, B. L., Ortiz, D., and Novick, P. (2006). Rabs and their effectors: achieving specificity in membrane transport. *Proc Natl Acad Sci USA* 103, 11821-11827.
- Gruenberg, J. (2001). The endocytic pathway: a mosaic of domains. *Nature Rev Mol Cell Biol* 2, 721-730.
- Hoogenraad, C. C., Milstein, A. D., Ethell, I. M., Henkemeyer, M., and Sheng, M. (2005). GRIP1 controls dendrite morphogenesis by regulating EphB receptor trafficking. *Nature Neurosci* 8, 906-915.
- Jaworski, J., Kapitein, L. C., Gouveia, S. M., Dortland, B. R., Wulf, P. S., Grigoriev, I., Camera, P., Spangler, S. A., Di Stefano, P., Demmers, J., *et al.* (2009). Dynamic microtubules regulate spine morphology and synaptic plasticity. *Neuron* 61, 85-100.
- Kennedy, M. J., and Ehlers, M. D. (2006). Organelles and trafficking machinery for postsynaptic plasticity. *Annu Rev Neurosci* 29, 325-362.
- Kulangara, K., Kropf, M., Glauser, L., Magnin, S., Alberi, S., Yersin, A., and Hirling, H. (2007). Phosphorylation of Glutamate receptor interacting protein 1 regulates surface expression of Glutamate receptors. *J Biol Chem* 282, 2395-2404.
- Malinow, R., and Malenka, R. C. (2002). AMPA receptor trafficking and synaptic plasticity. *Annu Rev Neurosci* 25, 103-126.
- Maxfield, F. R., and McGraw, T. E. M. (2004). Endocytic recycling. *Nature Rev Mol Cell Biol* 5, 121-132.
- McBride, H. M., Rybin, V., Murphy, C., Giner, A., Teasdale, R., and Zerial, M. (1999). Oligomeric complexes link rab5 effectors with NSF and drive membrane fusion via interactions between EEA1 and syntaxin 13. *Cell* 98, 377-386.
- Park, M., Penick, E. C., Edwards, J. G., Kauer, J. A., and Ehlers, M. D. (2004). Recycling endosomes supply AMPA receptors for LTP. *Science* 305, 1972-1975.
- Park, M., Salgado, J. M., Ostroff, L., Helton, T. D., Robinson, C. G., Harris, K. M., and Ehlers, M. D. (2006). Plasticity induced growth of dendritic spines by exocytic trafficking from recycling endosomes. *Neuron* 52, 817-830.
- Prekeris, R., Klumperman, J., Chen, Y. A., and Scheller, R. H. (1998). Syntaxin 13 mediates cycling of plasma membrane proteins via tubulovesicular recycling endosomes. *J Cell Biol* 143, 957-971.

- Sheng, M., and Hoogenraad, C. C. (2007). The postsynaptic architecture of excitatory synapses: a more quantitative view. *Annu Rev Biochem* 76, 823-847.
- Shepherd, J. D., and Huganir, R. L. (2007). The cell biology of synaptic plasticity: AMPA receptor trafficking. *Annu Rev Cell Biol Dev Biol* 23, 613-643.
- Steiner, P., Sarria, J. C. F., Glauser, L., Magnin, S., Catsicas, S., and Hirling, H. (2002). Modulation of receptor recycling by neuron-enriched endosomal protein of 21 kDa. *J Cell Biol* 157, 1197-1209.
- Steiner, P., Alberi, S., Kulangara, K., Yersin, A., Sarria, J. C., Regulier, E., Kasas, S., Dietler, G., Muller, D., Catsicas, S., and Hirling, H. (2005). Interactions between Neep21, GRIP1 and GluR2 regulate sorting and recycling of the glutamate receptor subunit GluR2. *EMBO J* 24, 2873-2884.
- Stinton, L. M., Selak, S., and Fritzler, M. J. (2005). Identification of GRASP-1 as a novel 97 kDa autoantigen localized to endosomes. *Clin Immunol* 116, 108-117.
- Sönnichsen, B., De Renzis, S., Nielsen, E., Rietdorf, J., and Zerial, M. (2000). Distinct membrane domains on endosomes in the recycling pathway visualized by multicolor imaging of rab4, rab5, and rab11. *J Cell Biol* 149, 901-913.
- Trischler, M., Stoorvogel, W., and Ullrich, O. (1999). Biochemical analysis of distinct rab5- and rab11 positive endosomes along the transferrin pathway. *J Cell Sci* 112, 4773-4783.
- van der Sluijs, P., Hull, M., Webster, P., Goud, B., and Mellman, I. (1992). The small GTP binding protein rab4 controls an early sorting event on the endocytic pathway. *Cell* 70, 729-740.
- Vitale, G., Rybin, V., Christoforidis, S., Thornqvist, P. O., McCaffrey, M., Stenmark, H., and Ye, B., Liao, D., Zhang, X., Zhang, P., Dong, H., and Huganir, R. (2000). GRASP-1: a neuronal rasGEF associated with the AMPA receptor/GRIP complex. *Neuron* 26, 603-617.
- Ye, B., Yu, W. P., Thomas, G. M., and Huganir, R. L. (2007). GRASP-1 is a neuronal scaffold protein for the JNK signaling pathway. *FEBS Lett* 581, 4403-4410.
- Zerial, M. (1998). Distinct rab-binding domains mediate the interaction of rabaptin-5 with GTP-bound rab4 and rab5. *EMBO J* 17, 1941-1951.
- Zerial, M., and McBride, H. (2001). Rab proteins as membrane organizers. *Nature Rev Mol Cell Biol* 2, 107-117.

Deletion of *FMRI* in Purkinje Cells Enhances Parallel Fiber LTD, Enlarges Spines, and Attenuates Cerebellar Eyelid Conditioning in Fragile X Syndrome

S.K.E. Koekkoek,^{1,6} K. Yamaguchi,^{3,6} B.A. Milojkovic,^{1,6} B.R. Dortland,^{1,6} T.J.H. Ruigrok,¹, R. Maex,¹, W. De Graaf,¹ A.E. Smit,¹ F. VanderWerf,¹ E. Bakker,² R. Willemsen,² T. Ikeda,³ S. Kakizawa,³ K. Onodera,³ D.L. Nelson,³ E. Mientjies,² M. Joosten,² E. De Schutter,⁴ B.A. Oostra,² M. Ito,³ and C.I. De Zeeuw¹,

¹Department of Neuroscience, Erasmus MC, Rotterdam, The Netherlands, ²Institute of Clinical Genetics, Erasmus MC, Rotterdam, The Netherlands, ³Laboratory for Memory and Learning and Laboratory for Behavior Genetics, ⁴Brain Science Institute, RIKEN, Wako, Japan, ⁵Laboratory of Theoretical Neurobiology, University of Antwerp, Antwerp, Belgium, ⁶Department of Molecular and Human Genetics, Baylor College of Medicine, Houston, Texas. ⁶These authors contributed equally to this work.

Neuron, Vol. 47, 339–352, August 4, 2005

Chapter 4

Deletion of *FMR1* in Purkinje Cells Enhances Parallel Fiber LTD, Enlarges Spines, and Attenuates Cerebellar Eyelid Conditioning in Fragile X Syndrome

S.K.E. Koekoek,^{1,6} K. Yamaguchi,^{3,6}
 B.A. Milojkovic,^{1,6} B.R. Dortland,^{1,6} T.J.H. Ruigrok,¹
 R. Maex,⁴ W. De Graaf,¹ A.E. Smit,¹ F. VanderWerf,¹
 C.E. Bakker,² R. Willemsen,² T. Ikeda,³ S. Kakizawa,³
 K. Onodera,³ D.L. Nelson,⁵ E. Mientjes,² M. Joosten,²
 E. De Schutter,⁴ B.A. Oostra,² M. Ito,³
 and C.I. De Zeeuw^{1,*}

¹Department of Neuroscience

²Institute of Clinical Genetics

Erasmus MC

P.O. Box 1738

3000 DR Rotterdam

The Netherlands

³Laboratory for Memory and Learning and Laboratory
 for Behavior Genetics

Brain Science Institute, RIKEN,

Wako, Saitama 351-0198,

Japan

⁴Laboratory of Theoretical Neurobiology

University of Antwerp

B2610 Antwerp

Belgium

⁵Department of Molecular and Human Genetics

Baylor College of Medicine

Houston, Texas

Summary

Absence of functional FMRP causes Fragile X syndrome. Abnormalities in synaptic processes in the cerebral cortex and hippocampus contribute to cognitive deficits in Fragile X patients. So far, the potential roles of cerebellar deficits have not been investigated. Here, we demonstrate that both global and Purkinje cell-specific knockouts of *Fmr1* show deficits in classical delay eyelid conditioning in that the percentage of conditioned responses as well as their peak amplitude and peak velocity are reduced. Purkinje cells of these mice show elongated spines and enhanced LTD induction at the parallel fiber synapses that innervate these spines. Moreover, Fragile X patients display the same cerebellar deficits in eyelid conditioning as the mutant mice. These data indicate that a lack of FMRP leads to cerebellar deficits at both the cellular and behavioral levels and raise the possibility that cerebellar dysfunctions can contribute to motor learning deficits in Fragile X patients.

Introduction

Fragile X syndrome is the most common, known monogenic cause of mental retardation (De Vries et al., 1997; Turner et al., 1996). Clinically the syndrome is characterized by mental retardation, hyperactive behavior, attention deficits, facial abnormalities, and macro-

orchidism (Hagerman and Hagerman, 2002). The gene involved is the Fragile X mental retardation 1 gene, *FMR1*, which contains in the 5' UTR region a polymorphic CGG repeat (Fu et al., 1991; Verkerk et al., 1991). In Fragile X patients, this repeat spans more than 200 CGG units, which, in turn, causes methylation of the promoter region of *FMR1* and thereby functionally inactivates the gene. Due to inactivation of *FMR1*, its protein, FMRP, is absent in patients, while it is normally expressed in a panneuronal fashion (Verheij et al., 1993; Bakker et al., 2000).

A mouse model for Fragile X syndrome has been created by interruption of the mouse *Fmr1* gene (The Dutch-Belgian Fragile X Consortium, 1994). This knockout mouse shows behavioral and cognitive abnormalities comparable to the symptoms found in Fragile X patients, and several of these symptoms can be linked to a dysfunction of a particular brain region. For example, their enhanced startle responses to auditory stimuli and their reduced freezing behavior in response to both contextual and conditional fear stimuli indicate a malfunction of the amygdala (Chen and Toth, 2001; Nielsen et al., 2002; Paradee et al., 1999). Similarly, the tendency of the knockout mice to show a deficiency in their ability to learn the position of a hidden escape platform in a water maze task suggests hippocampal dysfunction (D'Hooge et al., 1997; Dobkin et al., 2000). To date, a potential contribution of cerebellar dysfunctions to the deficits in Fragile X patients has not been elucidated.

The pathological cellular mechanisms that may underlie the cortical behavioral and cognitive deficits described above are probably related to dysfunctions at the level of dendritic spines and their input. The dendritic spines of pyramidal cells of both Fragile X patients and *Fmr1* knockout mice are unusually long and irregular (Comery et al., 1997; Irwin et al., 2001; Rudelli et al., 1985). Since these spines appear morphologically immature, FMRP has been suggested to be involved in spine maturation and pruning, as well as in synaptogenesis (Comery et al., 1997). Indeed, FMRP and *Fmr1* mRNA are present in spines and/or dendrites, and FMRP is translated in response to activation of the type 1 metabotropic glutamate receptors (mGluR-1) in synaptoneuroosomes (Weiler et al., 1997). The function of FMRP as an inhibitor of translation of bound mRNAs in vitro, including its own mRNA and that of proteins involved in microtubule-dependent synapse growth and function, indicates that FMRP may act as a regulator of activity-dependent translation in synapses (Brown et al., 2001; Li et al., 2001; Miyashiro et al., 2003). This possibility is supported by the finding that the induction of mGluR1-dependent long-term depression (LTD) is enhanced in pyramidal cells of the hippocampus in *Fmr1* knockout mice (Huber et al., 2002). Thus, altered hippocampal LTD in Fragile X patients may interfere with normal formation and maintenance of synapses required for particular cognitive functions.

Metabotropic GluR1-dependent LTD, which appears to require rapid translation of mRNA, can also be in-

*Correspondence: c.dezeuw@erasmusmc.nl

⁶These authors contributed equally to the present study

duced at the parallel fibers (PF) to Purkinje cell (P cell) synapses in the cerebellum (Coesmans et al., 2003; Karachot et al., 2001). Absence of FMRP in cerebellar P cells could, therefore, similarly to the consequences of its absence in the pyramidal cells in the hippocampus, cause spine abnormalities in its dendrites, alter LTD induction at its PF inputs, and elicit abnormalities in motor learning behavior that specifically depends on intact cerebellar P cells, such as associative eyeblink conditioning, (Mauk and Donegan, 1997; Kim and Thompson, 1997; Yeo and Hesslow, 1998). Moreover, because the PF inputs to P cell spines compete to some extent with the climbing fiber (CF) input to their dendrites (Ichikawa et al., 2002), absence of FMRP may also affect the normal mono CF innervation of adult P-cells. Thus, to investigate the possibility that cerebellar deficits contribute to Fragile X syndrome, we tested the cerebellar learning capabilities of global and P cell-specific *Fmr1* knockout mice as well as those of Fragile X patients using classical eyeblink conditioning procedures. In addition, we investigated whether such behavioral deficits might be correlated to morphological and/or cell physiological abnormalities of the PF and CF input to P cells.

Results

Eyeblink Conditioning Is Affected in Both Global *Fmr1* Null Mutants and Purkinje Cell-Specific *L7-Fmr1* Knockouts

To find out whether a lack of FMRP can cause deficits in cerebellar eyeblink conditioning, we first subjected global *Fmr1* null mutant mice ($n = 10$) and wild-type littermates ($n = 9$), during four paired training sessions, to a classical eyeblink conditioning task (Koekkoek et al., 2002). The percentage of conditioned responses (CRs) in the global mutants was significantly reduced at sessions T2, T3, and T4 ($p < 0.05$, Student's *t* tests; $p < 0.005$, MANOVA) (Figure 1A). In addition, the global mutants showed significant deficits in both the peak amplitude and peak velocity of their CRs during training sessions T3 and T4, but not during sessions T1 and T2 (for both parameters at both T3 and T4, $p < 0.05$, Student's *t* tests) (Figures 1B and 1C). In contrast, the latencies to the onset and peak amplitude of the CRs were not significantly affected in the global null mutant (latency to onset: 109 ± 8 ms in mutants versus 102 ± 5 ms in wild-types; $p > 0.4$, Student's *t* test; latency to peak amplitude: 295 ± 14 ms in mutants versus 315 ± 15 ms in wild-types; $p > 0.3$, Student's *t* test). After two sessions of extinction, the percentages of CRs in both wild-types and global *Fmr1* null mutants were significantly reduced (in both cases, $p < 0.01$, Student's *t* tests). Moreover, when the conditioned stimulus (CS) and unconditioned stimulus (US) were randomly paired, virtually no CRs were observed. Finally, to determine possible effects of a lack of FMRP on the eyeblink reflex itself, we further analyzed the kinetics of the unconditioned responses (URs). The amplitudes (0.68 ± 0.03 mm) and peak velocities (44.9 ± 2.07 mm/s) of the URs in the mutants were not significantly different from those (0.73 ± 0.03 mm and 47.3 ± 2.04 , respectively) in wild-types ($p > 0.25$ for both comparisons; Student's *t* tests). Thus, it appears unlikely that differences in sen-

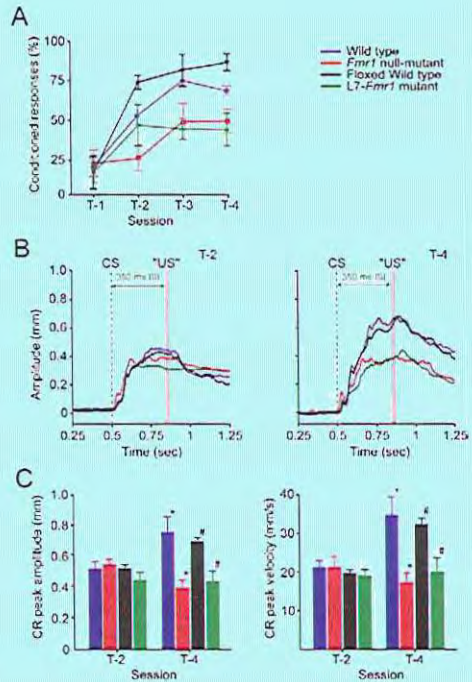


Figure 1. Eyeblink Conditioning Is Impaired in Both Global *Fmr1* Null Mutants and P Cell-Specific *L7-Fmr1* Mutants

(A) Mean percentages (\pm SEM) of significant CRs over 4 days of paired training for global *Fmr1* null mutants (red; $n = 10$) and wild-type littermates (blue; $n = 9$) as well as for *L7-Fmr1* mutants (green; $n = 7$) and floxed controls (black; $n = 8$). These data show that *Fmr1* mutants cannot improve the percentage of their CRs during the training as well as wild-types can. (B) Examples of data sets for training sessions T-2 (left) and T-4 (right), showing the average amplitude of CS-only responses of a representative global *Fmr1* null mutant (red), wild-type littermate (blue), *L7-Fmr1* mutant (green), and floxed control (black). Note that at T-4, both the wild-type animals and *Fmr1* mutants show reasonably well-timed responses around the moment when the US is supposed to take place ("US"), while the sizes of the responses of the *Fmr1* mutants remain fixed in amplitude over the training sessions. (C) Histograms showing average peak amplitudes and peak velocities of global *Fmr1* null mutants (red), wild-type littermates (blue), *L7-Fmr1* mutants (green), and floxed controls (black) at T-2 and T-4. In contrast to the *Fmr1* mutants, wild-type animals show a significantly increased peak amplitude and peak velocity at T-4 (for all comparisons, * $p < 0.05$ and # $p < 0.05$), but not at T-2. Error bars indicate SEM.

sitivity to the US among *Fmr1* null mutants and wild-types contribute to the differences in CRs.

Because the eyeblink paradigm in mice is largely controlled by the cerebellum (Koekkoek et al., 2003), the data described above suggest that a lack of FMRP in cerebellar neurons is at least partly responsible for the behavioral deficits. We therefore investigated to what extent the abnormal conditioning behavior can be explained by a lack of FMRP specifically in P cells, which form the main site of integration for the PF and

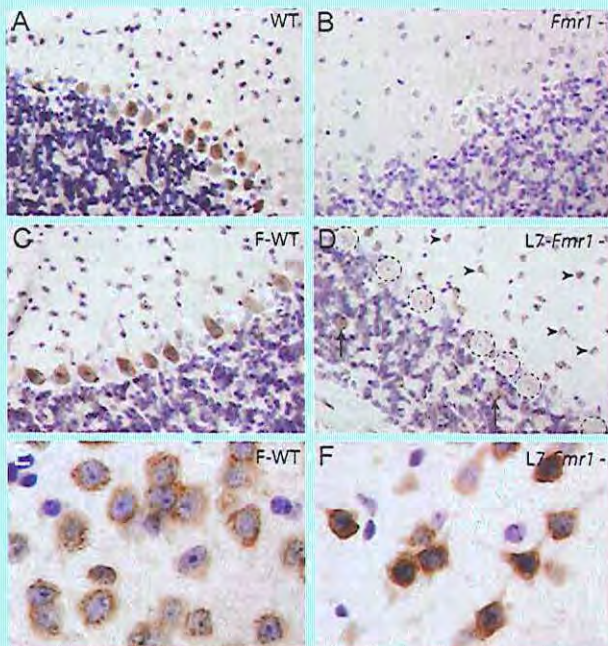


Figure 2. FMRP Expression in Wild-Type, Global *Fmr1* Null Mutant, Floxed Control, and *L7-Fmr1* Mutant Mice

FMRP expression in wild-type (A), global *Fmr1* null mutant (B), floxed control (C and E), and *L7-Fmr1* mutant (D and F) mice, using immunoperoxidase staining on paraffin sections. Note in (D) that the P cells of the *L7-Fmr1* mutant are not labeled (dashed circles), while Golgi cells (arrows) and stellate cells (arrowheads) are positively stained for FMRP in the same section. In contrast, in cerebellar sections of the global *Fmr1* null mutant (B) or the wild-types (A and C), none or all of these types of neurons are labeled, respectively. In the cerebral cortex virtually all neurons were positively labeled both in the floxed wild-type (E) and the *L7-Fmr1* mutant (F).

CF inputs and are the sole output of the cerebellar cortex. P cell-specific *Fmr1* knockout mice were created using crossbreedings of *L7-cre* mice and floxed *Fmr1* mutants. Immunohistochemical analysis demonstrated that the *L7-Fmr1* knockout mice did not express FMRP, while their surrounding neurons in the cerebellum, as well as neurons outside the cerebellum, did (Figure 2). Like the global *Fmr1* null mutants the P cell-specific *L7-Fmr1* mutants ($n = 7$) showed a significantly reduced percentage of CRs on days T-3 and T-4 in comparison with both the wild-type littermates of the global *Fmr1* mutants and their floxed controls ($n = 8$ for both sessions and both control groups; $p < 0.05$, Student's *t* tests) (Figure 1A). Moreover, the positive CRs showed significantly lower amplitudes and velocities on days T-3 and T-4 (for both parameters, $p < 0.05$, Student's *t* tests; Figures 1B and 1C), while the timing properties were unaffected (latency to onset: 115 ± 18 ms in mutants versus 111 ± 8 ms in wild-types; $p > 0.7$, Student's *t* test; latency to peak amplitude: 296 ± 17 ms in mutants versus 302 ± 17 ms in wild-types; $p > 0.6$, Student's *t* test). In addition, the amplitudes and velocities of the URs did not differ from those in their controls ($p > 0.1$ for all comparisons; Student's *t* test). These data demonstrate that a lack of FMRP in P cells alone is sufficient to replicate the deficits in eyeblink conditioning described above for the global knockout.

Startle Responses Are Enhanced in Global *Fmr1* Null Mutants but Not in Purkinje Cell-Specific *L7-Fmr1* Knockouts

Since enhanced startle responses to auditory stimuli have also been associated with Fragile X syndrome

(Chen and Toth, 2001; Nielsen et al., 2002), we also analyzed the initial 60 ms periods, following the onset of the tone, of the eyeblink responses in both the global *Fmr1* mutants and P cell-specific *L7-Fmr1* mutants, as well as in their controls. This analysis showed that during all training sessions the peak amplitudes of the startle responses in the global *Fmr1* mutants, but not those in the P cell-specific *L7-Fmr1* mutants, were significantly higher than those of wild-types (for all sessions T1-T4, $p < 0.001$, Student's *t* tests) (Figure 3). Moreover, the percentage of startle responses was significantly increased during all sessions in the global *Fmr1* mutants, but not in the P cell-specific *L7-Fmr1* mutants ($p < 0.05$, MANOVA). These differences between the global and P cell-specific mutants suggest that a lack of FMRP in regions outside of the cerebellum can enhance the startle response, and therefore follows the notion that startle responses are controlled primarily by higher brain structures such as the amygdala (Paradee et al., 1999). In addition, these differences once again illustrate the sensitivity and specificity of the magnetic distance measurement technique (MDMT) recording method that we employ for eyeblink conditioning (Koekoek et al., 2002; De Zeeuw et al., 2004).

LTD Is Enhanced in Purkinje Cells of both Global *Fmr1* Mutants and *L7-Fmr1* Mutants

Because deficits in eyeblink conditioning have been associated with cell physiological deficits of the PF-P cell synapse (Shibuki et al., 1996; Koekoek et al., 2003), we investigated the induction of LTD and the efficacy of this synapse in slices of *Fmr1* mutants. LTD was in-

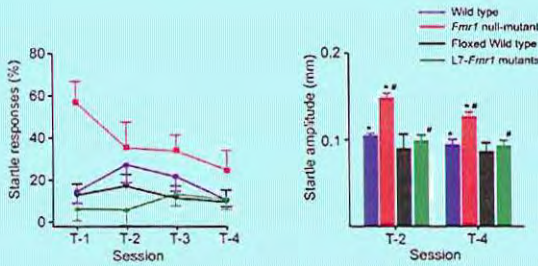


Figure 3. Startle Responses Are Enhanced in Global *Fmr1* Null Mutants, but Not in P Cell-Specific *L7-Fmr1* Mutants

(Left panel) The percentage of startle responses in wild-types and mutants during the initial 60 ms period of the eyeblink responses. Note that this percentage was significantly increased during all sessions in global *Fmr1* null mutants (red) as compared to wild-type littermates (blue), *L7-Fmr1* mutants (green), and floxed wild-type controls (black). (Right panel) Peak amplitudes of the startle responses of *Fmr1* null mutants were significantly higher than those of wild-type littermates, *L7-Fmr1* mutants, and floxed controls ($p < 0.001$ [* and #]; Student's *t* tests). Error bars indicate SEM.

duced by conjunctively applying PF stimuli and depolarizing pulses (single pulses, 140 ms duration; from -70 to $+10$ mV) at 1 Hz for 5 min after reaching stable recordings of EPSCs during PF stimulation at 0.2 Hz for 10 min (Miyata et al., 1999). Figure 4A shows that this conjunctive stimulation induced LTD in both wild-type ($n = 7$) and global *Fmr1* mutant mice ($n = 6$), as represented by a significant reduction in PF-EPSC (in both cases $p < 0.01$, Student's *t* tests). Hyperpolarizing pulse-evoked currents hardly changed in both wild-types and global *Fmr1* mutants ($p > 0.5$ in both cases, Student's *t* tests), implying that conjunctive stimulation does not affect access resistance, input resistance, or membrane capacitance. The change in access resis-

tance after conjunctive stimulation was no more than 2% on average in the cells used for analyses (10 wild-type and 10 mutant cells). During the 15 min period from 21 to 35 min after the onset of conjunctive stimulation, the mean amplitude of the PF-EPSCs was reduced to $70.4\% \pm 1.3\%$ in wild-types and to $60.7\% \pm 2.3\%$ in global *Fmr1* mutant mice. Thus, the induction of LTD in P cells of global *Fmr1* null mutants was significantly enhanced compared with that in wild-types ($p < 0.01$; Duncan's New Multiple Range Test) (Figure 4B). LTD was also induced using double shock stimulation of PFs at a 50 ms interval combined with the depolarizing pulse. The depression of PF-EPSC obtained with this double shock protocol in the global mutant mice was

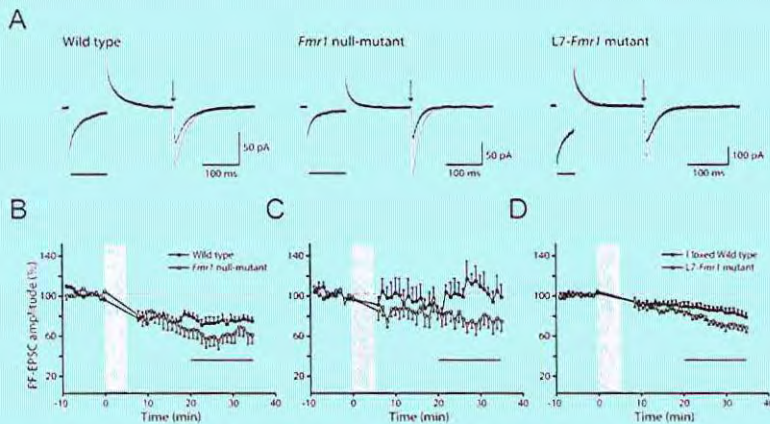


Figure 4. LTD Induction Is Enhanced in Purkinje Cells of Global *Fmr1* Null Mutants and *L7-Fmr1* Mutants

(A) Superimposed PF-EPSCs in three of the P cells recorded before conjunctive stimulation and 33 min (wild-type), 31 min (global *Fmr1* null mutant), or 32 min (*L7-Fmr1* mutants) after conjunctive stimulation, each trace representing an average of 12 traces. Note the stronger reduction of the PF-EPSCs in the mutants. Horizontal bars indicate hyperpolarizing pulses (2 mV, 100 ms) used for monitoring access resistance and input resistance, while downward arrows indicate moments of PF stimulation. (B) PF-EPSC amplitude is plotted against time before and after conjunctive stimulation averaged for 10 cells from seven wild-type mice and 10 cells from six global *Fmr1* null mutant mice. In each of these cells, 12 records successively acquired at 0.2 Hz were averaged to obtain PF-EPSC values for every minute. The shaded column indicates the period of conjunctive stimulation. (C) PF-EPSC amplitude is plotted against time for repetitive stimulation of PFs in global *Fmr1* null mutants. (D) PF-EPSC amplitude is plotted against time before and after conjunctive stimulation averaged for seven cells from seven floxed wild-type mice and six cells from six *L7-Fmr1* mutant mice. In (B)–(D), vertical bars extending either upward or downward from the plotted points indicate SEM.

72.5% \pm 1.1% ($n = 5$), which was relatively modest. Nevertheless, it was still enhanced compared to the depression of 81.8% \pm 0.9% ($n = 4$) ($p < 0.01$, ANOVA) obtained in wild-type mice with the same double shock protocol.

To find out whether the difference in LTD induction between wild-types and global mutants is specific to conjunctive stimulation, we also tested the effect of repetitive stimulation of PFs only at 1 Hz for 5 min. Indeed, this stimulus paradigm induced depression to 75.6% \pm 2.5% of the baseline values in global *Fmr1* mutants, while it did not cause a significant reduction in PF-EPSCs of P cells in wild-types. In these experiments too, the difference between wild-types and mutants was greatest 20 min after onset of the tetanus protocol. Thus, LTD induction following repetitive stimulation of PFs alone in global mutant mice is comparable to that following conjunctive stimulation in wild-type mice ($p > 0.05$, ANOVA), but smaller than that following conjunctive stimulation in global *Fmr1* mutants ($p < 0.01$, ANOVA) (Figures 4B and 4C).

The differences in LTD induction between global mutants and wild-types raise the question of whether the general synaptic efficacy of the PF-P cell synapse is also affected in *Fmr1* mutants. We therefore investigated the relationships between stimulation strength and PF-EPSC amplitude; paired-pulse facilitation of PF-EPSCs, facilitation, and fatigue of PF-EPSCs; maximum amplitude of metabotropic glutamate receptor type 1 (mGluR1)-dependent slow PF-EPSCs, thresholds, and maximum firing rate of Na⁺-spikes; and maximum Ca²⁺ current and density of voltage-dependent Ca²⁺ channels in P cells. None of these parameters differed between global *Fmr1* mutants and wild-type littermates (see Table 1 in the Supplementary Data available with this article online). Thus, these control data suggest that the basic synaptic efficacy of the PF-P cell synapse is not affected in *Fmr1* mutants.

Since the PF input to the dendrites of a P cell competes with its CF input (Cesa et al., 2003; Kakizawa et al., 2000), the affected level of PF-LTD in *Fmr1* mutants may possibly be related to an abnormal CF input. We therefore investigated the strength and depression of CF-EPSCs, and we examined whether the global *Fmr1* mutants suffer from a persistent multiple CF input (Kano et al., 1998). The CF-EPSCs in mutant P cells did not show any significant anomaly in that both the absolute strength and paired-pulse depression in null mutants ($n = 7$) were indistinguishable from those in wild-types ($n = 7$) ($p > 0.4$ and $p > 0.16$, respectively, Student's *t* tests). The paired-pulse depression of the CF-EPSCs was 81.7% \pm 1.8% in P cells of the mutant mice compared with 77.5% \pm 2.3% in the wild-type mice. In regard to the number of CF inputs per P cell, we found that 60.4% of the P cells ($n = 48$) in wild-types tested at P21–48 showed a single-CF innervation, while double- and triple-CF innervations were observed in 35.4% and 4.2% of the cases, respectively. In mutant mice, single-, double-, and triple-CF innervations were observed in 75.6%, 22.2%, and 2.2% of the P cells ($n = 45$) tested, respectively. The percentage of single-CF innervation was in fact higher in the mutants than in the wild-types ($p < 0.01$, χ^2 test). Thus, the CF input to P cells in *Fmr1* mutants does not show any sign of a pre-

or postsynaptic deficit, and their development does not show any sign of a delay; in contrast, the normal development from multiple to mono-CF innervation is accelerated.

Finally, to investigate whether the enhancement in LTD induction is due solely to an intrinsic abnormality of P cells or whether it results from an interactive process between P cells and their surrounding neurons, we also investigated LTD of the PF-P cell synapse in cerebellar slices of the P cell-specific *L7-Fmr1* mutants. Here too, conjunctive stimulation induced LTD in both the P cell-specific *L7-Fmr1* mutant mice ($n = 6$) and the floxed controls ($n = 7$), as represented by a significant reduction in PF-EPSC (in both cases, $p < 0.01$, Student's *t* tests) (Figure 4D). Hyperpolarizing pulse-evoked currents changed minimally in both controls and mutants ($p > 0.35$ in both cases, Student's *t* tests), implying that conjunctive stimulation does not affect access resistance, input resistance, or membrane capacitance. The change in access resistance after conjunctive stimulation was no more than 3% on average in the cells used for analyses (seven control and six mutant cells). During the period from 21 to 35 min after the onset of conjunctive stimulation, the mean amplitude of the PF-EPSCs was significantly more reduced in *L7-Fmr1* mutant mice (72.9% \pm 1.3%) than in controls (83.2% \pm 0.8%) ($p < 0.01$; Duncan New Multiple Range Test). Thus, the enhancement in LTD induction found in global *Fmr1* mutants was also found in P cell-specific *L7-Fmr1* mutants, indicating that the difference with the wild-types can indeed be attributed to an intrinsic effect of the P cells themselves.

Morphology of Purkinje Cells

The finding that P cells in the cerebellum of *Fmr1* mutants show an enhanced level of LTD induction at the PF input to their dendritic spines raises the question of whether the dendritic tree of P cells in *Fmr1* mutants shows morphological abnormalities. As revealed by both calbindin immunocytochemistry and intracellular labeling with biotinylated dextran amine (BDA), the dendrites and axons of P cells of *Fmr1* null mutants appeared normal at the light microscopic level (Figure 5). The ramifications of the dendrites were not significantly different ($p > 0.6$, Student's *t* test) when analyzed with topological analyses for symmetry of arborizations (Van Pelt et al., 1992). The spine densities of distal dendrites with an average diameter smaller than 1.5 μm were 1.22 \pm 0.30 spines/ μm (mean \pm SD) and 1.18 \pm 0.27 spines/ μm (mean \pm SD) in *Fmr1* null mutants ($n = 7$) and wild-types ($n = 7$), respectively. Likewise, the spine density in dendritic fragments with an average diameter bigger than 1.5 μm (proximal category) was 1.26 \pm 0.27 spines/ μm (mean \pm SD) in *Fmr1* null mutants and 1.22 \pm 0.20 spines/ μm (mean \pm SD) in wild-types. Thus, unlike the pyramidal cells in cerebral cortical areas, the spine density of cerebellar P cells in *Fmr1* null mutants did not differ significantly from that in their wild-type littermates (distal versus distal, $p > 0.5$; proximal versus proximal, $p > 0.5$; total versus total, $p > 0.5$; Student's *t* tests).

In contrast, the shape of the spines of P cells in *Fmr1* null mutants differed from that in wild-types. Electron

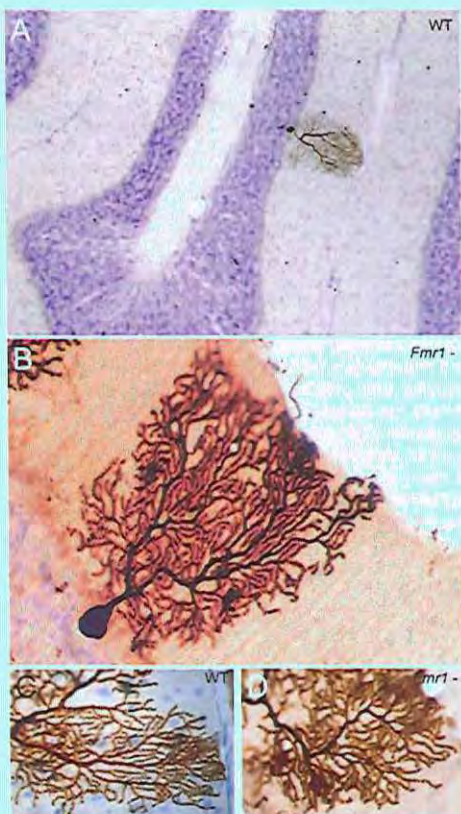


Figure 5. Dendritic Arborization of the Purkinje Cells in Global *Fmr1* Null Mutants Is Normal

Light microscopic images of the dendritic trees of P cells in wild-types (A and C) and *Fmr1* null mutants (B and D) that are retrogradely labeled with BDA. Both the topology of the P cell dendrites and the density of their spines appear normal.

microscopic analysis of calbindin-stained P cells showed that their spines were more irregular and longer (Figure 6A). The average lengths of the spine head and spine neck in *Fmr1* null mutants ($0.56 \pm 0.05 \mu\text{m}$ and $0.63 \pm 0.18 \mu\text{m}$, respectively; $n = 4$) were significantly greater than those in wild-types ($0.50 \pm 0.04 \mu\text{m}$ and $0.46 \pm 0.15 \mu\text{m}$, respectively; $n = 4$) ($p < 0.05$ and $p < 0.001$ for heads and necks, respectively; Student's *t* tests). The spine head diameter, spine head length/spine head diameter ratio, average spine neck diameter, and minimal spine neck diameter of *Fmr1* null mutants were not significantly different from those of wild-types (for all parameters, $p > 0.2$, Student's *t* tests). Finally, electron microscopic analyses of the spine densities did not reveal any difference, either, between mutants and wild-types ($p > 0.6$; Student's *t* test).

To find out whether the differences in lengths of spine

heads and necks were due to intrinsic changes of the P cells rather than an interaction with the environment, we also investigated the P cell spines in the *L7-Fmr1* mutant mice at the ultrastructural level (Figure 6B). The average lengths of the spine head and spine neck in *L7-Fmr1* mutants ($0.57 \pm 0.07 \mu\text{m}$ and $0.70 \pm 0.1 \mu\text{m}$, respectively; $n = 4$) were significantly greater than those in the floxed controls ($0.45 \pm 0.05 \mu\text{m}$ and $0.42 \pm 0.08 \mu\text{m}$, respectively; $n = 4$) ($p < 0.05$ and $p < 0.02$ for heads and necks, respectively; Student's *t* tests) (Figure 6C). No differences were observed in the densities of the spines ($p > 0.4$; Student's *t* test). Thus, similar to the global mutants, the P cell-specific *L7-Fmr1* mutants showed longer spines in which the necks were particularly elongated, while the number of spines appeared normal.

Eyeblink Conditioning Following Lesions of Cerebellar Nuclei in Trained Animals

The eyeblink data of the *Fmr1* mutants indicate that the output of the cerebellum to a large extent controls the conditioning process. However, since the mutants do not express FMRP in their P cells in early development or thereafter, we cannot exclude the possibility that secondary developmental aberrations downstream of the P cells do occur. This possibility may be especially valid for the global mutants, because the neurons involved in the eyeblink pathway downstream of the P cells also lack FMRP. We therefore investigated the change in CRs in the global *Fmr1* mutants ($n = 4$) and in their wild-type littermates ($n = 4$) after bilateral lesions of the anterior interposed nuclei, which form the ultimate cerebellar output mediating control signals for eyeblink responses (Yeo and Hesslow, 1998; Koekkoek et al., 2003). Figures 7A and 7B show an example of such lesions in an *Fmr1* mutant and their impact on the number of degenerating fibers in the superior cerebellar peduncles and the ipsilateral descending tracts, which are indicative for abundant damage in the anterior interposed nuclei (Teune et al., 2000). Following such lesions in trained wild-types and trained global *Fmr1* mutants, the percentages of CRs were reduced by $36\% \pm 11\%$ and $21\% \pm 6\%$, respectively. Both changes were significant ($p < 0.01$ and $p < 0.05$, respectively; Wilcoxon rank-sum test). In addition, the remnant responses showed a reduction in amplitude (for wild-types and global *Fmr1* mutants: $42\% \pm 9\%$ and $25\% \pm 8\%$, respectively) and latency to peak amplitude (for wild-types and global *Fmr1* mutants: $35\% \pm 1\%$ and $30\% \pm 8\%$, respectively) (Figure 7C). Both changes were significant for both wild-types and *Fmr1* mutants (for all comparisons, $p < 0.05$, Wilcoxon rank-sum tests). While percentages of CRs and CR amplitude values were significantly different between wild-types and null mutants after training session T-4 before the lesion ($p < 0.05$ and $p < 0.05$, respectively; Student's *t* tests), these differences disappeared after the lesions ($p = 0.25$ and $p = 0.3$, respectively; Student's *t* tests). The results of these experiments confirm that the main differences in eyeblink conditioning parameters, such as the changes in peak amplitude and peak velocity that we observed between unlesioned *Fmr1* mutants and their wild-type littermates, are largely due to a direct

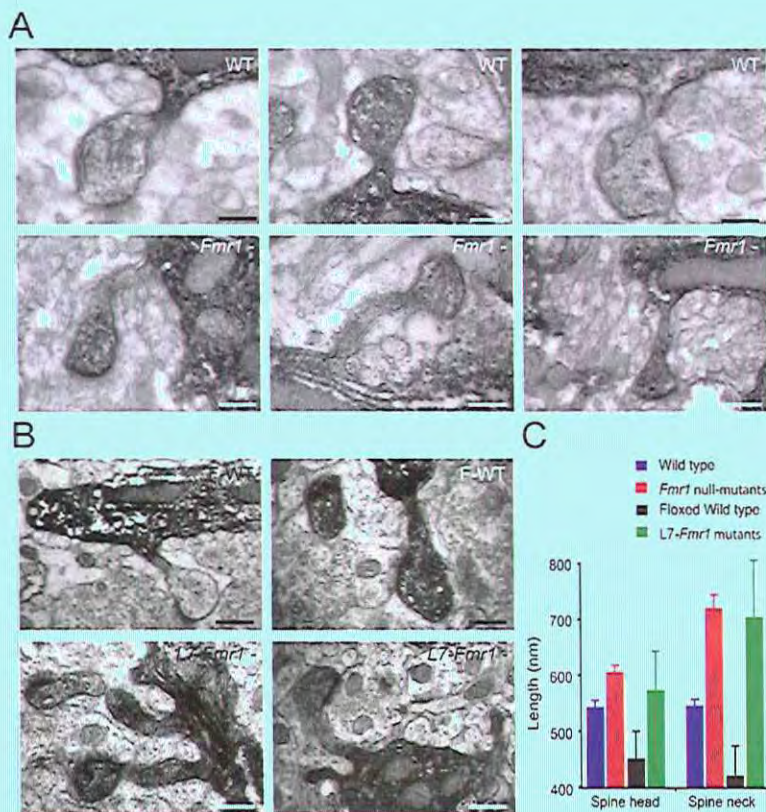


Figure 6. Ultrastructural Characteristics of Purkinje Cell Spines in *Fmr1* Null Mutants and *L7-Fmr1* Mutants Are Abnormal

(A) Electron microscopic images of the morphology of individual P cell spines in wild-types (WT; top panels) and global *Fmr1* null mutants (*Fmr1*⁻; bottom panels) that are labeled following immunocytochemistry with an antibody against calbindin. Note the longer and more irregularly shaped spines in *Fmr1* null mutants. Scale bars in micrographs of the wild-types represent 271 nm, 283 nm, and 260 nm, respectively (left to right). Scale bars in micrographs of the *Fmr1* mutants represent 297 nm, 309 nm, and 321 nm, respectively (left to right).

(B) Electron micrographs of individual P cell spines in floxed wild-types (F-WT; upper panel) and P cell-specific *L7-Fmr1* mutants (*L7-Fmr1*⁻; bottom panel) that are labeled following calbindin immunocytochemistry. Scale bars in micrographs of the floxed wild-types represent 279 nm and 257 nm, respectively (left to right). Scale bars in micrographs of the *L7-Fmr1* mutants represent 307 nm and 342 nm, respectively (left to right).

(C) Histograms of average lengths (+SD) of spine heads and spine necks in *Fmr1* mutants ($n = 194$), wild-type littermates ($n = 204$), *L7-Fmr1* mutants ($n = 124$), and floxed wild-type controls ($n = 113$).

difference in cerebellar control; in addition, they suggest that these differences are not due to secondary developmental aberrations downstream of their P cells.

Eyeblink Conditioning in Fragile X Patients

The data described above indicate that an animal model of Fragile X syndrome shows deficits in eyeblink conditioning and that this deficit is probably due largely to a lack of FMRP in cerebellar P cells. To find out whether a lack of functional FMRP in humans leads to the same deficits in cerebellar motor learning, we tested affected males ($n = 6$) and controls ($n = 6$), using an eyeblink conditioning task in which the eyelids are

conditioned to a tone. The patients showed severe deficits (Figure 8). The peak amplitude (0.14 ± 0.03 cm) and peak velocity (3.3 ± 0.7 cm/s) in affected Fragile X males were, on average, significantly lower ($p < 0.001$ and $p < 0.001$, respectively; Student's *t* test) than those in normal subjects (0.54 ± 0.06 cm and 10.0 ± 1.5 cm/s, respectively). When separated according to training session (T1, T2, T3, and T4), peak amplitudes in Fragile X patients were significantly smaller than those in controls after T2, T3, and T4 (for T2 and T3, $p < 0.05$; for T4, $p < 0.005$; Student's *t* tests), while peak velocities in Fragile X patients were significantly smaller after T3 and T4 (in both cases, $p < 0.05$, Student's *t* tests).

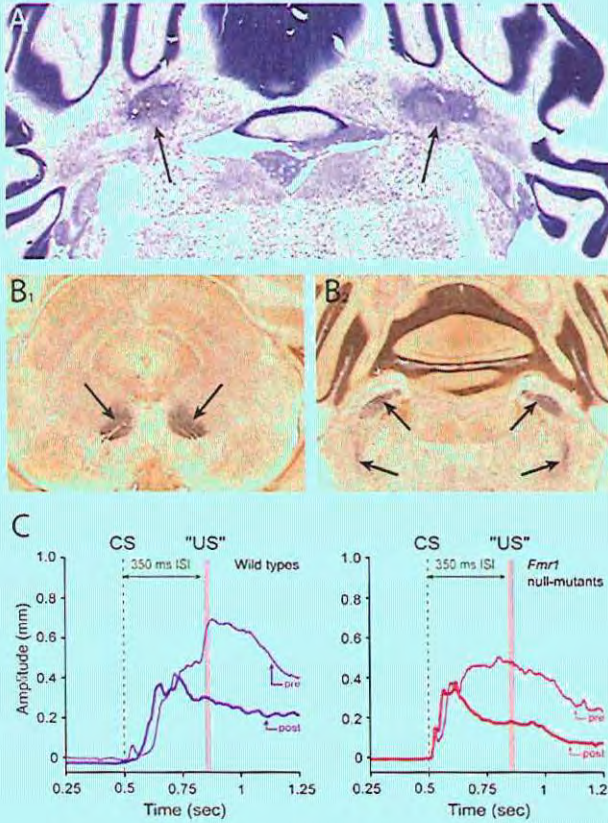


Figure 7. Bilateral Lesions of Anterior Interposed Nuclei Lead to Relatively Comparable Eyeblink Traces in Trained Wild-Types and *Fmr1* Null Mutants

(A) Example of bilateral lesion (arrows) of anterior interposed nuclei in Nissl-stained section of *Fmr1* null mutant.
 (B) Example of degenerated axonal fibers (silver staining is indicated by arrows) in the superior cerebellar peduncles (left) and ipsilateral descending tracts (right); the latter are indicative for lateral damage to the anterior interposed nucleus (Teune et al., 2000).
 (C) Traces showing the average amplitudes of the CRs in wild-types (left, blue) and *Fmr1* null mutants (right, red) before (thin line) and after (thick line) the lesions.

In addition, Fragile X patients showed a robust decrease in the number of CRs that were acquired during and after training (Figure 8C). The percentage of CRs was on average $80.3\% \pm 4.0\%$ in control subjects and $37.6\% \pm 2.7\%$ in affected males. For all sessions, the differences in the percentage of CRs were significant (T1, $p < 0.005$; T2, T3, and T4, $p < 0.001$; Student's *t* tests). In contrast, neither the average onset latency (0.87 ± 0.05 s) nor the average latency to peak amplitude of the CRs (0.95 ± 0.06 s) in affected males ($p = 0.29$ and $p = 0.30$, respectively; Student's *t* tests) differed from those in controls (0.92 ± 0.02 s and 1.02 ± 0.03 s, respectively). UR kinetics were analyzed to check for possible deficits in reflex pathways that may contribute to reduced motor learning (Figure 8C). Neither the mean amplitude (0.59 ± 0.05 cm) nor the mean velocity (13.4 ± 1.5 cm/s) of the responses in Fragile X patients differed from those in controls (0.57 ± 0.06 cm and 15.9 ± 2.0 cm/s, respectively) ($p = 0.88$ and $p = 0.31$, respectively; Student's *t* tests). Finally, when we subjected Fragile X patients and controls to randomly paired training paradigms, no CRs were observed. From these data, we conclude that Fragile X patients

show the same deficits in eyeblink conditioning as those that we observed in the animal models of Fragile X.

Modeling Deficits in Eyeblink Conditioning Associated with Enhanced LTD

The observation that *Fmr1* mutants show both deficits in eyeblink conditioning and enhanced PF LTD raises the question of whether these two factors are causally related. Such a relationship seems counterintuitive because PF LTD is assumed to form an important memory trace for cerebellar conditioning (Koekkoek et al., 2003; Mauk and Donegan, 1997; Yeo and Hessler, 1998). We therefore investigated whether enhanced LTD can lead to a diminished eyeblink response in a model (Figure 9). The model that we created is focused on the impact of P cells on cerebellar nuclei neurons and is based on the following assumptions: (1) during its time course, the CS activates consecutively different sets of granule cells (Medina and Mauk, 2000); (2) for each activated granule cell, the strength of LTD depends on the length of the time interval to the CF stimulus (Wang et al., 2000); (3) LTD at a PF synapse will decrease the re-

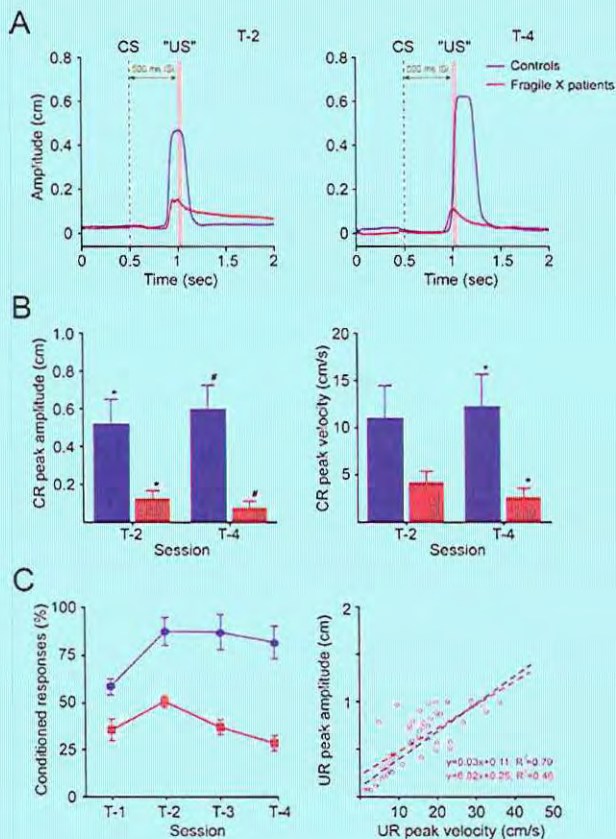


Figure 8. Eyeblink Conditioning Is Impaired in Fragile X Patients

(A) Examples of data sets for training sessions T-2 (left) and T-4 (right), showing the average amplitude of CS-only responses of a control subject (blue) and a Fragile X patient (red). (B) Histograms showing average peak amplitudes (left) and peak velocities (right) for all tested controls ($n = 6$) and Fragile X patients ($n = 6$) at T-2 and T-4. * indicates $p < 0.05$ and # indicates $p < 0.005$. (C) While the mean percentages (\pm SEM) of CRs in control subjects are significantly higher than those in Fragile X patients after each of the four training sessions (T1–T4; left), the kinetics of their unconditioned responses are indistinguishable from each other (right). Error bars indicate SEM.

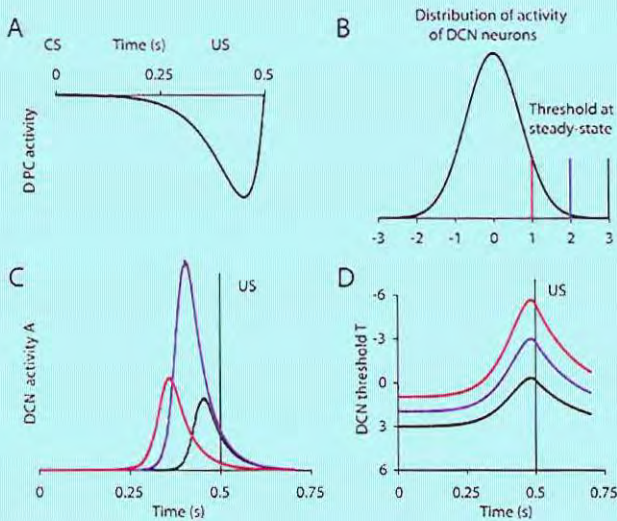
sponse of a P cell to that PF input; (4) fast release from inhibition drives cerebellar nuclei neurons effectively through postinhibitory rebound (Aizenman and Linden, 1999, 2000); (5) the strength of the response of a cerebellar nucleus neuron will be determined not only by instantaneous changes in firing rate of the afferent P cells but also by the steady-state level of the activity of cerebellar nuclei neurons (a depolarization of the average resting membrane potential of cerebellar nuclei neurons can, by diminishing deactivation of T-type Ca^{2+} channels, reduce the number of neurons that are available for postinhibitory rebound); (6) increased LTD in Fragile X results in reduced P cell activity and decreased inhibition of cerebellar nuclei neurons at the resting level; and (7) the motor response during a CR is determined by the instantaneous firing rate of a subpopulation of neurons in the cerebellar nuclei (Gruart et al., 1997). The details and formulas of the model are presented in the Supplementary Data (see Part II) and outlined in Figure 9. In short, the model demonstrates that a change in balance between excitation and inhibition in the cerebellar nuclei neurons, resulting from enhanced LTD at the

PF-P cell synapse, may cause a paradoxical impairment of the CR. The primary mechanism is exhaustion of the pool of cerebellar nuclei neurons capable of producing postinhibitory rebound when the CS relieves the cerebellar nuclei neurons of P cell inhibition.

Discussion

The present study shows that cerebellar abnormalities in Fragile X syndrome can occur at the morphological level, cell physiological level, and behavioral level. We found that a lack of FMRP results in a unique phenotypic combination of elongated P cell spines, enhanced LTD at the PFs that innervate these spines, and an impaired motor learning capability that is controlled by P cells. This unique combination reveals not only the extent to which cerebellar deficits may contribute to abnormalities in Fragile X syndrome but also possible clues about cerebellar function in general.

The abnormalities of dendritic spines that we observed in cerebellar P cells of both the global and cell-specific *Fmr1* null mutants mimic only partially those



activity (depicted in [A]) drives the threshold leftward, causing disinhibited neurons to produce a rebound response. The response is clearly strongest when starting from an optimal steady state (blue curve, wild-type). Both enhanced (red curve, Fragile X) and reduced (black curve) levels of steady-state DCN excitation reduce the response amplitude.

(D) Time evolution of the threshold (upward corresponding to disinhibition) during the responses computed in (C).

that have been described for pyramidal cells in the cerebral cortex (Comery et al., 1997; Hinton et al., 1991; Irwin et al., 2002). They follow the same pattern in the morphology of individual spines appearing as immature shaped processes with elongated necks and heads, but they differ in that their spine density is normal. Apparently, the density of spines in P cells is more tightly regulated by compensatory mechanisms than that in pyramidal cells is. The spine density in P cells is largely subject to a well-regulated process in which the CFs and PFs compete with each other for specific sites at the dendritic tree (Cesa et al., 2003; Kakizawa et al., 2000). It is therefore attractive to hypothesize that the accelerated elimination of multiple CF inputs that we found in our electrophysiological recordings of *Fmr1* null mutants reflects a mechanism that compensates for a slowdown in spine maturation. Such a view is supported by recent data obtained by Strata and colleagues, who showed that at least two different mechanisms are responsible for spine density and spine pruning in P cells, i.e., one dependent on activity in the CFs and another one that is activity-independent (Bravin et al., 1999; Strata et al., 2000).

One of our major findings is that a lack of FMRP leads to enhanced PF LTD without affecting the basic electrical properties of P cells. Interestingly, this difference between *Fmr1* mutants and their wild-type controls, which has not been described for any other cerebellar mutant before, occurs about 15 min after the offset of conjunctive stimulation of the PFs and CFs or about 15 min after repetitive stimulation of PFs alone. This period directly follows the critical time period during which the presence and expression of one or more

rapidly turned over protein(s) is/are required to induce LTD (Karachot et al., 2001). Thus, since FMRP can operate as a negative regulator of mRNA translation (Laggenbauer et al., 2001), one may assume that FMRP probably normally inhibits the translation of at least one of the proteins that is required for the expression of PF LTD 15 min after its induction. Similar time frames have been found for the impact of a lack of FMRP on the induction of LTD at the CA3-CA1 synapse in the hippocampus (Huber et al., 2002). Based on their recordings in hippocampal slices, Bear and colleagues proposed a model in which they suggest that FMRP serves to limit expression of homosynaptic LTD by inhibiting mGluR-dependent translation of local synaptic mRNAs that are involved in the stabilization of endocytosed AMPA receptors. Because PF LTD is also driven by activation of metabotropic glutamate receptors (Coesmans et al., 2003) and because PF LTD is ultimately also expressed as an endocytosis of AMPA receptors (Xia et al., 2000; Linden, 2001), their hippocampal model may also be applicable to cerebellar P cells. Considering the common specificity of the electrophysiological effects in both the hippocampus and cerebellum in that a lack of FMRP causes enhanced homosynaptic LTD without affecting basic electrophysiological properties, one would expect that the specific behavioral consequence of such a unique defect is prominently present. Unfortunately, the hippocampal deficits that can be observed in *Fmr1* null mutants subjected to spatial learning tests are partially controversial (see e.g., D'Hooge et al., 1997; Dobkin et al., 2000; Van Dam et al., 2000). Here, we show that when subjected to an associative eye-blink test, which allows us to detect deficits specific for

Figure 9. Mathematical Model Illustrating a Critical Sensitivity of the CR on the Steady-State Activity of P Cells (PCs) and Deep Cerebellar Nuclei (DCN) Neurons

(A) Time course of the presumed decrease in PC activity during CS presentation. This curve reflects the dependency of LTD on the relative timing of spikes in parallel and CFs during training (Wang et al., 2000).

(B) Representation of the level of excitation in the population of DCN neurons. Excitation is distributed as depicted by the standard normal curve. The blue vertical line indicates the steady-state position of the firing threshold before CS presentation; changes in PC activity cause the threshold to move leftward (disinhibition) or rightward (inhibition). Sub-threshold neurons are able to produce a rebound burst when disinhibited. The leftward-shifted steady-state threshold (red line, Fragile X) indicates the increased level of excitation that enhanced LTD is predicted to produce in the cerebellar nuclei (see Kenyon et al., 1998); the black-line threshold represents the case of a decreased steady-state excitation, due to decreased LTD or intrinsic excitability.

(C) Simulated rebound DCN activity during presentation of the CS. The decrease in PC activity (depicted in [A]) drives the threshold leftward, causing disinhibited neurons to produce a rebound response. The response is clearly strongest when starting from an optimal steady state (blue curve, wild-type). Both enhanced (red curve, Fragile X) and reduced (black curve) levels of steady-state DCN excitation reduce the response amplitude.

(D) Time evolution of the threshold (upward corresponding to disinhibition) during the responses computed in (C).

cerebellar motor learning, these global *Fmr1* null mutants do have a robust phenotype and that the same behavioral phenotype can be observed in P cell-specific *L7-Fmr1* mutants as well as in Fragile X patients themselves. All of them showed significantly less CRs, and they were all unable to increase the peak amplitude and peak velocity of their CRs during the training. In contrast, the latency to peak amplitude of the CRs was not significantly affected, indicating that learning-dependent timing is not severely impaired by a lack of FMRP. In this respect, the phenotype of LTD-enhanced *Fmr1* mutants diverges from that of LTD-deficient mutants. Transgenic mice in which PF LTD is selectively blocked by P cell-specific expression of an inhibitory peptide against multiple isoforms of protein kinase C (De Zeeuw et al., 1998) cannot adjust the timing of their CRs to the moment of onset of the US (Koekkoek et al., 2003). On the other hand, these LTD-deficient mice show, like the *Fmr1* mutants, a reduced percentage of CRs, and they are also unable to increase the peak amplitude and peak velocity of their CRs during the training. Thus, while the existence of PF LTD may be qualitatively necessary for the occurrence of learning-dependent timing of CRs, the exact level of PF LTD may be quantitatively responsible for the amount of CRs. Perhaps there is a level of expression of PF LTD that is optimal for attaining a maximum level of learned responses. Our model suggests that the CR may be impaired if the average level of the activity of cerebellar nuclei neurons is at a nonoptimal steady-state due to decreased inhibition by P cells. A mathematical model of cerebellar learning (Kenyon et al., 1998) predicted that enhanced LTD at the PF-P cell synapse would cause compensatory changes in the entire cerebello-olivary feedback loop. More particularly, an increased steady-state activity of cerebellar nuclei neurons would be needed to restore the balance between LTD and long-term potentiation (LTP) and to stabilize the weights of the PF-P cell synapses at nonsaturating values (see also Coesmans et al., 2004). The present model suggests that an altered steady-state level of the activity of cerebellar nuclei neurons may, in addition, impair the expression of the CR. Interestingly, the cerebellum may not be the only brain region in which an optimal rather than a maximum level of cellular plasticity is necessary for effective learning behavior. Several studies have demonstrated that a relatively mild enhancement of LTP induction in the hippocampus can be associated with impaired fear conditioning or spatial learning (Gu et al., 2002; Migaud et al., 1998).

Due to the unique aberration of enhanced LTD in *Fmr1* mutants and due to the unique combination of their deficits in classical conditioning, we have not only provided suggestive evidence for the potential importance of an optimal, instead of a maximum, level of PF LTD for cerebellar motor learning, but we have also shown that cerebellar deficits may be associated with learning deficiencies in Fragile X syndrome. Over the past decade, research on the potential roles of the cerebellum in cognitive processes has shown a remarkable advent. Investigations vary from transneuronal tracing studies, showing robust reciprocal and topographic connections between the cerebral and cerebellar cortex via the pons and thalamus (Kelly and Strick,

2003; Middleton and Strick, 1994), to clinical and neuropsychological studies, showing cognitive dysfunctions following cerebellar lesions (Leiner et al., 1993), and imaging studies, showing cerebellar activities correlated with cognitive activities (Kim et al., 1994; Vokaer et al., 2002). Thus, while a lack of FMRP in areas such as the cerebral cortex, amygdala, and hippocampus may induce cognitive symptoms in Fragile X syndrome, the current data allow us to conclude that a lack of functional FMRP in cerebellar P cells may equally well lead to deficits in motor learning in Fragile X patients.

Experimental Procedures

Eyeblink Conditioning in Mice

Wild-type and *Fmr1* mutant mice were prepared for eyblink conditioning according to the DMTD procedure as described by Koekkoek et al. (2002). In short, mice were anesthetized, using a mixture of nitrous oxide and halothane, and a promade connector was placed on the skull. A sensor chip linked to the connector was placed over the upper eyelid, while a magnet was attached to the lower eyelid. Mice were subjected to either a paired or a randomly paired procedure in four sessions. During one session, the subject received 64 trials grouped in 8 blocks. The trials were separated by a random intertrial interval (ITI) ranging from 20 s to 40 s. In the procedure of paired training, each block consisted of one US-only trial, six paired trials, and one CS-only trial. After four sessions of paired trainings the subject was allowed to rest for 1 day, followed by two sessions of extinction. In the extinction procedure, each block consisted of one US-only trial and seven CS-only trials. In the randomly paired procedure, the US occurred randomly in the ITI, while the CS was given as described in the paired trials. In the analyses of the eyelid movements, we considered a movement as a significant eyelid response when its amplitude was greater than the mean + 3 SDs of the amplitude of the movements that occurred in the 500 ms period before the onset of the CS. Such a response was considered to contain a startle response when movement occurred within the 60 ms period directly after the onset of the CS; when significant movement occurred after this period, it was considered a CR.

Cell Physiology

Mice were anesthetized with ether and decapitated (for details, see Llano et al., 1991). The cerebellum was excised, and slices were prepared from the vermis. The recording chamber was perfused with oxygenized saline containing 100 μ M picrotoxin. Recordings of P cells were obtained at 31.0°C, using an upright Nikon or Zeiss microscope, and whole-cell patch-clamp recordings were obtained with the use of borosilicate pipettes (resistance, 3–5 M Ω). Membrane current was recorded with a Multiclamp700A amplifier (Axon), while stimulation and online data acquisition were performed using pClamp 9 software (Axon). PFs and CFs were focally stimulated by applying pulses through glass pipettes positioned on the surface of the slice. Properties of voltage-gated Ca²⁺ channels in P cells were measured under voltage-clamp conditions. Slow EPSC caused by repetitive stimulation (8 pulses, 50 Hz) via type 1 metabotropic glutamate receptors (mGluR1) was measured in the presence of NBQX (10 μ M) (Batchelor and Garthwaite, 1997).

Generation of Purkinje Cell-Specific *Fmr1* Knockout Mice, *L7-Fmr1* Mutant Mice

We generated conditional knockout mice in which the first coding exon of *Fmr1* can be deleted through Cre-mediated recombination. In brief, the floxed *Fmr1* allele contains a lox site 2800 bp in front of exon 1 of the *Fmr1* gene and a second lox site 260 bp after exon 1 in intron 1 of the *Fmr1* gene. Mice expressing a *L7/PCP2-cre* transgene (Barski et al. 2000) were subsequently crossed with the floxed *Fmr1* mice to generate a P cell-specific *Fmr1* knockout mouse. To confirm that FMRP was selectively not expressed in P cells, adult mice were sacrificed and processed for immunohisto-

chemical analysis of FMRP expression (for details, see Bakker et al., 2000).

Cytology of Purkinje Cells

The morphology of P cells was investigated, using BDA injections or immunocytochemistry against calbindin. BDA injections (10% in 0.1 M phosphate buffer) were made following electrophysiological identification of the cerebellar nuclei. After the iontophoretic injections, the animals were allowed to recover for 5 days and then were subsequently anesthetized (Nembutal; 50 mg/kg) and perfused with 4% paraformaldehyde in 0.1 M phosphate buffer. The brains were removed and cut in sagittal sections, which were reacted with ABC complex and diaminobenzidine to visualize the BDA. Calbindin immunocytochemistry was performed by incubating the sections with rabbit anti-calbindin antibody, ABC, and diaminobenzidine. Some of the sections were investigated under the light microscope, while others were osmicated, embedded in Durcupan, and processed for electron microscopy (De Zeeuw et al., 1989). For analysis, Purkinje cell dendrites were divided into a proximal category of dendrites (with a diameter $\geq 1.5 \mu\text{m}$) and a distal category (with a diameter $< 1.5 \mu\text{m}$). Spine density was calculated by dividing the total number of spines per dendrite by the length of the dendrite. Total spine length was calculated by measuring the distance between the tip of the spine head and the base of the spine neck; spine head length was measured by multiplying the distance from the tip of the spine to the head diameter-intersection line by a factor of two; and spine neck length was calculated by subtracting the spine head length from the total spine length.

Cerebellar Lesions

The anterior interposed cerebellar nuclei were identified with the use of electrophysiological recordings in trained animals, and the lesions were subsequently made with the use of pressure injections of 200 nmol of N-methyl-D-aspartate. After recovery and new eyeblink recordings, the animals were anesthetized (Nembutal; 50 mg/kg) and transcardially perfused with 4% paraformaldehyde in 0.1 M phosphate buffer. The brains were removed and cut into sections, which were stained with silver reagents as described by Haasdijk et al. (2002).

Eyeblink Conditioning in Humans

Normal males and males with Fragile X syndrome were subjected to eyeblink conditioning procedures with the use of MDMT and video technology. MDMT as described by Koekkoek et al. (2002) was modified so it could be applied to human subjects. During MDMT recording, we simultaneously captured video frames for calibration purposes. The MDMT sensor was attached on the edge of the orbit below the right lower eyelid, while a NIB magnet was attached to the edge of the right upper eyelid. A headset containing the MDMT amplifier, MDMT power supply, puff nozzle, miniature camera, and headphones was mounted on the head of the subject. Subjects were seated before a monitor and allowed to watch a movie. The headset provided a head-free recording situation, which is necessary when dealing with mentally compromised patients. The puff nozzle was set to direct the air puff to the cornea close to the outer canthus of the eye at a distance of 15 mm. The puff had an intensity of 20 PSI at the source, while stimulus duration was set at 20 ms. The sound of the movie acted as background noise, and volume was adjusted to an average of 75 dB. The CS was a 650 Hz tone at 75 dB with a duration of 520 ms starting 500 ms prior to US delivery (interstimulus interval, 500 ms). The headset provided complete sound isolation from the environment. The training was divided into four training sessions with two blocks of eight trials each. Each block contained one CS-only and one US-only trial, which were randomly distributed. The ITI was randomly determined but always ranged from 10 s to 30 s. All data values were obtained from CS-only trials, with the exception of UR data values. In the randomly paired procedure, the US occurred randomly in the ITI, while the CS was given as in the paired trials. For analysis criteria, see Koekkoek et al. (2002).

Model

Simulations were performed with custom-written C code. Differential equations (see Supplemental Data) were integrated with the forward Euler method. In population models like the present one, there is an unavoidable lack of data to constrain all parameters. We therefore confirmed that the main finding, i.e., the critical dependence of the CR amplitude on the steady-state level of activity in P cells and neurons of the cerebellar nuclei, can be reproduced in models sharing these features: the instantaneous response of cerebellar nuclear neurons is dominated by rebound discharges, the rebound discharge depends on the level of inhibition, and the pool of neurons available for disinhibition, or the overall rebound response, can be exhausted.

Supplemental Data

Supplemental Data include a table and sections of text pertaining to cell physiology, the mathematical model used, and the results and can be found with this article online at <http://www.neuron.org/cgi/content/full/47/3/339/DC1>.

Acknowledgments

We thank E. Dalm, Ir. J. v.d. Burg, I. Nieuwenhuizen, L. Soverijnen, Dr. A.E. Smits, and Dr. L. Govaerts for their excellent assistance. The work in the group of C.I.D.Z. was supported by the Dutch Organization for Medical Sciences (NWO-PIONIER and ZON-MW), Life Sciences (NWO-ALW), Neuro-Biik consortium (Senter), and the European Community (EC). B.A.O., S.K.E.K., and D.L.N. were supported by NIH (NIH 5 RO1 HD38038) and FRAXA Research Foundation. E.D.S. and R.M. were supported by EC and IUAP and FWO (Belgium).

Received: February 13, 2004

Revised: November 29, 2004

Accepted: July 7, 2005

Published: August 3, 2005

References

- Alzenman, C.D., and Linden, D.J. (1999). Regulation of the rebound depolarization and spontaneous firing patterns of deep nuclear neurons in slices of rat cerebellum. *J. Neurophysiol.* 82, 1697–1709.
- Alzenman, C.D., and Linden, D.J. (2000). Rapid, synaptically driven increases in the intrinsic excitability of cerebellar deep nuclear neurons. *Nat. Neurosci.* 3, 109–111.
- Bakker, C.E., de Diego Otero, Y., Bontekoe, C., Raghoe, P., Luteijn, T., Hoogeveen, A.T., Oostra, B.A., and Willemson, R. (2000). Immunocytochemical and biochemical characterization of FMRP, FXR1P, and FXR2P in the mouse. *Exp. Cell Res.* 258, 162–170.
- Barski, J.J., Dethleffsen, K., and Meyer, M. (2000). Cre recombinase expression in cerebellar Purkinje cells. *Genesis* 28, 93–98.
- Batchelor, A.M., and Garthwaite, J. (1997). Frequency detection and temporally dispersed synaptic signal association through a metabotropic glutamate receptor pathway. *Nature* 385, 74–77.
- Bravin, M., Morando, L., Vercoli, A., Rossi, F., and Strata, P. (1999). Control of spine formation by electrical activity in the adult rat cerebellum. *Proc. Natl. Acad. Sci. USA* 96, 1704–1709.
- Brown, V., Jin, P., Ceman, S., Darnell, J.C., O'Donnell, W.T., Tenenbaum, S.A., Jin, X., Feng, Y., Wilkinson, K.D., Koeno, J.D., et al. (2001). Microarray identification of FMRP-associated brain mRNAs and altered mRNA translational profiles in fragile X syndrome. *Cell* 107, 477–487.
- Cesa, R., Morando, L., and Strata, P. (2003). Glutamate receptor delta2 subunit in activity-dependent heterologous synaptic competition. *J. Neurosci.* 23, 2363–2370.
- Chen, L., and Toth, M. (2001). Fragile X mice develop sensory hyperreactivity to auditory stimuli. *Neuroscience* 103, 1043–1050.
- Coesmans, M., Smitt, P.A., Linden, D.J., Shigemoto, R., Hirano, T., Yamakawa, Y., van Alphen, A.M., Luo, C., van der Geest, J.N., Kros,

- J.M., et al. (2003). Mechanisms underlying cerebellar motor deficits due to mGluR1-autoantibodies. *Ann. Neurol.* 53, 325-336.
- Coesmans, M., Weber, J.T., De Zeeuw, C.I., and Hansel, C. (2004). Bidirectional parallel fiber plasticity in the cerebellum under climbing fiber control. *Neuron* 44, 691-700.
- Comery, T.A., Harris, J.B., Willems, P.J., Oostra, B.A., Irwin, S.A., Weiler, I.J., and Greenough, W.T. (1997). Abnormal dendritic spines in fragile X knockout mice: maturation and pruning deficits. *Proc. Natl. Acad. Sci. USA* 94, 5401-5404.
- De Vries, B.B., van den Ouweland, A.M., Mohkamsing, S., Duivenvoorden, H.J., Mol, E., Gelsema, K., van Rijn, M., Halley, D.J., Sandkuijl, L.A., Oostra, B.A., et al. (1997). Screening and diagnosis for the fragile X syndrome among the mentally retarded: an epidemiological and psychological survey. Collaborative Fragile X Study Group. *Am. J. Hum. Genet.* 61, 660-667.
- De Zeeuw, C.I., Holstege, J.C., Ruigrok, T.J., and Voogd, J. (1989). Ultrastructural study of the GABAergic, cerebellar, and mesodiencephalic innervation of the cat medial accessory olive: anterograde tracing combined with immunocytochemistry. *J. Comp. Neurol.* 284, 12-35.
- De Zeeuw, C.I., Hansel, C., Bian, F., Koekkoek, S.K., van Alphen, A.M., Linden, D.J., and Oberdick, J. (1998). Expression of a protein kinase C inhibitor in Purkinje cells blocks cerebellar LTD and adaptation of the vestibulo-ocular reflex. *Neuron* 20, 495-508.
- De Zeeuw, C.I., Elgersma, Y., Hulscher, H.C., Dortland, B.R., Hensbroek, R.A., Ruigrok, T.J., and Koekkoek, S.K.E. (2004). Response to comment on "Cerebellar LTD and Learning-Dependent Timing of Conditioned Eyelid Responses". *Science* 304, 211C.
- D'Hooge, R., Nagels, G., Franck, F., Bakker, C.E., Reyniers, E., Storm, K., Kooy, R.F., Oostra, B.A., Willems, P.J., and De Deyn, P.P. (1997). Mildly impaired water maze performance in male Fmr1 knockout mice. *Neuroscience* 76, 367-376.
- Dobkin, C., Rabo, A., Dumas, R., El Idrissi, A., Haubenstock, H., and Brown, W.T. (2000). Fmr1 knockout mouse has a distinctive strain-specific learning impairment. *Neuroscience* 100, 423-429.
- Fu, Y.H., Kuhl, D.P., Pizzuti, A., Pieretti, M., Sutcliffe, J.S., Richards, S., Vorkerk, A.J., Holden, J.J., Fenwick, R.G., Jr., Warren, S.T., et al. (1991). Variation of the CGG repeat at the fragile X site results in genetic instability: resolution of the Sherman paradox. *Cell* 67, 1047-1058.
- Gruart, A., Pastor, A.M., Armengol, J.A., and Dolgado-García, J.M. (1997). Involvement of cerebellar cortex and nuclei in the genesis and control of unconditioned and conditioned eyelid motor responses. *Prog. Brain Res.* 114, 511-528.
- Gu, Y., McIlwain, K.L., Weeber, E.J., Yamagata, T., Xu, B., Antalfy, B.A., Reyes, C., Yuva-Paylor, L., Armstrong, D., Zoghbi, H., et al. (2002). Impaired conditioned fear and enhanced long-term potentiation in Fmr2 knock-out mice. *J. Neurosci.* 22, 2753-2763.
- Haasdijk, E.D., Vluga, A., Mulder, M.T., and Jaarsma, D. (2002). Increased apolipoprotein E expression correlates with the onset of neuronal degeneration in the spinal cord of G93A-SOD1 mice. *Neurosci. Lett.* 335, 29-33.
- Hagerman, R.J., and Hagerman, P.J. (2002). The fragile X premutation: into the phenotypic fold. *Curr. Opin. Genet. Dev.* 12, 278-283.
- Hinton, V.J., Brown, W.T., Wisniewski, K., and Rudelli, R.D. (1991). Analysis of neocortex in three males with the fragile X syndrome. *Am. J. Med. Genet.* 41, 289-294.
- Huber, K.M., Gallagher, S.M., Warren, S.T., and Boar, M.F. (2002). Altered synaptic plasticity in a mouse model of fragile X mental retardation. *Proc. Natl. Acad. Sci. USA* 99, 7746-7750.
- Ichikawa, R., Miyazaki, T., Kano, M., Hashikawa, T., Tatsumi, H., Sakimura, K., Mishina, M., Inoue, Y., and Watanabe, M. (2002). Distal extension of climbing fiber territory and multiple innervation caused by aberrant wiring to adjacent spiny branchlets in cerebellar Purkinje cells lacking glutamate receptor delta 2. *J. Neurosci.* 22, 8487-8503.
- Irwin, S.A., Patel, B., Idupulapati, M., Harris, J.B., Crisostomo, R.A., Larson, B.P., Kooy, F., Willems, P.J., Cras, P., Kozlowski, P.B., et al. (2001). Abnormal dendritic spine characteristics in the temporal and visual cortices of patients with fragile-X syndrome: a quantitative examination. *Am. J. Med. Genet.* 98, 161-167.
- Irwin, S.A., Idupulapati, M., Gilbert, M.E., Harris, J.B., Chakravarti, A.B., Rogers, E.J., Crisostomo, R.A., Larson, B.P., Mehta, A., Alcantara, C.J., et al. (2002). Dendritic spine and dendritic field characteristics of layer V pyramidal neurons in the visual cortex of fragile-X knockout mice. *Am. J. Med. Genet.* 111, 140-146.
- Kakizawa, S., Yamasaki, M., Watanabe, M., and Kano, M. (2000). Critical period for activity-dependent synapse elimination in developing cerebellum. *J. Neurosci.* 20, 4954-4961.
- Kano, M., Hashimoto, K., Watanabe, M., Kurihara, H., Offermanns, S., Jiang, H., Wu, Y., Jun, K., Shin, H.S., Inoue, Y., et al. (1998). Phospholipase cbeta4 is specifically involved in climbing fiber synapse elimination in the developing cerebellum. *Proc. Natl. Acad. Sci. USA* 95, 15724-15729.
- Karachot, L., Shirai, Y., Vigot, R., Yamamori, T., and Ito, M. (2001). Induction of long-term depression in cerebellar Purkinje cells requires a rapidly turned over protein. *J. Neurophysiol.* 86, 280-289.
- Kelly, R.M., and Strick, P.L. (2003). Cerebellar loops with motor cortex and prefrontal cortex of a nonhuman primate. *J. Neurosci.* 23, 8432-8444.
- Kenyon, G.T., Medina, J.F., and Mauk, M.D. (1998). A mathematical model of the cerebellar-olivary system I: self-regulating equilibrium of climbing fiber activity. *J. Comput. Neurosci.* 5, 17-33.
- Kim, J.J., and Thompson, R.F. (1997). Cerebellar circuits and synaptic mechanisms involved in classical eyelink conditioning. *Trends Neurosci.* 20, 177-181.
- Kim, S.G., Ugurbil, K., and Strick, P.L. (1994). Activation of a cerebellar output nucleus during cognitive processing. *Science* 265, 949-951.
- Koekkoek, S.K.E., Den Ouden, W.L., Perry, G., Highstein, S.M., and De Zeeuw, C.I. (2002). Monitoring kinetic and frequency-domain properties of eyelid responses in mice with magnetic distance measurement technique. *J. Neurophysiol.* 88, 2124-2133.
- Koekkoek, S.K., Hulscher, H.C., Dortland, B.R., Hensbroek, R.A., Elgersma, Y., Ruigrok, T.J., and De Zeeuw, C.I. (2003). Cerebellar LTD and learning-dependent timing of conditioned eyelid responses. *Science* 301, 1736-1739.
- Laggerbauer, B., Ostareck, D., Koidol, E.M., Ostareck-Loderer, A., and Fischer, U. (2001). Evidence that fragile X mental retardation protein is a negative regulator of translation. *Hum. Mol. Genet.* 10, 329-338.
- Leiner, H.C., Leiner, A.L., and Dow, R.S. (1993). Cognitive and language functions of the human cerebellum. *Trends Neurosci.* 16, 444-447.
- Li, Z., Zhang, Y., Ku, L., Wilkinson, K.D., Warron, S.T., and Feng, Y. (2001). The fragile X mental retardation protein inhibits translation via interacting with mRNA. *Nucleic Acids Res.* 29, 2276-2283.
- Linden, D.J. (2001). The expression of cerebellar LTD in culture is not associated with changes in AMPA-receptor kinetics, agonist affinity, or unitary conductance. *Proc. Natl. Acad. Sci. USA* 98, 14066-14071.
- Liano, I., Marty, A., Armstrong, C.M., and Konnerth, A. (1991). Synaptic- and agonist-induced excitatory currents of Purkinje cells in rat cerebellar slices. *J. Physiol.* 434, 183-213.
- Mauk, M.D., and Donegan, N.H. (1997). A model of Pavlovian eyelid conditioning based on the synaptic organization of the cerebellum. *Learn. Mem.* 4, 130-158.
- Medina, J.F., and Mauk, M.D. (2000). Computer simulation of cerebellar information processing. *Nat. Neurosci.* 3 (Suppl.), 1205-1211.
- Middleton, F.A., and Strick, P.L. (1994). Anatomical evidence for cerebellar and basal ganglia involvement in higher cognitive function. *Science* 266, 458-461.
- Migaud, M., Charlesworth, P., Dempster, M., Webster, L.C., Watabe, A.M., Makhinson, M., He, Y., Ramsay, M.F., Morris, R.G., Morrison, J.H., et al. (1998). Enhanced long-term potentiation and impaired learning in mice with mutant postsynaptic density-95 protein. *Nature* 396, 433-439.
- Miyashiro, K.Y., Beckel-Mitchener, A., Purk, T.P., Becker, K.G., Bar-

- ret, T., Liu, L., Carbonetto, S., Weiler, I.J., Greenough, W.T., and Eberwine, J. (2003). RNA cargoes associating with FMRP reveal deficits in cellular functioning in *Fmr1* null mice. *Neuron* 37, 417–431.
- Miyata, M., Okada, D., Hashimoto, K., Kano, M., and Ito, M. (1999). Corticotropin-releasing factor plays a permissive role in cerebellar long-term depression. *Neuron* 22, 763–775.
- Nielsen, D.M., Derber, W.J., McClollan, D.A., and Crnic, L.S. (2002). Alterations in the auditory startle response in *Fmr1* targeted mutant mouse models of fragile X syndrome. *Brain Res.* 927, 8–17.
- Paradee, W., Melikian, H.E., Rasmussen, D.L., Kenneson, A., Conn, P.J., and Warren, S.T. (1999). Fragile X mouse: strain effects of knockout phenotype and evidence suggesting deficient amygdala function. *Neuroscience* 94, 185–192.
- Rudelli, R.D., Brown, W.T., Wisniewski, K., Jenkins, E.C., Lauro-Kamionowska, M., Connell, F., and Wisniewski, H.M. (1985). Adult fragile X syndrome. Clinico-neuropathologic findings. *Acta Neuropathol. (Berl.)* 67, 289–295.
- Shibuki, K., Gomi, H., Chen, L., Bao, S., Kim, J.J., Wakatsuki, H., Fujisaki, T., Fujimoto, K., Katoh, A., Ikeda, T., et al. (1996). Deficient cerebellar long-term depression, impaired eyeblink conditioning, and normal motor coordination in GFAP mutant mice. *Neuron* 16, 587–599.
- Strata, P., Morando, L., Bravin, M., and Rossi, F. (2000). Dendritic spine density in Purkinje cells. *Trends Neurosci.* 23, 198–198.
- Teune, T.M., van der Burg, J., van der Moer, J., Voogd, J., and Ruijgrok, T.J. (2000). Topography of cerebellar nuclear projections to the brain stem in the rat. *Prog. Brain Res.* 124, 141–172.
- The Dutch-Belgian Fragile X Consortium. (1994). *Fmr1* knockout mice: A model to study fragile X mental retardation. *Cell* 78, 23–33.
- Turner, G., Webb, T., Wake, S., and Robinson, H. (1996). Prevalence of fragile X syndrome. *Am. J. Mod. Genet.* 64, 196–197.
- Van Dam, D., D'Hooge, R., Hauben, E., Reyniers, E., Gantois, I., Bakker, C.E., Oostra, B.A., Kooy, R.F., and De Deyn, P.P. (2000). Spatial learning, contextual fear conditioning and conditioned emotional response in *Fmr1* knockout mice. *Behav. Brain Res.* 117, 127–136.
- Van Polt, J., Uylings, H.B., Verwer, R.W., Pentney, R.J., and Woldenberg, M.J. (1992). Tree asymmetry—a sensitive and practical measure for binary topological trees. *Bull. Math. Biol.* 54, 759–784.
- Verhoij, C., Bakker, C.E., de Graaff, E., Keulemans, J., Willemsen, R., Verkerk, A.J., Galjaard, H., Reuser, A.J., Hoogeveen, A.T., and Oostra, B.A. (1993). Characterization and localization of the FMR-1 gene product associated with fragile X syndrome. *Nature* 363, 722–724.
- Verkerk, A.J., Pieretti, M., Sutcliffe, J.S., Fu, Y.H., Kuhl, D.P., Pizzuti, A., Reiner, O., Richards, S., Victoria, M.F., Zhang, F.P., et al. (1991). Identification of a gene (FMR-1) containing a CGG repeat coincident with a breakpoint cluster region exhibiting length variation in fragile X syndrome. *Cell* 65, 905–914.
- Vokaer, M., Bier, J.C., Elincx, S., Claes, T., Paquier, P., Goldman, S., Bartholome, E.J., and Pandolfo, M. (2002). The cerebellum may be directly involved in cognitive functions. *Neurology* 58, 967–970.
- Wang, S.S., Denk, W., and Haussler, M. (2000). Coincidence detection in single dendritic spines mediated by calcium release. *Nat. Neurosci.* 2, 1266–1273.
- Weiler, I.J., Irwin, S.A., Klintsova, A.Y., Spencer, C.M., Brazelton, A.D., Miyashiro, K., Comery, T.A., Patel, B., Eberwine, J., and Greenough, W.T. (1997). Fragile X mental retardation protein is translated near synapses in response to neurotransmitter activation. *Proc. Natl. Acad. Sci. USA* 94, 5395–5400.
- Xia, J., Chung, H.J., Wihler, C., Haganir, R.L., and Linden, D.J. (2000). Cerebellar long-term depression requires PKC-regulated interactions between *GluR2/3* and PDZ domain-containing proteins. *Neuron* 28, 499–510.
- Yeo, C.H., and Hessler, G. (1998). Cerebellum and conditioned reflexes. *Trends Cogn. Sci.* 2, 322–331.

Discussion

Chapter 5

Discussion

Dendritic spines are the small mushroom-shaped postsynaptic membrane specializations that protrude from the cell surface of neuronal dendrites and are the major sites of glutamatergic input in the brain. Spines are motile, exist in a variety of shapes ranging from mushroom-shaped to thin filopodia-like spines and correlate with the strength of the synapse, making them attractive structural candidates for learning and memory (Yuste and Bonhoeffer, 2001). The distinct responsiveness of thin, filopodia-like spines to synaptic activity has led to the suggestion that they are 'learning or plasticity spines', whereas the stability of mushroom spines suggests that they are 'memory spines' (Bourne and Harris, 2007) (Kasai et al., 2003). Several human mental retardation syndromes have been linked to altered spine morphology (Kaufmann and Moser, 2000; Newey et al., 2005).

Several models have been proposed to describe the molecular and cellular mechanism underlying spine morphology and plasticity (Bourne and Harris, 2007; Ethell and Pasquale, 2005). It is generally believed that changes in spine morphology are primarily based on tight coordination of actin dynamics (Ethell and Pasquale, 2005; Tada and Sheng, 2006) and membrane trafficking (Kennedy and Ehlers, 2006). However many fundamental issues are still unresolved. The studies in this thesis describe new mechanisms involved in spine and synaptic plasticity. In this chapter we will discuss the conclusions from the experimental work presented in this thesis.

The role of microtubules in spine morphology

Post-mitotic neurons show a very characteristic microtubule organization which is distinct from dividing cells. In mature neurons, most microtubules are not attached to the centrosome but form dense bundles running along the length of axons and dendrites cross-linked by microtubule-associated proteins, such as MAP2 and tau (Chen et al., 1992). Microtubule arrays within neuronal processes are highly organized with respect to their intrinsic polarity (Baas et al., 1988). Ultrastructural studies show that in axons, microtubules are generally long and uniformly oriented, with their plus-ends distal to the cell body, whereas in proximal dendrites microtubules are much shorter and exhibit mixed polarity (Jaworski et al., 2008). More distal thinner dendrites of higher order, however, contain unipolar microtubules oriented the same way as the axonal ones (Baas et al., 1988). This specialized microtubule organization has recently been visualized by following the microtubule plus end binding protein EB3 in living neuronal cells (Ahmad et al., 2006; Morrison et al., 2002; Stepanova et al., 2003). It was shown that in axons and distal dendrites all dynamic microtubule plus-ends point toward growth cones while in proximal dendrites significant EB3-GFP movement was directed towards the cell body (Stepanova et al., 2003). The major role of microtubules in mature neurons is to act as railways for motor-based transport. The polarized microtubule network can generate asymmetries in the neurons and direct specific motor proteins. In addition, the microtubule cytoskeleton serves as a primary spatial regulator of cell migration, axonal outgrowth and neuronal differentiation. At their growing tips, microtubules can recruit regulatory molecules (+TIPs) which function as signaling devices to regulate cytoskeleton dynamics and protein targeting at specific cellular locations (Basu and Chang, 2007; Lansbergen and Akhmanova, 2006). For example, +TIPs have recently been shown to be important for targeting of voltage gated potas-

sium (Kv1) channels into the axons (Gu et al., 2006) and gap junction formation (Shaw et al., 2007). It is therefore not surprising to find a strong functional interplay between microtubule dependent mechanisms and neuronal development and maintenance.

For a long time microtubules were considered to be predominately present along the dendrites in mature neurons but absent from dendritic spines. Most studies, typically visualizing microtubules using MAP2 antibodies or fluorescent constructs have only detected microtubules in the dendritic shaft. MAP2 preferentially binds stable microtubules and thus fails to label the dynamic microtubules. Some EM studies have detected the presence of microtubules in spines (Chicurel and Harris, 1992; Fiala et al., 2003), however it is unclear if the presence of microtubules has any influence on dendritic spine structure or function. In chapter 2 we visualized dynamic microtubules by GFP-tagged end binding protein 3 (EB3) and show that growing microtubules periodically depart from the dendritic compartment and enter dendritic spines in mature cultured hippocampal neurons. Furthermore, we demonstrate that dynamic microtubules labeled with EB3 affect spine morphology. Overexpression of EB3 leads to spine enlargement while EB3 knockdown leads to an increase in filopodia shaped spines. Dynamic microtubules entering the spine seem to be able to affect actin organization within spines. First, EB3 overexpression increases F-actin staining in the spine and a knockdown of EB3 decreases F-actin staining. We treated control and EB3 knockdown neurons with jasplakinolide and latrunculin B, drug that are known to increase actin polymerization and depolymerization, respectively. Jasplakinolide rescues the EB3 knockdown phenotype, while latrunculin B further enhances the phenotype. Second, p140Cap, a new binding partner of EB3, is involved in controlling actin organization. Endogenous p140Cap in hippocampal neurons localizes in spines and colocalizes with F-actin. Overexpression of p140Cap increases spine size and rescues the EB3 knockdown phenotype. Although it is clear that EB3 is involved spine plasticity, it remains unclear whether MTs need EB3 for spine entry. It will be interesting to investigate microtubule dynamics in neurons lacking EB3. Moreover, EB3 null mutant mice might provide a good model system to investigate the role of EB3 in microtubule dynamics and synaptic plasticity.

Aside from regulating the actin cytoskeleton in the spine via p140Cap, microtubules penetrating spines might be involved in other processes affecting spine morphology. The microtubule might provide a direct route from the dendrite into the spine for microtubule-dependent transport of cargo enabling fast recruitment of components necessary for spine growth and synaptic function. In cultured hippocampal neurons EB3-labeled MTs entering a spine can only be found in a small fraction (4%) of dendritic spines at any given time. The time EB3 can be detected in the spine is short (~3 sec). While microtubules are found in the spine for up to ~ 2 minutes (Hu et al., 2008). This is more than enough time for microtubule dependent motor proteins to travel along the microtubules and deliver their cargo at the synaptic site in the spine head. It is still unclear what triggers microtubule entry in a spine and why some spines are entered and other neighboring spines are not. Additional studies will be required to determine the signaling pathways triggering microtubules to enter the spine.

In other model systems, such as epithelial cells, it has been shown that microtubule plus ends can target cell-cell adhesion sites and affect the integrity of those sites (Akhmanova et al., 2009). Cadherin-based cell-cell adhesion sites are positively affected when targeted by microtubule plus ends. N-cadherin is a cell adhesion protein found in the synaptic cleft and might be a target for dynamic microtubules entering the spine.

Whether microtubules and adhesion proteins affect each other in the dendritic spine and if this possible interaction has any functional significance in spine plasticity needs to be investigated.

The role of endosomes in spine morphology

Based on uptake of extracellular gold particles (Cooney et al., 2002), visualizing clathrin assembly in living neurons (Blanpied et al., 2002), and pre-embedding immunogold electron microscopy (Racz et al., 2004), it was shown that dendritic spines contain endocytic machinery. The endosomal compartments are present in the spine head or immediately beneath the spine. Membrane trafficking from recycling endosomes is a common mechanism that cells employ to expand the plasma membrane, and target proteins in a polarized manner in such distinct processes as cytokinesis, cell-cell adhesion, phagocytosis, and cell fate determination.

Endosomal recycling at the synapse is an essential process to maintain synaptic strength and at the same time allow for synaptic plasticity. Recycling of receptors occurs continuously at the synapse, moving receptors from the synaptic membrane to an internalized pool of receptors and back to the cell membrane. A popular model is that recycling endosomes in close proximity to synapses or even within dendritic spines provide a local intracellular pool of glutamate receptors, such as AMPA-type glutamate receptors (Greger and Esteban, 2007; Kennedy and Ehlers, 2006). Interestingly, it has been found that recycling endosomes supply AMPARs for LTP. Stimuli that triggered LTP promoted AMPAR insertion and increased generalized recycling of cargo and membrane from endocytic compartments.

In chapter 3 we show that GRASP-1 can regulate endosomal trafficking in dendritic spines by connecting Rab4-positive early recycling endosomes with Rab11-positive late recycling endosomes. This endosomal recycling pathway is essential for maintenance of spine morphology. Overexpression of dominant negative forms of Rab4 or Rab11 disrupts this endosomal recycling which leads to a decrease in spine density in hippocampal neurons. Similarly, a knockdown of GRASP-1 in neurons leads to a decrease in the numbers of mushroom shaped spines and an increase in filopodia. We have shown that GRASP-1 is able to separate Rab4-positive endosomes from Rab-5 positive endosomes and link these Rab4-positive endosomes with Rab11-positive endosomes. In addition, we demonstrate that efficient AMPAR recycling depends on GRASP-1. In both control neurons and GRASP-1 knockdown neurons AMPAR surface labeling decreases quickly after AMPA stimulation, but while the amount of AMPAR at the surface completely recovers after an hour in control neurons this recovery is not seen in GRASP-1 knockdown neurons. Interestingly, chemically induced LTD by stimulation with NMDA affects the GRASP-1 localization. Colocalization of Rab4 and GRASP-1 disappears after NMDA activation, suggesting that NMDA activation might lead to inactivation of either Rab4 or GRASP-1, disabling the binding of endosomes, Rab4 and GRASP-1. This could block access to the recycling endosomal pathway and force internalized receptors into the lysosomal pathway. In this way, different forms of synaptic activity could regulate the sorting endosomal pathways by influencing the different Rab GTPase proteins bound to endosomes. A GRASP-1 KO mouse could be a nice model to further investigate the role of GRASP-1 in endosomal pathways and AMPAR recycling in the dendritic spine.

Fragile X syndrome and spine morphology

Fragile X syndrome is the most common heritable form of mental retardation; it is caused by a lack of expression of FMRP (fragile X mental retardation protein). FMRP is an RNA binding protein that associates with polyribosomes and is localized in neurons in RNA transport granules (Antar et al., 2005); (Wang et al., 2008). FMRP has been shown to influence the translation efficacy of several of its target mRNAs (Bagni and Greenough, 2005; Bardoni et al., 2006; Zalfa et al., 2007) and is therefore thought to be involved in the transport and/or the regulation of mRNA translation.

In chapter 4, we show spine abnormalities in Purkinje cells in the cerebellum from FMR1 knock-out mice, we demonstrate that these abnormalities cause deficits at cell physiological and behavioral level. Several other studies have shown that lack of FMRP results in an abnormal spine morphology in many other brain regions like the cerebrum (Comery et al., 1997; Hinton et al., 1991; Irwin et al., 2002) and the hippocampus (Pfeiffer and Huber, 2007). Dendritic spines of both FMR1 knock-out mice and Fragile X patients (Koukoui and Chaudhuri, 2007) have an immature filopodia-like morphology with long spine necks and small spine heads. It has been shown that FMRP is localized in dendritic spines of mature neurons and can bind to a subset of mRNAs involved in local translation, including mRNAs coding for synaptic proteins such as PSD95, CaMKII and GluR1/2 (Bassell and Warren, 2008). FMRP translation occurs after activation of metabotropic glutamate receptors (mGluR) (Huber et al., 2002) suggesting FMRP is an activity-dependent regulator of mRNA translation in spines. mGluR1/5-dependent LTD is enhanced in hippocampal neurons (Huber et al., 2002) and Purkinje cells (chapter 4) in FMR1 knock-out mice. The abnormal regulation of local mRNA translation in FMR1 knock-out mice may explain the increased AMPAR internalization at the synapse (Nakamoto et al., 2007). Blocking mGluR1/5 receptors with the antagonist MPEP normalizes AMPAR internalization and decreases local protein synthesis to normal levels in spines of FMRP deficient neurons (Dolen et al., 2007). Furthermore, lack of FMRP leads to a lower motility of mRNA and lower association of mRNA and kinesin in dendrites (Dichtenberg et al., 2008). Suppression of FMRP or blocking of mRNA transport from the soma to spines in wild type neurons lead to a filopodia like spine morphology as seen in *Fmr-1* KO neurons (Dichtenberg et al., 2008). To what extent the disrupted mRNA transport in dendrites contributes to the abnormal spine morphology seen in FMRP knock-out mice is not yet fully clear. Further studies are required to determine the exact processes through which FMRP influences spine morphology, AMPAR internalization and synaptic plasticity.

Concluding remarks and future directions

At the moment a spine grows, transport of receptors, PSD components and membrane components to the spine head is needed to enable the spine to enlarge its membrane surface and to incorporate more receptors in the synaptic membrane to increase its synaptic strength. The narrow spine neck separates the spine head from the dendritic shaft, limiting transport between those two parts of a neuron (Alvarez and Sabatini, 2007). A fast and highly regulated form of transport is needed to enable the fast plasticity seen in spines (Fig. 1). Microtubules invading spines could provide a pathway for this fast and regulated transport. Microtubule invasion of a spine is an activity-dependent process (Hu et al., 2008) and leads to growth of the spine (chapter 2). The microtubule grows quickly into spine and stays in the spine long enough for microtubule dependent motor proteins to deliver their cargo in the spine head. In contrast to the dendrite where microtubules have a mixed orientation, microtubules in the spine have a uniform polarity with their plus-end in the spine head and their minus end in the dendritic shaft. Thus in this way microtubules could enable polarized cargo transport, as kinesin motors can only move into the spine and dynein/dynactin motors can only traffic out of the spine. Interestingly, several components of the dynein complex have been identified in postsynaptic density (Cheng et al., 2006).

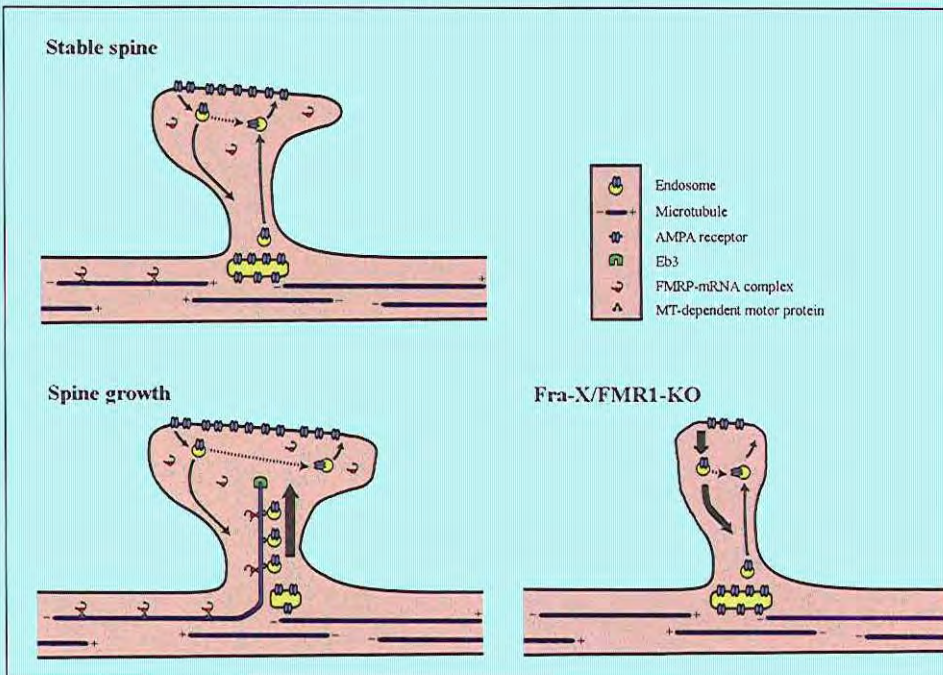


Figure 1: Model for the role of microtubules, endosomes and FMRP in spine plasticity.

In a stable spine AMPA receptors are constantly recycled from the synaptic membrane to an intracellular pool and *vica versa*. After invasion of a microtubule into the spine endosomes can be transported from the intracellular pool to the spine head by kinesins, shifting the equilibrium in endosomal recycling toward exocytosis which leads to spine growth, more AMPA receptors at the synaps and thus increased synaptic strength. FMRP is involved in the transport of a subset of mRNAs to the spine and in the regulation of translation of this subset of mRNAs. FMRP may regulate the translation of proteins involved in endosomal transport or AMPA receptor recycling. If so, lack of FMRP may cause the equilibrium in endosomal recycling shift toward endocytosis, leading to AMPA receptor internalization and increased LTD.

Several questions raised by the current study remain unanswered. Do microtubule dependent spine and dendrite alterations play a direct role in neurological diseases? How are spine microtubule dynamics influenced by synaptic activity? Furthermore, it has recently been shown that after LTP induction, transport of Rab11 positive recycling endosomes containing AMPA receptors from the dendritic shaft into the spine to the spine head is enhanced (Wang et al., 2008). It is tempting to speculate that these recycling endosomes are directed into the spine by microtubule dependent machinery. It would be interesting to find out whether GRASP-1 has a role in this process. Although technically challenging, it will be worthwhile monitoring AMPAR recycling in the absence GRASP-1 in living neurons. Furthermore, electrophysiological measurements in hippocampal slices need to be performed to reveal the *in vivo* role of GRASP-1 at synapses.

The fact that FMRP can associate with kinesin motors raises the intriguing possibility that also FMRP dependent mRNA transport can use spine microtubules as trafficking routes to the postsynaptic site (Fig. 1). In this model we show possible mechanisms in which FMRP can affect dendritic spine plasticity. Also in this study several questions remain unanswered. What is the link between mGluR1/5 dependent LTD and AMPAR recycling? Does FMRP regulate mRNA translation of any protein involved in AMPAR recycling? Could FMRP influence indirectly endosomal Rab GTPase activity?

It will be interesting to further investigate the cytoskeletal and trafficking mechanisms underlying synaptic plasticity. Moreover, we need to identify the molecular components involved in these processes and determine how these molecules function in a complex synaptic protein network in order to regulate dendritic spine morphology and plasticity. Furthermore, understanding how different neural stimuli, such as LTP and LTD, regulate spine plasticity and modify neuronal connections will be important to fully understand the cellular basis of learning and memory. As dendritic spine abnormalities are found in many neuropathologies, understanding the molecular processes underlying dendritic spine morphology and plasticity will also be useful to gain further understanding in those neuropathologies.

Reference

- Ahmad, F. J., He, Y., Myers, K. A., Hasaka, T. P., Francis, F., Black, M. M., and Baas, P. W. (2006). Effects of dyactin disruption and dynein depletion on axonal microtubules. *Traffic* 7, 524-537.
- Akhmanova, A., Stehbens, S. J., and Yap, A. S. (2009). Touch, grasp, deliver and control: functional cross-talk between microtubules and cell adhesions. *Traffic* 10, 268-274.
- Alvarez, V. A., and Sabatini, B. L. (2007). Anatomical and physiological plasticity of dendritic spines. *Annu Rev Neurosci* 30, 79-97.
- Antar, L. N., Dictenberg, J. B., Plociniak, M., Afroz, R., and Bassell, G. J. (2005). Localization of FMRP-associated mRNA granules and requirement of microtubules for activity-dependent trafficking in hippocampal neurons. *Genes Brain Behav* 4, 350-359.
- Baas, P. W., Deitch, J. S., Black, M. M., and Banker, G. A. (1988). Polarity orientation of microtubules in hippocampal neurons: uniformity in the axon and nonuniformity in the dendrite. *Proc Natl Acad Sci U S A* 85, 8335-8339.
- Bagni, C., and Greenough, W. T. (2005). From mRNP trafficking to spine dysmorphogenesis: the roots of fragile X syndrome. *Nat Rev Neurosci* 6, 376-387.
- Bardoni, B., Davidovic, L., Bensaid, M., and Khandjian, E. W. (2006). The fragile X syndrome: exploring its molecular basis and seeking a treatment. *Expert Rev Mol Med* 8, 1-16.
- Bassell, G. J., and Warren, S. T. (2008). Fragile X syndrome: loss of local mRNA regulation alters synaptic development and function. *Neuron* 60, 201-214.
- Basu, R., and Chang, F. (2007). Shaping the actin cytoskeleton using microtubule tips. *Curr Opin Cell Biol* 19, 88-94.
- Blanpied, T. A., Scott, D. B., and Ehlers, M. D. (2002). Dynamics and regulation of clathrin coats at specialized endocytic zones of dendrites and spines. *Neuron* 36, 435-449.
- Bourne, J., and Harris, K. M. (2007). Do thin spines learn to be mushroom spines that remember? *Curr Opin Neurobiol* 17, 381-386.
- Chen, J., Kanai, Y., Cowan, N. J., and Hirokawa, N. (1992). Projection domains of MAP2 and tau determine spacings between microtubules in dendrites and axons. *Nature* 360, 674-677.
- Cheng, D., Hoogenraad, C. C., Rush, J., Ramm, E., Schlager, M. A., Duong, D. M., Xu, P., Wijayawardana, S. R., Hanfelt, J., Nakagawa, T., *et al.* (2006). Relative and absolute quantification of postsynaptic density proteome isolated from rat forebrain and cerebellum. *Mol Cell Proteomics* 5, 1158-1170.
- Chicurel, M. E., and Harris, K. M. (1992). Three-dimensional analysis of the structure and composition of CA3 branched dendritic spines and their synaptic relationships with mossy fiber boutons in the rat hippocampus. *J Comp Neurol* 325, 169-182.
- Comery, T. A., Harris, J. B., Willems, P. J., Oostra, B. A., Irwin, S. A., Weiler, I. J., and Greenough, W. T. (1997). Abnormal dendritic spines in fragile X knockout mice: maturation and pruning deficits. *Proc Natl Acad Sci U S A* 94, 5401-5404.
- Cooney, J. R., Hurlburt, J. L., Selig, D. K., Harris, K. M., and Fiala, J. C. (2002). Endosomal compartments serve multiple hippocampal dendritic spines from a widespread rather than a local store of recycling membrane. *J Neurosci* 22, 2215-2224.
- Dictenberg, J. B., Swanger, S. A., Antar, L. N., Singer, R. H., and Bassell, G. J. (2008). A direct role for FMRP in activity-dependent dendritic mRNA transport links filopodial-spine morphogenesis to fragile X syndrome. *Dev Cell* 14, 926-939.

- Dolen, G., Osterweil, E., Rao, B. S., Smith, G. B., Auerbach, B. D., Chattarji, S., and Bear, M. F. (2007). Correction of fragile X syndrome in mice. *Neuron* *56*, 955-962.
- Ethell, I. M., and Pasquale, E. B. (2005). Molecular mechanisms of dendritic spine development and remodeling. *Prog Neurobiol* *75*, 161-205.
- Fiala, J. C., Kirov, S. A., Feinberg, M. D., Petrak, L. J., George, P., Goddard, C. A., and Harris, K. M. (2003). Timing of neuronal and glial ultrastructure disruption during brain slice preparation and recovery in vitro. *J Comp Neurol* *465*, 90-103.
- Greger, I. H., and Esteban, J. A. (2007). AMPA receptor biogenesis and trafficking. *Curr Opin Neurobiol* *17*, 289-297.
- Gu, C., Zhou, W., Puthenveedu, M. A., Xu, M., Jan, Y. N., and Jan, L. Y. (2006). The microtubule plus-end tracking protein EB1 is required for Kv1 voltage-gated K⁺ channel axonal targeting. *Neuron* *52*, 803-816.
- Hinton, V. J., Brown, W. T., Wisniewski, K., and Rudelli, R. D. (1991). Analysis of neocortex in three males with the fragile X syndrome. *Am J Med Genet* *41*, 289-294.
- Hu, X., Viessmann, C., Nam, S., Merriam, E., and Dent, E. W. (2008). Activity-dependent dynamic microtubule invasion of dendritic spines. *J Neurosci* *28*, 13094-13105.
- Huber, K. M., Gallagher, S. M., Warren, S. T., and Bear, M. F. (2002). Altered synaptic plasticity in a mouse model of fragile X mental retardation. *Proc Natl Acad Sci U S A* *99*, 7746-7750.
- Irwin, S. A., Idupulapati, M., Gilbert, M. E., Harris, J. B., Chakravarti, A. B., Rogers, E. J., Crisostomo, R. A., Larsen, B. P., Mehta, A., Alcantara, C. J., *et al.* (2002). Dendritic spine and dendritic field characteristics of layer V pyramidal neurons in the visual cortex of fragile-X knockout mice. *Am J Med Genet* *111*, 140-146.
- Jaworski, J., Hoogenraad, C. C., and Akhmanova, A. (2008). Microtubule plus-end tracking proteins in differentiated mammalian cells. *Int J Biochem Cell Biol* *40*, 619-637.
- Kasai, H., Matsuzaki, M., Noguchi, J., Yasumatsu, N., and Nakahara, H. (2003). Structure-stability-function relationships of dendritic spines. *Trends Neurosci* *26*, 360-368.
- Kaufmann, W. E., and Moser, H. W. (2000). Dendritic anomalies in disorders associated with mental retardation. *Cereb Cortex* *10*, 981-991.
- Kennedy, M. J., and Ehlers, M. D. (2006). Organelles and trafficking machinery for postsynaptic plasticity. *Annu Rev Neurosci* *29*, 325-362.
- Koukoui, S. D., and Chaudhuri, A. (2007). Neuroanatomical, molecular genetic, and behavioral correlates of fragile X syndrome. *Brain Res Rev* *53*, 27-38.
- Lansbergen, G., and Akhmanova, A. (2006). Microtubule plus end: a hub of cellular activities. *Traffic* *7*, 499-507.
- Morrison, E. E., Moncur, P. M., and Askham, J. M. (2002). EB1 identifies sites of microtubule polymerisation during neurite development. *Brain Res Mol Brain Res* *98*, 145-152.
- Nakamoto, M., Nalavadi, V., Epstein, M. P., Narayanan, U., Bassell, G. J., and Warren, S. T. (2007). Fragile X mental retardation protein deficiency leads to excessive mGluR5-dependent internalization of AMPA receptors. *Proc Natl Acad Sci U S A* *104*, 15537-15542.
- Newey, S. E., Velamoor, V., Govek, E. E., and Van Aelst, L. (2005). Rho GTPases, dendritic structure, and mental retardation. *J Neurobiol* *64*, 58-74.
- Pfeiffer, B. E., and Huber, K. M. (2007). Fragile X mental retardation protein induces synapse loss through acute postsynaptic translational regulation. *J Neurosci* *27*, 3120-3130.

- Racz, B., Blanpied, T. A., Ehlers, M. D., and Weinberg, R. J. (2004). Lateral organization of endocytic machinery in dendritic spines. *Nat Neurosci* 7, 917-918.
- Shaw, R. M., Fay, A. J., Puthenveedu, M. A., von Zastrow, M., Jan, Y. N., and Jan, L. Y. (2007). Microtubule plus-end-tracking proteins target gap junctions directly from the cell interior to adherens junctions. *Cell* 128, 547-560.
- Stepanova, T., Slemmer, J., Hoogenraad, C. C., Lansbergen, G., Dortland, B., De Zeeuw, C. I., Grosveld, F., van Cappellen, G., Akhmanova, A., and Galjart, N. (2003). Visualization of microtubule growth in cultured neurons via the use of EB3-GFP (end-binding protein 3-green fluorescent protein). *J Neurosci* 23, 2655-2664.
- Tada, T., and Sheng, M. (2006). Molecular mechanisms of dendritic spine morphogenesis. *Curr Opin Neurobiol* 16, 95-101.
- Wang, H., Dichtenberg, J. B., Ku, L., Li, W., Bassell, G. J., and Feng, Y. (2008). Dynamic association of the fragile X mental retardation protein as a messenger ribonucleoprotein between microtubules and polyribosomes. *Mol Biol Cell* 19, 105-114.
- Yuste, R., and Bonhoeffer, T. (2001). Morphological changes in dendritic spines associated with long-term synaptic plasticity. *Annu Rev Neurosci* 24, 1071-1089.
- Zalfa, F., Eleuteri, B., Dickson, K. S., Mercaldo, V., De Rubeis, S., di Penta, A., Tabolacci, E., Chiurazzi, P., Neri, G., Grant, S. G., and Bagni, C. (2007). A new function for the fragile X mental retardation protein in regulation of PSD-95 mRNA stability. *Nat Neurosci* 10, 578-587.

Summary
Samenvatting



Summary

The brain is an extensive network of neurons. Complex processes like sensor, motor and cognitive functions are processed and regulated in the brain. Learning and memory are also processes that take place in the brain. Neurons receive signals and pass these signals on to other neurons. Synapses are the points of contact between neurons at which communication between those neurons is possible. A synapse has a presynaptic compartment at the axon of the neuron that sends the signal and a postsynaptic compartment at the dendrite of the receiving neuron. Signal transmission over a synapse occurs when an electric stimulus triggers the presynaptic synapse to release neurotransmitters. Those neurotransmitters can bind to receptors at the postsynaptic compartment which can lead to an electric signal in the receiving neuron. Neurons can quickly adapt to new information by adjusting the amount of synaptic connections and the strength of those connections with other neurons and thereby changing the networks they are part of. New synapses can be made, existing synapses can disappear, grow or shrink. This synaptic plasticity is thought to be the mechanism behind learning and memory. Abnormalities in the synaptic connections between neurons are found in many neuropathologies.

In this thesis we try to gain further insight on the molecular processes involved in the plasticity of the postsynaptic compartment of the synapse, the dendritic spine.

Chapter 1 is an overview of the current knowledge of synaptic transmission, spine morphology and transport of synaptic proteins.

In **chapter 2** we describe how dynamic microtubules can enter a dendritic spine and modulate spine morphology. We describe the interaction between microtubule plus end binding protein EB3 and p140Cap, a protein localized in the spine. We show that dynamic microtubule, EB3 and p140Cap are essential for synaptic transmission and for maintaining spine morphology in hippocampal neurons. Knocking out EB3, p140Cap or disabling dynamic microtubuli leads to filipodia like spines. We show that EB3-labeled growing microtubule ends bind p140Cap and regulate the localization of p140Cap. p140Cap can interact with the actin binding protein cortactin. Thus, we propose a possible mechanism linking dynamic microtubuli entering spines, actin dynamics and synaptic plasticity.

In **chapter 3** we identify the protein GRASP-1 as a neuron specific effector of Rab4 and a key component of the molecular machinery that coordinates the endosomal system in dendrites. We show that GRASP-1 is necessary for AMPA receptor recycling, maintenance of spine morphology and endosomal mobility. GRASP-1 enables coupling between early and late recycling endosomes by binding Rab4 and the SNARE protein syntaxin 13. The data uncover a new mechanism for regulation of membrane receptor transport.

In **chapter 4** we investigate the effects on spine morphology of the absence of functional FMRP in neurons. In patients, a mutation in FMR1 results in the absence of FMRP which causes Fragile X syndrome. In a mouse model for Fragile X syndrome we show that the absence of FMRP results in abnormal spine morphology in Purkinje cells in the cerebellum and deficits on both cell physiological and behavioral level. Fragile X patients display the same deficits in motor learning as the mutant mice.

In chapter 5 we discuss the results we described in this thesis and possible directions for future studies to further investigate spine morphology and synaptic plasticity.

Samenvatting

De hersenen bestaan uit een uitgebreid netwerk van zenuwcellen, ook wel neuronen genaamd. Complexe processen zoals sensorische, motorische en cognitieve functies worden in de hersenen verwerkt en gereguleerd. Ook leren en geheugen zijn processen die in de hersenen plaats vinden. Neuronen kunnen signalen ontvangen en aan elkaar doorgeven. Deze communicatie verloopt via synapsen, de contactpunten tussen neuronen. De synaps bestaat uit een presynaptisch compartiment op een axon en een postsynaptisch compartiment op een dendriet. Signaal overdracht over een synaps komt tot stand doordat na een elektrische stimulans, neurotransmitters vrij komen uit het presynaptische compartiment die kunnen binden aan receptoren in het postsynaptische compartiment wat leidt tot een elektrische signaal in het postsynaptische neuron. Neuronen zijn in staat om zich snel aan te passen aan nieuwe informatie door het aantal verbindingen en de kracht van de verbindingen met andere neuronen aan te passen en hiermee veranderingen aan te brengen in de netwerken waarin ze zich bevinden. Dit gebeurt door nieuwe synapsen te maken en/of bestaande synapsen te laten groeien of verkleinen en wordt gezien als het mechanisme dat het brein in staat stelt tot leren en geheugen. Het is goed bekend dat bij veel neurologische aandoeningen afwijkingen worden gevonden in de synaptische verbindingen tussen neuronen. In dit proefschrift probeer ik meer inzicht te verschaffen in de moleculaire processen die betrokken zijn bij de plasticiteit van het postsynaptische compartiment van de synaps, de dendritische spine.

In **hoofdstuk 1** geef ik een overzicht van de huidige kennis op het gebied van synaptische transmissie, spine morfologie en de moleculaire processen die betrokken zijn bij het transport van synaptische eiwitten.

In **hoofdstuk 2** wordt beschreven dat dynamische microtubuli een dendritische spine in kunnen groeien en zo de morfologie van de spine kunnen beïnvloeden. We beschrijven de interactie tussen het plus eind bindende eiwit EB3 en het in de spine gelokaliseerde eiwit p140Cap. We tonen aan dat dynamische microtubuli, EB3 en p140Cap essentieel zijn voor synaptische transmissie en het in stand houden van spine morfologie in hippocampale neuronen. Het uitschakelen van dynamische microtubuli, EB3 of p140Cap in een neuron leidt tot onderontwikkelde spines, zogenaamde filipodia. We stellen een model voor waarin EB3 gebonden aan dynamische microtubuli kan binden aan p140Cap en daarmee de localisatie van p140Cap beïnvloedt. p140Cap kan een interactie aan gaan met het actine bindend eiwit cortactin. Dit geeft een mogelijk mechanisme hoe microtubuli invloed hebben op actine dynamiek in spines en op deze manier spine morfologie en synaptische plasticiteit kunnen beïnvloeden.

In **hoofdstuk 3** identificeren we het eiwit GRASP-1 als een neuron specifieke bindingspartner voor Rab4. GRASP-1 is betrokken bij de coordinatie van het endosomale systeem in dendrieten. We laten zien dat GRASP-1 essentieel is voor AMPA receptor recycling, spine morfologie en een functioneel endosomaal apparaat. GRASP-1 maakt een connectie tussen vroege en late recycling endosomen door een verbinding te vormen tussen Rab4 en het SNARE eiwit syntaxin 13. Op deze manier is GRASP-1 in staat om Rab4 gelabelde endosomen af te splitsen van Rab5 gelabelde vroege endosomen en ze te koppelen aan Rab11 gelabelde late recycling endosomen. GRASP-1 lijkt betrokken te zijn bij een nieuw mechanisme voor de regulatie van membraan receptor transport onder invloed van verschillende synaptische stimuli.

In **hoofdstuk 4** wordt gekeken naar de effecten van het ontbreken van het eiwit FMRP op spine morfologie. In mensen leidt het ontbreken van functioneel FMRP in neuronen tot het fragile X syndroom, een veel voorkomende vorm van mentale retardatie. We laten in een muizen model voor fragile X syndroom zien dat deze mutatie leidt tot een abnormale spine morfologie in Purkinje cellen in het cerebellum, veranderingen op celfysiologisch niveau en afwijkingen in het motorisch leergedrag in de eye-blink conditionerings test. Bij patiënten met het fragile X syndroom worden dezelfde afwijkingen gevonden in het motorisch leergedrag. FMRP is een voorbeeld van hoe een enkel eiwit invloed heeft op de spine morfologie in neuronen en uiteindelijk zelfs op gedrag of motoriek.

In **hoofdstuk 5** bespreken we de resultaten van het onderzoek beschreven in dit proefschrift en worden mogelijke richtingen voor toekomstig onderzoek bekeken om de mechanismen en processen betrokken bij spine morfologie en synaptische plasticiteit verder te ontrafelen.

Portfolio

Portfolio

Curriculum Vitae

Bjorn Robin Dortland

Geboren: 9 januari 1973 te Gouda

- | | |
|-------------|---|
| 1985 – 1990 | HAVO, rijkscholengemeenschap RSG, Gouda |
| 1990 – 1996 | Hoger Laboratorium onderwijs HLO, Zoologie, Delft |
| 1996 – 2002 | Analist, Erasmus MC, afdeling Celbiologie |
| 2002 – 2009 | AIO, Erasmus MC, afdeling Neurowetenschappen |

List of publications

Cai, Z., de Bruijn, M., Ma, X., Dortland, B., Luteijn, T., Downing, R. J., and Dzierzak, E.

Haploinsufficiency of AML1 affects the temporal and spatial generation of hematopoietic stem cells in the mouse embryo.

Immunity 2000 oct. 13, 423-431.

Akhmanova, A., Hoogenraad, C. C., Drabek, K., Stepanova, T., Dortland, B., Verkerk, T., Vermeulen, W., Burgering, B. M., De Zeeuw, C. I., Grosveld, F., and Galjart, N.

Clasps are CLIP-115 and -170 associating proteins involved in the regional regulation of microtubule dynamics in motile fibroblasts.

Cell, 2001, march 23, 104, 923-935.

Hoogenraad, C. C., Akhmanova, A., Howell, S. A., Dortland, B. R., De Zeeuw, C. I., Willemsen, R., Visser, P., Grosveld, F., and Galjart, N.

Mammalian Golgi-associated Bicaudal-D2 functions in the dynein-dynactin pathway by interacting with these complexes.

Embo J, 2001, august 1, 20, 4041-4054.

Hoogenraad, C. C., Koekkoek, B., Akhmanova, A., Krugers, H., Dortland, B., Miedema, M., van Alphen, A., Kistler, W. M., Jaegle, M., Koutsourakis, M., et al.

Targeted mutation of Cyln2 in the Williams syndrome critical region links CLIP-115 haploinsufficiency to neurodevelopmental abnormalities in mice.

Nat Genet, 2002, sept., 32, 116-127.

Stepanova, T., Slemmer, J., Hoogenraad, C. C., Lansbergen, G., Dortland, B., De Zeeuw, C. I., Grosveld, F., van Cappellen, G., Akhmanova, A., and Galjart, N.

Visualization of microtubule growth in cultured neurons via the use of EB3-GFP (end-binding protein 3-green fluorescent protein).

J Neurosci, 2003, apr 1, 23, 2655-2664.

Koekkoek, S. K., Hulscher, H. C., Dortland, B. R., Hensbroek, R. A., Elgersma, Y., Ruigrok, T. J., and De Zeeuw, C. I.

Cerebellar LTD and learning-dependent timing of conditioned eyelid responses.

Science, 2003, sep 19, 301, 1736-1739.

Dortland, B. R., Koekkoek, S. K., Yamaguchi, K., Milojkovic, B. A., Ruigrok, T. J., Maex, R., De Graaf, W., Smit, A. E., VanderWerf, F., Bakker, C. E., et al.

Deletion of FMR1 in Purkinje cells enhances parallel fiber LTD, enlarges spines, and attenuates cerebellar eyelid conditioning in Fragile X syndrome.

Neuron, 2005, aug 4, 47, 339-352.

Van Der Giessen, R. S., Koekkoek, S. K., van Dorp, S., De Gruijl, J. R., Cupido, A., Khosrovani, S., Dortland, B., Wellershaus, K., Degen, J., Deuchars, J., et al.

Role of olivary electrical coupling in cerebellar motor learning.

Neuron, 2008, may 22, 58, 599-612.

Dortland, B. R., Jaworski, J., Kapitein, L. C., Gouveia, S. M., Wulf, P. S., Grigoriev, I., Camera, P., Spangler, S. A., Di Stefano, P., Demmers, J., *et al.*

Dynamic microtubules regulate dendritic spine morphology and synaptic plasticity.

Neuron, 2009, jan 15, *61*, 85-100.

Hoogenraad C.C., Van Vlijmen T., Popa I., Dortland B.R., Wulf P.S., Govers R., Monti M., Heck A.J.R., Sanchez-Martinez E., Rehmann H., Jaarsma D., Van der Sluijs P.

Neuron specific Rab4 effector GRASP-1 coordinates membrane specialization and maturation of recycling endosomes.

Submitted

Dankwoord

Al sinds 1996 loop ik rond op het Erasmus, eerst bij celbiologie en daarna bij neurowetenschappen. Als iemand mij 13 jaar geleden verteld had dat dit uiteindelijk zou resulteren in een proefschrift, is de kans groot dat ik deze persoon voor gek verklaard had. Maar wonderbaarlijk genoeg is het toch zo ver gekomen.

Wetenschap doe je niet alleen en dit boekje is niet enkel mijn werk maar iets waar heel veel collega's een bijdrage aan geleverd hebben. Dit is het moment dat ik iedereen kan bedanken voor alle hulp op wetenschappelijk gebied. En daarnaast wil ik ook iedereen bedanken die mijn AIO tijd tot een gezellige periode gemaakt hebben, waarin ik enorm veel lol gehad heb en meestal met plezier naar mijn werk kwam.

Allereerst mijn promotor, Chris, zonder jouw overtuigingskracht was ik nooit aan dit promotietraject begonnen. Bedankt dat je me de kans gegeven hebt om te promoveren bij neurowetenschappen. Je hebt ooit tijdens een werkbespreking gezegd dat je hoopte dat "Bjorn de Promovendus" op zou bloeien. Ik hoop dat ik aan je verwachtingen heb voldaan.

Casper, zonder jouw hulp had ik dit hele promotie gebeuren nooit succesvol afgerond. We kennen elkaar al sinds de brugklas, gingen allebei naar het HLO, waren collega's bij celbiologie, ik was ooit jou paranimf en nu ben je mijn co-promotor. Ik kan daar de lol wel van inzien. Bedankt.

Natuurlijk wil ik ook mijn beide paranimfen, Phebe en Petra, bedanken. Ik ben blij dat jullie je taak zo serieus nemen en de eerste de beste gelegenheid gebruikten om mij, die gestresste, hardwerkende promovendus, in de maling te nemen door misbruik te maken van mijn onwetendheid op het gebied van prijzen van dameskleding. Phebe, ik zal mijn plekkie naast je op het lab best gaan missen. Je vind het vast niet erg als ik zo nu en dan nog een koffie kom drinken als ik heimwee krijg.

Alexander, we promoveren op dezelfde dag en stiekem ben ik wel een beetje jaloers dat jij straks alle stress 2 uur eerder achter je kan laten dan ik. Op het grote promotiefeest moeten we maar een paar biertjes drinken om het te vieren. Veel succes in Duitsland.

Lab 1271, waar serieuze wetenschap afgewisseld wordt met volstrekt onzinnige discussies, smerige verhalen en minder wetenschappelijke experimenten met droog ijs en vloeibare stikstof. Max, Nanda, Marijn, Mathijs, Myrrhe, Samantha, Dick, Eva, Lukas, Robert, Karin en Kah Wai, allemaal bedankt voor de gezelligheid zowel op het lab als er buiten.

Ook lab Koekoek bedankt. Hier heb ik geleerd dat er vele mogelijkheden zijn met een eyeblink opstelling. Je kan er mee meten, je kan er aan knutselen en je kan hem verhuizen. Om eerlijk te zijn, de tweede optie is het leukst en de laatste heb ik te vaak moeten doen. Maar uiteindelijk kan ik daardoor wel solderen als een dolle. Bas, Hester, Joel en Henk-Jan, het was een groot plezier om met jullie te werken.

Groep Akhmanova, Anna, Ilya, Daniel, Babette, Suzanna, Gideon, Rick, er wordt zoveel samen gewerkt tussen ons en jullie lab dat het soms wel lijkt of we 1 grote groep zijn. Jammer dat de werkbespreking altijd zo belachelijk vroeg in de ochtend was, anders was ik er graag wat vaker bij geweest.

Verder kan ik ook de lunchgroep niet vergeten te bedanken. Frank, Jeffrey, Rick (ooit win ik een potje squash van je), Marja, Michael en Suzanne, jullie hebben

jarenlang vol afgrijzen toe moeten kijken hoe ik mijn dagelijkse portie kantine voedselprutspulblubber naar binnen zat te werken. Hopelijk heeft dat jullie eetlust nooit bedorven. Het was altijd fijn dat er consequent niet over wetenschap gepraat werd tijdens de lunch.

Sara, Angélique, Doortje en Corina, urenlang heb ik jullie van je werk gehouden wanneer ik weer eens meer zin had in thee/koffie en een beetje kletsen dan in mijn experimenten. Uiteindelijk heeft jullie dat allemaal gelukkig niet weerhouden om ver voor mij te promoveren. Bedankt voor alle gezelligheid. Sara, speciaal voor jou bestaat er nu een foto waarop ik een andere kerel zoen. Die foto was niet makkelijk te maken, maar zeker de moeite waard om jou een beetje te shockeren. Al ben ik wel bang dat deze foto nog veel te vaak terug gaat komen op genante momenten.

En voor de collega's die ik niet bij naam genoemd heb, ook jullie hebben bijgedragen aan het feit dat ik het prima naar mijn zin gehad heb bij neurowetenschappen en daarvoor

Allemaal Bedankt.